LEABHARLANN CHOLÁISTE NA TRÍONÓIDE, BAILE ÁTHA CLIATH | TRINITY COLLEGE LIBRARY DUBLIN
Ollscoil Átha Cliath | The University of Dublin

Terms and Conditions of Use of Digitised Theses from Trinity College Library Dublin

Copyright statement

All material supplied by Trinity College Library is protected by copyright (under the Copyright and Related Rights Act, 2000 as amended) and other relevant Intellectual Property Rights. By accessing and using a Digitised Thesis from Trinity College Library you acknowledge that all Intellectual Property Rights in any Works supplied are the sole and exclusive property of the copyright and/or other IPR holder. Specific copyright holders may not be explicitly identified. Use of materials from other sources within a thesis should not be construed as a claim over them.

A non-exclusive, non-transferable licence is hereby granted to those using or reproducing, in whole or in part, the material for valid purposes, providing the copyright owners are acknowledged using the normal conventions. Where specific permission to use material is required, this is identified and such permission must be sought from the copyright holder or agency cited.

Liability statement

By using a Digitised Thesis, I accept that Trinity College Dublin bears no legal responsibility for the accuracy, legality or comprehensiveness of materials contained within the thesis, and that Trinity College Dublin accepts no liability for indirect, consequential, or incidental, damages or losses arising from use of the thesis for whatever reason. Information located in a thesis may be subject to specific use constraints, details of which may not be explicitly described. It is the responsibility of potential and actual users to be aware of such constraints and to abide by them. By making use of material from a digitised thesis, you accept these copyright and disclaimer provisions. Where it is brought to the attention of Trinity College Library that there may be a breach of copyright or other restraint, it is the policy to withdraw or take down access to a thesis while the issue is being resolved.

Access Agreement

By using a Digitised Thesis from Trinity College Library you are bound by the following Terms & Conditions. Please read them carefully.

I have read and I understand the following statement: All material supplied via a Digitised Thesis from Trinity College Library is protected by copyright and other intellectual property rights, and duplication or sale of all or part of any of a thesis is not permitted, except that material may be duplicated by you for your research use or for educational purposes in electronic or print form providing the copyright owners are acknowledged using the normal conventions. You must obtain permission for any other use. Electronic or print copies may not be offered, whether for sale or otherwise to anyone. This copy has been supplied on the understanding that it is copyright material and that no quotation from the thesis may be published without proper acknowledgement.

Modulating oxidative stress in the retina using gene therapy as a potential treatment for inherited retinopathies

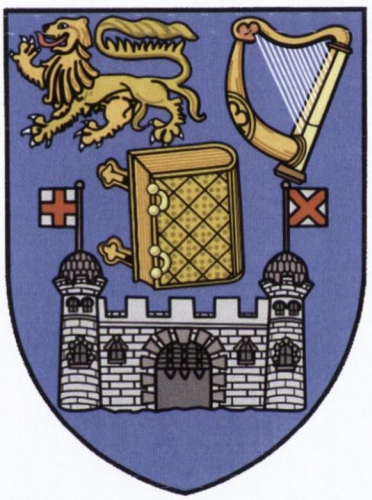

A thesis submitted to the University of Dublin for the Degree of Doctor of Philosophy

By

Gareth O'Dwyer
2014

Under the supervision of Professor Jane Farrar

Department of Genetics
Trinity College Dublin

Declaration

This thesis has not been previously submitted as an exercise for a degree at this or any other University. The work presented here is entirely my own except where noted. I agree to deposit this thesis in the university's open access institutional repository or allow the library to do so on my behalf, subject to Irish copyright legislation and Trinity College library conditions of use and acknowledgment.

Gareth O'Dwyer.

Gareth O'Dwyer

TRINITY COLLEGE
0 9 JUN 2014
LIBRARY DUBLIN
LIBRARY DUBLIN

Thesis 10400

Summary

The focus of this thesis was the exploration of genetic modulators of oxidative stress in transgenic mouse models of Retinitis Pigmentosa (RP). This disease can be inherited both dominantly and recessively and can be either X-linked or autosomal depending of the disease causing mutation. Patients of RP gradually lose their peripheral eyesight over years as rod cells die in the retina. Cone cells then begin to die leading to complete blindness. Evidence amassed over the past ten years has suggested that increasing levels of oxidative stress in the retina of these patients is causing cell death of rod and cone photoreceptor cells. In particular, cone cells seem to die secondary to rods as the levels of oxidative stress dramatically increase when rods die. In addition, this increase in oxidative stress appears to be common in many inherited and non-inherited retinal degenerations.

Based on these observations, two genetic therapies were created. The first of these was an RNA interference (RNAi) based therapy targeted at the *Rac1* gene. The protein encoded by this gene is known to activate the NADPH oxidase complex which produces ROS. Previous studies have shown that depleting this gene in the retina preserves eyesight in mouse models of RP. Therefore short interfering RNAs (siRNAs) were generated to target *Rac1* mRNA and were demonstrated to suppress expression of this gene *in vitro*. Subsequently, short hairpin RNAs (shRNAs) were developed based on the sequence of successful siRNAs for Adeno Aassociated Virus (AAV) mediated delivery to the mouse retina *in vivo*. This also resulted in suppression of endogenous mouse *Rac1* expression. Furthermore, of the two shRNA AAV vectors created, one was demonstrated to preserve visual function and rod and cone photoreceptor viability in a mouse model of RP.

In addition to the suppression of *Rac1*, a parallel project explored the use of *Thioredoxin1* (Trx) over-expression in the retina and the effect of this over-expression in two mouse models of RP. The *Trx* gene encodes an anti-oxidant protein which acts as a reducing agent within the cell cytoplasm. Previous studies have demonstrated that over-expression of this gene preserves retinal ganglion cell function and viability in several models of retinal degeneration. Furthermore, over-expression of *Trx* was shown to be protective of retinal photoreceptor cells in a

mouse model of RP. Therefore an AAV plasmid was generated which expresses the *Trx* gene. This plasmid was demonstrated to drive strong expression of *Trx in vitro*. Subsequently this plasmid was used to generate recombinant AAV vector to deliver this plasmid to retinal cells *in vivo*. The vector was demonstrated to drive strong expression of *Trx* in the photoreceptor cells *in vivo*. Delivery of the *Trx* AAV vector to two mouse models of RP failed to protect photoreceptor cell function or viability in these models. Possible reasons for this failure are also explored in this thesis.

Finally, a stain for ROS named dihydroethidium (DHE) was used to evaluate the levels of ROS in three mouse models of retinal degeneration frequently used by the TCD Ocular Genetics laboratory. Of these three, two were demonstrated to exhibit increased staining for ROS in the retina. In addition, ROS production in the retina was monitored using this stain after treatment of RP model mice with a *Rac1* targeted shRNA or a plasmid over-expressing *Trx*. No decrease in staining was observed for any constructs evaluated except for one shRNA which targets *Rac1*. This shRNA was the same construct which elicited an improvement in photoreceptor function and cell viability, suggesting that shRNA suppression of *Rac1* decreased the production of ROS and in turn increased the functionality of the retina by reducing ROS mediated pathology.

The experiments detailed in this thesis provide an indication that modulation of the retinal levels of reactive Oxygen species can provide functional benefit in mouse models of RP. Furthermore, it provides the motivation to carry out further characterisation of RNAi mediated suppression of *Rac1* expression within other animal models of RP as well as mouse models of other retinal degenerations for which oxidative stress is a contributing pathological factor.

Acknowledgments

There are many people who deserve thanks for helping me along the way of my four years in the laboratory. Firstly to Prof Jane Farrar for offering me this exciting project, for taking the time to provide help and support and for constantly challenging me to think analytically and view the bigger picture of this research. To Dr Sophia Millington-Ward who has been a constant guidance through the experimental work. To Dr Naomi Chadderton who took a lot of time to initially create the AAV vectors described in this thesis and who then taught me this intricate process. To Dr Mary O'Reilly who answered endless questions about the finer details of DNA cloning and who would always take the time to review (often puzzling) DNA sequences and restriction digests. To Dr Arpad Palfi who gratefully taught me histology. To Dr Paul Kenna who has taken a huge amount of time and effort to perform all the sub-retinal injections and ERG recordings. Without him this thesis would be meaningless. And to Dr Matthew Campbell who was incredibly helpful with western blot troubleshooting and was always ready to provide a second opinion on experimental design. I would also like to thank Science Foundation Ireland who have funded the work detailed within this thesis.
I would also like to thank my fellow students past and present with whom I have shared the more social aspects of a PhD study. They are Leanne Moore, Dr Anh Nyugen, Dr Clare Morgan, James Keaney, Ema Ozaki, Matt Carrigan, Ailbhe Brazel and especially Finnian Hanrahan whom I have known since being an undergrad in this department and who has become a close friend over these four years.
To those in the animal unit; Dave, Rebecca, Charlie and Caroline who have been a huge help with providing the mice for all of my *in vivo* work. In addition, I would also like to thank non-laboratory friends, especially Ger, Harry and Liam who have been there for regular tea breaks and car trips around Dublin.
I would also like to thank my family; my mam Laura, James, Jessica and Andrew who didn't quite understand what I did but were proud and supportive nonetheless. And finally to my girlfriend Claire, whom I met in the Farrar lab and who has been an absolute pillar these past four years. Here's to the next four years in UCD together. I love you very much.

I would like to dedicate this to my dad, Kevin, who never allowed me to doubt myself and who would have been incredibly proud to see me finish this PhD study.

List of Abbreviations

8-OH-dG: 8-oxo-2'-deoxyguanosine
AAV: Adeno Associated Virus
adRP: autosomal dominant Retinitis Pigmentosa
ALS: Amyothrophic Lateral Scclerosis
AMD: Age-Related Macular Degeneration
ANOVA: Analysis of Variation
B-PDE: β-Phosphodiesterase
CDS: Coding Sequence
CMV: Cytomegalovirus
CNTF: Ciliary Neurotrophic Factor
CNV: Choroidal Neovascularisation
DMEM: Dulbecco's Modified Eagle Medium
DMSO: Dimethyl Sulfoxide
DNA: Deoxyribonucleic Acid
DR Diabetic Retinopathy
dsRNA: double stranded RNA
EGFP: Enchanced Green Fluorescent Protein
ELISA: Enzyme Linked Immunosorbent Assay
ERG: Electroretinography
FACS: Fluorescence Activated Cell Sorting
GABA: γ-Aminobutyric Acid
GCL: Ganglion Cell Layer
GDP: Guanosine Diphosphate
GMP: Guanosine Monophosphate
GPCR: G-Protein Coupled Receptor
GTP: Guanosine Triphosphate
HNE: Hydroxynonenal
IFN: Interferon
INL: Inner Nuclear Layer
IPL: Inner Plexiform Layer
ITR: Inverted Terminal Repeat
LCA: Leber Congenital Amaurosis
LHON: Leber's Hereditary Optic Neuropathy
MCS: Multiple Cloning Site
miRNA: microRNA
MRPR2: Mouse Rhodopsin Promoter Reverse 2
NO: Nitric Oxide
NT: Non-Targeting
OIR: Oxygen Induced Retinopathy
ONL: Outer Nuclear Layer
OPL: Outer Plexiform Layer
PARP: Poly ADP Ribose Polymerase
PBS: Phosphate Buffered Saline
PCR: Polymerase Chain Reaction
Pfa: Paraformaldehyde
PRR: Proline Rich Region
PUFA: Poly-Unsaturated Fatty Acid
PX: Phox Homology

RAC1: Ras-related C3 botulinum toxin substrate 1
RdCVF: Rod-derived Cone Viability Factor
RISC: RNA-Induced Silencing Complex
ROS: Reactive Oxygen Species (or Rod Outer Segments)
RNA: Ribonucleic Acid
RNAi: RNA Interference
RNS: Reactive Nitrogen Species
RP: Retinitis Pigmentosa
RPE: Retinal Pigment Epithelium
siRNA: small interfering RNA
shRNA: short hairpinRNA
SSB: Single Strand Break
TPR: Tetricopeptide Repeat
Trx: Thioredoxin
UPR: Unfloded Protein Response

Contents

Chapter_1:_Introduction 8
1.1 The Eye: Structure and Function 9
1.2 Retinal Structure 9
1.3 Visual Transduction 11
1.4 Retinitis Pigmentosa 13
1.5 Clinical Symptoms and Assessment 14
1.6 Genetic Basis of RP 15
1.7 Oxidative Stress 16
1.8 Oxidative Stress in RP 17
1.9 Gene Therapy 19
1.10 Replacement Strategies and LCA Clinical Trials 21
1.11 RNA interference 23
1.12 RNAi and its uses in Gene Therapy 24
1.13 Gene Therapy for RP 27
1.14 Delivery Methods 29
1.15 Non-viral delivery 32
1.16 Objectives 34
Chapter 2: Materials and Methods 41
Section 2.1: Materials 42
2.1.1 Reagents for DNA cloning 42
2.1.2 Cell Culture Reagents 43
2.1.3 RNA Reagents 44
2.1.4 Protein Reagents 44
2.1.5 Reagents for Production of Recombinant AAV 46
2.1.6 Animals 46
2.1.7 Animal Reagents 46
2.1.8 Histology and Immunohistochemistry Reagents 47
2.1.9 Antibodies 47
2.1.10 FACS Reagents 48
2.1.11 Primers 48
Section 2.2 Methods 50
2.2.1 Cloning Methods 50
2.2.1.1 Determination of DNA/RNA Concentration by NanoDrop™ Spectrophotometry 50
2.2.1.2 Electrophoresis of DNA by Agarose Gel 50
2.2.1.3 DNA purification using PCR Purification and Gel Extraction Kits 50
2.2.1.3 DNA Purification by Phenol/Chloroform Extraction 51
2.2.1.4 DNA Amplification and isolation using Kits 51
2.2.1.5 Restriction Enzyme DNA Digestion 52
2.2.1.6 Blunting of 5' DNA sticky ends using Klenow Enzyme 53
2.2.1.7 Blunting of 3' DNA stick end using T4 DNA Polymerase 53
2.2.1.8 DNA Ligation 53
2.2.1.9 Polymerase Chain Reaction (PCR) 54
2.2.1.10 Inducing Competence in XL1-BlueMRA E. Coli 54
2.2.1.11 Transformation of competent cells 55
2.2.1.12 Colony PCR 55
2.2.1.13 Sequencing 56

2.2.2 Cell Culturing Protocols 56
2.2.2.1 Culturing Conditions 56
2.2.2.2 Cell Passaging 56
2.2.2.3 Cell Counting using a Haemocytometer 56
2.2.2.4 Freezing Cells 57
2.2.2.5 Thawing Cells 57
2.2.2.6 Transfection using Lipofectamine 2000® 57
2.2.3 RNA Protocols 58
2.2.3.1 General Treatment of RNA 58
2.2.3.2 Harvesting HeLa Cells and isolation of RNA 58
2.2.3.3 Harvesting Retina and isolation of Retinal RNA 59
2.2.3.4 RT-qPCR 59
2.2.4 Protein Protocols 61
2.2.4.1 Extraction of protein from HeLa cells 61
2.2.4.2 Extraction of protein from Mouse Retina 61
2.2.4.3 Quantifying Protein Concentration by BCA Aassay 61
2.2.4.4 Quantifying Protein Concentration by Fluorometry. 62
2.2.5 Western Blot Protocols 62
2.2.5.1 Preparation of SDS-PAGE Gel 62
2.2.5.2 Poly-Acrylamide Gel Electrophoresis 63
2.2.5.3 Transfer of protein to blot (Semi-dry) 63
2.2.5.4 Ponceau S Staining 64
2.2.5.5 Blocking Western Blots 64
2.2.5.6 Specific Probing of Protein with Antibody 64
2.2.5.7 Chemiluminescent Detection of Protein Bands 65
2.2.5.8 Stripping of Western Blots 65
2.2.6 Synthesis of Recombinant AAV 2/5 66
2.2.6.1 Triple Transfection 66
2.2.6.2 Harvesting and Purification of Recombinant AAV from HEK 293 cells 66
2.2.6.3 Determination of Viral Titre 68
2.2.7 Animal Procedures 68
2.2.7.1 Animal Housing 69
2.2.7.2 Mouse Genotyping 69
2.2.7.3 Subretinal delivery of AAV 69
2.2.7.4 Electroretinography 70
2.2.8 Histology and Immunohistochemistry 70
2.2.8.1 Fixing Retina using Paraformaldehyde and Sectioning 71
2.2.8.2 Immunostaining the Retina 71
2.2.9 Statistical Analysis 72
Chapter 3: Suppression of *Rac1 in vitro* and *in vivo* 73
3.1 Introduction 74
3.2 Materials and Methods 76
3.2.1 Cloning of the *RAC1* gene in to pcDNA3.1+ 77
3.2.2 Co-Transfection of siRNAs and CMV_RAC1 77
3.2.3 Isolation of RNA from HeLa Cells 78
3.2.4 RT-qPCR analysis of HeLa cell RNA 78
3.2.5 Isolation of Protein from HeLa Cells 78
3.2.6 Western Blotting 79
3.2.7 Annealing of oligonucleotides 79
3.2.8 Immunohistochemistry 79

3.3 Results 81
3.3.1 Design of siRNAs targeting *RAC1* 81
3.3.2 Expression of Rac1 in the Wildtype Retina 81
3.3.3 Cloning of the *Rac1* Gene in to a Mammalian Expression Vector 82
3.3.4 Suppression of *RAC1* mRNA in HeLa Cells 83
3.3.5 Suppression of *RAC1* Protein in HeLa Cells 84
3.3.6 Design of shRNA oligonucleotides 86
3.3.7 Cloning of the RAC1 shRNAs in to pAAV_MCS 86
3.3.8 shRNA mediated Suppression of *RAC1 in vitro* 87
3.3.9 Production of AAV 2/5 88
3.3.10 Histology of Eyes taken from Injected Wildtype Mice 89
3.3.11 Cloning of the CMV_EGFP DNA in to pAAV_shRAC1_1/3 90
3.3.12 Production of AAV 2/5 with new AAV plasmids 91
3.3.13 RT-qPCR Analysis of Suppression of *Rac1* mRNA *in vivo* 91
3.3.14 Western Blot Analysis of Suppression of Rac1 Protein *in vivo* 92
3.3.15 Immunohistochemical Analysis of Suppression of Rac1 *in vivo* 95
3.3.16 Effect of *Rac1* suppression on Retinal Structure and Function of injected hP347s transgenic mice 96
3.4 Discussion 101
Chapter 4:Expression of Recombinant Thioredoxin1 *in vitro* and *in vivo* 152
4.1 Introduction 153
4.2 Materials and Methods 160
4.2.1 Cloning of the Thioredoxin1 Gene 160
4.2.2 Transfection and Harvesting of HeLa Cells 160
4.2.3 Production of Recombinat AAV_Trx virus 161
4.2.4 RT-qPCR Analyses 161
4.2.5 Western Blotting 162
4.2.6 Immunohistochemistry 162
4.3 Results 163
4.3.1 Cloning of the Thioredoxin1 Gene into pAAV_MCS 163
4.3.2 Expression of Exogenous Thioredoxin1 mRNA in HeLa Cells 163
4.3.3 Expression of Exogenous Thioredoxin Protein in HeLa Cells 164
4.3.4 Production of Recombinant AAV 2/5 165
4.3.5 Expression of Exogenous *Trx* mRNA *in vivo* 165
4.3.6 Expression of Exogenous Trx protein *in vivo* 166
4.3.7 Immunohistochemical Analysis of Expression of Trx *in vivo* 167
4.3.8 Effect of Exogenous Trx Expression in Pro23His RP model Mice 168
4.3.9 Effect of Exogenous Trx Expression hP347S RP Model Mice 171
4.3.10 ERG analysis of Thioredoxin1 over-expressio n in wild type mice 173
4.4 Discussion 175
Chapter 5: Investigation of Dihydroethidium as a Retinal Marker of Oxidative Stress211
5.1 Introduction 212
5.2 Materials and Methods 217
5.2.1 Preparation of DHE solution 217
5.2.2 Administration of DHE by intraperitoneal injection 217
5.2.3 *Ex vivo* staining of the retina using DHE 218
5.2.4 Data Interpretation and Statistical Analysis 219
5.3 Results 220
5.3.1 Evaluation of DHE as a marker of Oxidative Stress *in vivo* 220
5.3.2 Evaluation of DHE as a marker of Oxidative Stress *ex vivo* 221

5.3.3 Examination of changes in retinal superoxide levels in disease model mice injected with recombinant *Thioredoxin* 222
5.3.4 Examination of changes in superoxide levels of RP disease model mice injected with shRNAs targeting *Rac1* 224
5.4 Discussion 227
Chapter 6: General Discussion 257
Chapter 7: Appendix 270

Table of Figures **Page**

Chapter 1:

Figure 1.1: Schematic of retinal structure 35
Figure 1.2: Diagram of Rhodopsin mediated hyperpolarisation 36
Figure 1.3: Fundus of healthy retina (left) and fundus of from a patient with mid stage RP 37
Figure 1.4: Examples of a typical ERG readout 38
Figure 1.5: Diagram of the RNAi Pathway 39

Chapter 3:

Figure 3.5.1: Schematic of the NADPH Oxidase complex upon assembly and activation of Rac1 112
Figure 3.5.2: Homology between siRNA target sequences and each species 114
Figure 3.5.3: Schematic of 'CMV-RAC1', a pcDNA3.1+ plasmid containing the human *RAC1* gene coding sequence 115
Figure 3.5.4: Restriction analysis of CMV_RAC1 with *HindIII* and *XbaI* 116
Figure 3.5.5: Secondary antibody only control for unspecific staining 117
Figure 3.5.6: Immunohistochemistry showing Rac1 Expression in Wilftype Retina 118
Figure 3.5.7: *RAC1* dissociation curve with first reverse primer 119
Figure 3.5.8: Actin dissociation curve 120
Figure 3.5.9: Standard curve of *RAC1* with first reverse primer 121
Figure 3.5.10: Standard curve of *ACTB* 122
Figure 3.5.11: Bar chart showing siRNA-mediated suppression of endogenous RAC1 in HeLa cells 123
Figure 3.5.12: *RAC1* dissociation using a new *RAC1* reverse primer 124
Figure 3.5.13: RAC1 standard curve with new primer 125
Figure 3.5.14: Suppression of RAC1 with new reverse primer 126
Figure 3.5.15: Western Blot showing suppression of RAC1 in vitro 127
Figure 3.5.16: shRNA design for cloning 128
Figure 3.5.17: Cloning of the shRNA in to pAAV 129
Figure 3.5.18: shRNA mediated suppression of *RAC1* in vitro 130
Figure 3.5.19: Retinal Histology showing EGFP expression from shRAC1 viruses 131
Figure 3.5.20: The pAAV_shRAC1_1 plasmid with CMV promoter driven EGFP 132
Figure 3.5.21: Restriction Enzyme Analysis of AAV_shRAC1_1/3 133
Figure 3.5.22: AAV_shRAC1_1 mediated suppression of *Rac1 in vivo* 134
Figure 3.5.23: AAV_shRAC1_3 mediated suppression of Rac1 *in vivo* 135
Figure 3.5.24: Western Blot showing Suppression of Rac1 *in vivo* 136
Figure 3.5.25: Densitometry Analysis of Rac1 suppression in vivo 137
Figure 3.5.26: Retinal histology showing immunofluorescence using a Rac1 specific antibody 138
Figure 3.5.27: Retinal Histology showing Rac1 Expression in NT20 and AAV_shRAC1_1 treated Eyes 139
Figure 3.5.28: Retinal Histology showing Rac1 expression in NT20 and AAV_shRAC1_3 treated eyes 140
Figure 3.5.29: Retinal histology of hP347S transgenic mice treated with AAV_shRAC1_1 at 4 weeks post injection using a cone specific marker (n=3) 141
Figure 3.5.30: Retinal Immunohistology of hP347S transgenic mice treated with AAV_shRAC1_3 at 4 weeks post injection using a cone cell specific marker (n=3) 142
Figure 3.5.31: Retinal Immunohistology of hP347S transgenic mice treated with AAV_shRAC1_3 at 16 weeks post injection using a cone specific marker (n=3) 143
Figure 3.5.32: Retinal Immunohistology of hP347S transgenic mice treated with AAV_shRAC1_3 at 16 weeks post injection using a rod specific antibody (n=3) 144
Figure 3.5.33: ERG analysis of AAV_shRAC1_1 injected hP347S transgenic mice at 4-12 weeks post injection (n=4) 145
Figure 3.5.34: ERG analysis of SH3 injected hp347s mice 4-14 weeks post injection (n=6) 148

Chapter 4:

Figure 4.5.1: Biochemical pathway showing the generation of reduced Trx by TrxR. 185
Figure 4.5.2: Vector Maps used for Thioredoxin Cloning 186

Figure 4.5.3: Agarose gel showing restriction digest of pTrx_AAV 187
Figure 4.5.4: Trx Dissociation Curve 188
Figure 4.5.5: Trx Standard Curve 189
Figure 4.5.6: CMV driven Expression of Thioredoxin in HeLa cells. 190
Figure 4.5.7: Overexpression of Trx in HeLa Cells 191
Figure 4.5.8: Overexpression of Trx in Injected Whole Retina where n=5 192
Figure 4.5.9: Western Blot showing overexpression of Trx *in vivo* where n=3 193
Figure 4.5.10: Immunohistochemistry of Trx_AAV Injected Wildtype Retinas where n=3 194
Figure 4.5.11: Immunohistochemistry of Trx_AAV injected P23H Mice at P10 where n=3 195
Figure 4.5.12: Immunohistochemistry of Trx_AAV injected P23H Mice at P22 where n=3 196
Figure 4.5.13: ONL thickness of P23H mouse left eyes and right eyes at 22 days post-injection of CMV_EGFP and Trx_AAV respectively where n=3 197
Figure 4.5.14: Electroretinographic Analysis of Trx_AAV injected P23H Mice at P22 where n=5 198
Figure 4.5.15: PNA staining of hP347S mice treated with Trx_AAV at 4 weeks post-injection where n=3 199
Figure 4.5.16: PNA staining of hP347S mice treated with Trx_AAV at 4 weeks post-injection where n=3 200
Figure 4.5.17: ERG analysis of Trx_AAV injected hP347S mice 4-16 weeks post injection where n=3 201
Figure 4.5.18: ERG analysis of Trx_AAV (1/2 dilution) injected hP347S mice 4 weeks post injection where n=3 204
Figure 4.5.19: ERG analysis of Trx_AAV (1/2 dilution) injected hP347S mice 12 weeks post injection where n=3 205
Figure 4.5.20: ERG analysis of 1/10 dilution of Trx_AAV injected hP347S at 6 weeks post injection where n=4 206
Figure 4.5.21: ERG responses of a range of Trx_AAV dilutions in wild type mice. 208

Chapter 5:

Figure 5.5.1: Molecular Structures of DHE and ethidium 236
Figure 5.5.2: *In vivo* DHE staining of the retinas of Rotenone Injected Eyes 237
Figure 5.5.3: *Ex vivo* DHE staining of retinal sections of wildtype and hP347S mice 238
Figure 5.5.4: Quantification of DHE staining intensity of wildtype and hP347 retinas (n=4) 239
Figure 5.5.5: *Ex vivo* DHE staining of retinal sections of wildtype and P23H mice 240
Figure 5.5.6: Quantification of DHE staining intensity of wildtype and P23H retinas 240
Figure 5.5.7: *Ex vivo* DHE staining of retinal sections of LHON model mice 241
Figure 5.5.8: Quantification of DHE staining intensity of LHON mouse model retinas 242
Figure 5.5.9: *Ex vivo* DHE staining of P22 P23H mice treated with Trx_AAV 243
Figure 5.5.10: Quantification of DHE staining intensity of P23H mice treated with Trx_AAV 244
Figure 5.5.11: *Ex vivo* DHE staining of hP347S mice treated with Trx_AAV 4 week post injection 245
Figure 5.5.12: Quantification of DHE staining intensity of hP347S mice treated with Trx_AAV 4 week post injection 246
Figure 5.5.13: *Ex vivo* DHE staining of hP347S mice treated with Trx_AAV 16 week post injection 247
Figure 5.5.14: Quantification of DHE staining intensity of hP347S mice treated with Trx_AAV 12 week post injection 248
Figure 5.5.15: *Ex vivo* DHE staining of hP347S mice treated with AAV_shRAC1_1 4 week post injection 249
Figure 5.5.16: Quantification of DHE staining of hP347S mice treated with AAV_shRAC1_1 4 week post injection 250
Figure 5.5.17: *Ex vivo* DHE staining of hP347S mice treated AAV_shRAC1_1 16 week post injection 251
Figure 5.5.18: Quantification of DHE staining intensity of hP347S mice treated with AAV_shRAC1_1 12 week post injection 252
Figure 5.5.19: *Ex vivo* DHE staining of hP347S mice treated with AAV_shRAC1_3 4 week post injection (n=6) 253
Figure 5.5.20: Quantification of DHE staining intensity of hP347S mice treated with AAV_shRAC1_3 4 week post injection (n=6) 254
Figure 5.5.21: *Ex vivo* DHE staining of hP347S mice treated with AAV_shRAC1_3 16 week post injection 255

Figure 5.5.22: Quantification of DHE staining intensity of hP347S mice treated with AAV_shRAC1_3 16 week post injection 256

Table of Tables Page

Chapter 3
Table 3.5.1: Schematic of a 24-well plate 112
Table 3.5.2: siRNA sequences 113
Table 3.5.3: ERG amplitude recordings of AAV_shRAC1_1 injected hP347S mice 147
Table 3.5.4: ERG amplitude recordings of AAV_shRAC1_3 injected hP347S mice 150
Chapter 4
Table 4.5.1: Schematic of 24-well plate of HeLa cells 184
Table 4.5.2: ERG amplitudes of left and right eyes of P23H mice P22 198
Table 4.5.3: ERG recordings of Trx_AAV injected hP347S heterozygous mice (n=3) 203
Table 4.5.4: ERG reccordings of Trx_AAV (1/2 dilution) injected hP347S heterozygous mice at 12 weeks post injection where n=3 204
Table 4.5.5: ERG recordings of Trx_AAV (1/2 dilution) injected hP347S heterozygous mice at 12 weeks post injection where n=3 205
Table 4.5.6: ERG recordings of Trx_AAV (1/10 dilution) injected hP347S heterozygous mice at 6 weeks post injetcion where n=3. 207

Chapter 1: Introduction

1.1 The Eye: Structure and Function

The eye is the primary light sensing organ of vertebrates. This organ takes sensory inputs in the form of light and uses a series of chemical isomerisations and protein signalling cascades to produce a nervous impulse which is then relayed to the brain for processing. The eye itself is composed of three primary tissue layers. The outer layer of the eye is composed of the sclera within the eye socket and the cornea which is exposed to the exterior of the head. The sclera is the white connective tissue which surrounds the entire posterior region of the eye. The cornea is a protective layer which covers the pupil and iris of the eye. The second layer of the eye is deep to the first layer and is composed of the choroid which provides a blood supply to the eye, the ciliary body which has a role in focusing light on to the retina and the iris which is the aperture which controls the amount of light entering the eye. The third and final layer of the eye is deep to the second layer and comprises the retina. This is the tissue in which light cues are received, resulting in a cellular signalling cascade which causes nervous impulses to be sent to the visual cortex of the brain, thus forming moving images referred to as 'sight' or 'vision'. The interior of the eye is composed of the vitreous humour, the aqueous humour and the lens. Both the vitreous humour and the aqueous humour have limited roles in the local immune system, serve to reduce refraction of light passing through the eye and maintain the intraocular pressure and shape of the eye. The lens is responsible for focusing incoming light on to the retina. The shape of this tissue (and hence its focusing properties) is controlled by the ciliary body (Ryan et al, 2001).

1.2 Retinal Structure

The retina is composed of three neuronal layers along with a melanin containing layer and a nerve fiber layer. The outermost layer of the retina is the melanin containing Retinal Pigment Epithelium (RPE). This layer separates the retina from the blood vessels of the choroid and facilitates the diffusion of glucose and other nutrients from the blood to the rest of the retina. The RPE also has a role in preventing photo-oxidative damage by absorbing excess light energy and recycles metabolites from the phototransduction cascade back to the retina (Saari et al, 2012, section 1.3). The most

basal neuronal layer of the retina in relation to the vitreous humour is the Outer Nuclear Layer (ONL) which contains the rod and cone photoreceptors of the retina which are responsible for converting incoming light into a nervous impulse. This impulse is then sent through the synapses which compose the Outer Plexiform Layer (OPL) which is located proximally to the ONL. These synapses connect the cell bodies of the ONL to the Inner Nuclear Layer (INL) which is again located proximally to the OPL. This is the second neuronal layer of the retina and comprises horizontal cells and bipolar cells which form synapses with other photoreceptors and amacrine cells respectively. Amacrine cells will then form synapses with the cells of the third neuronal cell layer, the Ganglion Cell Layer (GCL). Bipolar cells will also form synapses directly with the GCL. The synpases which form between bipolar cells and amacrine cells and ganglion cells reside in the Inner Plexiform Layer (IPL) which resides between the inner nuclear layer and the GCL (Farrar et al, 2002). Finally the retina is separated from the vitreous body by the nerve fiber layer and the inner limiting membrane. The nerve fiber layer relays electrical impulses from the ganglion cell layer whereas the inner limiting membrane comprises a membrane which is a modification of the periphery of the vitreous. All neurons in the retina are partially enveloped in müller cells (Ryan et al, 2001). Müller cells span the entire retina and serve to guide migrating neurons of the retina during development and also to control the extracellular environment of the retinal neurons (Ahmad et al, 2011, see figure 1.1).

Each rod and cone cell contains an abundance of G-Protein Coupled Receptors which act as light sensors, transducing a signal to 2nd messenger proteins after activation by light. In rods the photosensing receptor is Rhodopsin, a 7-transmembrane receptor present in the membranes of intracellular discs within the outer segments of the cells. The outer segments are typically made up of 1000-2000 membrane discs of which rhodopsin accounts for roughly half of the total weight. The intracellular discs are formed by invagination of the cell membrane which then pinches off to form a vesicle (Gomperts et al, 2009).

In cones, a similar cell structure is observed. Like rods, cones contain light sensing proteins called opsins. These lay in invaginations of the cone outer segment. These invaginations do not pinch off as in rods however and as such, there are no intracellular discs containing opsin proteins in cones. There are three types of cone depending on

the opsin held in the cell. L cones contain l-opsin which responds to light in the wavelength range of 555-565nm. M cones contain m-opsin which responds to light in the wavelength range of 530-537nm. Finally S cones contain s-opsin which responds to the wavelength range of 415-430nm. Cones are typically dispersed within the retina with rods. However the largest concentration of cones lies within the macula, particularly within the fovea which is an area of the retina largely responsible for maintaining visual accuity. The fovea contains mainly L and M cones as the lens of the eye tends to absorb the high frequency light received by S cones. Whilst playing little role in visual accuity, S-cones are still required for trichromatic vision (Purves et al, 2008).

Cones are typically less sensitive to light than rods. For example, rods can respond to one photon of light whereas cones require at least 100 photons before activation. Whilst inefficient, the lack of sensitivity is accounted for in the neural circuitry of both the rods and cones connecting them to the nerve fiber layer at the basal region of the retina. A group of rods is typically connected to a bipolar cell. A group of rod bipolar cells is in turn connected to just one rod amacrine cell which then relays the nerve impulse to the ganglion cells which connect to the nerve fibre layer. This means that rods have reduced spatial resolution. Cones, however, connect to just one bipolar cell which in turn connects to just one retinal ganglion cell meaning that each activated cone in a given area of the retina responds to just one neural circuit providing better spatial resolution than rods. Cones are typically concentrated in the fovea of the retina which is located directly opposite the aperture of the iris (the pupil). This allows a person a high level of visual acuity for objects directly in front of him/her whilst regions in the periphery of the visual field are typically blurrier (Mustafi et al 2009).

1.3 Visual Transduction

As mentioned above, the rod specific opsin, rhodopsin, is a 7 trans-membrane G-protein coupled receptor (GPCR). Unlike other systems however, whereby activation of the GPCR is induced by binding of the ligand to the receptor, rhodopsin is bound to its ligand in an inactivated state. The ligand needs to be activated by light to isomerise and activate rhodopsin. This ligand is 11-cis retinal, a long chain aldehyde which is

converted to all-trans retinal when it absorbs a photon. Isomerisation of 11-cis retinal induces the activation of rhodopsin which then activates transducin, a 2nd messenger protein, by exchanging transducin bound GDP for GTP. Transducin then dissociates into an α subunit and a βγ subunit. The α subunit then proceeds to activate cGMP phosphodiesterase which hydolyses cGMP to 5'GMP (Gomperts et al, 2009, see figure 1.2).

Unlike most neurons which depolarise and release neurotransmitter in response to a stimulus, rods are constantly depolarised to a membrane potential of -30mV and therefore constantly release their neurotransmitter glutamate to the cells of the inner nuclear layer. The constant depolarisation of cells is caused by the open state of ligand gated cation channels which maintain an influx of Ca^{2+} and Na^{+} ions into the rods. The channels are held open by cGMP. Activation of cGMP phosphodiesterase and hydolysis of cGMP causes the cation channels to close. Closure of these channels then causes hyperpolarisation of the cell to approximately -60mV which reduces glutamate release from the rods and induces the relay of the light signal through the retinal circuitry (Gomperts et al, 2009).

Rods must quickly recover from any light stimulus to continue to receive and process new stimuli. This quick recovery is achieved through a number of mechanisms. Firstly, photoisomerisation of 11-cis retinal to all-trans retinal causes the covalent bond binding the retinoid to rhodopsin to be broken, dissociating all-trans retinal. At this point the rhodopsin protein is said to be bleached as it cannot respond to further light stimuli. All-trans retinal is reduced to all-trans retinol in the rod cell outer segments. All-trans retinol is then taken up by the cells of the RPE where it is recycled to 11-cis retinal enzymatically. The RPE then supplies the rods with 11-cis retinal which itself maintains rhodopsin in an inactive state to prevent spontaneous activation (Surya et al, 1998). A second way in which rod activation is halted is through the activation of rhodopsin kinase. This enzyme is activated by the βγ subunit of transducin and so is activated immediately after activation of rhodopsin. Rhodopsin kinase then phosphorylates the intracellular C terminal of rhodopsin which is subsequently bound by arrestin. Arrestin prevents further interaction between rhodopsin and inactive transducin. Finally, following the closure of the ligand gated cation channels, Ca^{2+} concentration rapidly decreases. This decrease is detected through Guanylyl Cyclase

Activating Protein (GCAP); a member of the calcium binding EF hand family of proteins which is bound to guanylyl cyclase. When Ca^{2+} levels are low, GCAP proteins become less bound to Ca^{2+} which stimulates activation of guanylyl cyclase. Guanylyl cyclase serves to synthesise cGMP from GTP which then binds to cation channels, in turn opening them and returning the cell to a depolarised state (Kefalov, 2012).

Cones also respond to light in a similar fashion to rods. However, cones do not only receive 11-cis retinal from the RPE, as cones in retinas detached from the RPE regenerate light responses after photoreceptor bleaching whereas rods do not (Wang and Kefalov, 2009). Using a glial cell specific toxin to kill the glial cells of the retina, it was shown that these same cones do not regenerate light responses after bleaching, suggesting that the müller cells of the retina supply the cones with a retinoid which re-actiates the opsins of the cones. Cones regenerated their ability to sense light when supplied with 11-cis retinol, the alcohol precursor to the aldehyde 11-cis retinal. This suggests that cones have a converting enzyme which forms 11-cis retinal from 11-cis retinol. The identity of this enzyme is currently unclear (Wang and Kefalov, 2011). Recently, a homologue of the enzyme present in the RPE which converts all-trans retinal to 11-cis retinal was identified. This enzyme, RPE65C, is present in the müller cells of zebrafish (a cone-rich organism) and performed the same enzymatic function as RPE localised RPE65 (Takahashi et al, 2011). This enables cones to maintain a larger supply of chromophore for opsins than rods and allows cones greater visual accuity overall.

1.4 Retinitis Pigmentosa

Retinitis Pigmentosa (RP) is a group of inherited diseases of the eye which typically manifest as early as childhood depending on the disease causing mutation. RP symptoms become apparent at a median age of 10.7 years in autosomal recessive forms of the disease and 23.4 years in autosomal dominant forms (Ryan et al, 2001). RP initially causes rod photoreceptor cell death followed by cone cell death. This loss of rods before cones is due to the fact that the mutations which cause RP typically either affect rod specific proteins (section 1.6) or affect the recycling of all-trans retinal to 11-cis retinal which can be offset in cones due to their independent means of attaining 11-

cis retinal (section 1.3). The death of rods also shifts much of the oxidative stress associated with highly metabolic rods on to cones (Yu et al, 2000) and also results in a lack of Rod derived Cone Viability Factor (RdCVF) which is required by cones for survival (Cronin et al, 2010). This dystrophy of the outer nuclear layer is followed by progressive cell death in all layers of the retina.

1.5 Clinical Symptoms and Assessment

As mentioned in section 1.4, RP begins as a loss of rods followed by a loss of cones. This period of cell death thus presents itself as nyctalopia (night blindness) caused by the loss of rods which are highly sensitive to small amounts of light and are therefore important for vision in low light (scotopic vision). This is followed by 'tunnel vision' as rods in the rod-rich periphery of the visual field die. Peripheral vision loss proceeds slowly towards the central field of vision. Some areas of the visual field remain intact as the visual field contracts from the periphery. These areas recede with time until complete loss of vision occurs, concurrent with the death of remaining photoreceptor cells.

Other features of RP include early colour vision defects, photopsia (flashes of perceived light caused by defective photoreceptors), cataracts and abnormal vitreous caused by the degeneration of the RPE. Examinations of the fundus of RP patients typically show attenuation of the blood vessels of the choriocapilliaris (the region of the choroid which is closest to the retina), mottling of the RPE and bone spicule deposits (see figure 1.3). Bone spicule deposition is caused by leakage of pigment from the degenerating RPE into the interstitial spaces of the retina (Hartong et al, 2006).

The resulting loss of sight as an outcome of retinal degradation is assessed by a number of methods. Perimetry involves focusing the patient's sight on a fixed object or shape and presenting other objects at specified points in the visual field of the patient. This allows the patient's visual field to be assessed at various spatial regions of the retina. A dark adaptation test is used to determine the sensitivity of both rods and cones to specified intensities of light after the patient has been dark adapted for a certain amount of time. Patients with RP tend to show a much slower response to the light than

unaffected individuals. Finally, a third test of degenerating vision is obtained through electrophysiology, most commonly electroretinography (ERG). ERG involves recording the electrical response from the retina (using an electrode placed on the cornea of the patient) to a light stimulus. The resulting potential changes are graphed and the peak responses recorded (see figure 1.4). The a-wave corresponds to the hyperpolarisation of the photoreceptors whereas the b-wave corresponds to the responses of the cells of the inner nuclear layer (amacrine cells, horizontal cells and bipolar cells). Patients with RP typically show a smaller ERG response than unaffected individuals. The responses of the rods and cones can also be differentiated by performing the ERG under scotopic (dark adapted conditions) or photopic (well lit conditions) to measure rod response and cone response respectively (Ferrari et al, 2011; Milam et al, 1998).

1.6 Genetic Basis of RP

Much of our understanding of the molecular mechanisms of RP pathology come from genetic analyses of families in which RP is inherited. RP is typically inherited in a monogenic fashion, whereby the disease is caused by mutation at a single locus. However one form of digenic RP has been reported in which two mutated loci are required to establish the disease phenotype (Kajiwara et al, 1994). Approximately 50% of cases are sporadic and many cases can be syndromic, whereby the clinical manifestations of RP present along with other pathologies. One such case is Usher Syndrome in which photoreceptor degeneration occurs along with sensorineural deafness (Farrar et al, 2002). RP can be inherited in an autosomal dominant, autosomal recessive or X-linked fashion, reflecting the heterogenous nature of the underlying genetics of this disease. The number of disease loci associated with RP is frequently updated (https://sph.uth.edu/Retnet/sum-dis.htm#A-genes) and currently stands at over 65 associated genes (Anasagasti, 2012). The variance of RP means that targeted therapies will be required which tackle the most common subtypes of the disease. The genes which are most commonly associated with RP are Retinitis Pigmentosa GTPase Regulator (*RPGR*, 10-20% of all cases), Rhodopsin (*RHO*, 8-10% of all cases) and usherin (*USH2A*, ~3% of all cases) (Wright et al, 2010). Most other variants are quite rare with a minor allele frequency (MAF) of less than 0.01. Due to the number of

variants however, RP has a global prevalence of approximately 1 in 3500 to 5000 (Anasagasti et al, 2012).

1.7 Oxidative Stress

Oxidative stress is a state of intracellular distress caused by an imbalance between the creation of Reactive Oxygen Species (ROS) and their destruction, causing apoptosis. ROS include superoxide (O_2^-) and oxygen free radicals ($O_2^{\cdot-}$) amongst others. These species come from a variety of sources, the most prominent of which are the mitochondrion, the NADPH Oxidase complex (see section 1.9) and xanthine oxidase. Mitochondria are the greatest contributors of oxidative stress to a cell (Rafaello et al, 2011). This ocurs through a process termed 'mitochondrial leakage' whereby electrons from the normal process of oxidative phosphorylation react with oxygen to create oxygen free radicals (Chen et al, 2003). Xanthine Oxidase is an enzyme which converts xanthine and hypoxanthine into superoxide and uric acid (Murata et al, 2012). This reaction is part of the normal metabolism of purine nucleotides (Harzand et al, 2012). ROS can also react with nitric oxide (NO) to form peroxynitrite ($ONOO^-$), a Reactive Nitrogen Species (RNS) which is particularly reactive against biomolecules. NO is a signalling molecule which is formed by the three isoforms of Nitric Oxide Synthetase (NOS, Emerit et al, 2004).

ROS are normally cleared from within the cell through the action of a number of detoxification enzymes including catalase, glutathione reductase, glutathione peroxidase and Superoxide Dismutase (SOD) of which there are two forms; SOD1 which is located in the cytoplasm and the mitochondrial inner membrane and SOD2 which is located in the mitochondrial matrix (Raffaelo et al, 2011). The SOD enzymes convert superoxide to H_2O_2 which is then converted to H_2O by catalase and glutathione peroxidase (Fukai et al, 2011). However, in many cases the levels of ROS may rise to overwhelm the action of these enzymes or to inactivate them through protein modifications leading to even higher levels of ROS. In these cases, ROS will act pathologically against cells and tissues and have been implicated in many diseases.

ROS generally act through modification of biomolecules such as DNA, proteins and lipids to cause cellular damage. ROS will react with DNA to form DNA lesions, the most studied of which is the formation of 8-Hydroxyguanine (8-OH-dG). This modified guanine nucleotide forms when guanine is attacked by a hydroxyl free radical which itself is formed from free radical chain reactions of superoxide radical with water. Peroxynitrite can also react with DNA to form nitroguanine. These modifications will tend to create G to T transversions (Valko et al, 2006). ROS will also react with poly-unsaturated fatty acids (PUFAs) in a reaction termed 'lipid peroxidation'. The reaction of ROS with PUFAs begins a free radical mediated chain reaction between adjacent lipids, thus causing far more extensive damage than the initial chemical insult, resulting in the formation of hydroxynonenal (HNE) which has been shown to induce apoptosis (Wu et al, 2012). Lipid peroxidation can also form malondialdehyde which can cause DNA mutations (Valko et al, 2006). ROS will cause changes to the structure of proteins by oxidising indvidual amino acid residues and by oxidising cysteine residues causing formation of disulfide bridges. Peroxynitrite also causes protein changes through nitration of tyrosine residues (Valko et al, 2006). The vast variety of biological effects exerted by ROS and RNS means that these mechanisms of pathology have been implicated in cancer (Valko et al, 2007), neurological disorders (Emerit et al, 2004), cardiovascular disease (Chen et al, 2012), diabetes mellitus (Styskal et al, 2012), ageing (Muller et al, 2007) and ischaemia/reperfusion injury (Jaeschke et al, 2012).

1.8 Oxidative Stress in RP

Since photoreceptors are one of the highest oxygen consuming tissues in the body (Usui et al, 2009) alterations to the redox environment of the retina could have devastating consequences. The most studied example of oxidative stress contributing to pathology is Age-Related Macular Degeneration (AMD) in which oxidative stress has been clearly linked to disease progression (Cao et al, 2013; Zafrilla et al, 2013; Ugurlu et al, 2013). Oxidative stress has also been linked to diabetic retinopathy (Williams et al, 2013) and retinopathy of prematurity (Wang et al, 2013). It has already been demonstrated that inherited retinal degenerations cause an increase in oxidative species in the retina (Yu et al, 2004; Padnick-Silver et al, 2006). As rods die, they transfer the

oxygen rich environment of their cells to neighbouring cones (Shen et al, 2005). Rods also supply the cones with rod-derived cone viability factor (RdCVF) which contributes to cone viability and functionality. After rods die, supply of RdCVF to the cones decreases, contributing to cone cell death. RdCVF belongs to the family of thioredoxin-like proteins which are important for maintaining a reducing environment in the cell (Cronin et al, 2010). Mice which have no RdCVF show an increase of oxidative stress in the cones and subsequent death of these cells (Cronin et al, 2010). RdCVF has also been shown to protect cone cell lines *in vitro* from oxidative stress through over-expression of this gene (Wang et al, 2008). Another factor which suggests a role of oxidative stress in retinal degeneration is the up-regulation of p66Shc in NARP (Neuropathy, Ataxia, Retinitis Pigmentosa) patients which causes a direct increase in ROS through interaction with the mitochondrion (Lebiedzinska et al, 2012). Taken together, these results suggest that oxidative stress may be a key driver of secondary cell death in cones. Further evidence supporting this idea comes from the observations that a reduction in oxidative stress through antioxidants or reducing enzymes increases the longevity of cones in models of retinal degenerations (Lee et al, 2011; Lu et al, 2009). Finally, it has been demonstrated that increased expression of the anti-oxidant enzymes catalase and SOD2 in the *rd10* mouse model reduces cone cell death (Usui et al, 2009b). Less apparent is the role that oxidative stress plays in the death of rod cells. It is known that rods do experience photo-oxidative stress and that this stress is attributable to activation of Rac1 (Balasubramanian & Slepak 2003), the activating protein of the NADPH oxidase complex. Furthermore, a conditional *Rac1* knock out mouse model crossed with a mouse model of RP has been demonstrated to exhibit increased rod viability and visual function (Haruta et al, 2009). Of the various rhodopsin mutations, those belonging to the class II set of mutations have been demonstrated to contribute to oxidative stress which may cause apoptosis of these cells. Class II mutations in rhodopsin cause protein misfolding and subsequent retention of the rhodopsin protein in the endoplasmic reticulum (ER, Saliba et al, 2002). This class of rhodopsin mutations include the Pro23His amino acid substitution, the most prevalent form of rhodopsin mutation RP carried by approximately 10% of individuals with autosomal dominant RP in the US (Sohocki et al, 2001). Studies of Pro23His mutant rhodopsin have shown that retention of this protein causes ER stress (Tam & Moritz, 2006) which initiates the Unfolded Protein Response (UPR) Pathway. The UPR pathway in turn causes an increase in oxidative stress which causes apoptosis

(Malhorta et al, 2008). ER stress has also been shown to play a role in the pathogenesis of the T17M and S334ter mutated rhodopsin models of RP (Kunte et al, 2012, Shinde et al, 2012). Recently, evidence has emerged demonstrating that oxidative stress in a mouse and rat model of RP causes single strand breaks (SSBs) in nuclear DNA and that this activates PARP (Poly ADP Ribose Polymerase) which induces apoptosis. The authors also provided evidence for oxidative stress induced damage of DNA in patients of RP (Murakami et al, 2012). These data suggest that a potential route of therapy for RP may be the reduction of oxidative stress in photoreceptor

1.9 Gene Therapy

Gene therapy has emerged as a powerful tool for treating many inherited disorders such as cardiovascular disease, liver diseases and neurological diseases as well as HIV and cancer (Niewohner & Tannert, 2006). The definition of gene therapy as outlined by the Human Genome Project is 'a technique for correcting defective genes responsible for disease development' (http://www.ornl.gov/sci/techresources/Human_Genome/medicine/genetherapy.shtml). This correction is generally achieved through the suppression of disease causing genes, the addition of wild type versions of faulty genes or through the repair of mutated DNA which causes disease.

The use of gene therapy had been proposed in 1947, several years before the structure of DNA had been elucidated, by Clyde Keeler who predicted that gene therapy could be used to correct hereditary diseases through an unspecified process of 'gene cancellation' (Keeler, 1947). The idea of gene therapy as a viable course of medical genetic correction was illustrated in 1990 when the T cells of a patient suffering from adenosine deaminase severe combined immunodeficiency were treated with a gene therapy to supply a wild type version of the recessive mutated allele causing the gene. This resulted in a long term reconstitution of the immune system (Blaese et al, 1995). The field of gene therapy was delivered a serious setback in 1999, however, when a patient died of a large immune response to an adenovirus carrying a gene therapy for ornithine transcarbamylase deficiency (Phillips MI, 2012). The issues with immune responses against viral delivery agents continue to be an area of intense research as

more viral delivery agents and safer delivery methods are formulated (see section 1.14).

Many novel uses of gene therapy have been developed to combat various acquired and inherited diseases which do not rely on just suppression of mutant alleles or supply of wild type genes. Therapies targeting cancerous cells can target a set of related microRNAs with similar sequences that are highly expressed in these cancer cells (Brown & Naldini, 2009). This approach has been used to successfully up-regulate expression of E2F, a tumour suppressor, in leukaemic cells *in vitro* (Scherr et al, 2007). A novel approach to treating cancer involves the use of 'suicide gene therapy' whereby a non human enzyme is delivered to cancer cells which, when expressed, will metabolise a pro-drug in to an apoptosis inducing drug. The suicide gene therapy treatment has been used to treat many cancer models including leukaemia, glioma, bladder cancer, liver cancer, colon cancer and oral cancer (Duarte et al, 2012). A phase 1 clinical trial of this system using a viral thymidine kinase gene therapy and ganciclovir has demonstrated therapeutic benefit in patients suffering from glioblastoma multiforme (Duarte et al, 2012). Gene therapies against HIV have focused on targeting more than one gene in the HIV genome as this virus is highly proliferative and exhibits a greater mutation rate than mammalian cells. One gene therapy, in the form of a DNA vector, was transfected into haematopoietic progenitor cells which were then transfused into patients. This resulted in successful post-transfusion expression of the DNA based therapies with no related toxicity for up to 2 years (DiGiusto et al, 2010). This was a phase 1 trial however and the patients suffered from non-Hodgkin lymphoma (which is regularly treated with transfusion of haematopoietic progenitor cells) and had no HIV present in their blood. Currently there are a number of clinical trials under way for diseases such as renal failure, hypercholesterolaemia, hepatitis C and HIV (Davidson & McCray Jr, 2011). A number of gene therapies are also in clinical trials for eye diseases including Leber Congenital Amaurosis, Pachyonia congenita, non-artereric anterior ischaemic optic neuropathy, AMD, choroidal neovascularisation, macular degeneration, diabetic macular oedema and glaucoma (Davidson & McCray, 2011).

1.10 Replacement Strategies and LCA Clinical Trials

As mentioned in section 1.9, traditional gene therapy approaches involve either the suppression of the disease causing mutant allele (in dominant disorders), replacement of a wildtype version of the mutant allele (in recessive disorders) or a combination of both (see section 1.12). This section deals with the use of replacement strategies in gene therapy. It would be impossible to mention all the global research currently under way in this field and therefore I will mention replacement gene therapies which have reached human clinical trials for a wide range of inherited disorders (clinicaltrials.gov).

A phase II clinical trial is currently under way for Alpha-1 Antitypsin (AAT) Deficiency which is a disease caused by loss of protease inhibition in both the lungs and the liver (clinical trial NCT01054339). The therapy is an Adeno-Associated Virus (AAV, see section 1.14) carrying the wildtype AAT gene. This therapy has been injected intramuscularly in to nine patients with the hope of establishing a dose response curve, finding any possible adverse effects and measuring any changes in serum levels of AAT. A clinical trial for Duchenne Muscular Dystrophy is also currently underway. This disease can be caused by a mutation causing a premature stop codon formation in the large *Dystrophin* gene (clinical trial NCT00428935). The current phase I clinical trial involves injection of AAV containing a smaller version of the human dystrophin gene called *minidystrophin*. This will also be injected intramuscularly with the hope that the injected muscle tissue will show a loss of or slower degradation of muscle. This is just one of 104 clinical trials currently listed for DMD on the clinicaltrials.gov website.

The results of a clinical trial using gene therapy for X-linked haemophilia were reported in late 2011 (Nathwani et al, 2011). This trial tested the efficacy and safety of an AAV encoding coagulation factor IX (FIX), a gene which is mutated and has no activity in patients of this disease. The virus was injected in three cohorts of patients containing two men each and corresponding to low, intermediate and high doses of virus. All patients injected exhibited a small increase in levels of FIX activity for up to 16 months after administration which correlated with improved blood clotting in response to injury. Patients in the high dose group showed the highest increase in FIX activity but also displayed some increase in T cells carrying antibodies against the

serotype of the AAV. However these levels soon dropped to baseline serum levels after injection and caused no adverse effects. None of the patient cohorts received immunosuppressive therapies with the administration of the AAV therapeutic. Furthermore, a separate clinical trial has found evidence of transgene expresseion of factor IX ten years after AAV administration (Buchlis et al, 2012). While transgene expression remained too low to initially provide therapeutic benefit, it provides evidence of the longevity of a gene therapy in humans (Kay et al, 2000).

A number of clinical trials have taken place with patients suffering from Parkinson's disease. This disease is caused by loss of dopaminergic neurons in the substantia nigra of the brain. Loss of these neurons can lead to uncontrollable motor movements (dyskinesia). Clinical trials have thus far focused on the delivery of genes involved in the synthesis of dopamine, the delivery of genes involved in the synthesis of inhibitory neurotransmitter γ-Aminobutyric Acid (GABA) or the delivery of neurotrophic genes (Witt & Marks Jr, 2011). Whilst one of these trials is ongoing (clinical trial NCT01621581), the rest have shown some improvement to the lives of patients and have demonstrated the safety of the gene therapy itself. However, in some cases there has been an increase of dyskinesia as opposed to a decrease (Witt & Marks Jr, 2011).

The first clinical trials of a replacement gene therapy for retinal degeneration were for a condition named Leber Congenital Amaurosis (LCA). This is a form of early onset blindness which can be caused by mutation of the *RPE65* gene. Much work had been undertaken using AAV to deliver this gene to the naturally occurring LCA model of this disease, the Briard mixed dog (Ackland et al, 2001, Jacobson et al, 2006) as well as to mouse models of this disorder (Batten et al, 2005; Pang et al, 2006). Three separate human clinical trials have subsequently begun in both the UK and America. In addition, there are currently eight on-going clinical trials underway using AAV delivered *RPE65* to treat patients of LCA (clinicaltrials.gov). Bainbridge et al reported safety of this therapy in all three patients who received an injection but efficacy in only one of these patients (Bainbridge et al, 2008). A clinical trials for a similar therapy against LCA has also been carried out which demonstrated an increase in visual function in all three patients injected with the therapy (Maguire et al, 2008). The third human trial of an *RPE65* therapy reported a safe administration along with a varying increase in light sensitivity (Hauswirth et al, 2008). As well as demonstrating an

improvement of visual function, these studies provided a strong emphasis on the safety of the therapeutic and demonstrated no adverse effects or immune responses as a result of the viral injection. One patient demonstrated a macular tear but this was not noted by the patient, whose visual field improved overall after application of the therapy. Follow on studies of these patients have been completed and are discussed in detail in section 4.4.

1.11 RNA interference

RNA interference has emerged in the past 20 years as a powerful tool in functional studies of genes and phenotype and as a method to develop therapeutics against faulty genes. This phenomenon was first discovered in 1990 by Napoli and Jorgensen (Napoli et al, 1990) who noticed that the introduction of an exogenous chalcone synthase gene into petunia flowers decreased the levels of chalcone synthase rather than increasing them. This work was carried further by Romano and Macino in *Neurospora crassa* (Romano & Macino, 1992) and in *Caenorhabditis elegans* by Fire et al (Fire et al, 1991) who also noticed that introduction of antisense RNA into these organisms caused a similar effect on the genes containing sequence homology to the RNA in these organisms. In 1998, subsequent Nobel Prize winners Fire and Mello demonstrated that the introduction of dsRNA into *C. elegans* caused far greater suppression than either sense or anti-sense RNA did alone (Fire et al, 1998). Further work by others later elucidated this suppression pathway biochemically and determined that double stranded RNAs (dsRNAs) of 21-23nt in length were optimal for RNAi (Sen & Blau, 2006).

The introduction of these exogenous nucleic acids inadvertently invoked the utilisation of the RNAi pathway, an intracellular RNA degradation pathway used to resist infection and to regulate gene expression. In mammals, the main role of RNAi is thus far identified as a means of regulation of gene expression through the use of microRNAs (miRNAs). These are transcribed from genomic DNA as primary miRNAs (pri-miRNAs) and form a hairpin loop containing a 5' methyl cap and a 3' poly-A tail (Davidson & McCray Jr, 2011). pri-miRNAs are then processed by the microprocessor complex which is comprised of Drosha and DGCR8 (DiGeorge syndrome critical region 8) which removes the 5' and 3' regions of the pri-miRNA to form the ~70nt

precursor mRNA (pre-miRNA; Yeom et al, 2006). The pre-miRNA is then exported from the nucleus by the Exportin-5 gated nuclear pore where it is processed further by the Dicer complex. This process involves removal of the hairpin region of the pre-miRNA to form two strands of the mature 21nt miRNA. The mature miRNA is then loaded into the RNAse Argonaute (Ago) protein which forms part of the RNA Induced Silencing Complex (RISC; Rand et al, 2005). Ago will use only one strand of the miRNA (referred to as the guide strand) while the other strand (referred to as the passenger strand) is cleaved and discarded. This activated RISC complex then seeks out mRNAs with complementarity to the guide strand of the miRNA. Once found, the target mRNA is cleaved by Ago, therefore silencing expression of the target gene immediately before the translation step (Davidson & McCray Jr, 2011; Couto & High, 2010).

1.12 RNAi and its uses in Gene Therapy

The use of RNAi as a therapeutic began to be considered after it was first demonstrated that small interfering RNA (siRNA) molecules could be used to down-regulate gene expression in mammalian cells *in vitro* (Elbashir et al, 2001). This was followed by effective suppression of gene expression in the mouse liver and brain, illustrating that RNAi could be employed *in vivo* (Xia et al, 2002). Since then, many expression vectors and means of delivery have been formulated to deliver RNAi molecules to cells *in vitro* and *in vivo* (Boudreau et al, 2011). In 2010, siRNAs bound to nanoparticles which targeted solid tumours through protein ligands on the surface of the nanoparticles were successfully used to downregulate gene expression of *RPM2* (a target oncogene) in humans (Davis et al, 2010). RNAi has also been used in clinical trials to treat patients of AMD using a siRNA based therapy, resulting in improved visual acuity in some patients (Kaiser et al, 2010). A search of clinical trials which are currently using RNAi as a therapeutic revealed ten studies examining the effects of targeted RNAi molecules for diseases such as breast cancer (NCT00689065), Glaucoma (NCT01739244) and Hepatitis C (NCT01899092). These data demonstrate the viability of RNAi as an effective tool to modulate disease genes in humans.

The use of RNAi still holds many caveats for those who wish to use this tool as a therapy. Firstly, the therapy must be delivered in such a way as to ensure that the antisense strand is the strand which is incorporated in to the RISC. This so called 'guide strand' is selected by the RISC based on a thermodynamic bias (Birmingham et al, 2007). Greater thermodynamic instability of the siRNA duplex at the 5' end of the guide strand promotes stronger incorporation into the RISC and higher silencing efficiency. Chemical modification of the passenger strand can also block incorporation of this strand in to the RISC. RNAi efficacy may also be reduced if targeted to an area containing undocumented SNPs. The use of artificial RNAi relies on the endogenous miRNA pathway in which microRNAs recognise seed regions (of 2-7nt of the target sequence) to target a large array of mRNAs. Therefore, artificial RNAs may also have off target effects by targeting more than one transcript. However, chemical modifications to both strands of the RNAi molecule have been shown to reduce these off target effects by 90%, thus increasing the specificity and safety of RNAi molecules (Birmingham et al, 2007). Chemical modifications are only possible when delivering the RNAi molecules directly rather than delivery of vectors which express RNAi molecules (eg short hairpin RNA (shRNA) or microRNA (miRNA) cassettes) as post-transcriptional modification would be impossible after the delivery of the therapeutic. The dose of RNAi molecules delivered to the tissue of interest must also be taken in to account. Typically, shRNA expressing cassettes have been shown to have high expression compared to miRNA expressing cassettes (Chang et al, 2006). This results in a high level of toxicity both *in vitro* and *in vivo* compared to miRNA cassettes which may be expressed from a range of promoters resulting in efficient RNAi silencing with lower transcript levels of the RNAi molecule (Boudreau et al, 2009; McBride et al, 2008). miRNAs also seem to be better tolerated to cells as they more closely mimic the endogenous RNAi molecules (Boudreau et al, 2009). Saturation of the RNAi pathway has been shown to be responsible for shRNA toxicity (Grimm et al, 2010). The authors of this paper demonstrated that the argonaute proteins are the rate limiting step of the RNAi pathway and that saturation of these proteins as well as exportin-5 causes shRNA toxicity. This can be alleviated by co-expressing exportin-5, the argonaute genes and the shRNA and by using a relatively weak shRNA promoter (using the H1 promoter versus the U6 promoter). Together, these approaches resulted in greater RNA suppression of the target sequence for a longer period of time. As with any relatively

new technology, a great number of methods have been and continue to be employed to further optimise efficacy and reduce toxicity.

Despite the practical hurdles which this technology presents, RNAi has been demonstrated to possess a wide range of potential clinical applications. These continue to be refined to increase safety and efficiency. Some of the most promising results have come from studies of diseases of the central nervous system in which a gain of function dominant mutant protein causes neurotoxicity. One of the earlier examples of the use of RNAi in the pre-clinical treatment of a neurodegenerative disorder was the treatment of the transgenic SCA1 mouse model of Spinal Cerebellar Ataxia with a shRNA (Xia et al, 2004). This disorder induces severe ataxia (loss of muscle control) and dementia caused by a progressive loss of a specific set of neurons of the cerebellum (OMIM entry 164400). Treatment of a mutant version of the ataxin-1 disease causing allele with a targeted shRNA resulted in a significant improvement in rotarod response of these mice. The rotarod response is a method of evaluating motor response in mice and consists of a rotating cylinder upon which the experimental mouse is placed, first reported in 1968 (Jones & Roberts, 1968). The number of falls from the moving cylinder is then used as a measure of motor co-ordination. Studies of Huntinton's disease animal models have demonstrated that shRNAs directed against mutant Huntingtin protein (the protein causing disease pathology) injected in to the striatum of the brain of these animals improved behavioural responses in these mice, as measured by stride length and rotarod response of the injected mutant animals (Harper et al, 2005). A similar approach to treating a rodent model of Huntington's disease using cyclodextrin based carriers of Huntingtin targeted siRNA has also demonstrated an increase in rotarod response of these animals, however the beneficial effects of this therapeutic ceased shortly after the end of the administration regime (Godinho et al, 2013). This finding suggests that continued RNAi-mediated suppression of the mutant allele is crucial to maintain the beneficial effects gained from clearing the mutant allele which causes neurotoxicity. RNAi has also been demonstrated to have a beneficial effect in an animal model of the neurodegenerative disease Amyotrophic Lateral Scelrosis (ALS). A shRNA directed against the disease causing mutant *SOD1* gene in transgenic animals expressing this allele resulted in improved motor responses as measured by stride length and rotarod response. Injected animals also demonstrated a two-fold increase in lifespan, comparable to wild type animals. These results were

further reinforced by histology showing preservation of motor neurons in injected mice (Ralph et al, 2005). The publications outlined in this section reflect only a limited number of studies examining the use of RNAi in a pre-clinical setting to treat animal models of a range of disorders.

1.13 Gene Therapy for RP

One focus of the TCD Ocular Genetics laboratory has been to explore the development of treatments for Retinitis Pigmentosa using gene therapy, in particular by targeting treatments towards forms of RP caused by the mutant rhodopsin gene. Mutations in this gene cause the disease phenotype in approximately 30% of all autosomal dominant RP (adRP) patients (Hartong et al, 2006) making rhodopsin mutations the most common cause of adRP. There are over 150 mutations in rhodopsin which cause adRP (RetNet, http://www.sph.uth.tmc.edu/retnet/home.htm) which makes a mutation dependent approach both technically and economically difficult. Therefore a suppression and replacement strategy for therapy has been proposed (Millington-Ward et al, 1997). This approach involves suppressing the endogenous mutant rhodopsin of patients suffering from RP and replacing the suppressed rhodopsin with wild type rhodopsin under the control of the Rho promoter. The replacement rhodopsin is modified at degenerate bases of the codons in the region which is targeted by the RNAi based suppressor, making the replacement rhodopsin resistant to sequence specific RNA silencing while retaining the correct protein coding sequence. The suppression and replacement approach has been demonstrated to protect photoreceptors from cell death and prolong functionality and vision in murine models of RP (Millington-Ward et al, 2011; Chadderton et al, 2009; O'Reilly et al, 2008; O'Reilly et al, 2007).

This approach, however, is limited in its scope as it is applicable to only a small proportion of the total number of patients suffering from RP due to its gene-centric solution to treating retinal degeneration. A number of wider reaching therapies have been proposed to provide benefit or delay the degenerative effects of RP (Cepko, 2012). The first possible solution is the delivery of growth factors to the eye. As mentioned in section 1.8, as rods die, the supply of RdCVF to the cones decreases, resulting in a marked increase of cone cell death (Cronin et al, 2010). Purified RdCVF protein has been injected in to a rat model of RP and demonstrated to delay

photoreceptor cell death (Yang et al, 2009). Delivery of protein to the eye can create physiological problems after repeat injections, therefore an approach utilising *RdCVF* within an AAV expression vector is under way to treat RP in animal models (Cepko, 2012). Other growth factors are currently being tested as treatments for RP, including one clinical trial using Ciliary Neurotrophic Factor (CNTF, Sieving et al, 2006). A second approach to providing a therapy for a large number of RP patients involves the use of gene therapies which tackle the oxidative stress load of retinal cells. The reasons for this approach have already been outlined in section 1.8. It has been observed that increased expression of *glutathione peroxidase* (Lu, 2009), *catalase* and *SOD2* (Usui et al, 2009b) via AAV delivery (see section 1.14) has resulted in decreased photoreceptor cell death in models of RP. Direct injection of genes encoding anti-oxidant proteins also offers benefit as expression of the anti-oxidants remains localised in the retina and therefore does not pose the risks towards normal cellular functions which ROS carry out that may arise with a systemic administration of such antioxidants. Furthermore, the retina is protected from large molecules in the general circulation due to the blood-retina barrier which exists between endothelial cells of the choroid (Hosoya & Tachikawa, 2012). A third approach to treating RP with gene therapy is the relatively new idea of optogenetics. This involves the introduction of non-human light sensing molecules to the cells of the retina which directly cause hyperpolarisation of these cells in response to light (reviewed in Garg & Federman, 2013). This approach is promising as it bypasses the use of a complex signal transduction cascade which normally occurs in the retina. Therefore the number of patients which may receive the treatment is greatly increased as mutations of a range of genes in the visual transduction cascade should, in priniciple, become irrelevant after introduction of an optogenetic gene. These genes include *halorhodopsin* (from the archaebacterium *Natronomonas pharaonis*) and *channelrhodopsin2* (from the bacterium *Chlamydomonas rheinhardtii*). These genes have been introduced via AAV delivery to the photoreceptors (*halorhodopsin*, Busskamp et al, 2010) and to the bipolar cells (*channelrhodopsin2*, Doroudchi et al, 2011) in mouse models of RP. The introduction of these genes has been shown to increase light sensitivity with no immune response related toxicity after one year (Busskamp et al, 2010). Clinical assessement of patients of LCA and RP has determined that these patients would be best suited to introduction of an optogenetic therapy to the ganglion cell layer and would likely respond well to such a therapy,

further taking the idea of optogenetic therapies from animal models to a clinical setting (Jacobson et al, 2013).

1.14 Delivery Methods

The eye possesses a unique structure in the human body as an organ which is relatively easily accessible to introduction of various drugs. This organ also contains a relatively small and thin target tissue (the retina) which allows small volumes of therapeutic to be delivered with relatively greater efficiency compared to other organs or tissue types. Lastly, the eye is immunocompromised as it is separated from the blood by the blood-retina barrier, a layer of endothelial cells which contain tight junctions to prevent the passage in and out of large molecules. This excludes antibodies and cells of the immune system from entering the same space as the retina, therefore reducing the risk of an adverse immune reaction to a foreign delivery agent (for example, a virus). Given these advantages, the area of therapeutic delivery to the eye remains a subject of keen interest for many researchers as newer and more efficient therapies are developed. This section will deal with methods of delivery of gene therapies to the retina with a focus on viral delivery.

Although there are a number of viral delivery options available (such as adenovirus, lentivirus and herpes simplex virus, Davidson & McCray Jr, 2011), for delivery of DNA and RNA based therapeutics to the retina, the viral delivery agent of choice for many researchers is the Adeno Associated Virus (AAV). This virus was first discovered as a contaminant of adenovirus preparations as AAV requires a helper adenovirus to successfully thrive (Hoggan et al, 1996). These small viral particles were shown to replicate in cell cultures when co-infected with various 'helper' viruses which could replicate without the help of another virus. Subsequent work on AAV revealed that this virus was of the genus *dependovirus* and the family *paroviridae*. AAV is a non-pathogenic icosahedral ssDNA virus containing a genome of approximately 4.7kb in length. The genome itself contains two Inverted Terminal Repeats (ITRs), between which lay the *rep* and *cap* sets of genes. The *rep* and *cap* sets contain the *rep40*, *rep52*, *rep68* and *rep78* genes and the *VP1*, *VP2* and *VP3* genes which are responsible for

DNA replication and capsid formation respectively (Nonnemacher & Weber, 2012). These sets are replaced with a transgene of interest in gene therapy studies.

Subsequent to binding of the AAV to the cell surface, the virus is taken up in to the cells by invagination of the cell membrane. The virus is then loaded in to the golgi apparatus of the cell before retrograde transport occurs through this apparatus and in to the cytoplasm of the cell. It is believed that the acidic nature of the endosomal sac in which the virus is transported to the golgi apparatus changes the capsid conformation of the virus, exposing the VP1 and VP2 regions of the capsid to the exterior of the capsid. The VP1 region contains a phospholipase region which facilitates escape of the AAV from the golgi apparatus in to the cytoplasm. The VP1 region also contains three basic clusters (BC1-3) which allow the virus to travel in to the nucleus through a nuclear pore. The virus then uncoats to release the viral genome (Nonnemacher & Weber, 2012). Recently it has been shown that mutation of conserved tyrosine residues of the AAV capsid can greatly increase the efficacy of AAV transduction of the retina (Petrs-Silva et al, 2011). Mutation of these conserved tyrosine residues eliminates the possibility of intracellular phosphorylation of these residues. Phosphorylation of conserved tyrosine residues (Y444, Y500 and Y730) is believed to mark viral capsids for unbiquination and subsequent proteolysis (Petrs-Silva et al, 2011).

The tropism of AAV can be engineered to transduce different cell types of interest by changing the capsid and hence serotype of the virus. Currently, there are 12 different serotypes which have been evaluated *in vivo* (Watanabe et al, 2013) using the AAV2 genome. These viruses are therefore referred to as AAV2/1-12. A comparative analysis of seven different serotypes of AAV by Watanabe et al recently concluded that AAV 2/5 had the highest overall transduction efficiency of the neonatal mouse retina after subretinal injection. This serotype is the virus of choice for *in vivo* experiments carried out in the TCD Ocular Genetics laboratory. However, the same study also showed that much of this transduction was limited to the RPE and ONL layers of the retina. In contrast, the other serotypes tested exhibited greater transduction to other layers of the retina with AAV 2/8 and AAV 2/2 being the most efficient for transduction of the GCL whereas AAV 2/1 showed the best transduction of the retinal müller cells. In the adult mouse retina however, higher efficiency of transduction of the ONL and RPE has been observed using AAV2/8 (Natkunarajah et al, 2008).Therefore for *in vivo* experiments

in which the gene therapy is delivered at P0, AAV 2/5 is ideal for experiments which deal with gene defects which are pathological to rods, cones and cells of the RPE but AAV 2/8 may be more clinically relevant due to its higher pharmokinetic profile and range of retinals cell which it transduces. In larger animal models, introduction of AAV to the retina has mostly been limited to subretinal injection as opposed to intravitreal injection due to the low transduction efficacy of photoreceptors that this injection produces in rodents (Liang et al, 2001; Dudus et al, 1999). Experiments in large animal models have tended to mirror the transduction efficiencies and retinal tropism shown in mouse models. For instance, the AAV 2/5 virus has been shown to have greater efficacy than AAV 2/2 in canines (Weber et al, 2003). Caution must be exercised when basing human therapies on successful treatment in rodents as the transduction patterns may vary when introduced in to large animal models as humans and non-human primates possess a macula which is absent in mice (Asokan et al, 2012; Huber et al, 2010). Furthermore, the AAV 8 serotype has been characterised in Beagle dogs (Stieger et al, 2008). This study showed that this serotype has a much larger tropism range than AAV 5, resulting in transduction of cells of the RPE, ONL, INL and GCL. Transgene expression was also noted in neurons of the brain along the visual pathway including the optic nerve, optic chiasm, suprachiasmatic nucleus, lateral geniculate nucleus and superior colliculus suggesting transport of the virus across neural synapses.

An exciting area of AAV research is the directed evolution of AAV capsids. This process involves randomly mutating a library of AAV genomes and using these genomes to create a library of viruses which are then intravitreally injected. Subsequent to injection, the retinal layer of interest is excised and the DNA extracted to examine which viruses have transduced this layer. Successful AAVs are then subject to further mutation and the process repeated to induce directed evolution towards transduction of a tissue of interest. This approach to creating new AAV serotypes has recently been demonstrated to create an AAV (termed 7m8) which transduces all layers of the murine and non-human primate retina (Dalkara et al, 2013).

The second most popular choice of viral delivery to cells *in vivo* is the lentivirus delivery agent. These viruses are also considered to be non-pathogenic. Lentiviruses will integrate in to the host genome at regions of euchromatin and stably express

transgene from a chromosomal locus (Davidson & McCray, 2011). This feature of lentiviral delivery makes it an attractive delivery option to actively dividing cells as the viral DNA will not degrade or become lost over successive cell divisions. However this feature also makes lentiviral delivery a possible tumour-inducing agent due to insertional mutagenesis of proto-oncogenes. The safety of lentiviral delivery to the retina was recently tested in p53 knockout mice which are particularly prone to tumour formation in the retina (Balaggan et al, 2012). p53 -/- mice which had been subretinally injected were allowed to live until natural death occurred. The mice exhibited no change in lifespan compared to uninjected animals of the same genetic background and gene knockout background. Furthermore, examination of the eyes showed no evidence of tumour formation in any of the 98 eyes which had received a subretinal injection of lentivirus. These data suggest that lentiviral delivery is a safe delivery method of gene therapy to the eye. Lentiviruses can also be modified to become integrase deficient by targeted mutation of the catalytic region of the integrase region of the virus, greatly increasing the safety of these vectors (Banasik & McCray, 2010). The safety conerns regarding lentiviral delivery has meant that little work has been performed using this delivery method in the treatment of genetic disorders of the retina. Lentivirus is also a relatively poor transducing agent of the retina due to the presence of the interphotoreceptor matrix (IPM), an extracellular matrix surrounding the photoreceptors (Grüter et al, 2005). This reduces the efficacy of lentiviral delivery in adult mice as the IPM develops early in postnatal eye development. No evidence could be found in the scientific literature examining if the IPM also retards the transduction efficacy of AAV *in vivo*. Nonetheless, lentiviral vectors have been used to treat animal models of LCA (Kostic et al, 2011; Verrier et al, 2011), Stargardt disease (Kong et al, 2008), X-linked RP (Glaus et al, 2011) and Usher Syndrome (Hashimoto et al, 2007).

1.15 Non-viral delivery

In addition to the wide use of viral vectors for delivery of gene therapies to the retina, non-viral vectors have been explored as another option for delivery of DNA and RNA to the retina. These delivery agents are in theory a much more attractive system of delivery as they avoid the issue of integration in to the host genome and possible immunogenicity that may arise from delivery of a viral vector. Non-viral vectors also avoid the capsid packaging issue which arises with viral vectors due to the limited size

of the transgene that may be inserted in to a viral genome. For example, AAV has a limit of approximately 4.7kb which may be inserted between the ITRs of this genome (Wu et al, 2010).

The delivery agent which has received most attention in the literature is the liposome. These are particles of lipid which enclose around the DNA or RNA therapeutic. A number of different lipids such as TMAG (N-(α-trimethylammonioacetyl)-didodecyl-D-glutamate), DC-cholesterol (3-β[N-(N', N'-dimethylaminoethane)-carbomyl] cholesterol), DOTAP (1,2 dioleoyl-3-trimethyl amonium propane) and DOPE (1,2 dioleoyl-3-phoshpatidylethanolamine) have been used in particular, as these lipids are cationic and will therefore bind negatively charged DNA during assembly of the liposomes (Kachi et al, 2005). Liposomes are frequently injected either intravitreally or subretinally. Intravitreal injection of rabbits using a DOTMA (N-[1-(2,3 dioleoyloxy)propyl]-N,N,N-trimethylammonium) complexed plasmid resulted in expression of reporter gene in all layers of the retina (Kawakami et al, 2004). TMAG has also demonstrated high efficacy of delivery of DNA to the GCL and RPE layers of the retina following intravitreal injection (Masuda et al, 1996). In addition, DOTAP has been demonstrated to effectively transfect the RPE cells *in vitro* with plasmid DNA (Urtii et al, 2000). However, lipid based carriers of nucleic acids have fallen out of favour for delivery to the retina as other methods of non-viral delivery have demonstrated greater efficacy (Charbel-Issa & MacLaren RE, 2012).

Polymers which bind to the DNA or RNA therapeutic have also been employed with success to deliver nucleic acids to the retina. The most widely used polymers are PEI (Polyethylenimine) and PLL (Poly-L-Lysine). These polymers bind and condense DNA or RNA and allow passage of negatively charged nucleic acid across the negatively charged exterior of the cell membrane. Intravitreal injection of PEI bound to a plasmid containing a shRNA targeting melanopsin resulted in almost complete suppression of melanopsin in the GCL of treated eyes (Liao &Yau, 2007). Combining polymer and liposomal delivery has also been achieved by combining a lipid-lysine to lipidic aminocarboxylic acid. This delivery agent was used to deliver an antisense oligonucleotide targeting VEGF by intravitreal injection resulting in penetration of the therapeutic oligonucleotide to all layers of the retina (Marano et al, 2005). More recently, nanoparticles composed of lysine peptides were used to bind and deliver

plasmid DNA to the retina by subretinal injection and intravitreal injection (Farjo et al, 2006). This delivery method resulted in strong reporter gene expression in tissues of the eye by intravitreal injection and RPE and ONL expression by subretinal injection. The delivery agent was also bound to polyethylene glycol (PEG) as this has been shown to increase the efficacy of both liposomal and polymer based delivery agents (Bochot et al, 2002). More recently, the use of modified cyclodextrin has emerged as a powerful tool to introduce nucleic acids to neuronal cells *in vitro* (O' Mahony et al, 2012, 2013). Finally, apart from administration of DNA bound lipids or polymers, there are two other delivery options available to introduce foreign genetic material to the retina. These methods are electroporation and iontophoresis. These methods are applicable to neonatal animals however and much of the work has not progressed past animals larger than mice due to practical drawbacks. Electrophoresis involves the use of an electrical charge to permeate the cell membrane and allow introduction of DNA or RNA. This method has been demonstrated to be an effective delivery method in mice which were subretinally injected with naked plasmid DNA at P0 (Matsuda & Cepko, 2004). Electrodes were then placed on either side of the head and a small charge was passed through the head of the mouse. This resulted in transgene expression in the ONL, INL but not the GCL. The transgene expression also began to decrease 3-4 weeks after electroporation, possibly due to dilution by cell division during retinal development at this early stage of life. Iontophoresis is the use of an electrical charge to transfer negatively charged DNA through a tissue of interest. Iontophoresis has been used to introduce a reporter plasmid through the sclera of the eye to layers of the retina (Souied et al, 2008). This resulted in expression of the reporter gene 6 days after iontophoresis. The expression of the reporter gene was limited to the outer segments of the retina with some expression in the synaptic layers (the OPL and IPL). This expression rapidly decreased however and was not observed past day 14.

1.16 Objectives

The objective of this thesis was the exploration of AAV 2/5 delivery of an RNAi based construct to the murine retina of a model of retinitis pigemtosa in order to reduce expression of the *Rac1* gene. This set of experiments is detailed in chapter three and involves the use of quantitative analysis to determine the effect of RNAi on *Rac1* expression both *in vivo* and *in vitro*. Furthermore, functional effects of RNAi mediated

suppression were examined by immunohistochemistry and electroretinography (ERG) analysis. In parallel with this study, a separate study was undertaken to explore the effect of *Thioredoxin1* over-expression in two mouse models of RP. This data is presented in chapter four and in a similar manner to chapter three, quantitative analysis was undertaken to examine the functionality of a *Thioredoxin1* cDNA under the control of an expression plasmid both *in vitro* and *in vivo*. The functional effects of over-expression were then examined by immunohistochemistry and ERG analysis. Modulation of the expression of both of these genes was anticipated to decrease retinal oxidative stress. In the final part of this thesis the nuclear stain of superoxide, dihydroethidium (DHE), was utilised to characterise oxidative stress in three mouse models of retinal degeneration. This stain was also used to assay any changes in retinal superoxide which may arise following AAV delivery of either a *Rac1* shRNA or a *Thioredoxin1* cDNA.

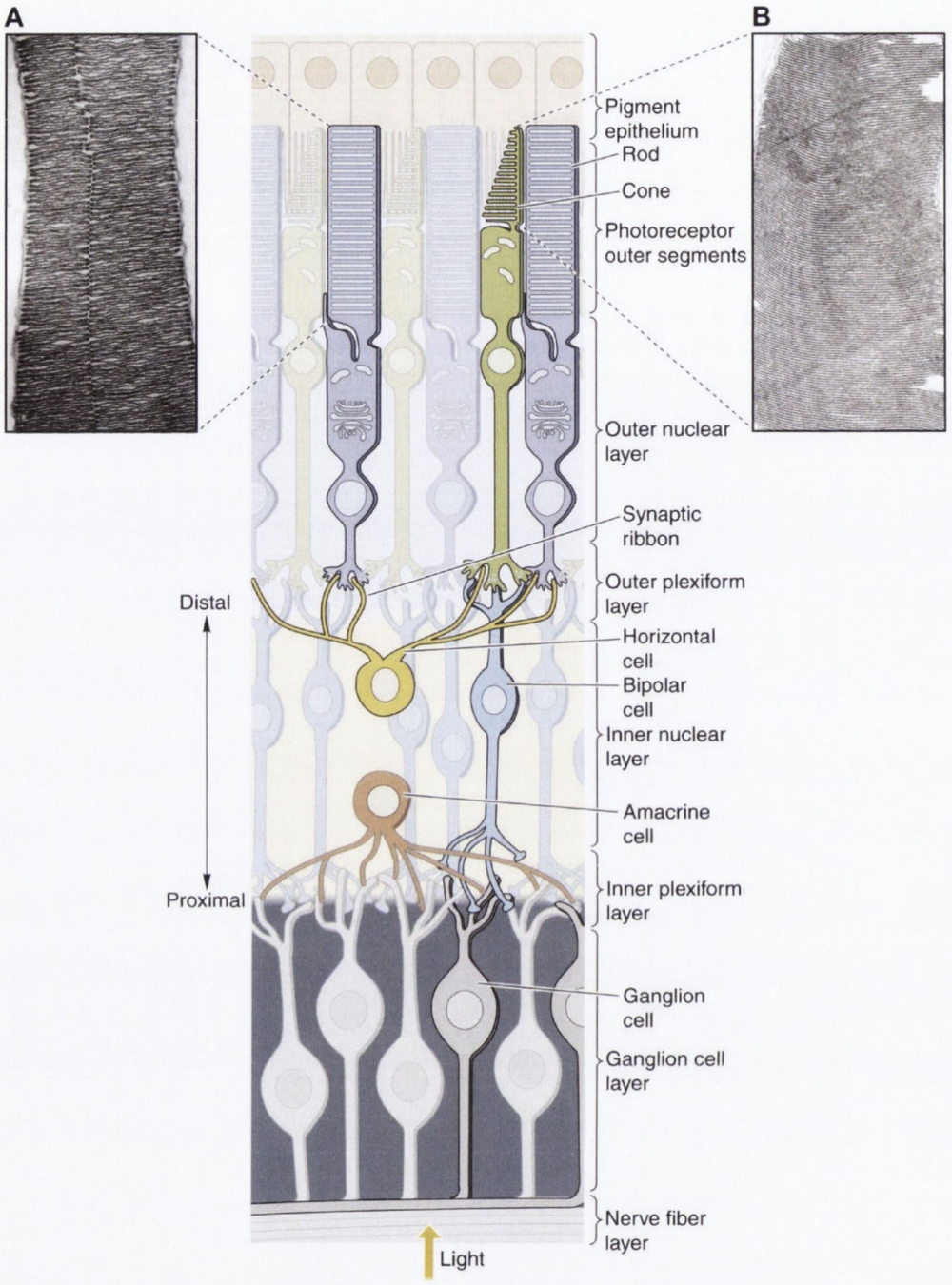

Figure 1.1: Schematic of retinal structure.

Figures A and B show Rod and Cone outer segment ultrastructure by electron microscopy respectively. These micrographs illustrate the presence of disks within the outer segments of the photoreceptors which contain the light sensing pigments of each type of photoreceptor. Also of note is the presence of three main nuclear layers in the neural retina, the ONL (made up of photoreceptors), the INL (made up of amacrine, bipolar and horizontal cells) and the GCL (made up of the ganglion cells). Adapted from Mustafi et al (2009).

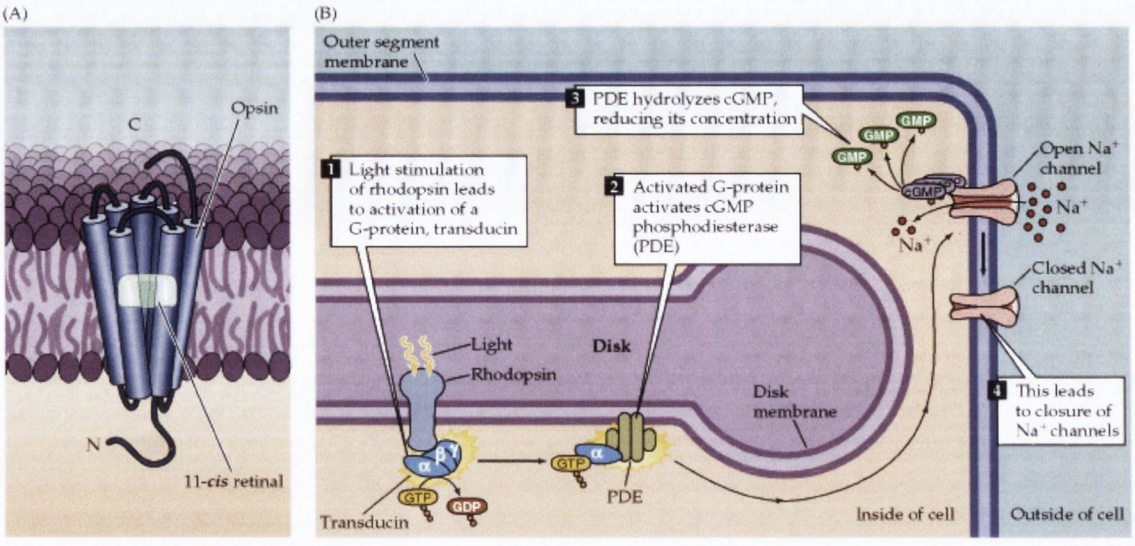

Figure 1.2: Diagram of Rhodopsin mediated hyperpolarisation

Rhodopsin is activated by isomerisation of 11 cis-retinal which induces a downstream cascade of signal transduction, beginning with the dissociation of the α and βγ subunits of transducin. This in turn causes activation of cGMP phosphodiesterase which acts to hydrolyse cGMP. The hydrolysis of cGMP induces the closure of cGMP gated ion channels which causes hyperpolarisation of the cell. Adapted from Purves et al, 2008.

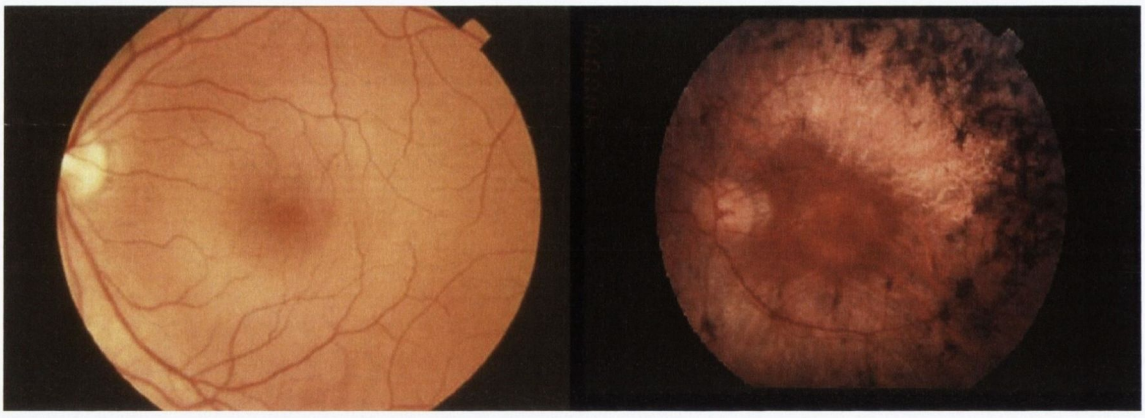

Figure 1.3 : Fundus of a healthy retina (left) and fundus of from a patient with mid stage RP (right).

The degenerating retina shows signs of bone spicule deposits in the retina as well as attenuation of the blood vessels. The macula also shows increased prominence, suggesting a possible macular oedema. Figures adapted from the National Institute of Health (http://www.nei.nih.gov/photo/eyedis/images/eye15-72.jpg) and Hamel et al (2006).

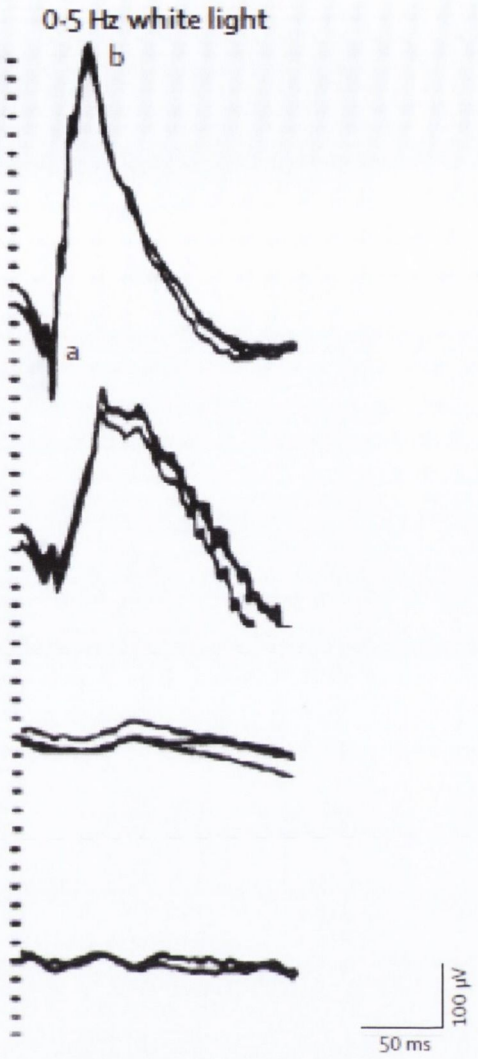

Figure 1.4: Examples of a typical ERG readout

This figure shows examples of ERG responses (from top to bottom) from a healthy individual, a 13 year old patient with autosomal dominant RP, a 9 year old patient with autosomal recessive RP and a 14 year old patient with X-linked RP. These graphs illustrate the variability of visual response of patients of RP based on the mode of inheritance of the disease and the mutated allele which causes the disorder. Adapted from Hartong et al (2006).

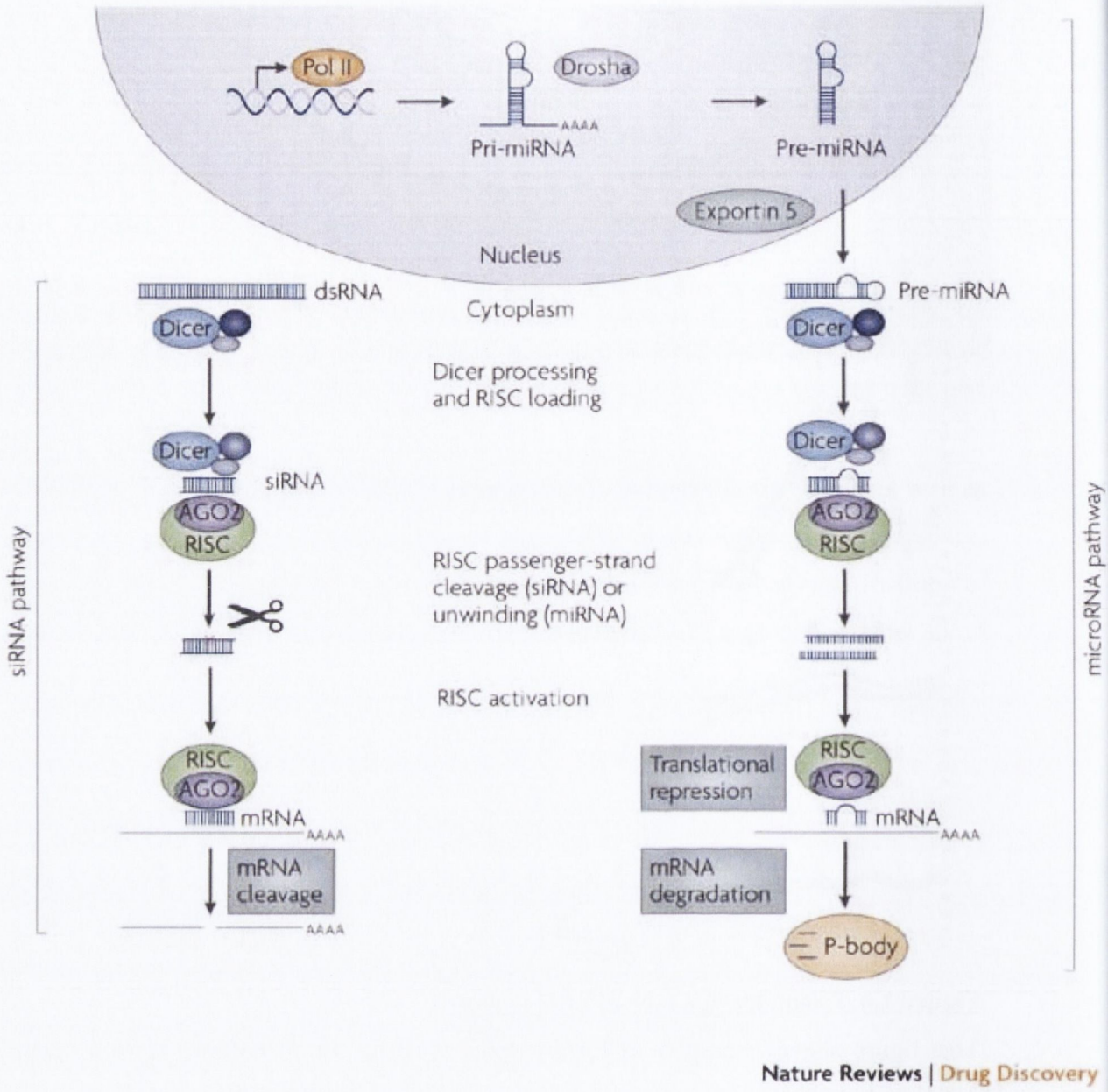

Figure 1.5: Diagram of the RNAi Pathway

This illustration shows the naturally occurring miRNA pathway on the right. It can be observed from this figure that miRNAs are first transcribed as pri-miRNAs before being processed by the Drosha complex to pre-miRNAs. Following this, the pre-miRNA is exported from the nucleus and undergoes more steps of processing before incorporation in to the RISC and suppression of mRNA translation, either by cleavage or translational repression in the P-body of the cell. Artificial shRNA constructs enter this pathway immediately prior to Dicer processing and subsequent to export from the nucleus. Artificial siRNAs are immediately incorporated in to RISC. Figure adapted from de Fougerolles et al, 2007.

Chapter 2: Materials and Methods

Section 2.1: Materials

2.1.1 Reagents for DNA cloning

Oligonucleotide annealing buffer: 0.025M NaCl

Restriction enzyme buffers (New England Biolabs):

1X NEBuffer 1 (pH 7 @ 25°C)	10mM Bis-Tris Propabe HCl, 10mM $MgCl_2$, 1mM Dithiothreitol.
1X NEBuffer 2 (pH 7.9 @ 25°C)	50mM NaCl, 10mM Tris-HCl, 10mM $MgCl_2$, 1mM Dithiothreitol.
1X NEBuffer 3 (pH 7.9 @ 25°C)	100mM NaCl, 50mM Tris-HCl, 10mM $MgCl_2$, 1mM Dithiothreitol.
1X NEBuffer 4 (pH 7.9 @ 25°C)	50mM Potassium Acetate, 20mM Tris-Acetate, 10mM Magnesium Acetate, 1mM Dithiothreitol.
Bovine Serum Albumin (BSA) (pH 7 @ 25°C)	BSA, 20mM KPO_4, 50mM NaCl, 0.1mM EDTA, 5% Glycerol.

- SuRE/CUT Buffer A (pH 7.9 @ 37°C, Roche): 33mM Tris-Acetate, 10mM Magnesium Acetate, 66 mM Potassium Acetate, 0.5mM Dithiothreitol.
- T4 Ligation Buffer (pH 7 @ 20°C, Roche): 0.66M Tris-HCl, 50mM $MgCl_2$, 10mM Dithiothreitol, 10mM ATP.
- T4 DNA Ligase (Roche).
- Klenow Enzyme (Roche).
- T4 DNA polymerase (Roche).
- Crimson *Taq*™ DNA polymerase (New England Biolabs).
- dNTP working solution: 2mM (Roche).
- Tris-Acetate EDTA buffer 10X (pH @ 25°C 8.2-8.4, Invitrogen): 0.4M Tris-Acetate, 10mM EDTA.
- Agarose (Sigma Aldrich).
- Xylene Cyanol (Electran) Dye (6X): 5.8mM Xylene Cyanol, 4.9M Glycerol.
- Bromophenol Blue (Electran) Dye (6X): 4.66mM Bromophenol Blue, 4.9M Glycerol.
- Ethidium Bromide (Sigma Aldrich): 10mg/ml.

- 100bp and 1kb DNA ladders (Fermentas).
- Luria Bertani (LB) Broth: 1% Tryptone (Oxoid), 0.5g Yeast Extract (Oxoid), 1% NaCl (Scharlau).
- LB/Agar: 1% Tryptone, 0.5% Yeast Extract, 1% NaCl, 1.5% BBL^{TM}Agar Grade A (BD Company)..
- 0.5M $CaCl_2$ (Sigma-Aldrich) Solution.
- 100mM $CaCl_2$ (Sigma-Aldrich) Solution
- 100mM $MgCl_2$ (Sigma-Aldrich) Solution.
- Glycerol (Sigma-Aldrich).
- 1X Crimson *Taq*^{TM} PCR Buffer (pH 8.5 @ 25°C, New England Biolabs): 12.5mM Tricine, 42.5mM KCL, 1.5mM $MgCl_2$, 6% Dextran Red Acid.
- 10X Tris-Triton: 0.57M Tris (pH9, Sigma-Aldrich), 0.57% Triton-X (Sigma-Aldrich).
- XL1-BlueMRA Competent Cells (Stratagene)

Antibiotics:

- Ampicillin (Sigma-Aldrich): Stock Solution: 49.6mM (in dH_2O)
  Working Solution: 0.124mM (in LB)
- Tetracycline (Sigma-Aldrich): Stock Solution: 22.5mM (in dH_2O)
  Working Solution: 0.056mM (in LB).

2.1.2 Cell Culture Reagents

- 1X Sterile Phosphate Buffered Saline (Gibco).
- Complete Dulbecco's Modified Eagle Medium(DMEM, Gibco): Dulbecco's Modified Eagle's Medium was supplemented with 10% heat inactivated Fetal Calf Serum FCS, 20µM L-Glutamine (Gibco) and 20µM Sodium Pyruvate (NaPyr, Gibco). The complete medium was stored at 4°C.
- 2X Freezing Media: 25% Dimethyl Sulfoxide (DMSO, Sigma-Aldrich), 25% FCS, 50% DMEM.
- Trypsin-EDTA (0.025%, Gibco)
- Trypan Blue (0.4%, Sigma-Aldrich)

- Lipofectamine® Transfection Reagent (Invitrogen).
- Opti-Mem® (Gibco).
- Ethanol (70%, TCD Hazardous Materials Facility).

2.1.3 RNA Reagents

- RQ1 DNase 10X Buffer (Promega): 400mM Tris-HCl (pH 8), 100mM $MgSO_4$, 10mM $CaCl_2$.
- RQ1 DNase Stop Solution (Promega): 20mM EGTA (pH 8).
- RQ1 DNase (Promega).
- Nuclease Free Water (Ambion).
- TRI-Reagent® (Sigma-Aldrich).
- Chloroform (Sigma-Aldrich).
- Isopropanol (Sigma-Aldrich).
- B-Mercaptoethanol (Sigma-Aldrich)
- Buffer RDD (Qiagen).
- Quantitect SYBR Green RT-PCR Kit (Qiagen).

2.1.4 Protein Reagents

- 10X Tris Buffered Saline (TBS, pH 7.5 @ 25°C). pH was adjusted using 1M HCl and 1M NaOH.
- 1X TBS-Tween. 1X TBS, 0.05% Tween-20 (Sigma-Aldrich).
- 1% Triton-X 100.
- 0.5M EDTA (pH8).
- Protease Inhibitor Solution: 1 Complete Mini-Protease Inhibitor Cocktail tablet (Roche) was dissolved in 1.5ml dH_2O.
- Cell Lysis Buffer: 0.1% Triton X-100, 1mM EDTA (pH8), 1X TBS, 15% Protease Inhibitor Solution.

- Tissue Lysis Buffer (pH 8.3): 62.5mM Trizma base (Sigma-Aldrich), 10mM Dithiothreitol (DTT, Sigma-Aldrich), 2% Sodium Dodecyl Sulfate (SDS, Sigma-Aldrich), 500µl Protein Inhibitor Solution.

- 1X PBS: Two tablets of PBS (Sigma-Aldrich) were dissolved in 400ml ddH_2O.

- 1.5M Tris-HCl (pH 8.8).

- 0.5M Tris-HCl (pH 6.8).

- 10% Ammonium Persulfate (APS) Solution.

- 10% Sodium Dodecyl Sulfate (SDS, pH 7.2)

- Prestained Protein Ladder Broad Range (Fermentas).

- Resolving gel for SDS-PAGE (Poly-Acrylamide Gel Electrophoresis, 12%): Gel solution was made up by adding the following reagents in order to a 50ml conical tube: 5ml 1.5M Tris HCl (pH 8.8), 6.6ml dH_2O, 8ml Bis-Acrylamide Solution (30%, Sigma-Aldrich), 200µl 10% SDS solution (pH 7.2), 200µl 10% APS solution, 10µl Tetramethylethylenediamine (TEMED, Sigma-Aldrich).

- Stacking gel for SDS-PAGE (4%): Gel solution was made up by adding the following reagents in order to a 50ml conical tube: 2.5ml 0.5M Tris-HCl (pH 6.8), 6.8ml dH_2O, 1.33ml Bis-Acrylamide (30%, Sigma-Aldrich), 100µl 10% APS Solution, 10µl TEMED (Sigma-Aldrich).

- 10X Running Buffer (pH8.6): 30.3g Trizma Base (Sigma-Aldrich), 144.2g Glycine (Sigma-Aldrich), 10ml 10% SDS Solution were dissolved in 800ml dH_2O. pH was adjusted to 8.6 using 1M NaOH and 1M HCl. Final volume was made up to 1L with dH_2O.

- 1X Transfer Buffer (pH 8.3): 3.03g Trizma Base (Sigma-Aldrich), 14.42 Glycine (Sigma-Aldrich), 200ml Methanol (Schlarau Chemie) were dissolved in 800ml dH_2O. pH was adjusted to 8.3 using 1M HCl and 1M NaOH. Final volume was made up to 1L with dH_2O.

- 5% Blocking Solution: 5% Marvel Dried Milk dissolved in 1X TBS.

- Ponceau S Solution: 0.1% Ponceau dissolved in 5% acetic acid (Sigma-Aldrich).

- Laemmli 4X Buffer (pH 6.8): 8% SDS, 20% β-Mercaptoethanol, 40% Glycerol, 0.008% Bromophenol Blue, 0.125M Tris-HCl.

- Amersham ECL™ Western Blotting Detection Reagent (GE Healthcare)

- 5X Professional Developer and Replenisher (Kodak)

- 5X GBX Fixer and Replenisher (Kodak)

- Super RX Fuji Medical X-Ray Film (Fujifilm).
- Lumocolor photocopy film (Staedtler).
- PVDF Immobilon Transfer Membrane (Millipore).
- Restore™ Western Blotting Stripping Buffer (Thermo-Scientific).

2.1.5 Reagents for Production of Recombinant AAV

- Plasmids: pAAV_MCS (Stratagene), pRep2/Cap521 (Hildinger et al, 2001), pHelper (Stratagene).
- Human Embryonic Kidney 293 (HEK 293) cells (ATCC).
- Transfection Buffer: 1M NaCl (Sigma-Aldrich, pH 5)
- Transfection Reagent: Polyethlenimine (Sigma-Aldrich): 0.1g/L, 150mM NaCl (pH5).
- Deoxycholic acid (Sigma-Aldrich).
- Caesium Chloride (Sigma-Aldrich).
- Slide-a-Lyzer (MSC/Fischer)

2.1.6 Animals

- Wildtype 129/SvHsd (Harlan, Loughborough, UK)
- Pro23His +/- crossed with Rho +/- on a 129/Sv background (Ollson et al, 1992).
- Human Pro347Ser +/- crossed with Rho +/- on a 129/Sv background (Li et al, 1996).

2.1.7 Animal Reagents

- Anaesthetic for sub-retinal injection: Medetomidine (1mg/g mouse weight), Ketamine (75mg/g mouse weight) via i.p. injection.
- Anaesthetic for ERG procedure: Ketamine (1.6mg/g mouse weight), Xylazine (0.16mg/g mouse weight) via i.p. injection.
- Topical Eye Dilation: 1% Cyclopentolate, 2.5% Phenylephrine.
- Analgesia: 1% Amethocaine, Vidisic gel

- Anaesthesia Reversal Agent: Atipamezole Hydrochloride (10mg/g mouse weight) via i.p. injection.

2.1.8 Histology and Immunohistochemistry Reagents

- 4% w/v Paraformaldehyde (Sigma-Aldrich) Solution (pH 7.4)
- 4% Pfa with 5% acetic acid.
- 10%, 20%, 30% w/v Sucrose (Sigma-Aldrich) solution in 1X PBS.
- Optimal Cutting Temperature (OCT) compound (VWR)
- Poly-Lysine coated glass slides (Thermo Scientific).
- Blocking Solution: Donkey Serum (Sigma-Aldrich, 10%), Triton-X (Sigma-Aldrich, 0.3%) in 1X PBS.
- Antibody Solution: Donkey Serum (2%), Triton-X (0.1%) in 1X PBS.
- 4,6 Diamidine-2-Phenylindole-Dihydrochloride (DAPI) solution: 0.01% w/v (Sigma-Aldrich).
- Aqua PolyMount coverslip Mounting solution (Polysciences).
- Dihydroethidine (DHE, Invitrogen) Solution: 5μM in Dimethyl Sulfoxide (DMSO, Sigma-Aldrich).
- Liquid Blocker PAP Pen (Sigma-Aldrich).

2.1.9 Antibodies

Primary Antibodies

- Mouse Anti-Rac1 antibody (Millipore). Reacts with Human, Mouse and Rat epitopes. Used at 1:100 dilution for immunohistochemistry
- Chicken Anti-Rac1 antibody (Abcam). Reacts with Human, Mouse and Cow epitopes. Used at 1:2000 dilution for western blot.
- Mouse Anti-Rac1 antibody (BD Biosciences) Reacts with Human epitope. Used at 1:1000 dilution for western blot.
- Rabbit Anti-Thioredoxin1 (Abcam). Reacts with Human and Mouse epitopes. Used at 1:200 dilution for immunohistochemistry and 1:1000 dilution for western blot.
- Rabbit Anti-β-Actin antibody (Abcam). Reacts with Human and Mouse epitopes. Used at 1:1000 dilution for western blot.

Secondary Antibodies

- Goat Anti-Chicken antibody (Abcam) fused to Horseradish Peroxidase (HRP). Used at 1:3000 dilution
- Goat Anti-Rabbit antibody (Abcam) fused to HRP. Used at 1:2000 dilution.
- Goat Anti-Mouse antibody (Abcam) fused to HRP. Used at 1:2000 dilution.
- Mouse Anti-Mouse antibody (Invitrogen) fused to CY3. Used at 1:500 dilution
- Goat Anti-Chicken antibody (Invitrogen) fused to CY3. Used at 1:500 dilution

2.1.10 FACS Reagents

- Hank's Balanced Saline Solution (HBSS, Gibco).
- Trypsin EDTA (10mg/ml in PBS, Sigma Aldrich)
- Trypsin Inhibitor (20mg/ml in PBS, Roche).
- Propidium Iodide (PI, 1mg/ml, Sigma-Aldrich).

2.1.11 Primers

Rac1 Cloning Primers

*Rac1*_gCF	5'AAGCAAAAGCTTATGCAGGCCATCAAGTGTGT3'
*Rac1*_gCR	5'AAGCAATCTAGATTACAACAGCAGGCATTTTC3'

RT-qPCR Primers

*Rac1*_qF	5' GATGCAGGCCATCAAGTGTG 3'
*Rac1*_qR	5' CCATCTACCATAACATTGGC 3'
Rac1_gR_new	5' CATTGGTTGTGTAACTGATC 3'
*Trx*_qF	5' AGGCTTCAAGCTTTTCCTTG 3'
*Trx*_qR	5' TGACTGCCAGGATGTTGCTG 3'
*ACTB*_F	5' TCACCCACACTGTGCCCATCTACGA 3'
*ACTB*_R	5' CAGCGGAACCGCTCATTGCCAATGG 3'
*Gapdh*_F	5' TTTGGCAATGTGGAAGGGCT 3'
*Gapdh*_R	5' TTCAGGGATGATGTTCTGGG 3'
EGFP_F	
EGFP_R	

Sequencing Primers

AAV_chk_F	5' CGATGGGGGTGTTCTGCTGGTA3'
AAV_chk_R	5' AACCGCATCGAGCTGAAGGG 3'
H1_F	5' GATTCGAACGCTGACGTCATC 3'
H1_R	5' GGTGATTTCCCAGAACAC 3'
M13_F	5' CAGTCACGACGTTGTAAAACG 3'
MRP_R	

Short Hairpin RNA PCR Cloning primers

shRAC1_1F	5'GATCCCCGTGTCCGTGCAAAGTGGTATTTCAAGAGAAT ACCACTTTGCACGGACATTTTTTCTAGAGGAAA3'
shRAC1_1R	5'AGCTTTTCCCTAGAAAAAATGTCCGTGCAAAGTGGTATT CTCTTGAAATACCACTTTGCACGGACACGGG3'
shRAC1_3F	5'GATCCCCGGAAGAGGAAGAGAAAATTTCAAGAGAATTT TCTCTTCCTCTTCTTTTTTCTAGAGGAAA3'
shRAC1_3R	5'AGCTTTTCCCTAGAAAAAAGAAGAGGAAGAGAAAATTC TCTTGAAATTTTCTCTTCCTCTTCCGGG3'

Section 2.2 Methods

2.2.1 Cloning Methods

2.2.1.1 Determination of DNA/RNA Concentration by NanoDrop™ Spectrophotometry

Nucleic acid solution concentrations were evaluated using the Nanodrop™ 1000 Spectrophotometer. This measures the absorbance of both RNA and DNA at wavelength 260nm. The units of absorbance are used to calculate the concentration of either nucleic acid. One unit of absorbance is equivalent to 50µg/ml of dsDNA or 40µg/ml of ssRNA. The purity of the sample can be evaluated by calculating the absorbance ratio of 260nm/280nm. This measures the absorbance of nucleic acid over the absorbance of protein (280nm). A ratio of 1.7 and above is considered 'clean'. Measurements were made by loading 2µl of nuclease free water onto the optical surface of the spectrophotometer to determine a blank measurement. 2µl of samples were subsequently loaded to determine their DNA or RNA concentrations.

2.2.1.2 Electrophoresis of DNA by Agarose Gel

Agarose gels were made by dissolving various amounts of agarose in 1X Tris-Acetate EDTA Buffer (TAE) depending on the concentration of agarose required. These typically ranged from 0.8% to 2.5% agarose. 1µl of Ethidium Bromide (EtBr, Sigma-Aldrich) was dissolved in 30ml of agarose solution and this was poured into a gel cast. A comb was then placed into the agarose solution and the solution was left to set at room temperature. When the gel was set, 10µl of DNA sample containing a 1:6 dilution of loading dye (either Xylene Cyanol or Bromophenol Blue) was loaded into the gel. The gel was electrophoresed at 80-100V for an appropriate amount of time. The DNA intercalated with EtBr was visualised using a UV transilluminator (Hoieffer).

2.2.1.3 DNA purification using PCR Purification and Gel Extraction Kits

DNA was purified from reaction solutions using a PCR Purification Kit (Fermentas) according to the manufacturer's instructions. Briefly, a 1:1 volume of binding buffer

was added to the DNA solution. This was then centriguged through a purification column. The column, containing the DNA, was then washed twice with wash solution by centrifugation before the DNA was eluted. For DNA fragments shorter than 500bp a 1:1 volume of isopropanol was added to the DNA solution before purification. Following purification the DNA was eluted into 50µl of nuclease free water.

DNA was purified from 1% agarose gels using a Gel Extraction Kit (Fermentas) according to the manufacturer's instructions. The DNA was first visualised under UV lamp and this region of agarose gel was excised using a sterile scalpel blade. This piece of gel was then melted with binding buffer at 65°C before being centrifuged through a purification column. The column was then washed twice with wash solution before elution. Following purification the DNA was eluted into 50µl of nuclease free water.

2.2.1.3 DNA Purification by Phenol/Chloroform Extraction

A 1:1 volume of Tris buffered phenol was mixed with the DNA solution. This was then centrifuged at 13,000rpm for 90 seconds. The aqeuous (top) phase was pipetted out and placed in a new eppendorf tube. To this a 1:1 volume of phenol/choloroform mixture (1:1) was added and mixed. This was then centrifuged at 13,000rpm for 90 seconds. The aqeuous phase was pipetted out and placed in a new eppendorf tube. To this a 1:1 volume of 96% choloroform solution was added. This was centrifuged at 13,000rpm for 90 seconds. The aqueous phase was pipetted into a new tube. A 2.5:1 volume of 96% ethanol was added to the aqueous phase and this mixture was chilled on ice for 20 minutes. This was then centrifuged at 13,000rpm for 20 minutes. At this stage a pellet of nucleic acid was usually visible at the bottom of the tube. The supernatant was removed and discarded. 200µl of 70% ethanol was mixed with the pellet to wash the DNA. This mixture was then centrifuged at 13,000rpm for 10 minutes. A pellet was again observed. The ethanol supernatant was removed and discarded and the pellet was allowed to air-dry in a laminar flow hood (MDH Ltd.). The pellet was then dissolved in 20µl nuclease free water.

2.2.1.4 DNA Amplification and isolation using Kits

Minipreparation: A transformed colony was picked and inoculated into 5ml of LB containing Tetracycline and Ampicillin. This was left to grow overnight at 37°C in an orbital shaker. The culture was then centrifuged at 3000rpm for ten minutes to pellet the cells. The DNA was extracted using the materials and methods described in the GenJet™ Plasmid Miniprep Kit protocol (Fermentas). The DNA was eluted in 50µl dH_2O.

Maxipreparation: A transformed colony was picked and inoculated into 5ml of LB containing Tetracycline and Ampicillin. This was left to grow for 8 hours at 37°C in an orbital shaker. 1ml of this culture was then subcultured into 200ml of LB containing Tetracycline and Ampicillin and incubated for 12-16 hours at 37°C in an orbital shaker. The culture was then centrifuged at 3000 rpm for 30 minutes to pellet the cells. The DNA was extracted using the materials and methods described in the HiSpeed® Plasmid Purification protocol (Qiagen). The DNA was eluted in 1ml dH_2O.

Megapreparation: A transformed colony was picked and inoculated into 5ml of LB containing Tetracycline and Ampicillin. This was left to grow for 8 hours at 37°C in an orbital shaker. 5ml of this culture was then subcultured into 600ml of LB containing Tetracycline and Ampicillin and incubated for 16 hours at 37°C in an orbital shaker. The culture was then centrifuged at 6000rpm for 15 minutes at 4°C to pellet the cells. The DNA was then extracted using the materials and methods described in the EndoFree® Plasmid Purification Handbook (Qiagen). The DNA was then eluted in 2-3ml dH_2O.

2.2.1.5 Restriction Enzyme DNA Digestion

Restriction Enzyme digestion was performed using various enzymes (New England Biolabs, NEB). These enzymes are stored in glycerol at -20°C. The digestion reaction was carried out in a 50µl reaction. The amount of enzyme used varied from 0.5µl to 2µl (10-40 units of enzyme/reaction) depending on the amount and length of DNA to be treated. For reactions in which more than one restriction enzyme was used, the total enzyme mixture added was kept under 3µl as glycerol tends to inhibit enzymatic reactions at concentrations over 5%. 5µl of the appropriate NEB buffer and 5µl of 10X

BSA (Bovine Serum Albumin, NEB) were also added to the reaction mixture. The remaining volume of reaction mixture was made up with nuclease free water. The reaction mixture was then incubated at 37°C for 2 hours. For sequential digestions on the same fragments of DNA, the DNA was PCR purified between digests using the PCR purification kit (Fermentas).

2.2.1.6 Blunting of 5' DNA sticky ends using Klenow Enzyme

For blunt cloning of an insert into a vector, both vector and insert must first be blunted. This is performed by inserting nucleotides opposite the open nucleotides of the sticky end of the DNA. The addition of nucleotides to a sticky end which has a 5' overhang is performed using Klenow enzyme. 6µl of Roche buffer A, 2µl of dNTP solution (2mM) and 2µl of klenow enzyme (Roche) were added to 50µl of DNA solution. This was incubated at 37°C for 30 minutes. The resulting DNA soultion was purified using the PCR purification kit (Fermentas) before ligation.

2.2.1.7 Blunting of 3' DNA stick end using T4 DNA Polymerase

In many cases, a restriction digest will leave a 3' sticky end instead of a 5' sticky end. In this instance T3 polymerase (Roche) was used to fill these ends. 6µl of Roche buffer A, 2µl of dNTP solution (2mM) and 2µl of polymerase were added to 50µl of DNA solution. This was incubated at 12°C for 10 minutes before incubation at 80°C for 10 minutes to inactivate the enzyme. The resulting DNA solution was purified using the PCR purification kit (Fermentas) before ligation.

2.2.1.8 DNA Ligation

Ligations were performed to ligate two compatible ends of DNA, typically to insert an insert into a vector. The relative concentrations of vector to insert were previously determined by visualising band intensity on an agarose gel under UV light illumination. The vector:insert ratio was usually kept at 10:1 and 100:1 in order to flood the reaction with insert DNA and inhibit the closure of the digested vector DNA. These reactions were carried out in a 10µl reaction volume. After the DNA was added

the remaining reaction volume was made up with 1µl T4 Ligase (1unit/µl, Roche), 1µl T4 Ligase Buffer (Roche) and nuclease free water. A vector digest control without ligase was also set up to account for the background number of colonies which form from undigested vector. A ligase control was performed which contained no insert and so would be unable to close and ligate (unless the vector had been blunted previously).

2.2.1.9 Polymerase Chain Reaction (PCR)

DNA was PCR amplified using the Crimson *Taq* DNA Polymerase kit (New England Biolabs). The PCR reactions were all made up to a final volume of 25µl. This was made up of 5µl Crimson *Taq* Reaction Buffer (New England Biolabs), 2.5µl 2mM dNTP Solution (containing all 4 nucleoside tri-phosphates required for DNA replication, Roche), 1µl 10µM Forward Primer, 1µl 10µM Reverse Primer, 0.2µl Crimson *Taq* DNA polymerase (New England Biolabs), 1-5µl DNA template and 10-14µl nuclease free water. This reaction mixture was mixed by pipetting and placed in a PCR thermal cycler (MJ Research Inc.). The PCR program was then initiated. This heats the reaction mixture to 94°C for 5 minutes which denatures the DNA into two strands. After this, 35 cycles of 95°C for 1 minute, 55°C for 1 minute and 72°C for 1 minute are completed. The 55°C step is the annealing step which allows the primers to bind to the recently denatured DNA. The 72°C step is the extension step which allows the DNA polymerase to synthesise a new strand of DNA complementary to the original DNA downstream of either primer. When the thermal cycler returns to 95°C, the DNA is denatured again allowing the cycle to begin for another round. At the end of these cycles the reaction mixture is heated to 72°C for 10 minutes to allow extension of any unfinished reactions and then cooled to 10°C for an indefinite amount of time. Samples were taken from the PCR thermal cycler when the temperature reached 10°C.

2.2.1.10 Inducing Competence in XL1-BlueMRA E. Coli

A colony of *E. coli* Tet^+ were picked and cultured in 1ml of LB containing Tetracycline overnight. 200µl of this culture was then sub-cultured into 20ml of LB containing tetracycline. When the culture reached the log phase it was placed on ice for

30 minutes before centrifugation at 3000rpm for 10 minutes to pellet the cells. The log phase was determined by measuring the optical density (OD) of the culture. An absorbance of 600 was deemed to be a log phase density. The cells were then washed with 100mM $MgCl_2$ solution and re-centrifuged. The cells were again washed, this time in 10ml of 100mM $CaCl_2$ solution. The cells were then incubated on ice for 30 mins before centrifugation at 3000rpm for ten minutes. The pellet of cells was re-suspended in 1ml of 100mM $CaCl_2$ solution. These cells were aliquoted and used immediately for transformation. The cells were deemed to be transformable for upto 24 hours after this point. These cells were often frozen for later use by the addition of a 15% v/v of glycerol before snap freezing in liquid Nitrogen. The frozen aliquots of competent cells were then stored for up to 6 months at -80°C.

2.2.1.11 Transformation of competent cells

A 200µl aliquot of competent cells was used to transform either 1µl of DNA (Miniprep, 1:100 dilution) or 5µl of DNA (Ligated DNA) containing an Ampicillin resistance gene for selection. The DNA was added to the cells and this was left to incubate on ice for 30 minutes. The cells were then heat shocked at 42°C for 1 minute. After this the cells were placed on ice for 20 minutes before 1ml of warm LB was added to the tube. The LB suspension of cells was then incubated at 37°C for 1 hour in an orbital incubator. 200µl of the cell suspension in LB was then plated on to LB Agar plates containing tetracycline and ampicillin. These plates were incubated overnight at 37°C.

2.2.1.12 Colony PCR

Colony PCR is a quick way of performing a PCR directly from bacterial lysate to assess the presence or absence of a desired plasmid. A colony of interest was picked using a sterile cocktail stick and placed into a 0.6ml eppendorf tube containing 5µl of 1X Tris/Triton solution. This was heated to 95°C for 5 minutes and then cooled to 10°C. A normal PCR was then performed on the resulting lysate.

2.2.1.13 Sequencing

Sequencing reactions were performed off-site by the Source Biosciences sequencing facility at St James' Hospital, Dublin. Plasmid samples to be sequenced were diluted to 100ng/µl and 10µl of this sample was used for sequencing. Primers were diluted to 3.2pmol/µl and 10µl of each primer to be used were used for sequencing.

2.2.2 Cell Culturing Protocols

2.2.2.1 Culturing Conditions

All cell types used were grown in complete DMEM at 37°C in a humidified chamber in the presence of 5% CO_2. Procedures involving cells were carried out in a laminar flow cabinet (Bio-Sciences). Cell medium was replaced with fresh medium every 1-2 days. Growth of cells was monitored by light microscopy (Olympus CK30).

2.2.2.2 Cell Passaging

Cells were passaged when their confluency reached approximately 80-90%. Medium was aspirated from the cell monolayer which was then washed with 1X PBS. The cells were then treated with 1-2ml of 0.25% Trypsin-EDTA solution (Gibco) for 1-2 minutes at 37°C. The flask was then examined under the microscope to confirm the removal of the cells from the bottom of the flask. At this stage the cells were treated with 10ml of warm media to inactivate the trypsin. This cell suspension was pipetted up and down to break any clumps of cells that may be in the suspension. 1-5ml of this suspension was then transferred to a new flask containing warm media. This was then left to incubate until the cells reached an appropriate passaging confluency.

2.2.2.3 Cell Counting using a Haemocytometer

Cells were trypisned and resuspended in DMEM as described previously. A 20µl aliquot of the cell suspension was then taken, to which 20 µl of Trypan Blue was added. This stains dead cells, allowing one to count live cells only. The stained cell

suspension was then placed on to a haemocytometer and a coverslip was placed on top of the suspension. Live cells per 1mm square grid were counted in quadruplicate and the average of the counts was taken as the number of cells x 10^4/ml within the cell suspension. This number was then multiplied by two to take in to account the 1:1 dilution of the suspension with trypan blue.

2.2.2.4 Freezing Cells

Cells were trypsinised as described previously and resuspended in 10ml of medium. This cell suspension was then transferred to a falcon tube and centrifuged at 1000rpm for 5 minutes. The resulting supernatant medium was discarded and the cell pellet was re-suspended in 1ml of fresh medium. 1ml of freezer medium was then added dropwise to the cell suspension and the suspension was mixed. The suspension was then transferred to a Cryo Tube™ (Nunclon) and placed in a freezing container containing isopropanol. This was placed at -80°C to cool slowly over 24 hours. After this time, the cells were kept at -80°C or in liquid nitrogen for long term storage.

2.2.2.5 Thawing Cells

A Cryo Tube™ containg frozen cells was thawed in a water bath at 37°C until approximately ¾ of the vial was thawed. The cells were then transferred to 10ml of chilled complete DMEM to prevent DMSO damage. This cell suspension was centrifuged at 1000rpm for 5 minutes and the supernatant was discarded. The pellet of cells was then resuspended in 5ml of warm complete DMEM before being transferred to a cell culture flask containing warm medium. The cells were left to incubate at 37°C for 24 hours at which point the medium was changed.

2.2.2.6 Transfection using Lipofectamine 2000®

HeLa cells were plated onto a 24-well plate at a density of $2x10^5$ cells in a total volume of 500µl and left to grow for 24 hours. After this time the cells should be 90-100% confluent. The cells were then transfected according to the Lipofectamine 2000®

(Invitrogen) instructions. In the case of co-transfections, 0.4µg of DNA was added with 16pmoles of siRNA solution. The non-targeting siRNA is scramble siRNA which has no known targets in the cell line used. The sequence of this NT siRNA is 5' UUCUCCGAACGUGUCACGU 3'. The cells were harvested 24 hours after transfection.

2.2.3 RNA Protocols

2.2.3.1 General Treatment of RNA

Due to its susceptibility to degradation, RNA was treated with greater care than with a DNA sample. RNA was dissolved in nuclease free water using filtered RNase free pipette tips. RNA solutions were contained in pre-sterilised nuclease-free eppendorf tubes. The RNA was constantly kept on ice when used and stored at -20°C.

2.2.3.2 Harvesting HeLa Cells and isolation of RNA

Cells were first aspirated of medium and washed in 1X PBS. The cells were then treated with Trizol® Reagent (Invitrogen, 250µl per well), mixed and left to lyse for 10 minutes. Lysate from the 4 wells transfected with the same siRNA were then collected and pooled into an eppendorf tube. 200µl of chloroform (Scharlau) was added to the tubes and mixed with the lysate. The lysates were then centrifuged at 13,000 rpm for 20 minutes at 4°C. The resulting aqueous phase was collected and transferred to a new eppendorf tube. A 5/6 volume of isopropanol was added to the aqueous phase and mixed. This was left at room temperature for 10 minutes before centrifugation at 13,000rpm for 10 minutes at 4°C. The supernatant was discarded and the resulting pellet was washed with 1ml of 75% ethanol solution. This suspension was then centrifuged at 13,000rpm for 5 minutes. The supernatant was again discarded and the pellet left to air-dry in a laminar flow hood. The pellet was then dissolved in 50µl of nuclease-free water. This RNA solution was treated to remove any remaining DNA. 5µl of RQ1 DNase (Promega) and 6µl of RQ1 DNase buffer were added to the solution which was then left to incubate at 37°C for 60 minutes. 6.5µl of stop solution was added and the RNA solution was left to incubate at 80°C for 10 minutes to inactivate

the DNase enzyme. The concentration of RNA was evaluated using the Nanodrop™ spectrophotometer as described previously.

2.2.3.3 Harvesting Retina and isolation of Retinal RNA

Retinas were extracted from euthanized mice and immediately placed in HBSS. The lens and RPE was removed and the retina was placed in to β-Mercaptoethanol containing buffer RLT. The retinal tissue was then gently homogenised by pipetting. The extraction of RNA from the homogenised extract was then carried out using the RNeasy® Mini Kit (Qiagen) according to the methods specified by the manufacturer. On column DNA digestion was also carried out during this isolation using the RNase Free DNase set (Qiagen) according to the manufacturer's instructions.

2.2.3.4 RT-qPCR

Real Time Reverse Transcription quantitaive PCR (RT-qPCR) is a method used during the course of this PhD to detect expression level changes of genes of interest after treatment with siRNAs. The RT-qPCR technique used was one step RT-qPCR, whereby reverse transcriptase was used to create cDNA from the RNA directly before the cDNA was amplified via PCR. Two house-keeping genes were used to normalise the different samples in order to obtain relative expression changes at the mRNA level. The housekeeping genes used were *GAPDH* and *ACTB*. *GAPDH* encodes an enzyme involved in glycolysis. It is considered to be ubiquitously expressed across most cell types. *ACTB* encodes β-Actin, a protein involved in the cellular cytoskeleton. This is also considered to be ubiquitously expressed.

A reaction master mix was first generated using the QuantiTect SYBR® Green RT-PCR kit (Qiagen). This contains the DNA dye SYBR which fluoresces when bound to double stranded DNA. It is used to quantify the amount of dsDNA produced during the PCR process. The kit also contains an RT mix which contains reverse transcriptase for creating cDNA from the mRNA collected from cell lysates.

RNA samples were first diluted to 0.5-3ng/µl. RNA from the non-targeting samples and this was used to make 4 serial dilutions to create a standard curve for the gene of interest. The RNA samples for the standard curve were plated onto a 96-well qPCR plate (Applied Biosystems) in duplicate in a volume of 4.5µl. The RNA samples to be quantified were plated in triplicate in a volume of 4.5µl. A nuclease-free water well was also included as a negative control. To these wells, 15.5µl of master mix was added and mixed with the RNA samples. This Master Mix contains the enzymes and reagents required for the RT-PCR along with primers specific to the RNA of interest. The plate was covered with an optical adhesive film (Applied Biosystems) and the plate was placed into a Real-Time PCR Systems machine model 7300 (Applied Biosystems). The reverse transcription/PCR program was activated. This comprises: 20 minutes at 50°C (Reverse transcription), 95°C for 15 minutes (Activation of DNA polymerase), 37 cycles of 95°C and 60°C for 15 seconds (denaturation) and 1 minute (Annealing) respectively and 95°C for 15 seconds, 60°C for 30 seconds and 95°C for 15 seconds (Dissociation). The dissociation step is performed to determine whether or not the primers used are specific as two or more dissociation peaks at different temperatures indicate two PCR products resulting from non-specific binding. The dissociation step will also detect primer dimers. The dissociation step perfomes this task by determining fluorescence of PCR products at a range of temperatures. The detected fluorescence is then graphed against temperature, providing the melting temperature of the product. A graph exhibiting more than one peak indicates the presence of primer dimers and/or non-specific binding.

The cDNA which was amplified was relatively quantified by measuring the number of PCR cycles a DNA fragment underwent before reaching an arbitrary fluorescence threshold. The name given to the number of these cycles is the Ct value. Therefore the lower the Ct value, the higher the quantity of gene of interest cDNA. The Ct values from the serial dilution wells were used by the ABI 7300 systems software to create a standard curve. This is a best fit line using the Ct values corresponding to arbitrary quantities previously specified by the researcher. The most accurate standard curves are those with R^2 values approaching 1 and a slope of -3.33. The standard curve is then used to assign numbered quantities to the sample RNA wells bases on their Ct values.

2.2.4 Protein Protocols

2.2.4.1 Extraction of protein from HeLa cells

Plated cells were aspirated and washed with 1X PBS 48 hours after siRNA treatment. The cells were then treated with 150µl of cell lysis buffer and scraped with a plastic cell scraper (Sarstedt). The lysate was then collected and transferred to a 2ml glass specimen tube. A magnetic stirring bar was added and the lysate was stirred on a magnetic stirring plate for 1 hour at 4°C. The lysate was then transferred to a 1.5ml eppendorf tube and centrifuged at 12,000rpm for 30 minutes at 4°C. After centrifugation the supernatant was transferred to a new eppendorf tube and stored at -20°C.

2.2.4.2 Extraction of protein from Mouse Retina

Retinas were extracted from euthanized mice and immediately washed using 1X PBS. The retinas were then placed in tissue lysis buffer. The retinas were homogenised by brief sonication before the resulting homogenised tissue was centrifuged at 13,000 rpm for 30 minutes at 4°C. The supernatant of the homogenate was then removed and stored at -20°C.

2.2.4.3 Quantifying Protein Concentration by BCA Aassay

Protein from cell and tissue lysates was quantified for equal loading on to a western gel. Protein concentration was measured using the BCA assay kit (Pierce). This uses bicinochonic acid (BCA) to detect Cu^{+} ions formed by the chelation and reduction of Cu^{2+} by proteins. An intense purple colour is formed by the BCA when it is chelated to Cu^{+} ions which can then be measured by spectrophotometry at 562nm. Bovine Serum Albumin (BSA) of a known concentration (2mg/ml) is provided in the kit to create a standard curve with which to quantify the concentration of unknown protein samples.

A series of serial BSA dilutions spanning 0-2mg/ml was first generated and plated in triplicate on a 96 well flat bottom plate (Nunclon) in a volume of 10µl per well. Protein

samples were then diluted 1/5 in lysis buffer and plated in triplicate in the same volume. Each well then received 200µl of BCA Reagent before the plate was closed, wrapped in tin foil and placed at 37°C for 30 minutes.When this time elapsed, the plate was placed in to a plate reader (Rosys Anthos). This measured absorbance at 595nm at each well. Absorbances of the BSA serial dilutions were then used to plot protein concentration against absorbance. This standard curve was used to determine the concentrations of the protein samples. Finally the protein concentrations were multiplied by 5 to account for the dilution factor.

2.2.4.4 Quantifying Protein Concentration by Fluorometry.

Another method of quantifying protein was the use of the Qubit® Fluorometer 2.0 (Invitrogen). Briefly, this quantifies protein by using a protein specific fluorophore provided in the Qubit® kit according to the instructions provided by the manufacturer. The kit also provides three know protein standards against which an unknown protein sample can be analysed. However, the protein must first be diluted 1:100 as the presence of Triton-X and SDS can interfere with the absorbance readings of the protein. After dilution, 10µl of protein sample is incubated with Qubit® buffer for 15 minutes at room temperature before being placed in to the fluorometer. This then provides a concentration of protein based on the standard curve established by the known standard. The resulting concentrations are then multiplied by 100 to take in to account the dilution factor.

2.2.5 Western Blot Protocols

2.2.5.1 Preparation of SDS-PAGE Gel

Protein samples were run on a Sodium Dodecyl Sulfate (SDS) Poly Acrylamide gel to separate the proteins by size with a ladder. The gels were prepared within an AE-6450 Dual Mini Slab kit (ATTO Biosciences) cast. The cast was first thoroughly washed and

assembled using a rubber gasket and a pair of clamps. The integrity of the assembled cast was tested using water to ensure no leaks were present. The water was then drained off and the cast was dried using filter paper. A resolving gel mixture was then made and poured into the cast until the mixture level reached 3cm from the top of the plates of the gel cast. The resolving gel was then left to solidify before the stacking gel solution was made and poured over the resolving gel until it reached the top of the plates. A comb was then placed between the plates at the top of the cast in to the stacking gel and this was left to solidify.

2.2.5.2 Poly-Acrylamide Gel Electrophoresis

When sufficiently solid, the comb was removed form the gel along with the plate clamps and the gaskets. The cast containing the gel was placed into the electrophoretic chamber with largest plate facing outwards. The cast was held securely on either side of the electrodes using pressure platens. The space between the two gel casts in the electrophoretic chamber was filled with 1X Running buffer along with the lower half of the electrophoretic chamber.

Protein samples were diluted in 4X Laemmli Buffer before being heated to 95°C for 10 minutes in a heating block to denature the proteins. The pre-stained ladder (New England Biolabs) was heated to 95°C for 2 minutes. 10µl of ladder was loaded into the gel. The volume of sample loaded depended on the concentration of the protein within the sample; however the volume of sample in one lane did not exceed 20µl. This is to ensure that all sample lanes contain an equal amount of total protein and to ensure that the intesity of the band observed on the x-ray film is the outcome of experimental treatment and not of unequal loading. The gel rig was then closed and connected to a power supply (Consort EV202). The gel was run at 60mA until the dye front of the ladder reached the bottom of the gel.

2.2.5.3 Transfer of protein to blot (Semi-dry)

Immediately before the gel had finished its run, a transfer rig (AE-6688 Horizblot, ATTO) was set up. Within this, 4 pieces of filter paper (3mm chromatography paper,

Whatman) were placed on top of each other. Each piece of filter paper was soaked in 1X transfer buffer before being placed on the transfer rig. A PVDF membrane (Immobilon) was then activated by soaking in 100% methanol for 20 seconds. This membrane was placed on top of the stack of filter paper. After the gel had run, the gel cast was removed from the gel rig and the plates separated. The stacking gel was cut from the resolving gel and discarded. The resolving gel was then placed onto the PVDF membrane before 4 more transfer buffer soaked pieces of filter paper were placed over the gel. The transfer rig was closed and connected to a power pack (EV202, Consort). The transfer was run for 1.5 hours at 80mA.

2.2.5.4 Ponceau S Staining

The PVDF blot was removed from the transfer rig after the 1.5 hour time had elapsed and was placed into an open container and stained with Ponceau S solution. This stains all proteins in the blot and is used to ensure that proteins have transferred from the gel to the PVDF membrane. Stained proteins will show up as dark red bands on the blot indicating a successful transfer. The Ponceau S was then poured off of the blot and 1X TBS was added to wash the blot. The blot was left in TBS on an orbital shaker (Bellco) for ten minutes at which point the TBS was poured off and fresh TBS was added. This was repeated twice to remove all Ponceau stain from the membrane.

2.2.5.5 Blocking Western Blots

The western blot should be blocked before any immunostaining occurs to block proteins in the blot which may bind non-specifically to the antibody used against the protein of interest. The blocking agent used was a 5% milk solution (Marvel) in 1X TBS. This is added to the blot after the Ponceau S solution has been washed off the blot. The milk solution stayed on the blot for 1 hour on an orbital shaker at room temperature. The blot was then washed 4 times with 1X TBS on the orbital shaker at room temperature for 10 minutes per wash.

2.2.5.6 Specific Probing of Protein with Antibody

Primary antibody was diluted according to the manufacturer's recommendations in 10ml of blocking agent. This was then poured over the blot which was subsequently covered in tin foil and placed on an orbital shaker. The blot was left at 4°C overnight. The following morning, the primary antibody solution was poured off of the blot and the blot was washed 4 times with 1X TBS. The secondary antibody was diluted according to the manufacturer's recommendations in 10ml of blocking solution. This was then poured over the blot which was left to incubate on an orbital shaker at room temperature for 2 hours. After this time the blot was again washed 4 times with 1X TBS.

2.2.5.7 Chemiluminescent Detection of Protein Bands

The blot was taken to a dark room. Here the chemiluminescence substrate was prepared. 1ml of reagent A was mixed with 1ml of reagent B from the Amersham ECL western blotting kit (GE Healthcare). This contains luminol which is oxidised by the horseradish peroxidase conjugate of the secondary antibody. The oxidised luminol then luminesces. The reagent A/B mixture was poured over the blot and left to incubate for 30 seconds. The blot was then placed between two sheets of transparent acetate paper (Staedtler) and placed in a cassette. A sheet of X-ray film was then placed on top of the acetate containing the blot and the cassette was closed. After 1 minute had passed the x-ray film was removed and placed into developing solution (Kodak). A new sheet of x-ray film was then placed on top of the acetate containing blot to be left for a longer period of time. This was continued with longer periods of x-ray film exposure to the blot. Meanwhile the x-ray film in the developer was washed in water, placed in fixing solution (Kodak) and then washed in water again. This development process was performed for all x-ray films exposed to the western blot.

2.2.5.8 Stripping of Western Blots

In order to confirm the equal loading of each well in the western gel, the blot was re-probed with an antibody against β-Actin protein. This is a housekeeping protein which should be expressed ubiquitously and be observed as bands of equal intensity after chemiluminescence detection. Before this can be performed, the blot must first be

stripped of antibodies against the protein detected in the previous chemiluminescence detection. The blot was therefore incubated in Restore Western Blot Stripping Buffer (Sigma-Aldrich) for 30 minutes on an orbital shaker at room temperature. The blot was then washed 4 times before the anti-β-Actin antibody was applied to the blot as described previously.

2.2.6 Synthesis of Recombinant AAV 2/5

2.2.6.1 Triple Transfection

Recombinant AAV was produced using the triple transfection method described by Xiao et al, 1998. This eliminated the use of adenovirus in AAV production (see AAV section, introduction) through the use of two separate vectors along with the vector encoding the altered AAV genome containing the inserted sequences of interest. 50 150 mm cell culture plates of HEK 293 cells were grown to 90% confluency before transfection with 625µg recombinant pAAV, 1250µg pHelper and 625µg pRep2/Cap5 DNA. The appropriate volumes of these three plasmids were placed in a 50ml sterile tube. This was made up to 50ml with transfection buffer. This solution was then mixed with 50ml of transfection reagent and left to incubate at room temperature for 8 minutes. 2ml of this solution was then pipetted on to each of the 50 HEK 293 plates. These plates were returned to the cell incubator for 5 hours to allow transfection of the vectors in to the cells. After this time, the media was changed on each plate and the cells were left to incubate recombinant virus for 48 hours in the cell incubator.

2.2.6.2 Harvesting and Purification of Recombinant AAV from HEK 293 cells

After 48 hours of incubation the HEK293 containing AAV were aspirated of media and dislodged from the plate using a cell scraper. These cells were collected in 2x50ml tubes and made up to 50ml with sterile 1X PBS. The cells were then frozen at -80°C and then thawed at 37°C. This freeze/thaw was repeated twice to lyse the HEK293 cells and release the intracellular viral particles. RNase and DNase were then added to the cell lysates which were then incubated at 37°C for 30 minutes. The supernatant

containing the released viral particles was then separated from the cell debris by centrifugation at 1000rpm for 20 minutes. Deoxycholic acid (final concentration of 0.5%) was then added to the supernatant and left to incubate at 37°C for 30 minutes.

Caesium Chloride ($CsCl_2$, 454mg/ml) was then added to the supernatant. A $CsCl_2$ gradient was then set up within Polyallomer ultracentrifuge tubes (Beckman). This was performed by pipetting 9ml $CsCl_2$ solution (816.5mg/ml) in to the tube. On top of this, 9ml of $CsCl_2$ solution (548.3 mg/ml) was gently layered, taking great care not to mix the two fractions. The supernatant containing $CsCl_2$ was then gently layered on top of these fractions. These tubes were then ultracentrifuged at 26,000 rpm in a vacuum at 4°C for 18 hours (Beckman Coulter L-100 XP). The purpose of this centrifugation is to separate the viral particles from the cell lysate and other impurities.

After centrifugation, fractions from the $CsCl_2$ gradient were sequentially collected in eppendorf tubes by piercing the polyallomer tube with a 16 gauge sterile needle. These fractions were then analysed using a refractometer (Thermo Electron Corporation). This records the refractive index of the fraction which is dependent on the concentration of $CsCl_2$ present as it is known that intact and full viral particles (as opposed to capsids which are empty of DNA) migrate to a known region of $CsCl_2$ concentration during ultracentrigugation. The fractions with AAV specific refractive indexes of 1.373-1.368 were pooled and placed in to a new $CsCl_2$ gradient of 548.3mg/ml in a smaller polyallomer tube. These were centrifuged as before at 59,000 rpm. Fractions were again collected within the refractive index range of between 1.373-1.368 and pooled. This pool of viral particles was centrifuged once more at 59,000 rpm. Fractions were again collected corresponding to the refractive index range for AAV.

The resulting suspensions of virus were injected in to Slide-a-Lysers (10 KDa, MSC). These were then washed 10 times in 1L of 1X PBS. This removes the $CsCl_2$ and other small molecular weight contaminants from the viral prep. After the 10 washes the viral suspension was removed by syringe and aliquoted before being placed at -80°C for storage.

2.2.6.3 Determination of Viral Titre

In order to adequately assess the number of viral particles that will be delivered to a mouse eye, the concentration of viral genomes (vg, the viral titre) must first be evaluated. 1µl of each viral fraction is first treated with 7U of DNase (Qiagen) for 30 minutes at 37^0C. The DNase is then inactivated for 10 minutes at 70^oC. The viral preparation is then treated with 7U of proteinase K for 1 hour at 50^oC followed by enzyme inactivation at 95^oC for ten minutes. Viral titre is evaluated by qPCR of the viral DNA using a serial dilution of viral DNA of known titre. The serial dilution ranges from $2.5x10^{11}$ to $2.5x10^7$ vg/ml in 10x dilutions. A reference virus of known titre is also included in the analysis against which final titres of the samples can be normalised. The reference virus must contain a locus of the same sequence as the virus of unknown titre as this assay is PCR based. For this reason the qPCR is carried out using CMV promoter specific primers as this region is common to all viruses synthesised during the course of this study. The qPCR is then carried out as follows: one step of 50^oC for 30 seconds, one step of 95^oC for 15 minutes and 46 steps of 95^oC for 15 seconds followed by 60^oC for 1 minute. The resulting data are then used to determine the titre of the unknown virus by comparing the CT values of the unknown virus against the standard curve of the known virus and by comparing the sample values against the reference virus. The values given must also be multiplied by 1000 to take in to account dilution due to addition of DNase and proteinase K and the fact that the viral DNA will be single stranded compared to the standards which are double stranded (see AAV section, introduction). The resulting titres are given in units of viral genomes per ml (vg/ml).

2.2.7 Animal Procedures

All experiments using animals were conducted in compliance with the ARVO statement for the Use of Animals in Ophthalmic and Vision Research (http://www.arvo.org/policies/statement_for_the_use_of_animals_in_ophthalmic_and_visual_research/) and in accordance with the EU Directive for the Protection of Vertebrate Animals used for Experimental and other Scientific Purposes (86/609/EEC).

2.2.7.1 Animal Housing

All animals were housed by the staff of the Ocular Genetics animal unit under the direction of TCD Biosciences Unit. These mice were kept under Specific Pathogen Free (SPF) conditions in Individually Ventilated Cages (IVCs). These cages were kept at a constant temperature of 21°C with 12h of light and 12h of dark per day. Neonate pups were kept with their mother until fully weaned whereupon the males and females were separated in to different cages. Adult mice were kept at numbers of no more than three for males and no more than four for females in one cage. Mice were euthanized by CO_2 asphyxiation followed by confirmation of death by cervical dislocation as outlined by the Handbook of Laboratory Animal Management and Welfare (Wolfensohn & Lloyd, Blackwell Publishing). Mouse pups must be euthanized by immersion in a closed chamber containing a volatile anaesthetic followed by decapitation to confirm death.

2.2.7.2 Mouse Genotyping

Mouse genotyping was carried out subsequent to extraction of genomic DNA from tail or ear clips. The DNA was extracted using the ReliaPrep® gDNA Tissue Miniprep System (Promega). Briefly, mouse tissue was placed in to an eppendorf containing 100µl of tissue lysis buffer with 20µl of proteinase K. This was vortexed and placed at 56°C overnight. The sample was then centrifuged at 8,000 rpm for 5 minutes to remove any remaining tissue and the supernatant was taken. The DNA was then extracted according to the manufacturer's protocols. Transgene specific PCR was then carried out on the extracted DNA and the PCR products were run on a gel to determine genotype.

2.2.7.3 Subretinal delivery of AAV

All subretinal injections of AAV were carried out by Dr Paul Kenna. Prior to injection, adult mice were given anaesethic via i.p. injection. The eyes were then covered with a topical hydrating and dilating agent and covered with a cover slip. A small puncture was then made in the sclera and 3µl of AAV suspension in sterile 1X PBS was

delivered to the subretinal space via 34 gauge needle. This causes a localised retinal detachment which typically resolves over the course of the following 48 hours. Following injection, the mice were injected with anaesthesia reversing agent, placed under a heat lamp (as anaesthesia induces a drop in core body temperature) and monitored until recovery.

Newborn mice were first chilled on ice to induce anaesthesia. Since mice do not open their eyes fully until at least P10 a small cut is made on to the eyelid. AAV is then delivered to the subretinal space. The mice were then warmed at 33°C for 30 minutes before being returned to their mother.

2.2.7.4 Electroretinography

All electroretinography was carried out Dr Paul Kenna. Prior to ERG recording, the mice to be analysed were dark adapted for 12 hours and all analyses were carried out under dim red light to eliminate external light interfering with the results of the procedure. Mice were anaesethised via i.p. injection and the eyes were dilated and small contact lens electrodes were placed on the corneas of the eyes (Goldwire electrodes, Roland Consulting). A ground electrode was placed on the tail and a reference electrode was placed 1mm from the temporal canthus (the region of the cornea at the edge of the eye where the eyelids meet). The responses of both eyes were recorded simultaneously with a full visual field flash of light. Rod-mediated (scotopic) responses were recorded using a dim flash of white light of flash intensity of 3 candelas/m^2/s at an intensity of -25dB. The mixed rod/cone response was then measured using maximal intensity. The eyes were then adapted to light of 30 candelas/m^2 for 30 minutes before the cone mediated response was recorded using maiximal flash intensity. The a-wave was measured from its peak to the basleine while the b-wave was measured from either the a-wave or from the baseline (to measure scotopic response).

2.2.8 Histology and Immunohistochemistry

2.2.8.1 Fixing Retina using Paraformaldehyde and Sectioning

Mice were euthanized and the eyes enucleated using forceps and the eyes were placed in 1X PBS to wash. The eyes were then placed in 4% paraformaldehyde for 4 hours at room temperature or overnight at 4°C. After this time, the Pfa was replaced with 1XPBS. At this point a corneal incision was made at the iris and the lens was removed. The eyes were then washed 3 times for 5 minutes each in 1x PBS. The eyes were placed in 10% sucrose (Fluka Analytical) solution for 30 minutes. Subsequently. the eyes were placed in 20% sucrose solution for 1 hour. Finally the eyes were placed in 30% sucrose solution overnight at 4°C. An equal volume of OCT (Optimal Cutting Temperature, VWR) solution was added to the sucrose solution and the eyes were rotated for 30 minutes at room temperature. The eyes were then placed in casts containing OCT. The eyes were adjusted to the desired orientation before the cast was placed in a plastic container containing isopropanol. This plastic container was then placed in liquid Nitrogen. This reduces the temperature of the OCT compound, freezing it and encapsulating the eyes within the OCT. The isopropanol slows the freezing process slightly to reduce the chance of cracking the cast and to preserve the integrity of the OCT blocks. The eyes were then sectioned into 12µm sections using a cryostat (Model CM1850, Leica). The sections were placed onto a Poly-D Lysine coated glass slide (Thermo Scientific) and left to dry. The slides loaded with the sections were left at -20°C.

2.2.8.2 Immunostaining the Retina

Slides loaded with sections were removed from -20°C and left to dry for 10 minutes at room temperature. The slide borders were marked with PAP pen. Blocking solution (5%) was placed over the sections and the sections were placed in a humidified chamber for 1 hour at room temperature. The blocking solution was then removed by tapping the side of the slides against absorbent paper. Antibody solution containing antibody of appropriate dilution was then placed over the sections and the slides were placed back in the humidified chamber. The chamber was incubated at 4°C overnight for primary antibody binding. The slides were then washed for 5 minutes, 3 times with 1x PBS. The secondary antibody solution was then added to the sections and the slides

were placed back in the humidified chamber to incubate at room temperature for 2 hours. The chamber was covered in tin foil to keep the sections in a dark environment. Slides were washed in 1x PBS before DAPI stain (Sigma, 1:10,000) was applied to the slides and left to incubate at room temperature for 5 minutes. The slides were then washed twice for 5 minutes in 1x PBS before mounting solution was placed over the sections and a coverslip placed over the sections. Sections were immediately examined under the fluorescent microscope if possible. If not the sections were placed at 4°C until required. Slides were not examined after 48 hours from secondary antibody staining.

2.2.9 Statistical Analysis

An unpaired two way student's t-test was used to evaluate the p-values attached to the mRNA suppression analysis *in vitro* and for the DHE staining analysis comparing wild type mice to mouse models of retinal degeneration. A paired two way student's t-test was employed when comparing data between the left (control treated) and right (AAV treated) eyes. P-values were calculated using Data Desk version 6.0. A p-value of ≤ 0.05 was determined to be statistically significant. For statisitical analysis using ANOVA, the Prism v5.01 program was used to assess significance. This was used for comparison of the effect of different dilutions of AAV on the ERG response of injected animals. The n number for all experiments is presented as the number of animals examined for a particular experiment. ERG analyses are time consuming and can be time sensitive if repeated over the course of days. Therefore for each animal only one set of results was collected for each animal at a given time-point. Quantitaive DHE analysis was undertaken by examining 9 micrographs for each experimental animal used. All other experiments (such as RNA and western blot band intensity experiments) were carried out three times on each sample where the n number in these experiments refers to the number of experimental animals.

Chapter 3: Suppression of *Rac1 in vitro* and *in vivo*

3.1 Introduction

The NADPH Oxidase complex is a group of five proteins which bind together to form an enzyme which produces superoxide (O_2^-) by transferring an electron to molecular oxygen (O_2). This enzyme complex was first discovered in phagocytes which were shown to create a respiratory burst in response to engulfing of bacteria. O_2^- serves a number of bactericidal functions such as generating H_2O_2 as a co-substrate for peroxidases in neutrophils, monocytes and eosinophils. In neutrophils, O_2^- reacts with chlorides to form HOCl which is itself a strong antimicrobial agent (Babior et al, 2002). This respiratory burst was shown to be absent from patients with the disease Chronic Granulomatous Disease, leading to the first identification of a protein in the NADPH Oxidase complex, NOX2 (Segal et al, 1978). This catalytic subunit (also known as $gp91^{phox}$) was soon found to have a number of homologs (NOX1, NOX3, NOX4, NOX5, DUOX1 and DUOX2) which could also act as the catalytic subunit of the NADPH Oxidase. The NADPH Oxidase complex also consists of a transmembrane anchoring protein ($p22^{phox}$), and two scaffold proteins ($p67^{phox}$ and $p47^{phox}$). $p67^{phox}$ and $p47^{phox}$ also have two homologues NOXA1 and NOXO1 respectively which function with NOX1 and DUOXA1 and DUOXO1 which interact with the DUOX proteins. This complex is then activated by the G-protein Rac1, or its homologue Rac2. In 1993, a sixth component was discovered, $p40^{phox}$, however the action of this cytosolic protein is not required for activation of the complex. The function of this protein may be redundant with the role of $p47^{phox}$, as a wildtype phenotype is preserved in $p47^{phox}$ murine knockout models through the action of $p40^{phox}$ (Fan et al, 2009).

The current model of the NADPH Oxidase complex is as follows: NOX2 is constitutively bound to $p22^{phox}$, both of which are transmembrane proteins. $p47^{phox}$ is then activated by phosphorylation of the specific serine residues S303, S304, S359 and S370. Phosphorylation of $p47^{phox}$ is carried out by protein kinase C and to a lesser extent by the kinase Akt. Phosphorylation causes the protein to change conformation, exposing two SH3 domains, a Proline Rich Region (PRR) and a Phox Homolgy (PX) domain. The SH3 domains then interact with $p22^{phox}$ and the PX domain interacts with the cell membrane which together cause translocation of $p47^{phox}$ to the assembling NADPH Oxidase complex. The PRR domain interacts with the SH3 domains of

$p67^{phox}$ causing translocation of this protein to the complex. Finally, Rac1 is localised to the complex through binding to the tetricopeptide repeats (TPR) of the $p67^{phox}$ protein. $p67^{phox}$ also recruits $p40^{phox}$ to the complex, completing the assembly of the NADPH Oxidase (Bedard & Krause, 2007). $p47^{phox}$ is therefore responsible for assembly of the proteins of the complex whereas $p67^{phox}$ is responsible for transferring an electron from NADPH to $gp91^{phox}$. $gp91^{phox}$ then transfers this electron to O_2 to form superoxide (see figure 3.5.1).

The main activator of the NADPH Oxidase complex is the Rac1 Rho GTPase. This protein plays a role in actin re-organisation, axonal guidance, cell migration, DNA synthesis and cell transformation (Bosco et al, 2009). Apart from superoxide production through activation of NADPH oxidase, the main role of Rac1 is in cell cytoskeletal dynamics by directing actin at the leading edge of cells (in particular, neurons; deCurtis, 2008). Like all GTPases, Rac1 is itself activated by Guanine-Exchange Factors (GEFs) of which there are several which activate Rac1 (Schmidt & Hall, 2002). This protein is crucial for activation of the Nox2 containing NADPH Oxidase whereas Rac1 only increases superoxide output of Nox1 containing NADPH Oxidase and is not required for production of superoxide (Miyano & Sumimoto, 2007). Of the seven NOX proteins expressed in humans, only NOX2 and NOX4 have been shown to be expressed in the retina (Groeger et al, 2009). Given the role that Rac1 has in activation of NADPH Oxidase, it has been proposed that this protein may play a role in oxidative stress in many tissues. It has previously been mentioned that Rac1 is involved in photo-oxidative damage in rods (section 1.8, Balasubramanian N & Slepak VZ 2003; Haruta et al, 2009). Evidence for the role of Rac1 in retinal degeneration first appeared in a paper which detailed the delay of cone death in a retinal degeneration model after inhibition of the NADPH Oxidase (Usui et al 2009). The authors used apopcynin to inhibit the NADPH Oxidase complex in the retinas of transgenic *rd1* mouse models of RP carrying the mutant PDE involved in the visual transduction cascade (see section 1.3). This reduced levels of oxidative stress and delayed the onset of cone cell death. Furthermore, depletion of Rac1 in a *Rac1* knockout transgenic mouse confers protection to photoreceptors exposed to photo-oxidative damage (Haruta et al, 2009). These data provide a stong suggestion that lowering the retinal levels of Rac1 results in benefit to both rods and cones in models of oxidative stress induced retinal degeneration. Rac1 is known to be involved in Age-Related Macular

Degeneration (AMD) by acting downstream of VEGFR within the RPE and facilitating invasion of choroidal cells into the RPE, the first step of neovascularisation which causes blindness in patients of AMD (Wang et al, 2011). Furthermore, Rac1 plays a role in neurite outgrowth of cones during normal eye development (Oblander & Brady-Kalnay, 2010).

Given the role of the NADPH Oxidase and Rac1 in the generation of superoxide in the retina, it was decided to create RNAi molecules which target the *Rac1* mRNA with the aim of reducing oxidative stress mediated retinal damage in transgenic RP mouse models. RNAi mediated suppression of other components of the NADPH Oxidase has already demonstrated a reduction in oxidative stress related injury in other models of retinal degeneration. Li et al (2008) reported a 75% reduction in the occurrence and spread of neovascularisation in laser induced CNV models of mice which had received a shRNA targeting $p22^{phox}$ by sub-retinal AAV delivery. This suppression reduced oxidative stress mediated expression of VEGF in the RPE of these mouse models of AMD which in turn reduced neovascularisation. Li et al (2010) have also shown a reduction in oxidative stress mediated neovascularisation in the db mouse model of diabetes by delivering shRNA against Nox4 by intravitreal adenoviral delivery. Injection of this virus caused a decrease in the activity of NADPH Oxidase, a reduction in vascular permeability, a reduction in VEGF expression and an overall reduction in neovascularisation. Groeber et al (2009) have shown that siRNA mediated suppression of Nox2 and Nox4 reduced production of H_2O_2 in 661W cells, a retina derived cell line. However the viability of the cells which had received these siRNAs was not examined. The siRNAs designed within this thesis were tested for suppression efficacy against *Rac1 in vitro* and shRNA constructs based on successful siRNA sequences were synthesised and incorporated in to an AAV genome for subsequent investigation of shRNA efficacy *in vivo*. Furthermore these AAV preparations were examined for any effect they may have on the visual function of a mouse model of RP.

3.2 Materials and Methods

All materials used within the methods detailed in this chapter are listed in section 2.1.

3.2.1 Cloning of the *RAC1* gene in to pcDNA3.1+

To obtain a measurable quantity of *RAC1* mRNA and protein in HeLa cells, it was decided to clone the *RAC1* gene in to a eukaryotic expression vector named pcDNA3.1. *RAC1* was first sequenced using Rhodopsin promoter specific primers from an expression plasmid kindly provided by Dr Naomi Chadderton of our research group. It was known that *RAC1* was under the control of the Rhodopsin promoter in this plasmid and therefore a primer directed at this segment of DNA should sequence through the *RAC1* gene. The primer used was MRPR2 (Mouse Rhodopsin Promoter Reverse 2). Sequencing revealed an absence of suitable restriction sites either upstream or downstream of this gene, immediately eliminating the possibility of directly excising the gene from the expression plasmid and ligating it in to pcDNA3.1. Sequencing also revealed that the full sequence of the gene was not present in this plasmid. Rather, the coding sequence or CDS from the start to stop codon of human *RAC1* was present. This sequence corresponds to nucleotides 242-820 of the *RAC1* cDNA sequence (NM_006908). It was therefore decided to PCR amplify the human *RAC1* CDS from this plasmid using primers that would bind to either end of the gene. These primers would also contain unique restriction sites upstream from the primer binding sites that could facilitate the cloning of the amplified gene in to pcDNA3.1+. The sites chosen were *HindIII* and *XbaI*.

3.2.2 Co-Transfection of siRNAs and CMV_RAC1

HeLa cells were co-transfected using Lipofectamine® transfection reagent as outlined in section 2.2.2.6. The wells were treated with the transfection mix according to the plate schematic presented in table 3.2.1. Briefly, for each column of 4 wells treated with the same reagents 1.8µg of CMV_RAC1 DNA and 72pmol of siRNA were mixed and the total volume of the mixture was made up to 225µl with Optimem. In a separate eppendorf tube, a lipofectamine mix was made up by diluting Lipofectamine reagent 1:25 in Optimem. Each tube was incubated at room temperature for 5 minutes. 225µl of the lipofectamine mix was then pippetted in to each siRNA mix. This was pippetted

up and down and incubated at room temperature for 30 minutes. 100µl of the mixture was then pipetted dropwise on to each well as detailed by the plate schematic presented in table 3.2.1. The cells were incubated at 37°C for 24 hours or 48 hours prior to harvesting of cells for RNA or protein extraction respectively.

3.2.3 Isolation of RNA from HeLa Cells

Cells that had been treated with siRNA were harvested as outlined in section 2.2.3.2. RNA was extracted using Trizol, treated with DNase and the concentration recorded using the Nanodrop. RNA concentrations of pooled wells usually ranged from 100-300ng/µl.

3.2.4 RT-qPCR analysis of HeLa cell RNA

RNA harvested from HeLa cells was analysed by RT-qPCR as outlined in section 2.2.3.4. Serial dilutions were created by diluting NT (non-targeting) RNA 1:20 in nuclease free water. This dilution was assigned the arbitrary quantity of 125 and three further serial 5X dilutions of this solution were made and assigned the quantities 25, 5 and 1. All RNA samples to be quantified were diluted to a concentration of 2ng/µl. All standards were pipetted in to duplicate wells and all unknown samples were pipetted in to triplicate wells. A negative control containing RT mix and nuclease free water was also included.

3.2.5 Isolation of Protein from HeLa Cells

Protein was harvested from HeLa cells as outlined in section 2.2.4.1. Each column of wells of the 24-well plate was pooled. The lysates of cells which received NT siRNA and CMV_RAC1 were used as both a positive control of CMV_RAC1 driven *RAC1* expression and a negative control of siRNA efficacy. The lysates from un-transfected cells were used as a negative control of exdogenous *RAC1* expression. All protein samples had their respective protein concentrations analysed by BCA assay (see section 2.2.4.3) to ensure equal loading of total protein on to the SDS-PAGE gel.

3.2.6 Western Blotting

Western blotting was carried out as outlined in section 2.2.5. Briefly, all lysate samples to be run on the gel were boiled for ten minutes in SDS containing buffer to induce denaturation. Due to the relatively small size of the RAC1 protein (21kDa), the semi dry transfer was undertaken for one hour only at 80mA (for two blots) to prevent RAC1 protein from passing through the PVDF membrane completely. The primary antibody used to probe for RAC1 was chicken anti-RAC1 (Abcam). Due to the relatively high expression of RAC1 in the lysates from cells which received CMV_RAC1 plasmid, these blots were exposed to x-ray film for no longer than 30 minutes. After this time, the RAC1 specific band would begin to 'burn off' the x-ray film (disappearance of the band on the x-ray film due to overexposure to the western blot). Subsequent to probing of RAC1, the blot was stripped and re-probed overnight using an actin specific antibody (Abcam). This was performed to ensure equal loading of protein lysates in to each well of the western gel.

3.2.7 Annealing of oligonucleotides

Oligonucleotides were resuspended in annealing buffer at a final concentration of 10pmol/µl. This was incubated at 95°C for 5 minutes before incubation at 18°C overnight. The annealed construct was then purified using the Fermentas PCR purification kit. The annealed oligonucleotide construct was subsequently cloned into the pSuper plasmid.

3.2.8 Immunohistochemistry

Immunohistochemistry was carried out as detailed in section 2.2.8. For antibody staining of the Rac1 protein, a modified protocol was undertaken for some experimental eyes. For this protocol, the eyes were fixed in 4% Pfa with 5% v/v acetic acid (Sigma-Aldrich). Subsequent to fixation and sectioning, the slides were covered with ice-cold 4% Pfa with 2% acetic acid solution and incubated at room temperature for 30 minutes. The slides were washed 2x5 minutes with PBS before being covered in ice cold 5% v/v acetic acid in ethanol and incubated at room temperature for two minutes. The slides were again washed 2x5 minutes in PBS. The slides were then

blocked in 8% BSA v/v in PBS for thirty minutes at room temperature. Subsequently, the slides were probed with anti-Rac1 antibody as outlined in section 2.2.8.

A stain for a cone specific lectin was also undertaken in this chapter using the Peanut Agglutinin (PNA) probe (Invitrogen). The PNA probe requires no secondary antibody as it is already bound to a fluorophore. Therefore, the slides were mounted with coverslips following washing of the PNA solution and viewed immediately by fluorescent microscopy.

The dilutions of antibodies used in this chapter are listed below.

Primary

Mouse 4D2 rod-specific antibody: 1:100

PNA: 1:500

Mouse Rac1 (Millipore): 1:100

Chicken Rac1 (Abcam): 1:100

All secondary antibodies and their dilutions used are listed in section 2.1.9. These antibodies were tested for unspecific staining to ensure that any primary antibody staining was specific and not a result of secondary antibody binding to epitopes within the retina. The results of this test are presented in figure 3.5.5.

3.3 Results

3.3.1 Design of siRNAs targeting *RAC1*

Three siRNAs were designed to target *Rac1* mRNA using online programs designed to provide siRNA sequences based on a number of criteria which contribute to high efficacy and silencing potential (for more information regarding efficacy parameters of siRNAs see Birmingham et al, 2007). The siRNAs were also designed against regions of homology between mouse, human and pig *Rac1* coding sequence regions should the siRNA be used in further studies in large animal models or in potential human clinical trials. The sequences of *Rac1* used to generate siRNA sequences were taken from the NCBI UniGene database of coding sequences (http://www.ncbi.nlm.nih.gov/unigene/). The accession numbers of each sequence are as follows: Human NM_006908, Mouse NM_009007 and Pig AK_231937.1. The first two siRNA sequences (RAC1_1 and RAC1_2) were designed using the Genscript Corporation siRNA target finder (http://www.genscript.com/siRNA_target_finder.html). The third siRNA (RAC1_3) was found using the Dharmacon siRNA tool (http://www.thermoscientificbio.com/design-center/?redirect=true, now owned by Thermo Scientific). RAC1_1 targeted nucleotides 517-535 of the human *RAC1* sequence, a region of complete homology between human and mouse but containing three mismatches to the pig sequence. RAC1_2 targeted nucleotides 806-824 of the human *RAC1* sequence, a region of homology between all three species. RAC1_3 targeted nucleotides 788-806 of the human *RAC1* sequence, however this region is homologous between human and mouse only. siRNA molecules with these sequences were subsequently obtained from Ambion with HPLC purification to ensure high purity. The siRNA molecules also had 3' overhangs of dTdT which has been shown to be important for efficient silencing in mammalian cells (Elbashir et al, 2001). The siRNA molecules were shipped pre-annealed to form a dsRNA molecule. The siRNAs were then dissolved to a final concentration of 100μM in nuclease free water and kept at -80°C. Aliquots for ready use were kept at a concentration of 20μM at -20°C. The siRNA sequences are provided in table 3.5.2 and their homology to the mRNA sequences of human, mouse and pig *Rac1* sequences is provided in figure 3.5.2.

3.3.2 Expression of Rac1 in the Wildtype Retina

Prior to further work being carried out in testing siRNAs *in vitro*, it was decided to examine the retinas of wildtype mice to determine the expression pattern of Rac1 in these mice. This is important as sufficient expression of Rac1 must be present in the retina for RNAi mediated suppression to have any functional or physiologically relevant results. Therefore three wildtype strain 129/SvHsd mice were euthanised at 4 weeks of age and the eyes were enucleated and immunostained with anti-Rac1 antibody (Millipore) as outlined in section 2.2.8. A no primary antibody control was also included in the analysis. A representative image of both the Rac1 immunostain and the no primary antibody control are shown in figure 3.5.6. This shows expression of Rac1 across all layers of the retina, with slightly higher expression in the nuclear layers of the retina (ONL, INL and GCL). These layers are marked by the blue DAPI stain that is overlaid on these images. The immunostain seems also to be specific as the no antibody control shows no staining. This result is promising as the AAV 2/5 containing an RNAi agent targeted against *Rac1* will preferentially transduce the ONL, where Rac1 expression appears to be quite high.

3.3.3 Cloning of the *Rac1* Gene in to a Mammalian Expression Vector

Prior to the testing of suppression of the three siRNAs targeting *Rac1*, the *Rac1* gene coding sequence (ie the Open Reading Frame, ORF) was cloned in to an expression vector in order to allow co-transfection of both the siRNA and the target gene in to HeLa cells. The coding sequence of *Rac1* (CDS, the sequence of the gene from start to stop codons excluding introns) was present in a vector already present in the laboratory from a previous collaboration. This plasmid was sequenced to confirm the presence of *Rac1*. Sequencing revealed presence of the complete sequence of the human *RAC1* CDS (see appendix). Primers containing the cloning restriction sites (*XbaI* & *HindIII*) were designed against each end of the CDS. The CDS was subsequently PCR amplified and cloned in to the pcDNA3.1+ mammalian expression vector using the *XbaI* and *HindIII* restriction enzymes. This placed the *Rac1* CDS downstream of the Cytomegaloviris (CMV) promoter, a promoter which induces strong expression of downstream sequences in eukaryotic cells. A schematic of this new plasmid, termed CMV_RAC1, is presented in figure 3.5.3 and shows the relative position of the human *RAC1* gene, promoter and the restriction sites used for cloning. This plasmid was

sequence verified (see appendix) and restriction digest verified (see figure 3.5.4) before it was maxi-prepped for later use in co-transfections.

3.3.4 Suppression of *RAC1* mRNA in HeLa Cells

HeLa cells were co-transfected with CMV_RAC1 plasmid DNA and the three *RAC1* specific siRNAs in 24 well plates using the lipofectamine transfection reagent. Transfections were repeated 3 times to evaluate RNAi-mediated suppression at the mRNA level via Trizol extraction. RNA harvested from treated cells was analysed by RT-qPCR using *RAC1* and *ACTB* (the gene encoding β-Actin, a housekeeping gene used to normalise expression quantities from sample to sample) specific primers. This demonstrated only one peak on the dissociation curve for both sets of primers (presented in figures 3.5.7 and 3.5.8). The melting temperature of the *RAC1* amplicon which was produced by the dissociation analysis was approximately 77°C, a figure which closely mirrors the melting temperature of 78°C calculated *in silico* (http://www.promega.com/techserv/tools/biomath/calc11.htm). The standard curve for *RAC1* amplification had a slope of -3.237 and an R^2 value of 0.993 (figure 3.5.9). The standard curve for *ACTB* amplification had a slope of -3.00 and an R^2 value of 0.994 (figure 3.5.10). These data indicate reliable and specific primer binding and amplification of either *RAC1* or *β-Actin* mRNA derived cDNA as the slopes of each standard curve closely approached the 'ideal' slope of -3.33, which would indicate 100% efficiency.

The standard curve data were then used to quantify relative mRNA transcript levels of both *RAC1* and *ACTB* in each of the treated samples. The quantity data from the *ACTB* samples were used to normalise the quantity data from the *RAC1* data. Since *ACTB* is a house keeping gene with ubiquitous expression, this normalisation allows for discrepancies in well loading to be minimised. These data demonstrated *RAC1* suppression of approximately 74%, 75% and 76% for the siRNAs RAC1_1, RAC1_2 and RAC1_3 respectively, compared to the NT quantities which were set at 100% for the purpose of expression analysis (figure 3.5.11). A standard two way unpaired student's T-test performed on the raw data of these results showed all three values correspond to a P-value of less than 0.05 confirming statistical significance. It was later

discovered that the primers specific to *RAC1* were picking up endogenous mRNA only, as one of the primers bound to an exon which lay downstream of the *Rac1* coding sequence. Since the CMV_RAC1 plasmid contained only the CDS of the *RAC1* gene, the primers must have only been amplifying endogenous mRNA and therefore figure 3.5.11 demonstrates suppression of endogenous *RAC1* expression in HeLa cells. Therefore, a new reverse primer (Rac1_gR_new) was ordered which would bind to both the CDS of the *RAC1* gene and to endogenous *RAC1* mRNA and hence amplify mRNA produced both endogenously and exogenously. Again, the standard curve and dissociation curve of this new primer set were analysed. This showed that the new primer pair also produced only one amplification product (figure 3.5.12) whilst the standard curve (figure 3.5.13) of the serial RNA dilutions had a slope of -3.55 and an R^2 value of 0.971. These standard curve values were somewhat less precise than that which was achieved with the previous set of primers but still fall within the range of values which may be taken as accurate. A set of three repeat transfections were carried out in HeLa cells as before and the RNA isolated from each well. RT-qPCR analyses of these data demonstrated suppression of 68% and 53% for RAC1_1 and RAC1_3 respectively compared to control treated samples, which is presented in figure 3.5.14. RAC1_2 RNA was not included in the repeat analyses for reasons which will be explained in section 3.3.5. Again, a student's T-test performed on the raw data for each suppression figure produced a statistically significant P-value figure of less than 0.05 between the *RAC1* specific siRNA treated cells and the NT siRNA treated cells. These data suggest less efficient suppression of *RAC1* than what was originally demonstrated with the endogenous pre-mRNA specific primers. This may be explained by the fact that the new set of primers is detecting not only endogenous mRNA but also the mRNA produced from the CMV_RAC1 plasmid. It can be observed from figure 3.5.14 that cells which received NT siRNA and CMV_RAC1 plasmid expressed ~25-fold more *RAC1* mRNA than untransfected cells which express endogenous levels of *RAC1* only.

3.3.5 Suppression of *RAC1* Protein in HeLa Cells

In order to confirm suppression of RAC1, a western blot was performed on cell lysates from siRNA transfected HeLa cells. This was undertaken to demonstrate that RAC1 protein production is downregulated as a direct result of knock down of *RAC1* mRNA transcripts. A set of three transfections was carried out as before and western blots were carried out for each transfection, with the same result gained each time. The results of a representative of one of these western blots are presented in figure 3.5.15. For each lane which was loaded with protein lysate, β-Actin protein was also probed with a specific antibody. This allows the researcher to visually confirm equal loading of all samples. It can be observed from figure 3.5.15 that probing for β-Actin produced five lanes of equal density. These data further validate the observed RT-qPCR data demonstrating efficient suppression of *RAC1* mRNA (Figure 3.3.11) but at the protein level. Lane 3 which contained lysate from RAC1_1 and CMV_RAC1 treated cells showed a very faint band at 21kDa corresponding to RAC1 protein, similar to that seen in the lane loaded with lysate from untransfected cells. Lane 5 which was loaded with lysate from RAC1_3 and CMV_RAC1 treated cells shows no band at all, suggesting that this siRNA is the most potent as evaluated by western blot analysis.

However, the lane which was loaded with cell lysate from CMV_RAC1 DNA and RAC1_2 siRNA treated cells displays a heavy band corresponding to RAC1 protein at 21kDa, similar to what has been observed in the positive control lane (NT) which received the non-targeting siRNA and CMV_RAC1 DNA. This suggested that RAC1_2 siRNA did not suppress at all, in direct contradiction to the initial RT-qPCR results of cells treated with the same DNA and siRNA. Further investigation revealed that RAC1_2 siRNA had been targeted against an exonic region of the *RAC1* gene lying downstream of the *RAC1* CDS and therefore would suppress only endogenous mRNA. Due to an oversight in intial primer design, the initial experiments detailing suppression of *RAC1* mRNA were such that only endogenous RAC1 expression could be evaluated, therefore these data demonstrated efficient RAC1_2 siRNA mediated suppression since RAC1_2 would only bind to endogenous mRNA. The western blot data shown here brought these siRNA and primer design discrepancies to light, allowing a new set of RNA experiments to be carried out with revised primer design as described previously (see figure 3.3.14).

3.3.6 Design of shRNA oligonucleotides

For suppression of *Rac1* to be evaulated *in vivo*, shRNA constructs were assembled for cloning in to the pAAV_MCS plasmid, a cloning plasmid based on the AAV2 genome which is frequently used in the laboratory to create recombinant AAV DNA containing a transgene of choice. These constructs were created by designing oligonucleotides containing a shRNA sequence based on the sequences of the siRNAs which were deemed to be successful *in vitro* (see section 3.5.16 for the *Rac1* shRNA oligonucleotide sequences). Two oligonucleotide sequences were designed for each siRNA chosen; RAC1_1 and RAC1_3. These oligonucleotides contained both the siRNA sequence and the reverse complement sequence of the siRNA separated by a short string of nucleotides. This would therefore form a shRNA duplex containing a stem loop structure when transcribed from a pAAV vector *in vivo*. The second oligonucleotide is designed to bind to the first oligonucleotide to form a dsDNA molecule suitable for ligation in to a pre-digested plasmid. The oligonucleotides were also designed in such a way as to leave overhangs on either end of the dsDNA molecule. These overhangs form an open restriction site (sticky site) which may bind to a sticky site formed by restriction digest of a vector of choice. These overhangs were therefore used to clone the dsDNA shRNA molecules in to the pSuper vector, as first demonstrated by Brummelkamp et al, 2002. The plasmid restriction sites chosen for this were *BglII* and *HindIII*. The oligonucleotides were annealed as described in section 2.2.

3.3.7 Cloning of the RAC1 shRNAs in to pAAV_MCS

All shRNAs used in this laboratory are typically expressed from the H1 promoter, a polymerase III promoter first described to express shRNAs by Brummelkamp et al, 2002. This allows for stringent expression of short transcripts such as shRNA. The H1 promoter is present in the MCS of the pSuper vector (Oligoengine) and therefore the shRNAs were cloned in to the MCS of this vector using the *BglII* and *HindIII* sites present on either end of the shRNA duplex and within the pSuper MCS (see figure 3.5.17). The region encoding the shRNA, H1 promoter, PGK promoter and EGFP of these newly cloned plasmids (pSuper_EGFP_Rac1_1/3) was then excised using *HindIII* and *AflII* sites. These sticky sites were blunted by filling in the nucleotides

complementary to the nucleotide overhangs using Klenow enzyme and T3 polymerase. Meanwhile a non essential region of the pAAV vector was excised using *NotI* restriction sites. These create blunt nicks in DNA (ie no 5' or 3' overhangs) and therefore the excised region from pSuper which had been blunted could be cloned between these *NotI* sites. These new plasmids were named pAAV_shRAC1_1 and pAAV_shRAC1_3. All newly cloned vectors were restriction digested and sequenced (see appendix) prior to proceeding to ensure the desired sequence had been obtained. Restriction digests were carried out using the *PstI* and *EcoRI* enzymes to confirm the integrity of the AAV plasmid. Due to the repeat sequences of the ITR fragments present, the AAV plasmid is prone to homologous recombination during cloning and mega-preparation (Yan et al, 2005). Therefore the plasmid is digested with these enzymes and run on an agarose gel after miniprepping positive colonies and megaprepping prior to the process of viral production. Obtaining full length bands as predicted using the restriction map of the completed vector demonstrates that no recombination has occurred as smaller than expected bands or bands of the incorrect size would appear if recombination had resulted in splitting the vector in two or reversing the orientation of the insert sequence respectively (see figure 3.5.21 for a representative image of a restriction digest of another pAAV plasmid examined during the course of this study). The final pAAV_shRAC plasmids were mega-prepped to create sufficient quantities for triple transfection of HEK293 cells and harvesting of AAV with this recombinant genome.

3.3.8 shRNA mediated Suppression of *RAC1 in vitro*

Each shRNA was evaluated for suppression efficacy in HeLa cells prior to production of AAV using these plasmids. To do this, the NT20, pAAV_shRAC1_1 and pAAV_shRAC1_3 plasmids were transfected in to HeLa cells. NT20 is a non-targeting AAV plasmid whose shRNA is based on 'scramble' siRNA sequence which does not target any known mRNA sequences (see section 2.1 for sequence). The NT20 plasmid is used to produce non targeting AAV for use in experiments examining the effects of a particular shRNA *in vivo* and therefore acts a control. CMV_RAC1 plasmid was not co-transfected in to these cells with the AAV plasmids as the efficiency of a successful transfection of two plasmids to each cell in a particular well is quite low due to the

limitations of the transfection reagent in delivering large plasmids. However it was known that suppression of endogenous *RAC1* expression could be observed as suppression of endogenous mRNA had previously been demonstrated using the *RAC1* specific siRNAs (see figure 3.5.11). Wells of HeLa cells were again transfected with 0.4µg of DNA in quadruplicate and RNA was harvested from these cells for RT-qPCR analysis using the Rac1_gF and Rac1_gR_new primers. The resulting data are presented in figure 3.5.18. These data show relative suppression values of 34.66% and 37.66% for pAAV_shRAC1_1 and pAAV_shRAC1_3 respectively. The suppression values fail to closely mirror the higher values achieved using the RAC1_1 and RAC1_3 siRNAs and CMV_RAC1 plasmid. However it must be noted that for a plasmid the size of pAAV_shRAC1/3 (~4.5kb) 0.4µg of DNA is 0.28pmole. Therefore the number of plasmids delivered to a well of HeLa cells is ~57 times less than the number of siRNA molecules that were delivered in earlier experiments. Although many copies of the shRNA are produced by H1 promoter mediated expression in these cells, the shortfall in the initial number of plasmid molecules compared to siRNA molecules results in fewer HeLa cells being transfected. siRNAs are also much smaller molecules and will therefore permeate the cell far easier than a large plasmid where RNAi mediated suppression occurs. Of course these points are merely speculation as to why the suppression efficacy of the shRNA constructs was reduced compared to the synthesised siRNAs as there were no experiments undertaken to evaluate the number of shRNA transcripts produced from the H1 promoter in the 24 hours that the HeLa cells were left to incubate. It was decided not to take lysate from shRNA treated HeLa cells for western blot analysis given the low endogenous expression seen at the protein level in this cell type (see UNT lane, figure 3.5.13). Furthermore, the pAAV_shRAC1 constructs were later used to evaluate the suppression of endogenous mouse suppression *in vivo* subsequent to delivery of these constructs to the mouse retina by viral delivery.

3.3.9 Production of AAV 2/5

To generate the molecular tools require to evaluate RNAi mediated suppression of mouse *Rac1 in vivo*, recombinant AAV 2/5 viruses were generated as described in

section 2.2.6. Three viruses were generated containing NT20, pAAV_shRAC1 and pAAV_shRAC3 viral genomes by the triple transfection method using AAV DNA, pHelper and 2/5 capsid DNA. NT20 is the standard non-targeting shRNA virus used in this laboratory as a non-targeting shRNA control against which targeting shRNAs are compared for *in vivo* analysis. Various fractions of resulting virus based on their respective refractive indices were titred by qPCR using EGFP specific primers as described in section 2.2.6.2. The viral titres in viral genomes/ml (vg/ml) for each fraction were as follows; NT20: $1.014x10^{12}$, $2.13x10^{12}$, AAV_shRAC1: $1.129x10^{12}$, $2.284x10^{12}$, AAV_shRAC3: $2.989x10^{12}$. The fractions with the highest titre were taken for subsequent sub-retinal injection in mice. However for sub-retinal delivery, each shRNA encoding viral vector was titre matched to the NT20 virus which was injected in to the contralateral eye to the shRNA injected eye (ie. in every injected mouse, NT virus would be injected in to the left eye and shRNA virus would be injected in to the right eye).

3.3.10 Histology of Eyes taken from Injected Wildtype Mice

To ensure successful viral transduction of AAV 2/5 vector to the retina, eyes were taken from wildtype 129/SvHsd mice which had been sub-retinally injected with AAV_shRAC1_1/3 viruses and NT20 virus. Sub-retinal injections were carried out as described in section 2.2.7.3. The viral titre of AAV_shRAC1_1 was $2.13x10^{12}$ vg/ml and therefore the number of viral particles in a 3µl volume delivered to the sub-retinal space was approximately $6.39x10^{9}$. NT20 was diluted to the same titre as AAV_shRAC1_1 to ensure an equal number of viral genomes delivered to both eyes with each virus. The viral titre of AAV_shRAC1_3 was $2.989x10^{12}$ vg/ml but this had to be titre matched to NT20 and therefore was diluted to the NT20 titre of $2.284x10^{12}$ vg/ml. The approximate number of viral genomes of each virus delivered to the sub-retinal space of either eye was $6.852x10^{9}$. The virus was incubated in the sub-retinal space for 3 weeks post injection before euthanisation of the animals and harvesting of the eyes. The eyes were then sectioned as described in section 2.2.8.1. A successful transduction can easily be ascertained from histology by looking for EGFP mediated fluorescence in the retina as each AAV 2/5 vector contains EGFP under the control of a promoter and therefore should readily express EGFP. Representative micrographs of

retinal sections of both *Rac1* shRNA injected right eyes and the contralateral NT20 injected left eyes are presented in figure 3.5.19. These histological images show poor EGFP expression from the *Rac1* shRNA containing AAV 2/5 vectors compared to the NT20 vector. A literature search later suggested that the PGK promoter used to drive expression of EGFP in the AAV_shRAC viruses had been a poor choice as this promoter has little activity in the adult retina, apart from some limited expression in the INL and RPE compared to the strong CMV promoter driven EGFP expression observed in NT20 treated eyes (Kostic et al, 2003). AAV 2/5 tends to transduce cells of the RPE and ONL only and therefore the PGK promoter would have very poor activity independent of the viral titre delivered.

3.3.11 Cloning of the CMV_EGFP DNA in to pAAV_shRAC1_1/3

Due to the relatively poor expression of EGFP from the PGK promoter in both pAAV_shRAC1_1/3 viruses, it was decided to excise this region of the plasmid and replace it with CMV driven EGFP. The NT20 AAV 2/5 vector also contains an EGFP but this reporter gene is driven by the CMV promoter. It was anticipated that this CMV promoter driven EGFP DNA segment would greatly increase EGFP expression to practical levels due to the strong fluorescence observed in NT20 injected retinas (figure 3.5.19). To do this, the pAAV_shRAC1_1/3 vectors were restriction digested with *AflII* which cuts at the end of the EGFP gene and *SphI* which cuts just before the start of the PGK promoter. This region was subsequently discarded after separation of both bands by agarose gel electrophoresis. Meanwhile, the NT20 vector was restriction digested with *AflII* which cuts at the end of the EGFP gene and *StuI* which cuts just before the start of the CMV promoter. The resulting sticky ends of *AflII* will have complete complementarity and therefore would readily ligate. The *StuI* site will create a blunt nick and therefore the *SphI* nick (which is sticky) had to be blunted using T4 DNA polymerase as outlined in section 2.2.1.7. The CMV_EGFP fragment from NT20 was then ligated in to the previously linearised pAAV_RAC1_1/3 vectors. These newly cloned vectors were subsequently restriction digested (see figure 3.5.21) and sequenced to confirm the integrity and correct sequence of the plasmid (see figure 3.5.20 and appendix). The names of both vectors remained the same.

3.3.12 Production of AAV 2/5 with new AAV plasmids

The newly cloned pAAV plasmids containing CMV driven EGFP and H1 driven shRNA were used to produce recombinant AAV2/5 in HEK 293 cells as previously outlined and explained in more detail in section 2.2.6. EGFP specific primers were again used to evaluate the titre of virus produced by this protocol. Three fractions were collected for each virus and the titres (in vg/ml) of each refractive index fraction were as follows; NT20: $2x10^{11}$, $2.4x10^{11}$, $3.89x10^{11}$, AAV_shRAC1_1: $1.91x10^{11}$, $1.93x10^{11}$, $3.6x10^{11}$, AAV_shRAC1_3: $2.1x10^{11}$, $6.8x10^{11}$, $6.8x10^{11}$. Again, the highest titre fraction of each virus was used for subsequent sub-retinal injection. Each shRNA encoding virus was injected at the same concentration as the NT20 virus in the contralateral eye. Therefore the un-diluted delivered viral titre in a 3µl volume would be as follows; NT20: $1.17x10^{9}$vg, AAV_shRAC1_1: $1.08x10^{9}$ and AAV_shRAC1_3: $2.04x10^{9}$. Adequate dilutions of each virus were made to ensure equal titre delivery of each virus to each eye immediately prior to injection.

3.3.13 RT-qPCR Analysis of Suppression of *Rac1* mRNA *in vivo*

Wildtype mice (strain 129) were injected at 6 weeks of age with equal titres of NT20 and shRAC1 virus to each eye by subretinal injection. The left eye received $1.08x10^{9}$ vg of NT20 and the right eye received the same number of viral particles of AAV_shRAC1_1. The virus was incubated for two weeks before euthanisation of the mice and harvesting of the retinas. At this time the retina was extracted and the fluorescent regions of the retina cut away from the non-fluorescent regions in order to take the transduced region only. RT-qPCR analysis was then undertaken on RNA extracted from this region of the retina. Each right eye sample value was normalised against the value given for the contralateral eye to allow for a direct comparison within each experimental animal. These values were then averaged and the standard deviation calculated. The results of this analysis are presented in figure 3.5.22. Figure 3.5.22 demonstrates a decrease of 68.33% (±3.8%) of *Rac1* expression in the region of the retina transduced with AAV_shRAC1_1. A standard two way paired student's t-test performed on this data of this RT-qPCR confirmed the significance of this difference, producing a p-value of 0.0005.

Expression analysis of *Rac1* was also undertaken on five animals injected with AAV_shRAC1_3. RNA was isolated and analysed by RT-qPCR in the exact same manner as the AAV_shRAC1_1 analysis. This revealed a 52.4% (±7.47%) decrease in *Rac1* expression in the right eyes of these animals (see figure 3.5.23). Statistical significance of this decrease was confirmed by two way paired student's t-test which produced a P-value of 9.64×10^{-5}.

3.3.14 Western Blot Analysis of Suppression of Rac1 Protein *in vivo*

Verification of *Rac1* suppression at the mRNA level was performed at the protein level by western blot analysis. Wildtype mice strain 129 were injected at 6 weeks of age with same titre of virus in to the sub-retinal space in each eye. The left eye received NT20 AAV and the right eye received titre matched AAV_shRAC1_1 or AAV_shRAC1_3. The virus was incubated in these mice for three weeks before euthanisation and harvesting of the retinas. The retinas were then extracted and viewed under a fluorescent microscope. Regions of the retina which had been transduced with AAV fluoresced green due to the presence of EGFP in these tissues. This region of green was excised from the rest of the retina and placed in to tissue lysis buffer. The protein was then extracted, the total protein concentration assayed by fluorometry and the lysate samples run on an SDS-PAGE gel. The resulting western blot was probed for both Rac1 and β-Actin and the results of this western blot are presented in figure 3.5.24. This western blot shows the expression of Rac1 and β-Actin proteins in the retinas of three mice which received NT20 and either of the *Rac1* shRNA viruses. Unfortunately complete equal loading could not be achieved for this experiment due to the highly variable results of both BCA assay and protein fluorometry on total protein sample of mouse retina origin compared to the highly reliable results that these assays provide on protein from cell culture lysates. This tends to occur for many of the western blots carried out in the laboratory on retinal protein due to the inadvertent excision of the RPE layer during extraction of the retina. Therefore, while the total protein concentration of each sample has been accurately recorded, the relative levels of β-Actin may vary amongst samples due to the varying amounts of RPE tissue in each sample. Of the three western blots carried out on this set of protein samples using different protein sample loading volumes, the figure of the western blot provided in

this study demonstrates the best equal loading of β-Actin that was achieved. This western blot is presented in figure 3.5.24.

The first set of data in the western blot is from the mice which received NT20 in the left eye and pAAV_shRAC1_1 virus in the right eye (lanes L1-3 and R1-3 respectively). From this, it can be observed that the left eyes of these mice show bands of similar intensity for both β-Actin and Rac1. Both 1L (Left Eye) and 3L Rac1 bands are of similar intensity. 2L shows a heavier Rac1 specific band but this lane also shows an equally heavy β-Actin specific band suggesting all three left eyes have similar levels of Rac1 expression. The bands from the contralateral eyes are indicated by the same number as their left eye counterparts (1-3) and are labelled R (Right Eye). These eyes show a clear decrease in Rac1 protein with no visible bands present in the lanes marked 1R and 2R. These eyes also show a clear β-Actin specific band, similar in intensity to the β-Actin band observed in the 1L and 2L lanes, suggesting that this decrease is mediated by shRNA mediated suppression. Lane 3R shows a visible Rac1 specific band with much lower intensity than that seen in lane 3L. The β-Actin band in the 3R lane is also less intense than the same band in the 3L lane however. This would suggest that the lower intensity of the Rac1 band in 3R is not completely the result of shRNA mediated suppression and may be due to unequal loading.

The second set of data in this western blot is from mice 4-6 which had received NT20 in their left eyes and AAV_shRAC1_3 virus in their right eyes (L-4-6 and R4-6). The pattern of Rac1 expression compared to β-Actin expression in lanes 4L and 5L is similar to what was observed in lanes L1 and L2 with bands of similar intensity difference. 6L shows a Rac1 band of far less intensity compared to 4L and 5L. However the β-Actin specific band in this lane is also much weaker compared to those seen in lanes 4L and 5L suggesting that all left eyes in this group have a similar level of Rac1 expression. Meanwhile the Rac1 specific bands in the lanes loaded with protein from right eye all show a similar intensity. Importantly these lanes also demonstrate a β-Actin specific band intensity similar to each other. Lanes 4R and 5R in particular show similar β-Actin specific band intensity to their left eye counterparts with a concomitant decrease in Rac1 specific band intensity compared to lanes 4L and 5L. This suggests shRNA mediated suppression of Rac1 has occurred in these eyes. Lane 6R has a much heavier β-Actin band and a Rac1 specific band that is slightly

fainter if not of similar intensity than its left eye counterpart. This would also be suggestive of shRNA mediated suppression of Rac1 as the weak β-Actin band of 6L suggests less total protein has been loaded in this lane compared to 6R. Therefore the Rac1 specific band in this lane should in theory be more intense than what is observed and heavier than its right eye counterpart.

Due to the unequal loading of protein samples observed in this experiment, an analysis of the differences in band intensity was undertaken using the ImageJ imaging program. This computer program allows one to measure the pixel intensity of bands quantitatively in order to compare samples. The method of calculating band intensity was taken from the National Insititute of Health (NIH) guidelines on accurately measuring band intensity (http://rsb.info.nih.gov/ij/docs/guide/user-guide.pdf). Briefly, areas of the same size were used to measure the band intensity of each band. The band intensity is then graphed as a curve with the peak of the curve indicating the centre of the band. The area under the curve was then calculated to provide a quantity of band intensity. The quantities of each Rac1 specific band were then normalised against their corresponding β-Actin specific bands. The normalised values of the bands were then averaged within each set and a standard deviation was calculated for each set. A two way paired student's t-test was performed to measure statistical significance. The resulting data were graphed as bar charts and are presented in figure 3.5.25. This analysis demonstrates that AAV_shRAC1_1 suppresses Rac1 expression by 81(±28)% and that AAV_shRAC1_3 suppresses Rac1 expression by 60(±19)%. Statistical analysis revealed that only the suppression by AAV_shRAC1_3 was significant with a P-value of 0.04; suppression by AAV_shRAC1_1 reached a P-value of only 0.07. These data indicate that AAV_shRAC1_3 is mediating potent suppression of Rac1 *in vivo*.

Overall, these western blot data demonstrate that the shRNAs targeting *Rac1* expressed from the AAV vector injected in to these eyes are functional. While AAV_RAC1_1 virus displayed a much more prominent change in Rac1 expression compared to NT20 injected contralateral eyes, this change was apparent in only two out of three mice injected with this construct. The second virus, AAV_RAC1_3, demonstrated a much smaller change in Rac1 expression. This suppression did not alter by much variation across all three mice that had been injected with this construct. Formal quantification

revealed that only one shRNA construct suppressed Rac1 expression by a statistically signficant amount. However, must also be remembered that the process of western blotting is also subject to variation due to the many steps involved in this protocol and therefore discrete changes in protein levels are difficult to readily quantify.

A final observation of this western blot is the presence of extra bands just above the Rac1 specific bands. These bands are far too small to be homodimers of Rac1 as their size is only ~24kDa (as sized by the protein ladder on this blot, not shown). The possible identity of this band is discussed in section 3.4.

3.3.15 Immunohistochemical Analysis of Suppression of Rac1 *in vivo*

Further verification of the suppression of *Rac1 in vivo* was undertaken by immunohistochemical analysis. Wildtype mice strain 129 were sub-retinally injected at 6 weeks of age as before and the eyes were harvested after 3 weeks of viral incubation. These eyes were fixed, sectioned and probed with anti-Rac1 antibody (Millipore) and anti-mouse secondary CY3 antibody. All sections were analysed by fluorescent microscopy. The resulting micrographs of these sections are presented in figures 3.5.27 for AAV_shRAC1_1 and 3.5.28 for AAV_shRAC1_3. These images demonstrate no discernible decrease in Rac1 antibody staining between the control and shRNA injected retinas in the transduced regions of the retina. Some changes in the intensity of staining are observed between the images of the left and right eyes, however these changes appear to affect all layers of the retina and not just the transduced layers (the RPE and ONL) suggesting that these changes in intensity are due to differences in staining efficacy rather than a difference in protein expression. These images also demonstrate EGFP expression in the ROS of the retina rather than in the ONL. This is believed to be an artefact of the acetic acid fixing process as an ONL fluorescence pattern is observed prior to antibody staining and does not occur on retinal sections which are fixed using 4% paraformaldehyde without 5% acetic acid. Retinal sections taken from animals which had been injected with AAV_shRAC1_1 or AAV_shRAC1_3 but fixed with 4% paraformaldehyde without 5% acetic acid also demonstrate EGFP expression in the ONL, suggesting that the EGFP fluorescence pattern observed using the Millipore antibody fixation protocol is not a functional

effect of *Rac1* suppression. A second set of data using a different fixation protocol and antibody is presented in figure 3.5.26. These representative micrographs of AAV_shRAC1_1 and AAV_shRAC1_3 treated right eyes and contralateral NT20 treated left eyes were probed using the Abcam antibody. Again, no discernible decrease in Rac1 staining is observed between the left and right eyes. Possible reasons for these contradictory results (based on the demonstrated efficacy of the shRNAs by RT-qPCR and western blot analysis *in vivo*) are discussed in section 3.4.

3.3.16 Effect of *Rac1* suppression on Retinal Structure and Function of injected hP347s transgenic mice

The human P347S transgenic mouse was first described by Li et al, 1996. This mouse model contains a human rhodopsin allele which has a specific mutation which causes an amino acid change at position 347 from proline to serine. This allele was first isolated from a human patient of autosomal dominant RP and used to create a knock in mouse model which displays an RP-like retinal degeneration phenotype. The line which is carried in the TCD Ocular Genetics laboratory has been bred on to a 129/SvHsd background and is frequently crossed with rhodopsin knockout mice (engineered by Humphries et al, 1997) in a heterozygous manner to breed a P347S +/- Rho +/- mouse. This creates a mouse which carries only two alleles of rhodopsin; one wild type rhodopsin allele and one P347S allele (as the P347S transgene is not at the rhodopsin locus and therefore a +/- designation means the presence of one allele only rather than the presence of one wild type allele). This bi-allelic system is therefore a true representation of a patient of RP carrying the autosomal dominant P347S mutation in a heterozygous fashion and is used for all studies of hP347S mice detailed in this thesis. The transgenic line bred by this laboratory is derived from the C2 line of transgenic clones first described by Li et al, 1996. This line (on a wild type background) has an expression level similar to the wild type allele, further emulating the genetic environment of patients of RP. Retinal degeneration begins slowly after birth and by P30 there are only 4-5 rows of nuclei remaining in the ONL. By 4 months of age these mice have only 1-2 layers remaining in the ONL. Rod isolated ERG b-wave analysis of P347S +/- Rho +/- animals has previously produced an average ERG

amplitude of 34.9μV and 16.9μV at 6 weeks and 20 weeks of age respectively (Millington-Ward et al, 2011).

3.3.16.1 Effect of *Rac1* suppression on ERG response of injected hP347S transgenic mice

Four transgenic mice carrying the hP347S rhodopsin mutation in a heterozygous manner were sub-retinally injected with NT20 in the left eye and with AAV_shRAC1_1 at P21. These mice were subsequently analysed by electroretinography at 4, 8 and 12 weeks post injection. The ERG analysis provides three data sets detailing rod, cone and maximal (both rod and cone) responses to light. The data sets are further divided in to two data sets for each response detailing the a-wave response (that of the photoreceptors) and the b-wave response (that of the cells of the INL, Asi & Perlman, 1992). The amplitudes of each ERG response recorded in these four mice were averaged and a standard deviation was calculated for each response. The resulting data are presented as bar charts in figure 3.5.33. P-values were calculated by two way paired student's t-test. Due to the fact that the rod a-wave response is in fact an artefact of the ERG process, the rod a-wave data will not be discussed in great detail. This is due to the low light intensity used to elicit the rod ERG response. For experimental purposes, the rod a-wave can be derived from the maximal a-wave as the mouse retina is largely composed of rods and a greater light intensity flash (2 log units greater than the rod response) is used to elicit the maximal a-wave response amplitude compared to the rod a-wave (Paul Kenna, personal communication). However the rod a-wave data are nonetheless presented to provide a complete overview of the ERG analyses. Figure 3.5.33 demonstrates that treatment of hP347S mice with AAV_shRAC1_1 provides no protection to rod, cone or maximal ERG responses at any time point analysed. In fact, of the four time points which reached statistical significance, all four showed that treatment with the *Rac1* shRNA decreased visual function in these mice. These four time points were 4 week Rod b-wave, 4 week Cone b-wave, 4 week maximal b-wave and 12 week maximal b-wave. All ERG amplitudes and their standard deviations are presented in table 3.5.3. Some slight protection of the rod and cone b-wave amplitudes can be observed at the 12 week time point but these data points failed to reach statistical significance. The ERG

data provided here suggest that suppression of *Rac1* is detrimental to the visual function of the hP347S transgenic mouse at 4 weeks post injection, however an increase in the n number of these experiments would be required to adequately determine if this shRNA is having a negative functional effect on the visual response of this mouse model.

To determine if suppression of *Rac1* using the second shRNA containing virus would have any different effects on ERG response, six hP347S heterozygous mice were sub-retinally injected with NT20 in the left eye and AAV_shRAC1_3 in the right eye at P21. ERG data were recorded at 4, 8 and 14 weeks post injection. The ERG data were averaged across the six injected mice and standard deviations were calculated for each data point. The resulting amplitude quantities and SD values are presented in bar chart form in figure 3.5.34. Again, p-values were calculated by two way paired student's t-test. It can be observed from figure 3.5.34 that AAV_shRAC1_3 is protective of b-wave function in rod, cone and maximal responses. Of the time points taken, five groups reached statistical significance to show an improvement in visual function. These time points were 14 week rod-b wave (61% amplitude increase compared to control eye), 4 week cone b-wave (17% increase), 4 week maximal b-wave (20% increase), 14 week maximal b-wave (53% increase) and 8 week maximal a-wave (114% increase). The P-values of these data sets are 0.053, 0.012, 0.04, 0.0097 and 0.026 respectively. These data reflect an overall trend for increased protection of b-wave visual function at all time points observed. However one time point reached statistical significance to show a decrease in visual function in the right eye compared to the left eye (P=0.032). This decrease was recorded for the 14 week maximal a-wave response (62% decrease in amplitude compared to left eye). These data suggest that suppression of *Rac1* by AAV_shRAC1_3 is protective of the b-wave function of rods and cones in the degenerating retina.

3.3.16.2 Effect of Rac1 supression on retinal histology of hP347S transgenic mice

The positive effect which AAV_RAC1_3 mediated *Rac1* suppression contributes to visual function in hP347S RP mouse models was further scrutinised by examining the histology of eyes treated with this construct. Heterozygous mice were sub-retinally

injected at P21 with equal viral titres of NT20 in the left eye and AAV_shRAC1_3 in the right eye. Two time points of three mice each were taken at 4 weeks and 16 weeks post injection. These eyes were fixed, sectioned and stained with AlexaFluor® bound Peanut Agglutinin (PNA). PNA is a plant derived lectin which preferentially binds to β-galactose. It has been known for many years that PNA acts as a selective marker for cones in the retina (Bridges, 1981). The resulting sections were analysed by fluorescent microscopy and representative images taken from each eye examined of the 4 week and 16 week time-points are presented in figures 3.5.30 and 3.5.31 respectively. These images reflect the trend observed in all slides observed; three slides for each eye containing 14 retinal sections. At 4 weeks post injection, little difference in cone density is observed between the NT20 and AAV_shRAC1_3 treated eyes in the EGFP positive region of the retina. However, at 16 weeks post injection, a clear difference in cone density can be observed between the NT20 and AAV_shRAC1_3 treated eyes. Figure 3.5.31 demonstrates a discernible increase in cone density in the AAV_shRAC1_3 treated retina, with little or no cones remaining in the left eyes of these mice. These data suggest that suppression of *Rac1* improves the viability of cone cells in the hP347S model of retinal degeneration. Due to the negative effect which AAV_shRAC1_1 has had on the ERG response of injected animals, these animals were not analysed in as much depth as AAV_shRAC1_3 as the purpose of this thesis was to identify nucleic acid based vectors which have a positive effect on visual function in mouse models of RP. However, PNA staining was undertaken on AAV_shRAC1_1 sub-retinally injected animals at 4 weeks post injection and representative micrographs of these animals are presented in figure 3.5.29. In much the same manner as AAV_shRAC1_3 at this time point, no discernible difference in the density of cones between the NT20 and AAV_shRAC1_1 injected eyes has been observed in these animals at 4 weeks post injection.

The ERG analysis of AAV_shRAC1_3 treated animals demonstrated increased visual function of the rod mediated response, as presented in figure 3.5.34 which reveals a 61% and 53% increase in rod and maximal b-wave response amplitude compared to the contralateral NT20 treated eye. Therefore, it was decided to stain retinal sections taken from three 16 week post injection animals for rhodopsin. Rhodopsin is the main visual pigment of rod cells and therefore acts as a marker of rod cells. The antibody chosen was the 4D2 anti-rho antibody which was presented as a gift to the laboratory

from Prof Robert Molday (Hicks & Molday, 1986). Representative micrographs of rhodopsin staining in all three animals are presented in figure 3.5.32. Again, the images presented are representative of the trend observed in all sections examined; three slides per eye with fourteen sections per slide. This demonstrates a clear increase in rod survival in the regions of the retina transduced with AAV_shRAC1_3 compared to NT20 control treated eyes. The left eyes of these mice show very little staining of rod cells in EGFP expression regions of the retina whereas the right eyes display a marked increase in rhodopsin staining of the outer segments and the ONL. Although no overall thickness in the ONL is observed in these images, these data strongly suggest that AAV_shRAC1_3 mediated suppression of *Rac1* is preserving rod cell longevity in the hP347S transgenic model of RP.

3.4 Discussion

Since the discovery of RNA interference more than twenty years ago, many approaches to the utilisation of this powerful phenomenon have been explored for the treatment of genetic disorders (Martinez et al, 2013). This has proven especially evident in the treatment of genetic diseases of the eye as this organ is highly amenable to introduction of foreign agents due to its thin layer of retinal tissue and protection from systemic immune response due to the presence of a blood-retinal barrier (Hosoya & Tachikawa, 2012). Autosomal dominant RP accounts for 30-40% of all cases of RP, making this form of the disorder the most common sub-type (Rossmiller et al, 2012). For this reason, RNAi has been used to promising effect in animal models of adRP as down-regulation of the mutant allele must be carried out to reduce the pathological effect of this gene on the wild type allele and return visual functionality to the retina (Kiang et al, 2005; O' Reilly et al, 2007; Gorbatyuk et al, Chadderton et al, 2009; 2007; Millington-Ward et al, 2011; Farrar et al, 2012). Despite advances by various groups to treat adRP with RNAi, these studies are largely limited to models of RP manifested by a rhodopsin mutation. Unless a gene therapy is individually designed for every patient, this approach would exclude a large cohort of patients with mutations in other genes, of which there are currently 54 loci associated with autosomal dominant, autosomal recessive and X-linked RP (https://sph.uth.edu/retnet/sum-dis.htm#B-diseases). Therefore an alternative approach to treating patients of RP is to target the retinal pathology which occurs downstream of the causative mutation. Some success has been achieved by delivery of neurotrophic factors, such a ciliary neurotrophic factor (CNTF) amongst others, to the retina of mouse models of RP (Dong et al, 2007; Li et al, 2010; Ohnaka et al, 2012) and proof of principle studies researching the release of neurotrophic factors from implants have been carried out in patients of RP (Kauper et al, 2012). These therapeutic approaches act by stimulating cell survival but fail to address the underlying causative mutation and therefore only slow retinal degeneration rather than reversing or preserving visual function.

In recent years the role of oxidative stress has become a new focus of attention in terms of the pathology of retinal degeneration. As previously discussed in sections 1.7 and 1.8, the over-production of reactive oxygen species has been shown to occur in many models of retinal degeneration, including retinitis pigmentosa (Lebiedzinska et al,

2012; Murakami et al, 2012; Usui et al, 2009; Usui et al, 2009b; Shen et al, 2005). Furthermore, a conditional Rac1 knockout transgenic mouse (in which Rac1 expression is reduced by approximately 50% in the rod photoreceptors) which was crossed with a mouse model of RP has been demonstrated to increase visual function in these mice (Haruta et al, 2009). In addition, pharmacological inhibition of the NADPH oxidase complex (for which Rac1 acts as an activator) has been demonstrated to preserve cone visual function in a mouse model of RP (Usui et al, 2009). Therefore a gene therapy which aims to reduce the burden of retinal ROS should in theory reduce photoreceptor cell death. This approach to preserving visual function has been the focus of the research contained within this chapter which details RNAi mediated down-regulation of *Rac1* expression in the photoreceptors of a transgenic mouse model of autosomal dominant RP.

Initially, siRNA sequences targeted at the *Rac1* gene were generated *in silico* using the GenScript and Dharmacon online siRNA finder tools. From these studies, five siRNA sequences were generated to target regions of homology between murine, human and porcine *Rac1* mRNA sequences (figure 3.5.2). The three siRNA sequences which targeted the regions of highest homology were chosen for further study *in vitro*. Prior to *in vitro* analysis however, a Rac1 specific antibody was used to examine the expression profile of *Rac1* in the wildtype retina (figure 3.5.6). This experiment was performed to ensure that Rac1 was expressed in the retina and would therefore be amenable to RNAi-mediated suppression. Determining the expression profile of Rac1 was also important as later delivery of *Rac1* targeted shRNAs would be carried out by AAV 2/5 which preferentially transduces the photoreceptors of the ONL and epithelial cells of the RPE (Watanabe et al, 2013). Therefore no RNAi induced phenotype would be expected if *Rac1* expression was not observed in the ONL. This experiment revealed that Rac1 is ubiquitously expressed in all layers of the retina, including the synaptic layers (figure 3.5.6). Stronger expression of Rac1 was observed in the nuclear layers of the cell (which are stained with DAPI), results which agree with previous studies which demonstrated expression in the nuclear layers but no expression in the plexiform layers (Mitchell et al, 2007). Rac1 is known to have a role in synapse formation of the photoreceptors and therefore expression in the OPL would be expected (Sherry & Blackburn, 2013). Furthermore Rac1 expression has been observed in both the inner and outer plexiform layers (Belmonte et al, 2006). These publications

suggest that the Rac1 expression profile observed in the experiments detailed in this chapter is a reliable reflection of retinal expression of this gene.

Analysis of the three *Rac1* specific siRNAs (RAC1_(1-3)) demonstrated potent suppression of *Rac1* mRNA in HeLa cells (figure 3.5.11). Publications concerning siRNA mediated suppression of *Rac1* tend to provide no quantitative data with which to compare the results presented here. However transfection of HeLa cells with *Rac1* siRNA has been shown to completely ablate Rac1 protein expression when transfected lysates are examined by western blot analysis (Mitsushima et al, 2009). When confirmation of suppression at the protein level was carried out by western blot, a large Rac1 specific band appeared in the lane loaded with cell lysate from RAC1_2 treated HeLa cells. This result highlighted two oversights in the initial design of these experiments. The first oversight was the fact that RAC1_2 had in fact been designed to target a region of the *Rac1* gene which was exonic but was partially excluded from the CDS of *Rac1*. This siRNA targets nucleotides 806-822 of the human *Rac1* mRNA sequence, a region which is part of the 6th exon of this gene (nucleotides 690-2341). However, the protein coding sequence extends from nucleotide 242 to 820 and therefore the last two nucleotides of RAC1_2 will not bind efficiently to CMV_RAC1 expressed *Rac1* mRNA since this region lies within the 3' UTR and not the CDS. Since the HeLa cells had been transfected with a *Rac1* coding sequence expressing plasmid, no suppression of exogenous *Rac1* could occur as the transfected coding sequence contained only the CDS of the gene from start to stop codon. This in turn led to the discovery of the second oversight which involved the design of a RT_qPCR primer which had its binding site partially outside of the CDS of *Rac1*. This explains the apparent suppression of *Rac1* in HeLa cells at the mRNA level as the primers would amplify only endogenous mRNA which is susceptible to RNAi suppression in the same manner as the exogenously transfected *Rac1* sequence. These discrepancies were quickly rectified and the mRNA experiments repeated with a new RT-qPCR primer designed to detect both endogenous and exogenous *Rac1* cDNA. In addition, RAC1_2 was not used again during the course of this PhD study as the remainder of this study examined only the effects of RAC1_1 and RAC1_3 as these siRNAs were demonstrated to suppress Rac1 protein.

Subsequent to a re-analysis of *Rac1* suppression using RAC1_1 and RAC1_3, a set of cloning experiments was initiated to create a recombinant AAV plasmid which expresses shRNAs targeting *Rac1* mRNA for subsequent use in the production of recombinant AAV 2/5 vectors in HEK293 cells. This cloning strategy aimed to create an AAV genome which would express H1 promoter driven shRNAs containing either the RAC1_1 or RAC1_3 siRNA sequences as well as a PGK (phosphoglycerate kinase) promoter driven EGFP marker gene to enable identification of AAV transduced cells in the mouse retina. When a successful set of AAV plasmids had been engineered, AAV 2/5 was produced by the method of triple transfection of HEK293 cells (Drittani et al, 2001). These plasmids were also used to examine shRNA mediated suppression of endogenous HeLa cell *RAC1* mRNA *in vitro*. Co-transfection of the shRNA AAV plasmids with CMV_RAC1 was not undertaken as the probability of a successful transfection of the same cell with two large plasmids was deemed too low to represent a reliable quantification of RNAi mediated suppression. This assumption is based on prior observations by other members of the TCD Ocular Genetics laboratory. The transfectcion of pAAV_shRAC1 plasmids in to HeLa cells demonstrated suppression of *Rac1* with both plasmids, although the level of suppression was much lower than that which was achieved using the *Rac1* siRNAs (figure 3.5.18). The discrepancy between the suppression efficacy of the siRNAs and shRNAs is most likely due to inadequate transfection of all cells in a well. Nonetheless, the result demonstrates that the shRNAs are functioning to suppress *Rac1* mRNA.In this case no western blot analysis was undertaken as no Rac1 specific band was detected in the un-transfected wells of earlier experiments (figure 3.5.15), suggesting that Rac1 is expressed at low levels (compared to CMV_RAC1 transfected cells) and may not be amenable to production of informative western blot results. Although high titres of both *Rac1* shRNA expressing and non-targeting shRNA control viruses were achieved, poor expression of EGFP was noted in the retinas of animals which had been sub-retinally injected with these viruses compared to the non-targeting virus (NT20) which expresses EGFP from a CMV promoter (figure 3.5.19). This suggested that the PGK promoter was a less efficient promoter than what was required, a surprising result given that phosphoglycerate kinase is a key enzyme involved in glycolysis. A literature search revealed the PGK promoter to have poor activity in the ONL of the mouse retina, the layer to which AAV 2/5 will preferentially transduce (Kostic et al, 2003).

Following these initial experiments examining the functionality of vectors containing PGK promoter driven EGFP expression, it was decided to re-clone both AAV shRNA plasmids to contain CMV promoter driven EGFP sequences. The newly cloned plasmids were then used to produce recombinant viruses containing the *Rac1* targeted shRNAs. These viruses produced reliable EGFP expression in the ONL following sub-retinal injection, at levels comparable to NT20 injected eyes. This EGFP signal was then used to excise transduced regions of retinas of AAV treated wild type mouse eyes for mRNA and protein analysis of *Rac1* expression. These *in vivo* experiments were performed to validate previous suppression data *in vitro*. RT-qPCR analysis confirmed that both AAVs were down-regulating *Rac1* expression *in vivo* (figures 3.5.22 and 3.5.23). The RT-qPCR data demonstrated a higher level of suppression than that which had been achieved using the same shRNA sequence *in vitro* as a selection of green cells was undertaken for this experiment, representing a more accurate representation of *Rac1* suppression. Interestingly AAV_shRAC1_1 suppressed *Rac1* expression to the same quantitative extent that had been observed using the RAC1_1 siRNA in HeLa cells (approximately 68%). Western blot analysis of EGFP positive regions of the retina also revealed suppression of Rac1 at the protein level using both viral vectors (figure 3.5.24). Interestingly a second band appeared at approximately 24-26kDa in the lanes loaded with lysates from both *Rac1* shRNA AAVs (excluding one lane loaded with AAV_shRAC1_1). A set of two bands have been observed for many published western blots using a Rac1 specific antibody (Smerling et al, 2007; Lin et al, 2012; Sharma & Mayer, 2008; Boo et al, 2007; Wei et al, 2013). More recently an extra band of similar size has been observed by western blot analysis using a Rac1 specific antibody in CHO cells (Fernandez et al, 2013). However in the CHO cells treated with *Rac1* siRNA no difference in band intensity was observed between the upper and lower bands. This extra band may be Rho-GDI bound Rac1, an inactive form of Rac1 which is found in the cytosol. A band of the same molecular weight similar to the extra band observed in this western blot has been observed previously in macrophage cells using a Rac1 specific antibody (Bromberg et al, 1994). This extra band was identified as RhoGDI by fractionation of cell lysates that were purified by column chromatography to produce Rac1 and RhoGDI specific bands at 21kDa and 24kDa respectively (Pick et al, 1993). Furthermore, a band of similar size was also observed in protein samples from mouse RPE cells using a Rac1 specific antibody (Mao Y & Finneman SC, 2012). However in this study the Rac1 band present was a dominant negative mutant of Rac1

named N17. This form of Rac1 cannot exchange bound GDP for GTP and therefore cannot become active and translocate to the membrane. RhoGDI is an inhibitor of Rac1 activation and therefore will bind only to GDP bound Rac1, explaining why this mutant may be appearing as a different band to the wild type version of the protein. While this may offer an explanation as to the identity of this extra band in the Rac1 experiments detailed in the current study, the extra band appears preferentially in lanes from eyes which received Rac1 specific shRNA. It is known that the RhoA family of GTPases (including RhoA, Cdc42 and Rac1) are part of an integrated pathway of crosstalk which can cause increases and decreases of expression (Guilluy et al, 2011). Therefore a decrease in *Rac1* expression caused by shRNA mediated suppression may have an effect on this network. A downstream effector of Rac1 activation is Pak1 (p21 Protein Activated Kinase), a kinase involved in cytoskeletal re-arrangements at focal adhesion points of cells (Delorme-Walker et al, 2011). The activated form of this protein has been shown to phosphorylate RhoGDI, inducing dissociation of RhoGDI from Rac1, which in turn causes Rac1 activation in what is termed a positive feedback loop (DerMardirossian C et al, 2004). Suppression of Rac1 will in theory result in less activation of Pak1 and may therefore cause decreased inactivation of RhoGDI. This could explain the pattern observed in this western blot as any remaining Rac1 protein remaining in shRNA treated retina will readily be bound to RhoGDI. A problem with this theory however is that no second bands were observed in siRNA treated HeLa cells. However HeLa cells are a human carcinoma derived immortal cell line and therefore will have a completely different expression profile to the mouse retina. This theory also fails to explain why these second bands have far greater intensity than any other bands on the blot, including NT20 lanes which in theory should have a much greater pool of intracellular Rac1 protein. A second possibility is that this band represents a homologue of Rac1 (such as CDC42 (~22kDa), RhoA (~23kDa), Rac2 (~21kDa) or Rac3/Rac1b (~21kDa)) which has been up-regulated to functionally compensate for the loss of Rac1 protein expression. While CDC42 is known to be expressed in the photoreceptors (Heynen et al, 2011) Rac2 has been shown to have no expression in the retina (Haruta et al, 2009). Given the vital role of Rac1 in a number of physiological functions and its intergral part of numerous pathways (including upstream and downstream signalling partners along with various guanine exchange factors and inhibitors), a microarray analysis of AAV_shRAC1 injected retinas would be ideal to provide a reasonable clue as to the identity of this extra band.

The final set of experiments aimed at validating Rac1 suppression *in vivo* examined retinal sections from eyes which had been treated with *Rac1* shRNAs. This revealed no suppression of Rac1 in the ONL of treated eyes compared to control eyes using a Rac1 specific antibody (Millipore). The experiment was repeated with a different Rac1 antibody (Abcam) but this resulted in the same outcome. Little information could be gleaned from a review of the literature regarding immunohistochemical staining of a *Rac1* RNAi agent treated retina. RNAi targeted Rac1 suppression in the retina has been used by other research groups (Mao & Finneman, 2012; Li et al, 2012) but neither group performed Rac1 specific antibody staining of sections taken from these mice. It is believed that no suppression of Rac1 was observed as the primary antibody used for these experiments is also detecting the protein of the extra band that was observed when *Rac1* shRNA AAV treated eyes were analysed by western blot. An increase in expression of this protein will mask any decrease in Rac1 staining which would result from shRNA mediated suppression. Despite this lack of evidence for Rac1 suppression *in vivo* as examined by immunohistochemistry, the RT-qPCR and western blot analysis has shown that these shRNAs are functioning *in vivo* and providing adequate suppression of endogenous *Rac1* expression at the mRNA and protein level.

The final set of experiments detailed in this chapter examined the effect that *Rac1* suppression would have in the retina of hP347S heterozygous transgenic mouse models of RP. All animals treated with the RAC1_1/3 viruses were sub-retinally injected at P21 (weaning age), a later time point than the P5 injections that have previously been carried out using rhodopsin suppression and replacement viruses in this lab (O' Reilly et al, 2007). The later injection time point was performed as Rac1 is known to play a role in ganglion cell axonal growth and neurite outgrowth in the OPL (Lorenzetto et al, 2013). Therefore, it was anticipated that suppression of Rac1 during postnatal development of the retina may have adverse effects on the functionality of the retina. These animals were analysed at various time points ranging from 4 weeks to 16 weeks post-injection and were examined by electroretinography (for further details of ERG see section 1.5) and immunohistochemistry. The first set of animals analysed by electroretinography were four mice which had been treated with AAV_shRAC1_1. These mice were analysed at 4, 8, and 12 weeks post-injection. Despite robust demonstration of the efficacy of this shRNA *in vitro* and in wild type mice, no

improvement in ERG response amplitude was recorded in these mice at any time point examined (figure 3.5.32). In fact, at 4 weeks post injection all b-wave responses were statistically significantly lower in the AAV_shRAC1_1 treated eyes compared to the NT20 injected eyes. The fact that this lower response occurred in the b-wave response is interesting as the b-wave is considered to be more clinically relevant as it is a response elicited by neuronal hyperpolarisation as opposed to GPCR induced hyperpolarisation (Asi & Perlman, 1992). ERG response remained lower in the *Rac1* shRNA treated eye at all time-points. These data suggest that suppression of *Rac1* is detrimental to visual function, contrary to the model of oxidative stress induced degeneration which has been a central theme of this thesis. Interestingly a completely different result was observed when 6 heterozygous mice carrying the same mutation were treated with AAV_shRAC1_3 (figure 3.5.33). An increase in b-wave response was recorded in the AAV_shRAC1_3 at all time points (4 week, 8 weeks and 14 weeks post injection). This increase reached statistical significance at 14 weeks for the rod b-wave response, 4 weeks for cone b-wave response and 4 and 14 weeks for maximal b-wave response. The discrepancy between AAV_shRAC1_1 and AAV_shRAC1_3 is difficult to speculate upon as both viruses suppressed *Rac1* expression to a similar extent.

Due to the lack of functional benefit observed by ERG analysis of AAV_shRAC1_1 injected animals, little histology was undertaken on animals injected with this virus. The purpose of this thesis was to explore possible gene therapies which reduce oxidative stress and improve the visual function in mouse models of RP. In addition, the hP347S transgenic mouse model of RP is a valuable resource used by many members of the TCD Ocular Genetics laboratory and therefore it was decided to focus on the virus with most promise as AAV_shRAC1_3 was the only virus which invoked an improvement in visual function and a decrease in reactive oxygen species (see section 5.3.4).

Animals which had been injected with AAV_shRAC1_3 were sacrificed for immunohistochemistry at two time-points at 4 weeks and 16 weeks post injection. Retinal sections from the first time point were stained with fluorescent tag bound peanut agglutinin (PNA) which specifically binds to surface saccharides of cone cells in the retina. This experiment revealed no difference in cone density between NT20

and AAV_shRAC1_3 treated eyes (figure 3.5.29). Cone cells are fully formed in the mouse retina by P10 (Fei Y, 2003), however the degenerating effects of the P347S rhodopsin mutation may not have affected the cell viability of cones at this stage of the disease as cone cell death is secondary to rod cell death in RP (Cronin et al, 2010). Therefore, suppression of *Rac1* will likely have no impact on cone cell density at this time-point when the mice are only 7 weeks old. At 16 weeks post-injection a clear difference in cone density is observed between control and AAV_shRAC1_3 treated eyes (figure 3.5.30). The eyes which received *Rac1* shRNA display a clear increase in cone cell density compared to NT20 injected eyes, in which little or no PNA staining is observed in the retina. No quantitative analysis was undertaken as counting of individual cells bound to PNA was deemed to be impossible given the resolution provided by fluorescent microscopy as evidenced in figure 3.5.30. However, this trend was observed in all slides observed (three slides per eye containing 14 sections per slide). These data suggest that AAV_shRAC1_3 is protective of cone cells at later stages of disease progression when rod cells have begun to die and the cone cells have become highly stressed due to increased levels of ROS. Given the protective effect of AAV_shRAC1_3 on ERG response at 16 weeks, it was decided to use an anti-rhodopsin antibody stain on retinal sections taken from hP347S heterozygous mice which had been treated with AAV_shRAC1_3 16 weeks prior. This experiment revealed a clear increase in rod cell density in the AAV_shRAC1_3 treated retina compared to the NT20 control (figure 3.5.31). Observation of these micographs suggest that no improvement in the thickness of the ONL has been achieved with treatment of AAV_shRAC1_3, a result which would be expected if suppression of *Rac1* is protective of both rod and cone photoreceptors. The size of the ONL is generally assayed by measuring the thickness of this layer from the optic nerve (where the thickness must be zero as the retina appears to invaginate to a point at this region of the retina) at set distances along the retina (Imai et al, 2010). ONL thickness measurements were not undertaken as severe thinning was observed across the retina in this transgenic model, with a thickness of only one layer of cells often observed in the transduced regions of the retina. The original paper detailing the pathology of this transgenic model determined that only 1-2 nuclear layers were preserved in this mouse line at 4 months of age (Li et al, 1996). The animals examined by immunohistochemistry in section 3.3.16.2 were almost 5 months of age when sacrificed, a time at which approximately one nuclear layer is expected within the

ONL. Therefore ONL thickness will not be addressed here as no scientifically sound measurement of this feature of retinal architecture could be undertaken due to the lack of resolution provided by fluorescent microscopy.

A puzzling outcome of this study was the discrepancy in effect between shRAC1_1 and shRAC1_3 treated animals. Theoretically there should be no difference in the phenotypes of AAV_shRAC1_1 and AAV_shRAC1_3 treated eyes as both shRNAs specifically target *Rac1* mRNA transcripts. Both constructs suppressed *Rac1* expression to a similar extent *in vitro* and *in vivo* (see figures 3.5.16, 3.5.19 and 3.5.20) so the difference observed cannot be a result of efficacy. It was hypothesised that the AAV_shRAC1_3 construct may target genes containing homologous sequences that could provide a compensatory functional effect in the absence of *Rac1*. However, sequence analysis of both constructs revealed no overlap in targeting between conserved sequences of *Rac1*, *Rac2* and *Rac1b* (*Rac3*) which may have provided compensation in the absence of *Rac1*. A general BLAST search revealed some sequence similarity between the AAV_shRAC1_1 target sequence with *Rac3* (17 of 19 nucleotides match) and *P2RY12* (13 of 19 nucleotides match, a receptor of ADP involved in platelet aggregation) but the E-values of both these hits reached 34, strongly indicating weak similarity when compared to an E-value of 0.035 when both siRNA target sequences are BLAST aligned with murine *Rac1*. A BLAST search of the pAAV_shRAC1_3 target sequence revealed no sequence similarity with any murine transcripts except *Rac1*. A second possibility for the difference in phenotype between the two sets of animals is the effect of off targeting of other transcripts. This is caused by targeting of the 3' UTR of transcripts which contain complementary regions to the seed regions (nt2-8 of the 19nt siRNA sequence) of the shRNA. Thse off targeting effects can be enhanced by a larger proportion of A and U nucleotides in the shRNA seed region and by specific nucleotides (such as U at position 1 and A or U at position 9) within the shRNA (Nielsen et al, 2007). Neither of the *Rac1* siRNAs contain a U at position 1; however both contain a U at position 9. In addition, both shRNAs possess a seed region containing A and U regions of 4/7nt and 5/7nt for Rac1_1 and Rac1_3 respectively. Whilst this does suggest a degree of off-targeting may occur, it does not explain the difference in response between the two constructs. A second explanation for the difference in phenotype is the possibility that the siRNA sequences produced by the shRNAs are immuno-stimulatory. The activation of Toll

like receptors (TLRs) has been demonstrated to be induced by introduction of siRNAs (Kariko et al, 2004) resulting in an innate interferon mediated immune response. Initially it was though that this activation of TLR was sequence independent, however it has subsequently been observed that certain sequence motifs within the siRNAs are more immunostimulatory than others, in particular the presence of poly-U repeats and GU rich regions (Jurk et al, 2011; Judge et al, 2005; Hornung et al, 2005). Analysis of the RAC1_1 and RAC1_3 siRNA sequences revealed no GU repeats in the antisense strand while there were poly-U repeats in both siRNAs (3(U) in RAC1_1 and 4(U), 2x2(U) in RAC1_3). However the sense strand of RAC1_1 contained three GU motifs (GUG, GUG and GU) compared to none in RAC1_3. Base substitution studies have demonstrated that a greater interferon response is induced by GU repeats than by poly-U motifs (Judge et al, 2005) and therefore this data tentatively suggests that RAC1_1 siRNA produced by processing of AAV_shRAC1_1 expressing shRNA may be much more immuno-stimulatory than AAV_RAC1_3. This in turn may induce retinal degeneration (as observed by ERG analysis at 4 weeks post-injection) as delivery of siRNA to the eye has been shown to induce TLR activation and induce cellular apoptosis in cells of the RPE after intra-vitreal injection (Kleinman et al, 2012). The difference in immuno-stimulatory properties of both sequences suggest that *Rac1* suppression may be beneficial in this mouse model of RP but that the beneficial effects have possibly been abrogated by the negative effects of AAV-shRAC1_1 mediated immune response.

The data in this chapter detail the cloning of the *Rac1* ORF in to an expression vector to produce full length Rac1 protein and the suppression of this full length mRNA and protein *in vitro*. Furthermore, siRNA mediated suppression of endogenous *Rac1* has been demonstrated *in vitro*. Additionally, shRNA sequences based on successful siRNAs have been cloned in to an AAV genome and this plasmid has been used to produce functional AAV vectors which were used to suppress *Rac1* expression *in vivo*. The functional effect of virally delivered shRNA against *Rac1* was then examined in a transgenic model of retinitis pigmentosa. The data presented in this chapter suggest that one of the two shRNA constructs designed to suppress *Rac1* is a functional suppressor of this gene in the mouse retina and that this suppression preserves ERG b-wave amplitude compared to control injected eyes. Additionally, this construct has preserved the viability of both rod and cone photoreceptors at the later stages of retinal

degeneration at up to 19 weeks of age in these animals. Although this construct has not preserved visual function to levels observed in wild type animals, it takes a step towards addressing oxidative stress as a functional effector of retinal pathology in RP and joins other therapeutic approaches reported in the literature which have been shown to preserve visual function in animal models of retinal degeneration. The effect of the *Thioredoxin* gene, responsible for direct scavenging of ROS, will be explored in two models of retinitis pigmentosa in chapter 4.

3.5 Figures & Tables

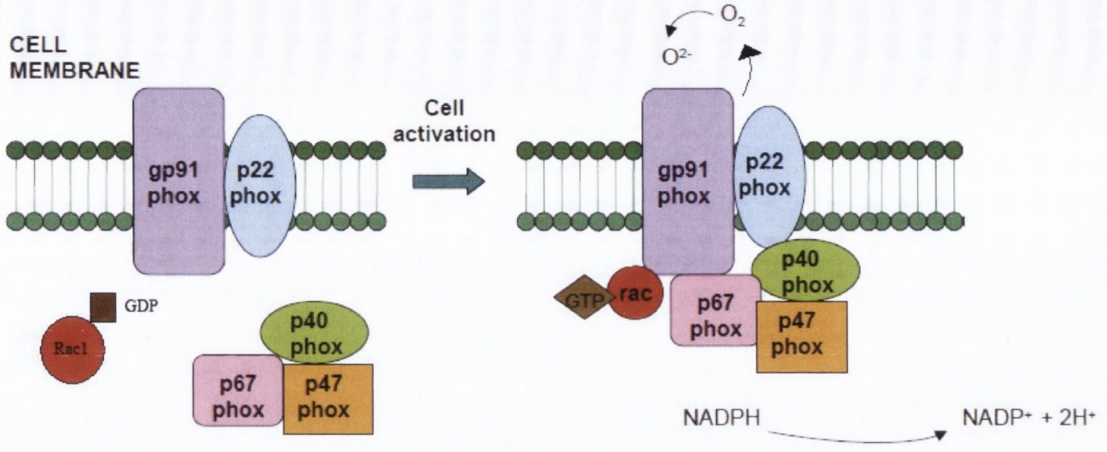

Figure 3.5.1: Schematic of the NADPH Oxidase complex upon assembly and activation of Rac1.

This schematic of the biochemical pathway leading to NADPH Oxidase production of superoxide shows assembly of the complex in the left panel. Rac1 becomes activated by a Guanine Exchange Factor (GEF) mediated exchange of Rac1 bound GDP for GTP. Rac1 then translocates to gp91phox where it recruits the non-membrane bound subunits of the complex to the cell membrane. After this has occurred, the NADPH Oxidase oxidises NADPH and passes this electron to molecular oxygen to form superoxide. Figure adapted from Assari (2006).

NT & CMV_RAC1	Untransfected	RAC1_1 & CMV_RAC1	RAC1_2 & CMV_RAC1	RAC1_3 & CMV_RAC1
1	1	1	1	1
2	2	2	2	2
3	3	3	3	3
4	4	4	4	4

Table 3.5.1: Schematic of transfection of 24-well plate

Cells were co-transfected according to this schematic. The RNA from each well in a column (wells 1-4) was pooled for later use in RT-qPCR analysis. One row of wells is not shown; this was left empty of cells. The untransfected column of wells was included to act as a control to demonstrate exogenous CMV promoter driven Rac1 expression from the CMV_Rac1 plasmid in transfected cells.

RAC1_1	5' UCCGUGCAAAGUGGUAUtt 3' 3'ACAGGCACGUUUCACCAUA 5'	Sense Antisense
RAC1_2	5' CCUGCUGUUGUAAAUGUtt 3' 3' ACGGACGACAACAUUUACA 5'	Sense Antisense
RAC1_3	5' GAAGAGGAAGAGAAAAUtt 3' 3' ttCUUCUCCUUCUCUUUUA 5'	Sense Antisense

Table 3.5.2: siRNA sequences

The sequences of each *Rac1* specific siRNA sense strand annealed to an antisense strand.

Rac1_1

```
   siRNA 1      (1) ----------------------------------------------------
Mouse Rac1    (396) TGCGTCCCCTCTCCTACCCGCAGACAGACGTGTTCTTAATTTGCTTTTCC
  Pig mRNA    (415) TACGTCCCCTGTCCTACCCACAAACAGACGTATTCTTAATTTGCTTTTCT
Human Rac1    (441) TACGCCCCCTATCCTATCCGCAAACAGATGTGTTCTTAATTTGCTTTTCC
 Consensus    (451) TACGTCCCCT TCCTACCCGCAAACAGACGTGTTCTTAATTTGCTTTTCC
                    501                                             550
   siRNA 1      (1) -------------------------TGTCCGTGCAAAGTGGTAT-----
Mouse Rac1    (446) CTTGTGAGTCCTGCATCATTTGAAAATGTCCGTGCAAAGTGGTATCCTGA
  Pig mRNA    (465) CTTGTGAGCCCTGCATCTTTTGAAAATGTTCGCGCAAAGTGGTACCCAGA
Human Rac1    (491) CTTGTGAGTCCTGCATCATTTGAAAATGTCCGTGCAAAGTGGTATCCTGA
 Consensus    (501) CTTGTGAGTCCTGCATCATTTGAAAATGTCCGTGCAAAGTGGTATCCTGA
                    551                                             600
   siRNA 1     (20) ----------------------------------------------------
Mouse Rac1    (496) AGTGCGACACCACTGTCCCAATACTCCTATCATCCTCGTGGGGACGAAGC
  Pig mRNA    (515) AGTGCGACACCATTGTCCCAACACTCCCATCATCCTGGTGGGGACGAAGC
Human Rac1    (541) GGTGCGGCACCACTGTCCCAACACTCCCATCATCCTAGTGGGAACTAAAC
 Consensus    (551) AGTGCGACACCACTGTCCCAACACTCCCATCATCCT GTGGGGACGAAGC
```

Rac1_2

```
  Pig mRNA    (715) CAGTGTTCGACGAAGCCATCCGAGCGGTTCTCTGCCCGCCCCCCGTCAAG
   siRNA 2      (1) ----------------------------------------------------
Mouse Rac1    (696) CAGTGTTTGACGAAGCTATCCGAGCGGTTCTCTGTCCCCCTCCTGTCAAG
Human Rac1    (741) CAGTGTTTGACGAAGCGATCCGAGCAGTCCTCTGCCCGCCTCCCGTGAAG
 Consensus    (751) CAGTGTTTGACGAAGC ATCCGAGCGGTTCTCTGCCCGCCTCCCGTCAAG
                    801                                             850
  Pig mRNA    (765) AAGAGGAAGAGGAAGTGCCTGCTGTTGTAAACGCCTGGGGCCCGGGG-CG
   siRNA 2      (1) ---------------TGCCTGCTGTTGTAAATGT----------------
Mouse Rac1    (746) AAGAGGAAGAGAAAATGCCTGCTGTTGTAAATGTCGGAGCCCCTCGTTCT
Human Rac1    (791) AAGAGGAAGAGAAAATGCCTGCTGTTGTAAATGTCTCAGCCCCTCGTTCT
 Consensus    (801) AAGAGGAAGAGAAAATGCCTGCTGTTGTAAATGTCTGAGCCCCTCGTTCT
                    851                                             900
  Pig mRNA    (814) GGGGCCCGTCCCGCCCCGAACCTTTGTCTGCTTTGCTCAAAT--------
```

```
   siRNA 2     (20) --------------------------------------------------
Mouse Rac1    (796) CGGTCCTG--CCTG---GAACCTTTGTACGCTTTGCTCAAAAAT------
Human Rac1    (841) TGGTCCTGTCCCTT--GGAACCTTTGTACGCTTTGCTCAAAAAAAAACAA
 Consensus    (851)  GGTCCTGTCCCT    GAACCTTTGTACGCTTTGCTCAAAAA
```

Rac1_3

```
   siRNA 3     (1) --------------------------------------------------
Mouse Rac1    (646) TGCTGTCAAATACCTGGAGTGCTCAGCTCTCACACAGCGAGGACTCAAGA
  Pig mRNA    (665) TGCTGTGAAATACCTGGAGTGCTCGGCGCTCACGCAGCGGGGCCTCAAGA
Human Rac1    (691) TGCTGTAAAATACCTGGAGTGCTCGGCGCTCACACAGCGAGGCCTCAAGA
 Consensus    (701) TGCTGT AAATACCTGGAGTGCTCGGCGCTCACACAGCGAGGCCTCAAGA
                    751                                             800
   siRNA 3     (1) ------------------------------------------------G
Mouse Rac1    (696) CAGTGTTTGACGAAGCTATCCGAGCGGTTCTCTGTCCCCTCCTGTCAAG
  Pig mRNA    (715) CAGTGTTCGACGAAGCCATCCGAGCGGTTCTCTGCCCGCCCCCCGTCAAG
Human Rac1    (741) CAGTGTTTGACGAAGCGATCCGAGCAGTCCTCTGCCCGCCTCCCGTGAAG
 Consensus    (751) CAGTGTTTGACGAAGC ATCCGAGCGGTTCTCTGCCCGCCTCCCGTCAAG
                    801                                             850
   siRNA 3     (2) AAGAGGAAGAGAAAAT---------------------------------
Mouse Rac1    (746) AAGAGGAAGAGAAAATGCCTGCTGTTGTAAATGTCGGAGCCCCTCGTTCT
  Pig mRNA    (765) AAGAGGAAGAGGAAGTGCCTGCTGTTGTAAACGCCTGGGGCCCG-GGGCG
Human Rac1    (791) AAGAGGAAGAGAAAATGCCTGCTGTTGTAAATGTCTCAGCCCCTCGTTCT
 Consensus    (801) AAGAGGAAGAGAAAATGCCTGCTGTTGTAAATGTCTGAGCCCCTCGTTCT
```

Figure 3.5.2: Homology between siRNA target sequences and each species

Each siRNA target sequence was compared across species to test the possible functionality of the siRNAs in mouse, pig and human. The yellow colouring of the nucleotides indicates complete homology between the siRNA and all three species. This analysis indicates that all siRNAs should have complete homology to mouse and human *Rac1* mRNA but mismatches exist between each siRNA and the pig sequence. However this feature makes these siRNAs ideal candidates for *in vitro* and *in vivo* suppression studies in human cells and mouse retina respectively.

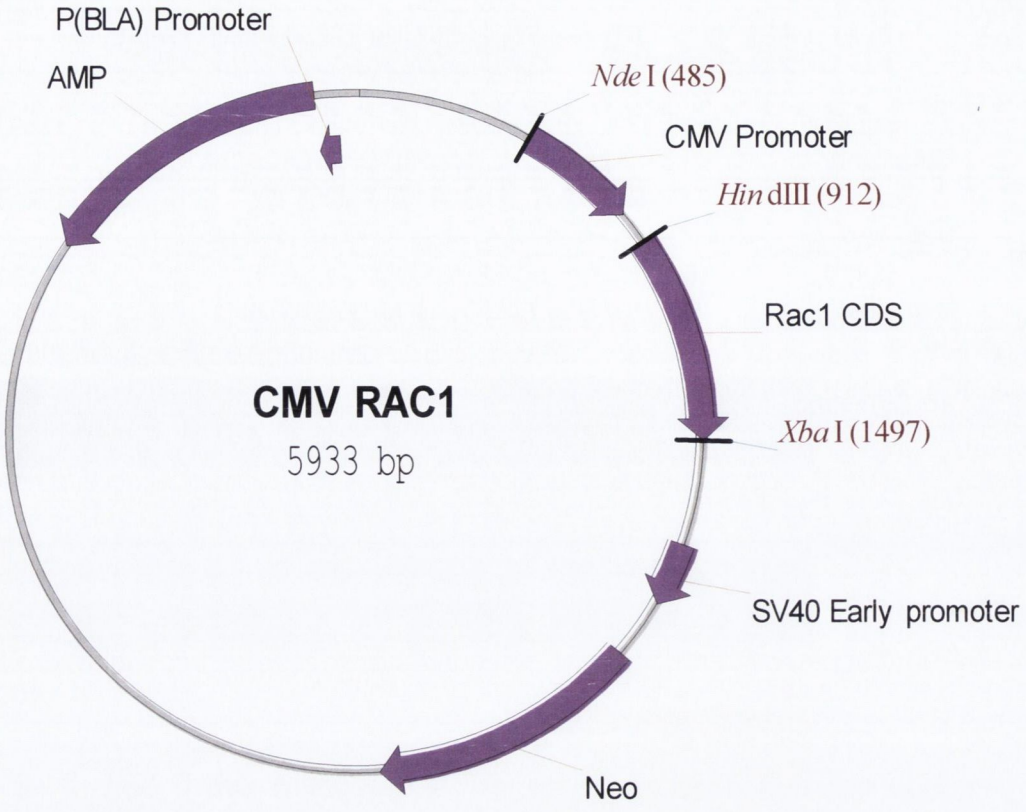

Figure 3.5.3: Schematic of 'CMV-RAC1', a pcDNA3.1+ plasmid containing the human *RAC1* gene coding sequence

The *HindIII* and *XbaI* sites used to clone the RAC1 CDS in to pcDNA3.1+ are marked in the figure at either end of the CDS. Placing the *HindIII* site on the 5' end of the gene and the *XbaI* site on the 3' end of the gene allowed this section of DNA to be cloned in to the plasmid in the correct orientation relative to the promoter (ie the start codon immediately downstream of the CMV promoter). The resulting plasmid was verified by restriction digest analysis and sequencing.

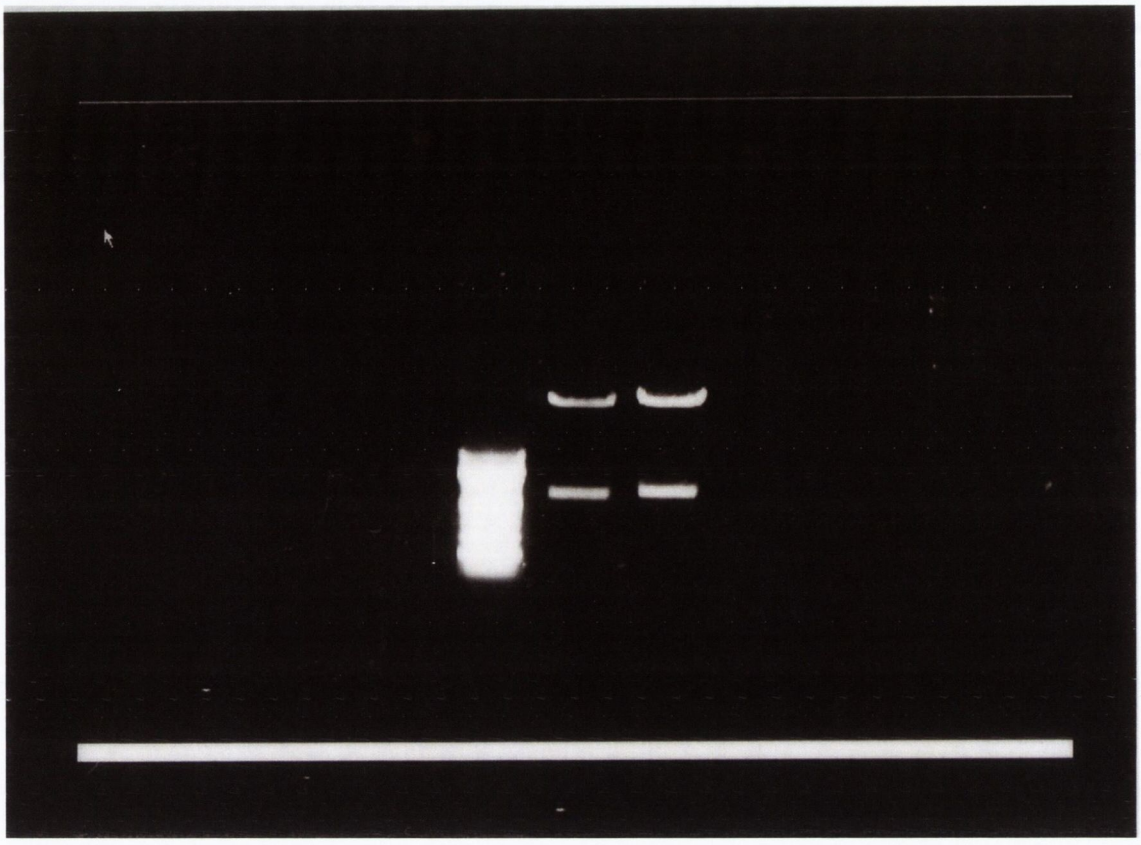

Figure 3.5.4: Restriction analysis of CMV_RAC1 with *HindIII* and *XbaI*

To ensure that the Rac1 insert had been cloned in to the pcDNA+ vector, a restriction digest was undertaken on two separate DNA minipreps using the cloning restriction sites *HindIII* and *XbaI* to excise the inserted fragment. This fragment is the lower band of approximately 600nt in length observed in this figure. The higher band observed is the rest of the CMV_RAC1 plasmid. No lower band would be expected if cloning had been unsuccessful as the *HindIII* and *XbaI* restriction sites are very close together in the pcDNA+ vector Multiple Cloning Site (MCS).

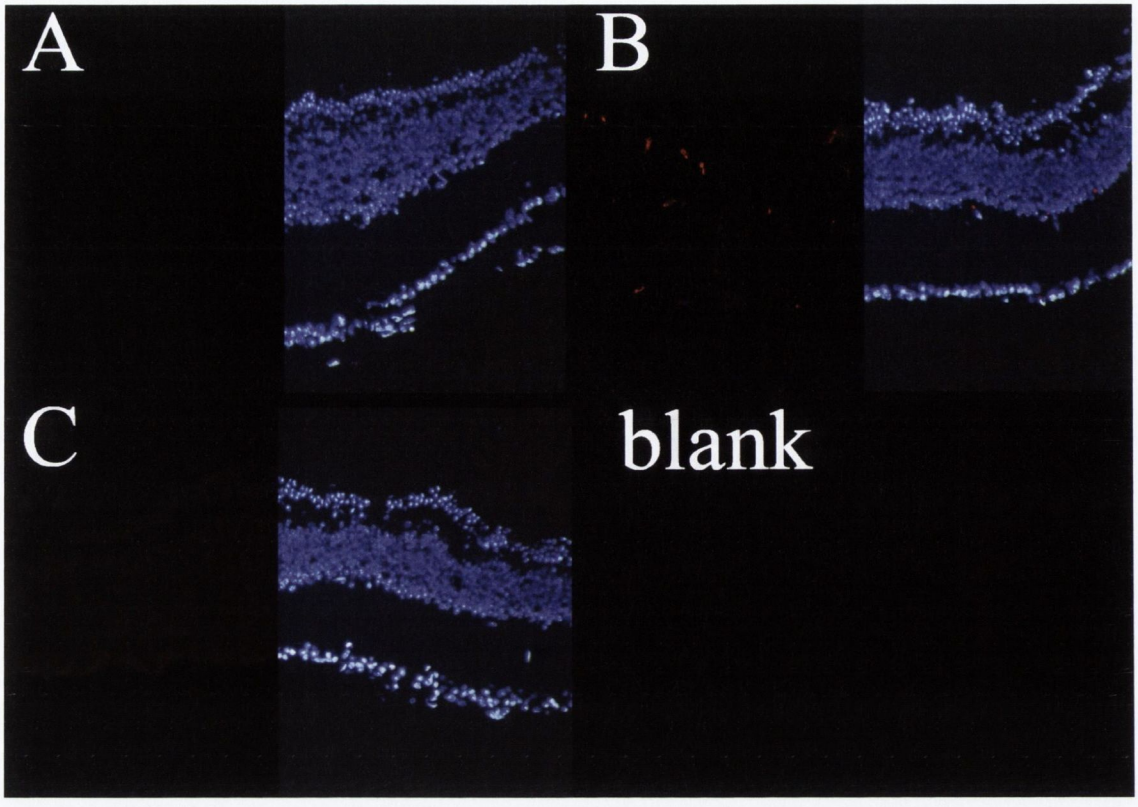

Figure 3.5.5: Secondary antibody only control for unspecific staining

During the course of this thesis, a number of different antibodies were used for immunohistochemistry. Prior to the use of these antibodies for immunohistochemistry, a negative control for unspecific retinal staining was undertaken by carrying out immunohistochemistry using antibody solution for an overnight 4°C incubation (when primary antibody would typically be placed upon slides). The following day the slides were probed using the three different secondary antibodies used in the course of this study. This figure shows the resulting negative stains obtained after incubation with A) Chicken Cy3 secondary antibody, B) Mouse Cy3 secondary antibody and C) Rabbit Cy3 secondary antibody. This demonstrated no staining of the retina using these antibodies.

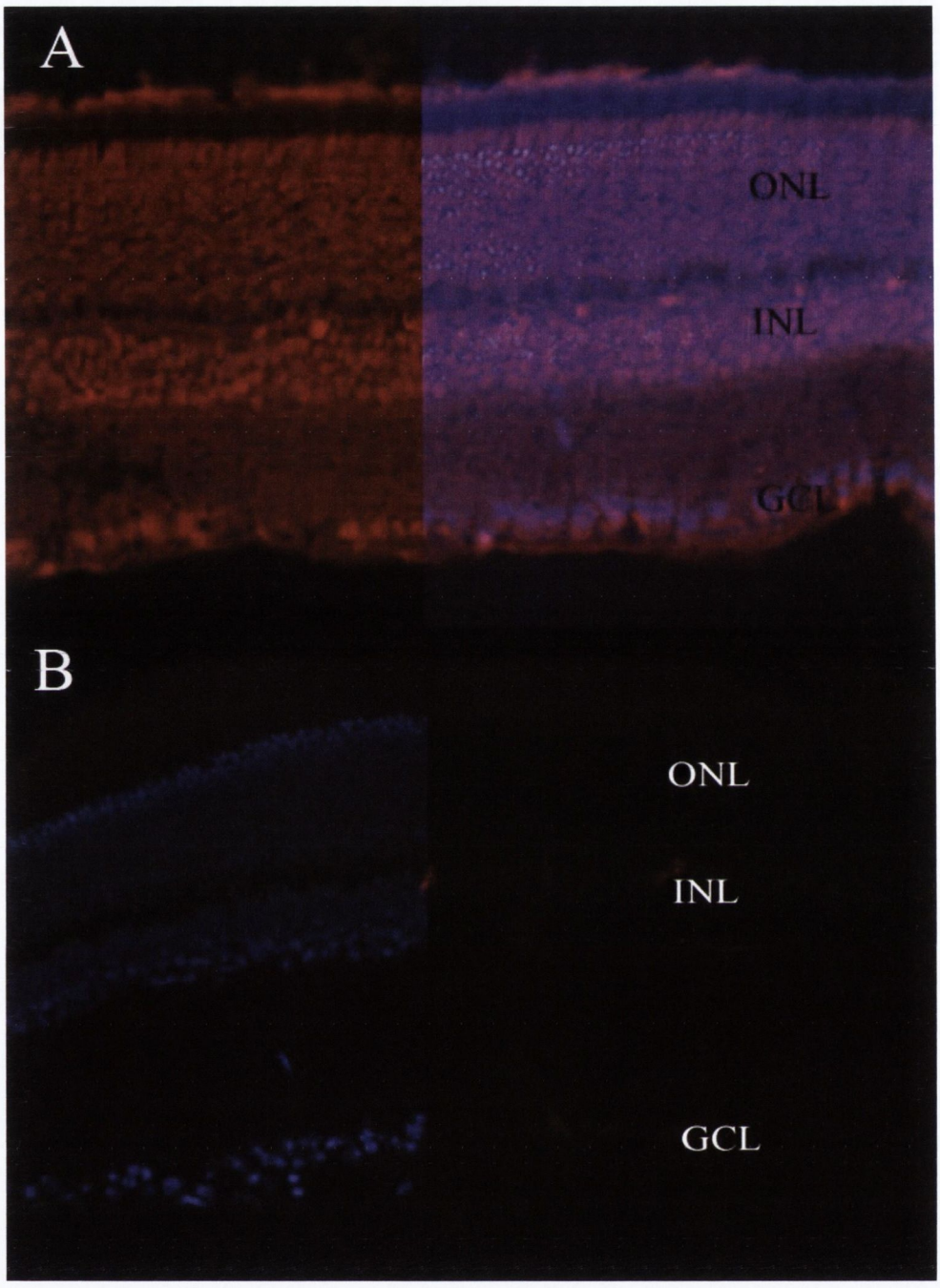

Figure 3.5.6: Immunohistochemistry showing Rac1 Expression in Wild type Retina

Representative sections showing (A) the expression of Rac1 in the retina and (B) the no primary antibody control. It can be seen from image A that Rac1 is expressed across all layers of the retina, with heavier expression in the cellular layers; the ONL (Outer Nuclear Layer), INL (Inner Nuclear Layer) and GCL (Ganglion Cell Layer). Meanwhile, image B shows little immunostaining with only unspecific autofluorescence of the choriocapilliaris and staining of some parts of the retina, most likely artefacts of the sectioning process.

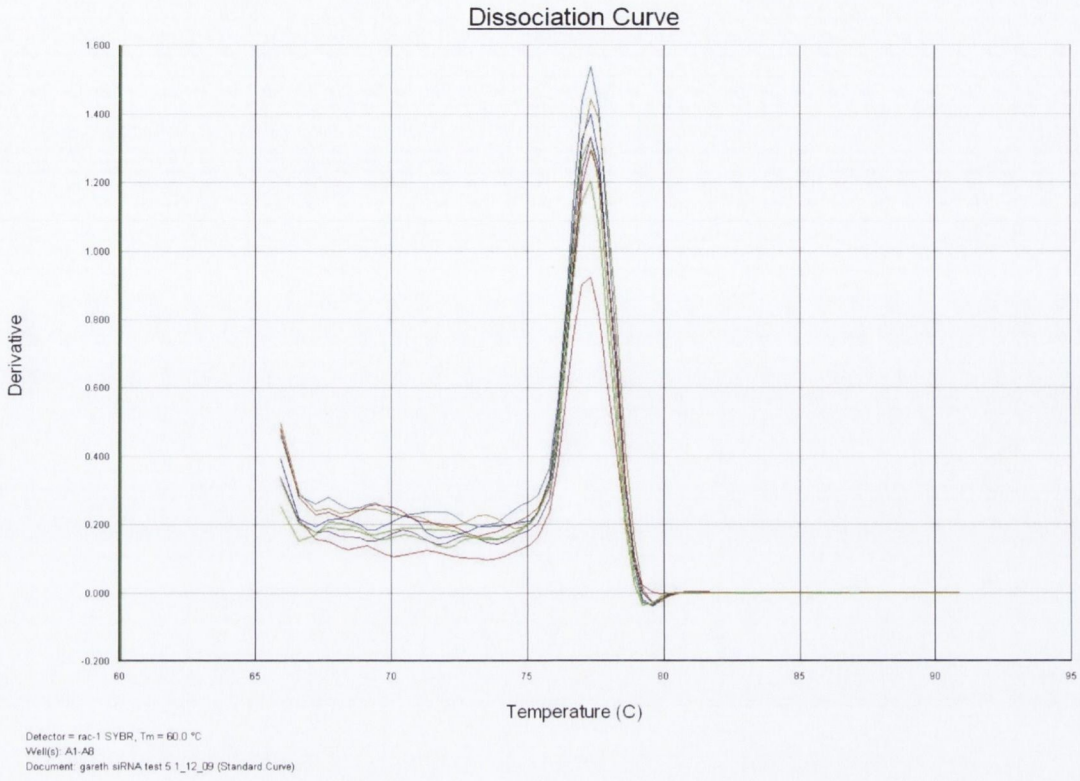

Figure 3.5.7: *RAC1* dissociation curve with first reverse primer

The dissociation curve is used to establish the number of amplicons produced by the qPCR process with a given set of primers. More than one amplicon is indicative of non-specific primer binding and/or the presence of primer dimers. More than one amplicon will skew the results of a RT-qPCR by creating unspecific SYBR fluorescence and by consuming more dNTPs. This dissociation curve indicates that the *RAC1* PCR product has a T_m of approximately 77°C and that the primers are specific to *RAC1* cDNA.

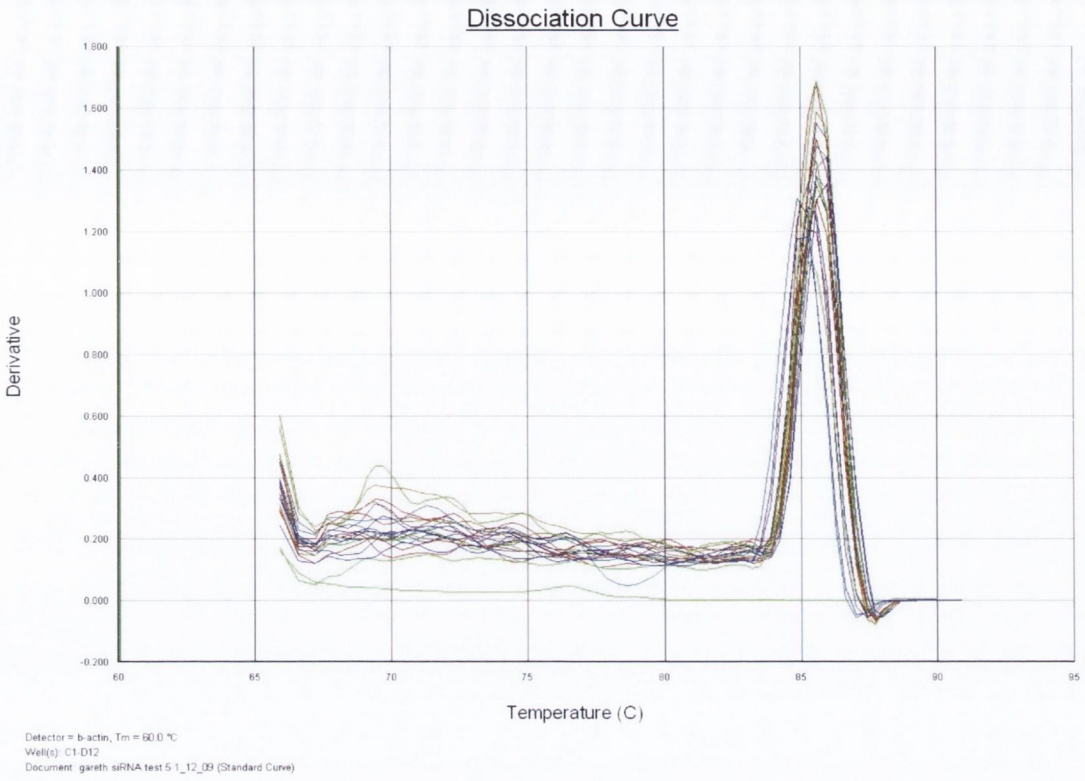

Figure 3.5.8: Actin dissociation curve

A dissociation curve was carried out during RTqPCR analysis to determine the number of separate amplicons produced by *ACTB* specific primers. The *ACTB* dissociation curve also indicates specific primer binding to the *ACTB* cDNA as one clearly discernible peak is observed in this graph. A T_m of approximately 86°C was recorded for this amplicon.

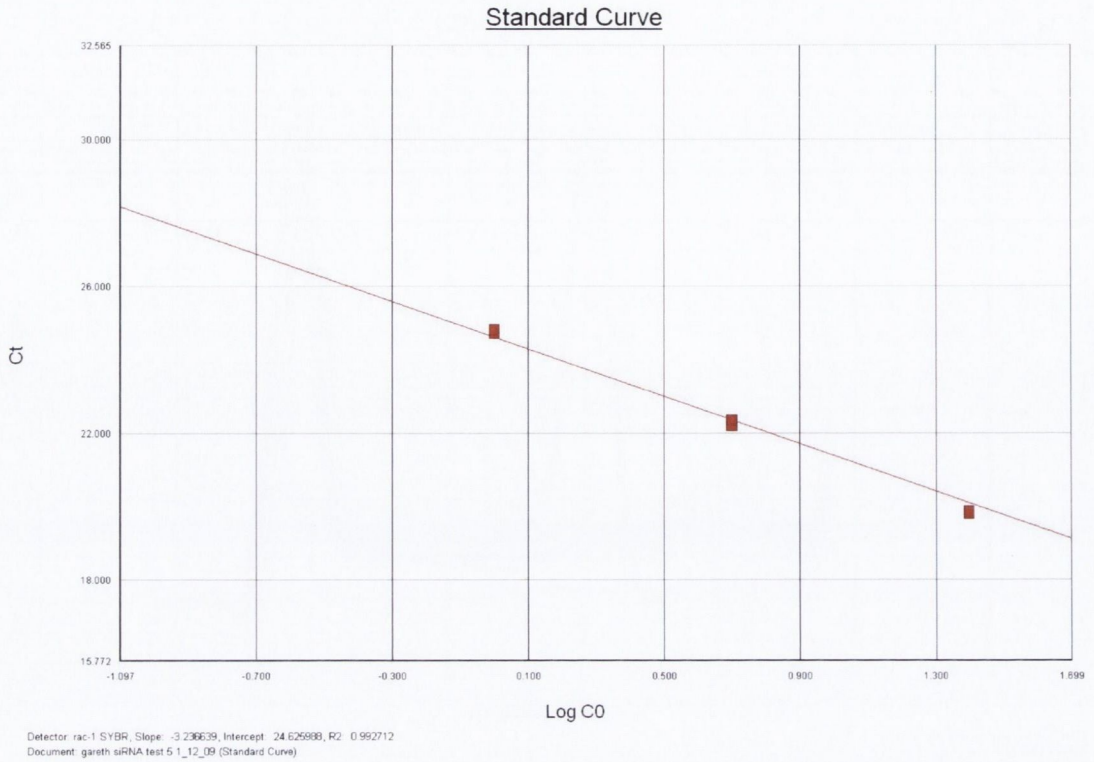

Figure 3.5.9: Standard curve of *RAC1* with first reverse primer

The standard curve was generated by making serial 5X dilutions of NT sample RNA and assigning these arbitrary quantities (shown here as a $LogC_0$, the Log_{10} of the concentration or quantity) differing by a factor of 5 to correlate to the Ct values produced by the qPCR. The Ct value is the PCR cycle number at a given point of analysis (called ΔRn) during the PCR that is determined by the researcher, generally when production of amplicons is in exponential growth (before the reaction slows due to dNTP depletion). All data are subsequently analysed at this point of the reaction. The slope and R^2 values are also taken from this curve. This standard curve provided an R^2 value of 0.993 and a slope of -3.237.

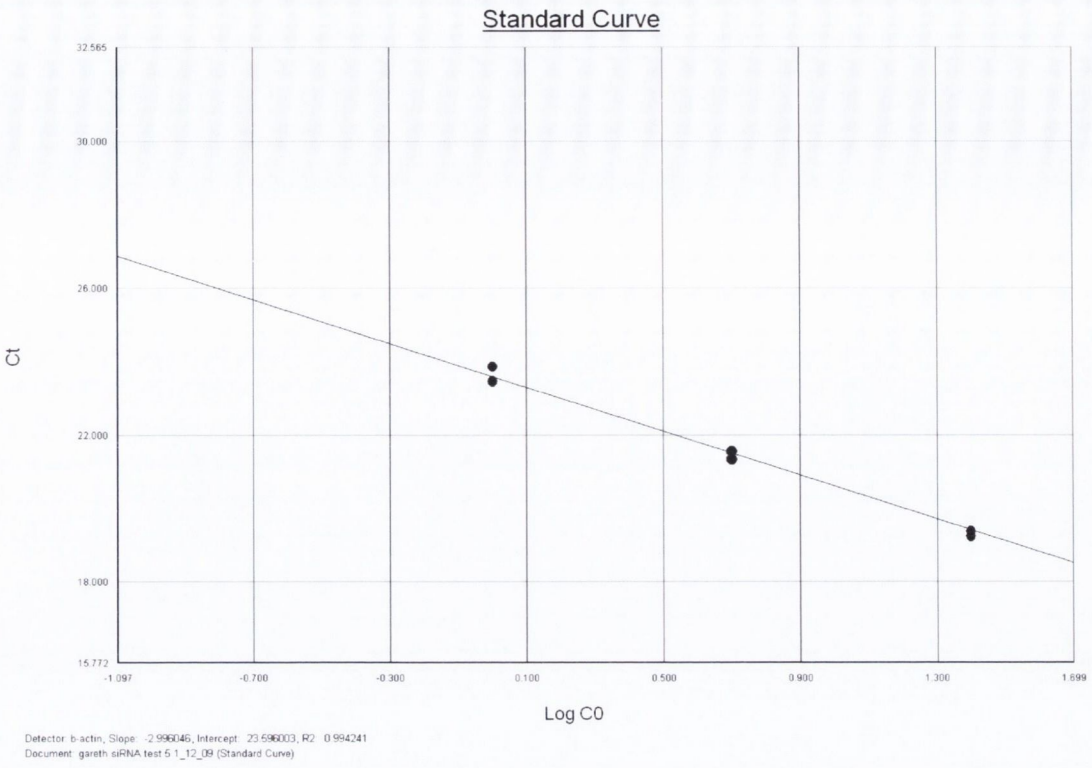

Figure 3.5.10: Standard curve of *ACTB*

This *ACTB* standard curve was used to calculate the slope and R^2 value which are the main determinants of a successful RT-qPCR. The standard curve was created using the same serial dilutions of NT RNA used to make the *RAC1* standard. This standard curve provided an R^2 value of 0.994 and a slope of -3.00.

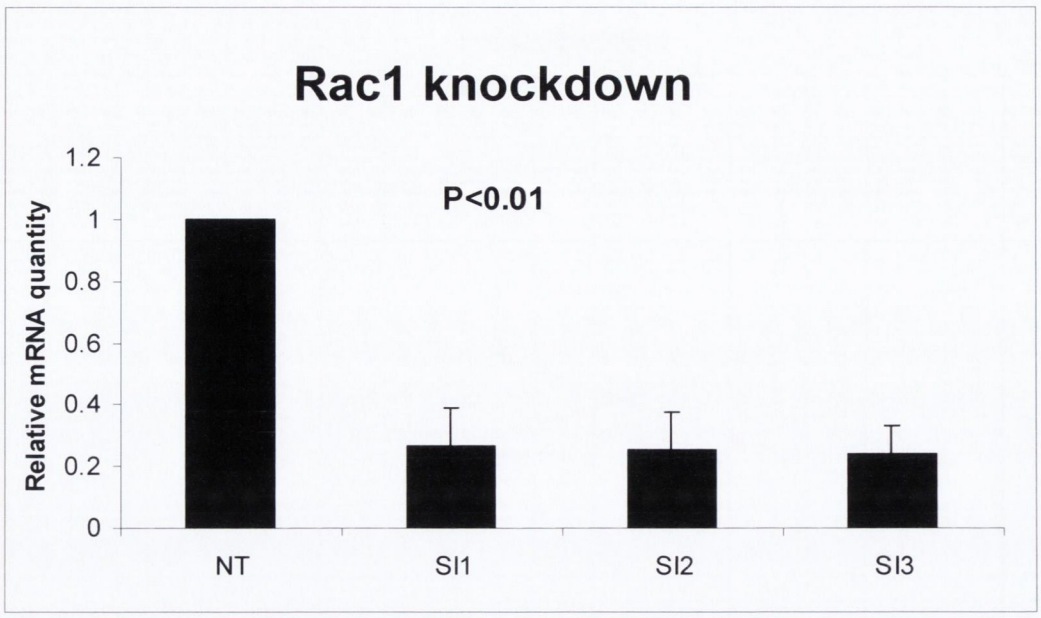

Figure 3.5.11: Bar chart showing siRNA-mediated suppression of endogenous *RAC1* in HeLa cells.

Suppression of endogenous *RAC1* in Hela cells as compared to non-targeting siRNA (NT) treated cells. The relative suppression for Rac1_1, Rac1_2 and Rac1_3 was 74% (±6%), 75% (±6%) and 76% (±4.5%) respectively. The P-values for Rac1_1, Rac1_2 and Rac1_3 suppression were 0.004853, 0.004761 and 0.004813 respectively. All three P-values were calculated by performing a two-way unpaired student's t-test. This demonstrates the efficacy of the siRNAs against endogenous human *RAC1* mRNA *in vitro*.

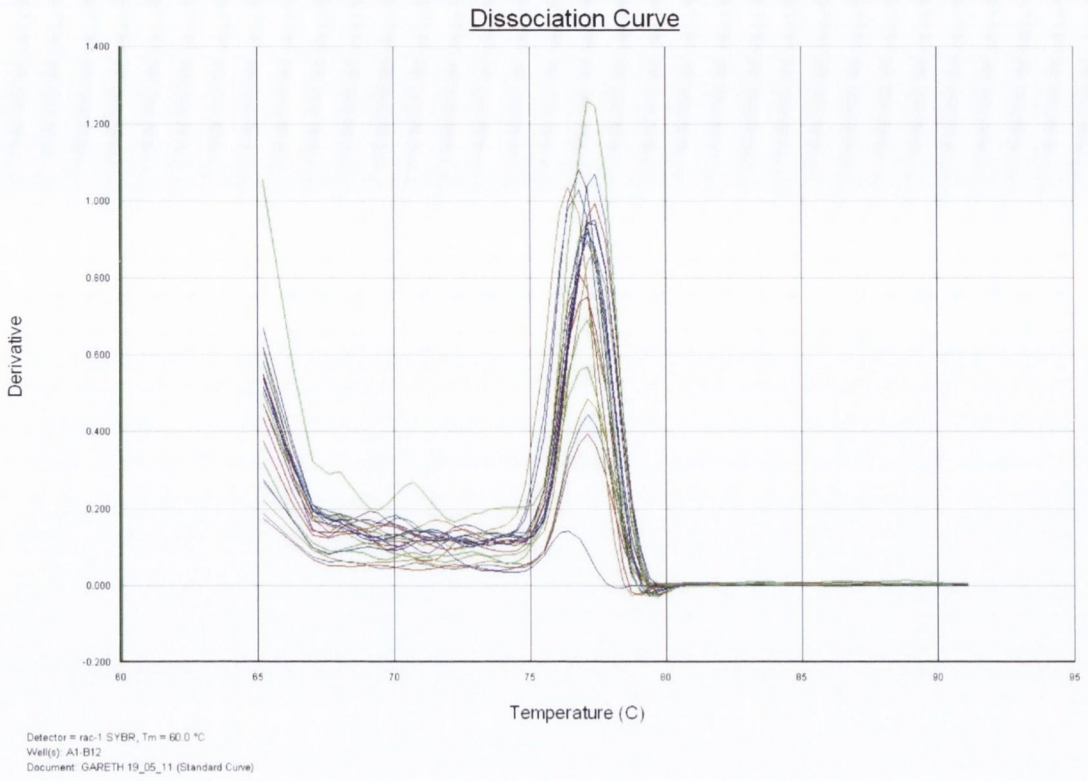

Figure 3.5.12: *RAC1* dissociation using a new *RAC1* reverse primer

Due to a mistake in initial primer design, a new reverse primer had to be synthesised to detect exogenous *RAC1* expression. This dissociation curve shows that the new set of primers produces one amplicon of 79bp with a T_m of 77.5°C.

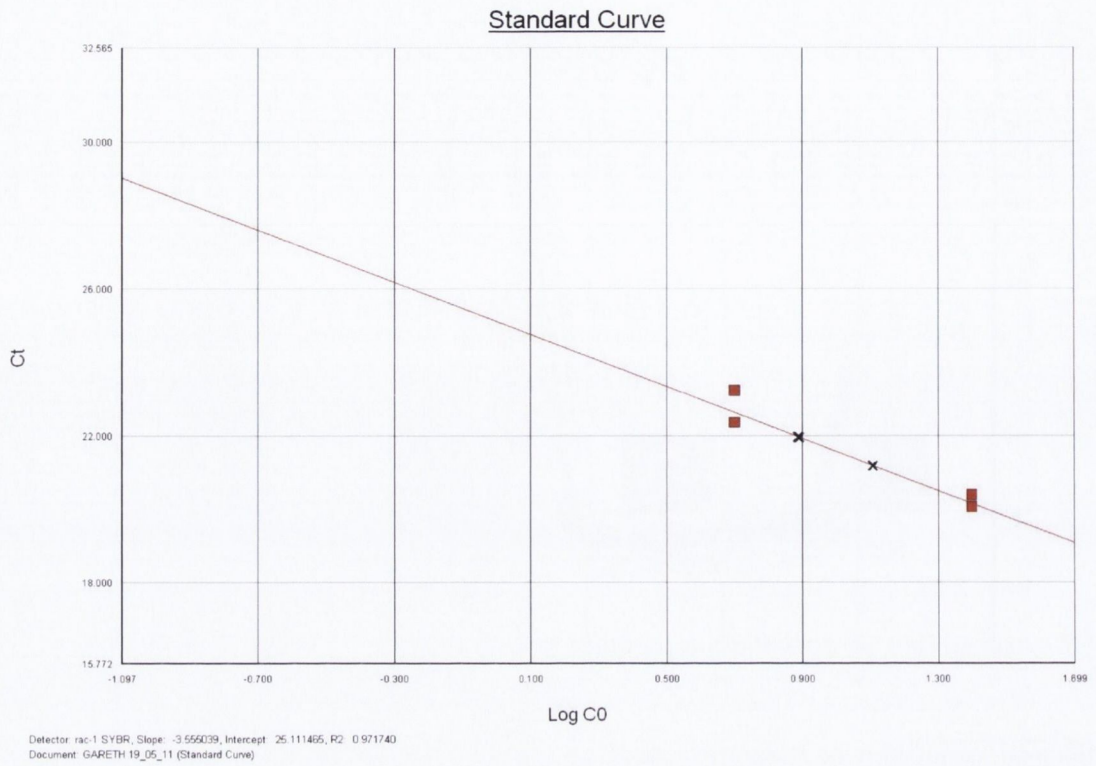

Figure 3.5.13: RAC1 standard curve with new primer

This standard curve was produced using Rac1_qF and Rac1_gR_new. This was produced using the same 5X dilution protocol as previous experiments. As was noted within the main body of text, this new set of primers displayed a less optimal detection efficiency of cDNA detection, however the R^2 values and slope fell within the range of values which can be taken as accurate. This standard curve provided an R^2 value of 0.971 and a slope of -3.55.

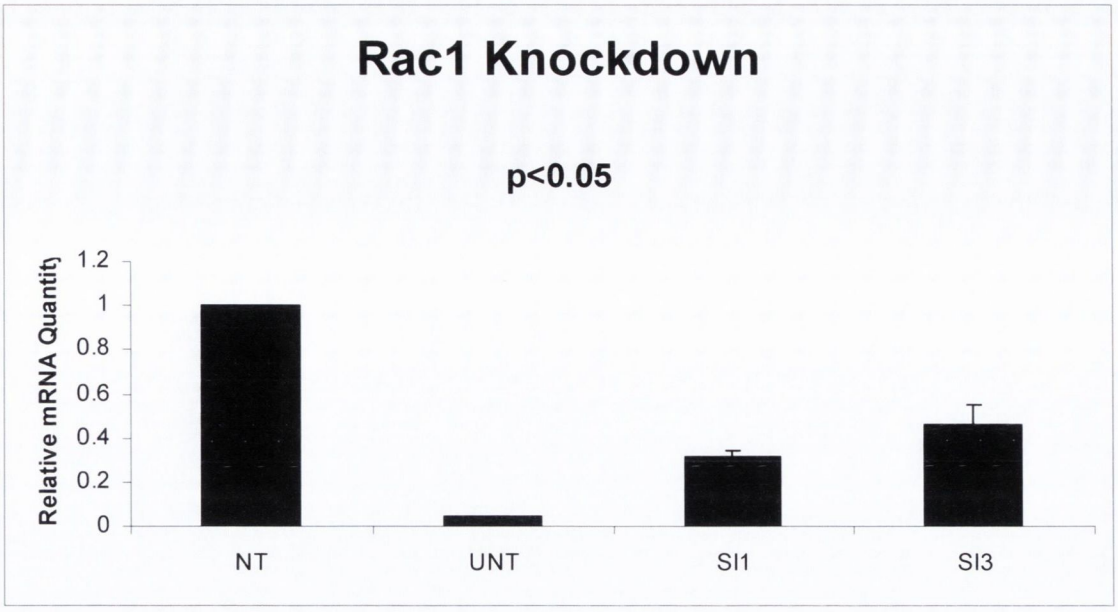

Figure 3.5.14: Suppression of RAC1 with new reverse primer

Suppression of both endogenous and exogenous expression of *RAC1* in HeLa cells. The relative suppression for Rac1_1 and Rac1_3 was 68% (±2%) and 53% (±9%) respectively. Untransfected cells showed 4% (±0.6%) expression of *RAC1* compared to non-targeting. The P-values for untransfected, RAC1_1 and RAC1_3 were 0.0001, 0.0197 and 0.0255 respectively. P-values were calculated using a two way unpaired student's t-test. This demonstrates the efficacy of RAC1_1 and RAC1_3 *in vitro* as well as the relatively low expression of cells which received no CMV_RAC1 expression plasmid (untransfected cells).

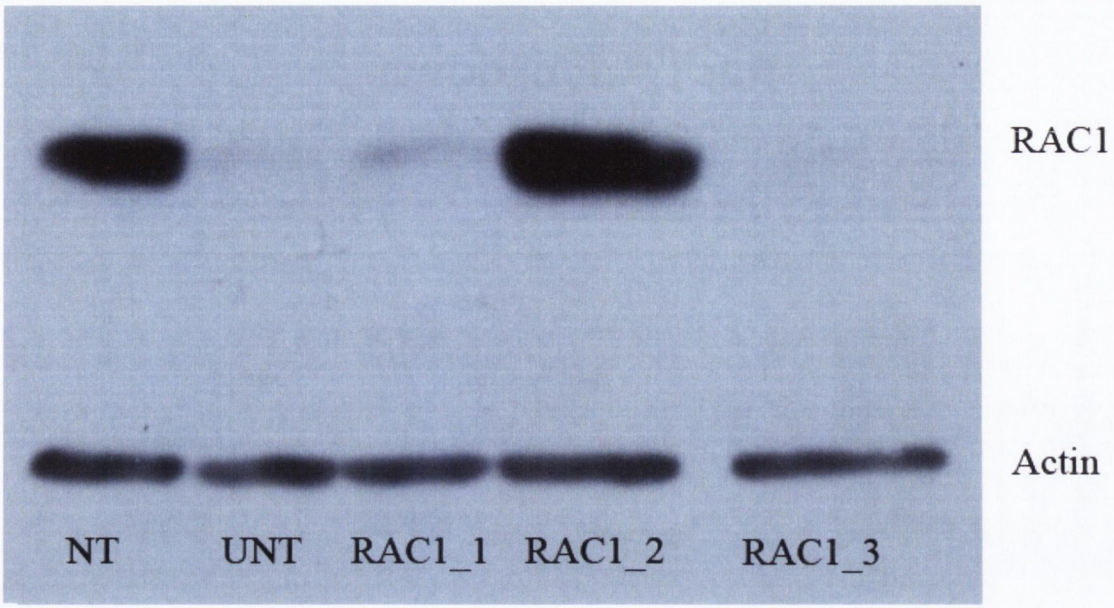

Figure 3.5.15: Western Blot showing suppression of RAC1 *in vitro*

This western blot is one of three blots carried out using the Abcam antibody against RAC1. The first lane is lysate from HeLa cells which were transfected with non-targeting siRNA (NT). and CMV_RAC1. The second lane is lysate from untransfected cells (UNT). Lanes 3-5 received the siRNAs indicated in the figure and CMV_RAC1. All RAC1 siRNA treated lanes showed almost complete suppression with the exception of lane 2 which has a heavy RAC1 specific band at 21kDa.

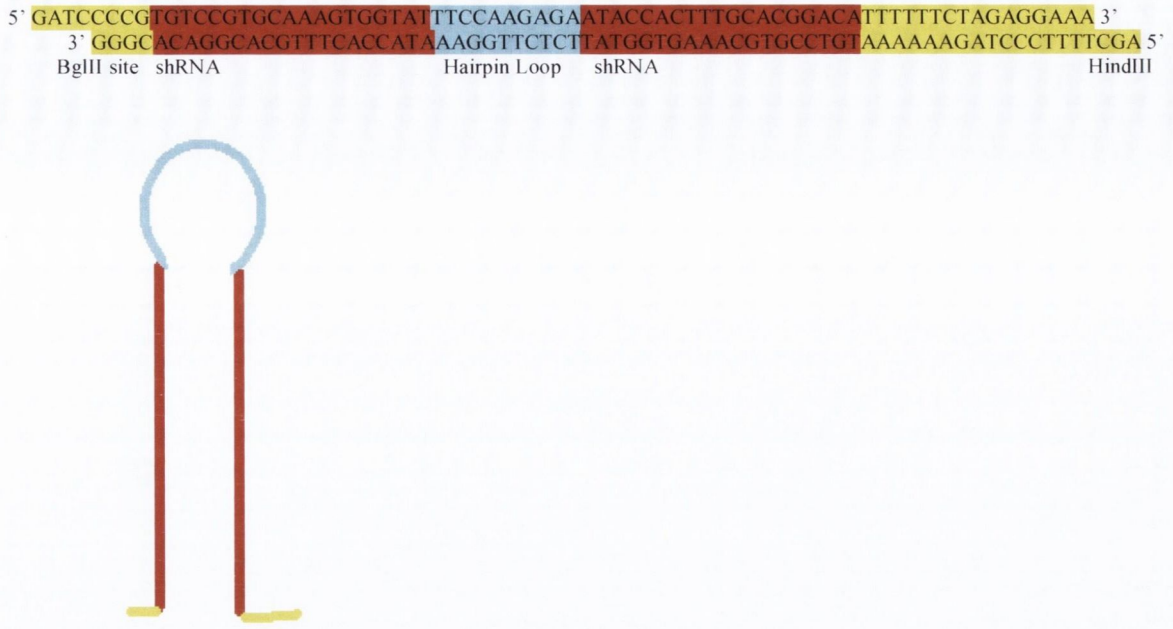

Figure 3.5.16: shRNA design for cloning

Sense and antisense complementary oligonucletoides were annealed to form a double stranded DNA oligomer. This oligomer was then cloned in to the pSuper vector using the *BglII* and *HindIII* sites indicated in the figure. This figure shows both the sequence of the shRNA and highlights the functional features of the shRNA construct based on the siRNA sequence of RAC1_1. The shape and features of the resulting RNA transcribed from this locus is shown below the sequence of the annealed oligonucleotides.

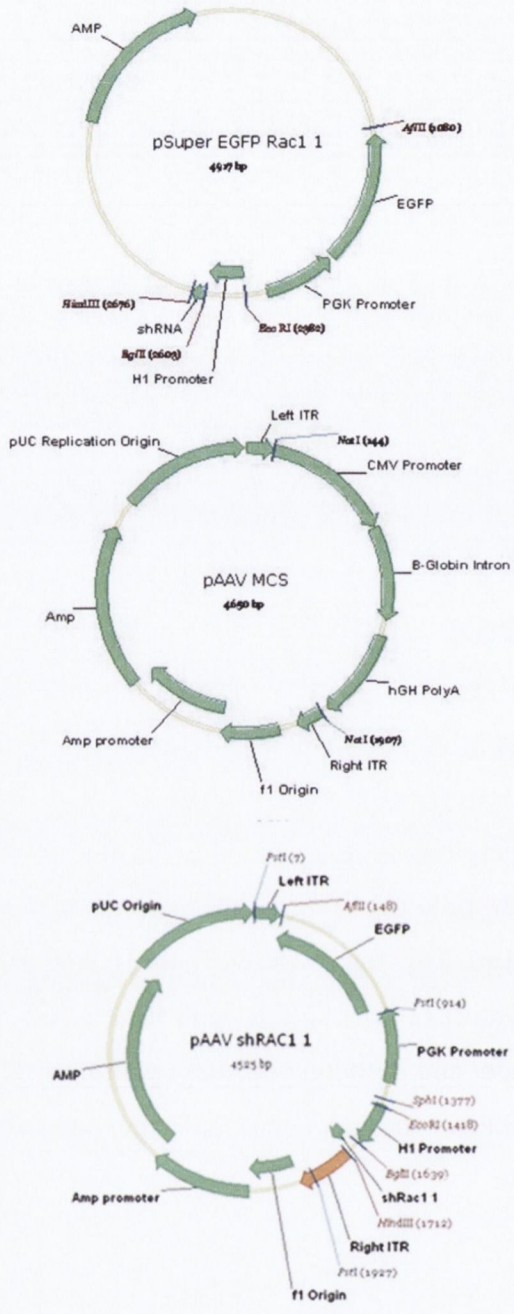

Figure 3.5.17: Cloning of the shRNA in to pAAV

Schematic showing the vector maps of pSuper_EGFP_Rac1_1, pAAV_MCS and pAAV_shRAC1_1. The shRNA was cloned in to pSuper.EGFP to create pSuper_EGFP_Rac1_1 using the *BglII* and *HindIII* sites marked on the vector. The H1 driven shRNA and PGK promoter driven EGFP section of DNA was then excised from pSuper, blunted and cloned in to pAAV_MCS using the *NotI* restriction sites marked on the pAAV_MCS vector. This produced the pAAV_shRAC1_1/3 vectors.

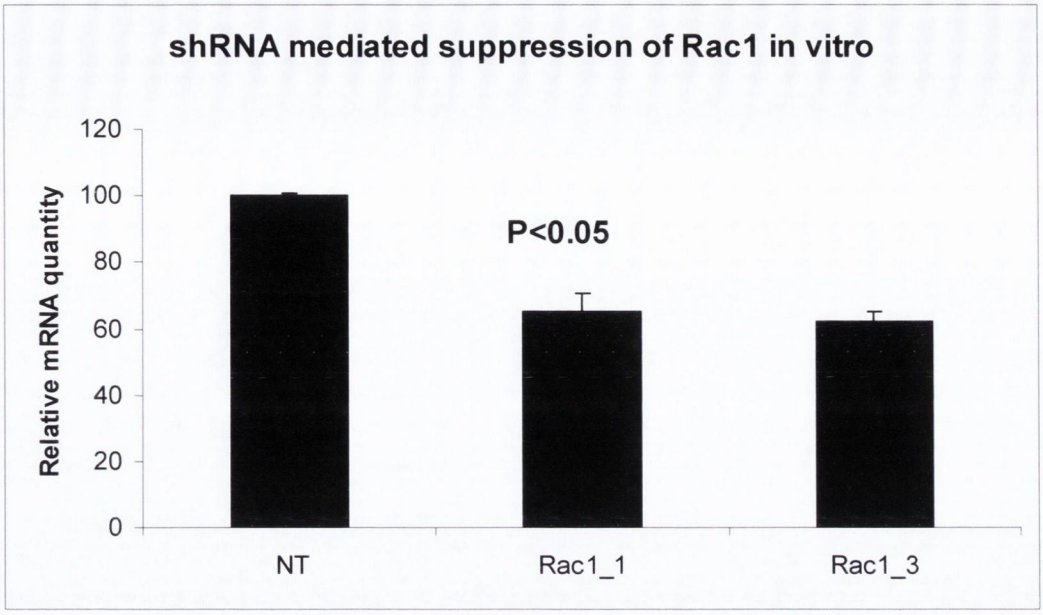

Figure 3.5.18: shRNA mediated suppression of *RAC1 in vitro*

Bar chart displaying the relative mRNA transcript quantities of pAAV_shRAC1_1 and pAAV_shRAC1_3 treated HeLa cells compared to NT20 treated cells. The relative suppression values are 34.66% (±10.1%) and 37.66% (±5.5%) for pAAV_shRAC1_1 and pAAV_shRAC1_3 treated cells respectively. The P-values for each of these shRNA data points were 0.014 and 0.004 respectively. P-values were calculated using a two way unpaired student's t-test. This chart demonstrates lower than expected suppression values based on the suppression data gleaned from the siRNA data of the same cell type.

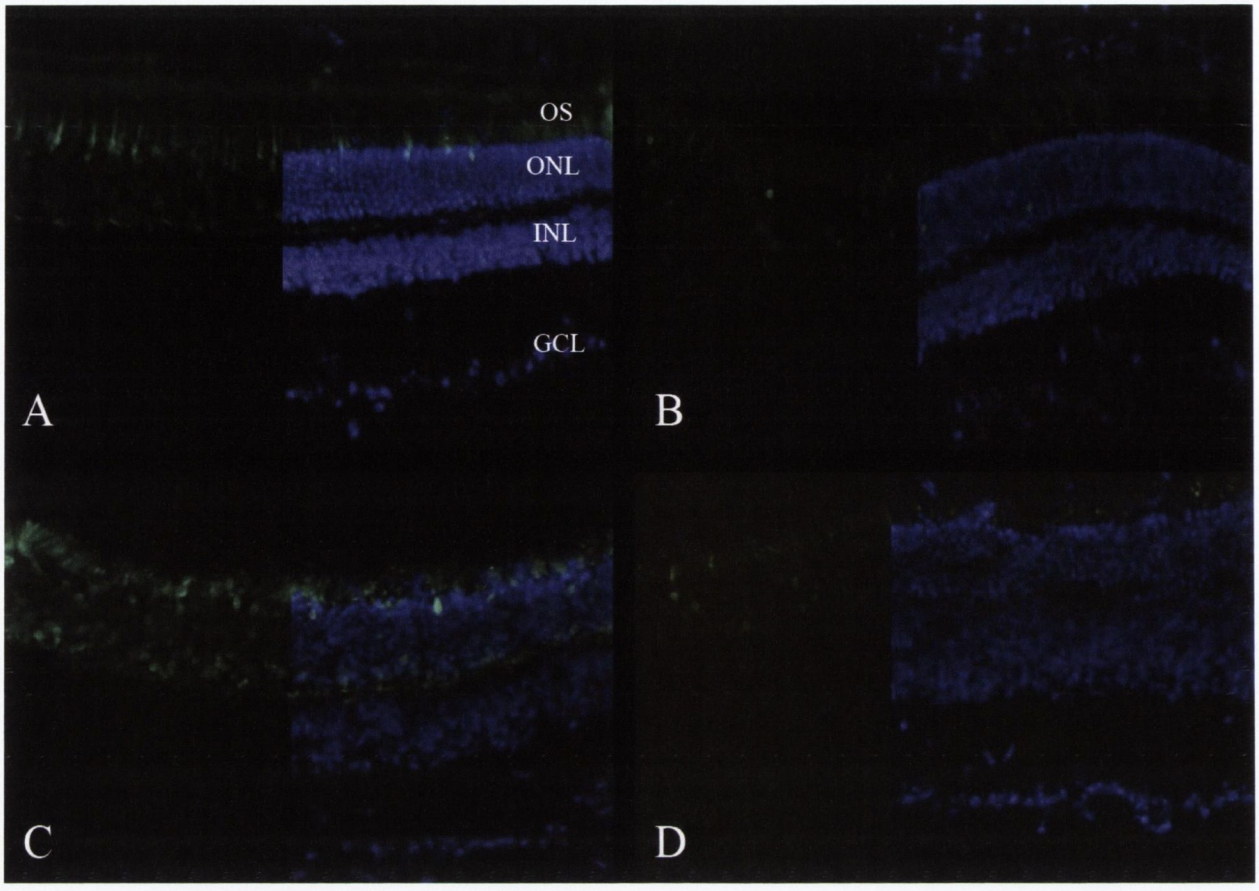

Figure 3.5.19: Retinal Histology showing EGFP expression from shRAC1 viruses

Retinal sections were examined to verify successful transduction of the pAAV_shRAC1_1/3 viruses. All images have been overlaid with the DAPI staining of the same section (in blue). DAPI will stain all layers containing a nucleus and therefore illustrate the positions of the ONL, INL and GCL. Images A and C show successful transduction and expression of EGFP from NT20 virus. Image B shows very low expression of EGFP from the pAAV_shRAC1_1 virus. This is from the contralateral eye to the eye from which image A was taken. Image D shows a similarly low expression of EGFP from pAAV_shRAC1_3 virus in the contralateral eye from which image C was taken. These data suggest either low expression of EGFP or poor transduction of these viruses to the retina. OS-Outer Segments, ONL-Outer Nuclear Layer, INL-Innear Nuclear Layer, GCL-Ganglion Cell Layer.

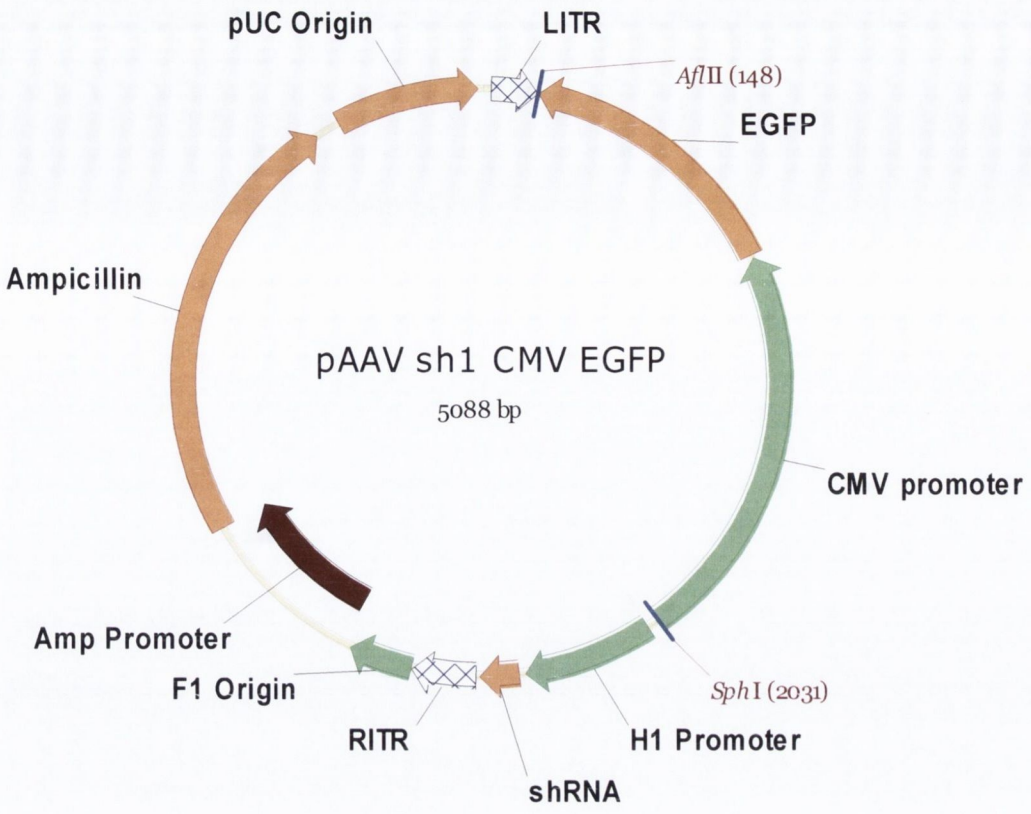

Figure 3.5.20: The pAAV_shRAC1_1 plasmid with CMV promoter driven EGFP

Due to the low EGFP expression obtained using the PGK promoter, a new AAV plasmid was cloned to contain CMV promoter driven expression of EGFP. This has been used numerous times by other members of the research group and had been shown to drive adequate expression of EGFP in NT20 AAV injected eyes. This figure illustrates the *AflII* and *Sph1* sites used to clone a CMV driven EGFP DNA segment from the NT20 plasmid in to the previous Rac1 shRNA AAV plasmid.

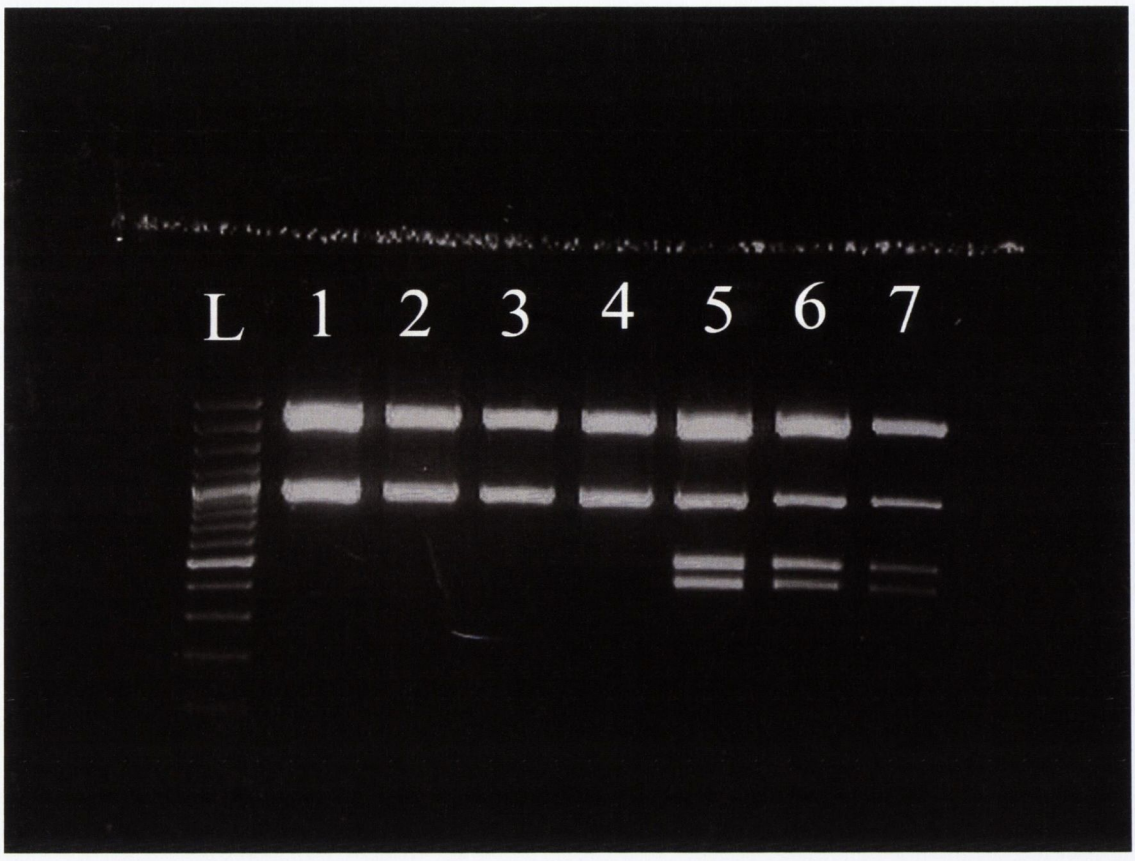

Figure 3.5.21: Restriction Enzyme Analysis of AAV_shRAC1_1/3

Restriction analysis of AAV_shRAC1_1 and AAV_shRAC1_3 with *PstI* (lanes 2&3 and lanes 4&5 respectively) and restriction analysis of AAV_shRAC1_1 and AAV_shRAC1_3 with *PstI+EcoRI* (lanes 6&7 and lane 8 respectively). This image of an agarose gel loaded with digested DNA show bands of the expected length of 2605, 934, 512 and 443 nucleotides for digestion with *PstI+EcoRI*. For digestion with *PstI* alone this gel shows the expected bands of 2605, 971 and 938 nucleotides. The resolution of this gel makes it impossible to distinguish the 971 and 938 bands due to their relatively large size in comparison with the lower bands.

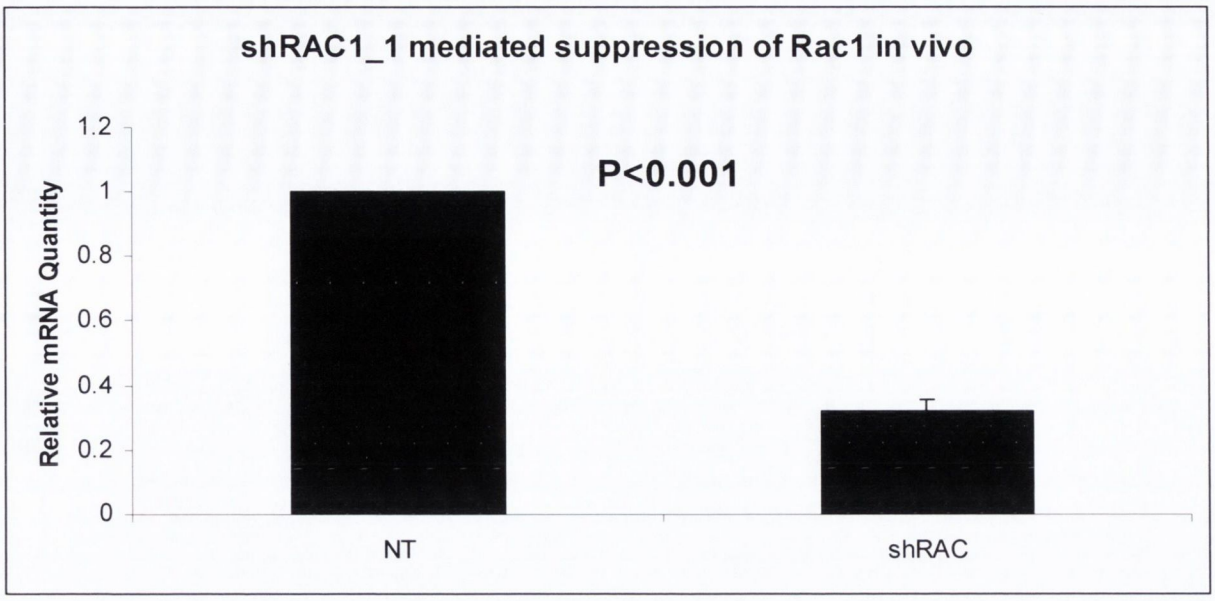

Figure 3.5.22: AAV_shRAC1_1 mediated suppression of *Rac1 in vivo*

Bar chart showing expression of *Rac1* mRNA in the retinas of eyes which received AAV_shRAC1_1 relative to *Rac1* expression levels seen in the contralateral retinas which received NT20. The relative expression level in the shRNA treated eyes was 31.66 (±3.8)% of the NT20 treated eyes. A two way paired student's t-test on this data produced a P-Value of 0.00051. This shows a functional effect of the shRNA on endogenous *Rac1* expression in the transduced region of the retina.

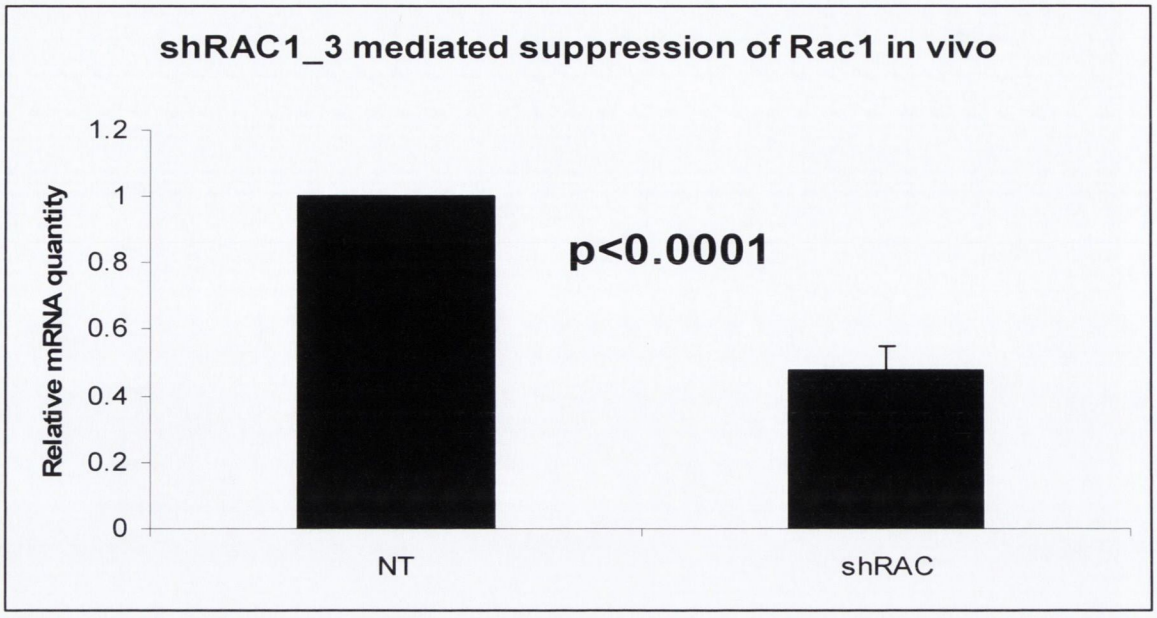

Figure 3.5.23: AAV_shRAC1_3 mediated suppression of Rac1 *in vivo*

Bar chart displaying the expression of *Rac1* mRNA in the retinas of eyes which received AAV_shRAC1_3 relative to *Rac1* expression levels seen in the contralateral retinas which received NT20. The relative expression level in the shRNA treated eyes was 47.60 (±7.47)% of the NT20 treated eyes. A two way paired student's t-test performed on this data produced a P-value of 0.0000964.

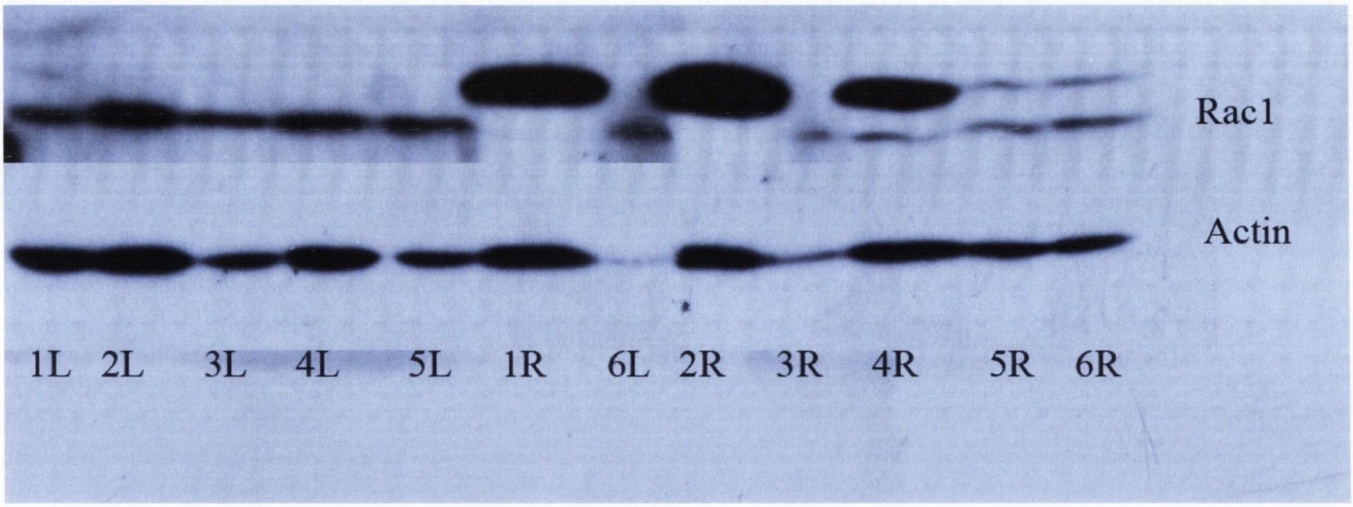

Figure 3.5.24: Western Blot showing Suppression of Rac1 *in vivo*

To confirm the mRNA suppression values obtained by RT-qPCR of Rac1 using pAAV_shRAC1/3, a western blot was carried out on retinal tissue which had been transduced with the Rac1 shRNA AAVs to confirm that transcriptional suppression also resulted in suppression of Rac1 protein expression. This figure demonstrates that both shRNAs discernibly suppress Rac1 protein in vivo. An unexpected result was the presence of an extra band just above the Rac1 band at 21kDa. This is thought to be RhoGDI, a GEF inhibitor of Rac1.

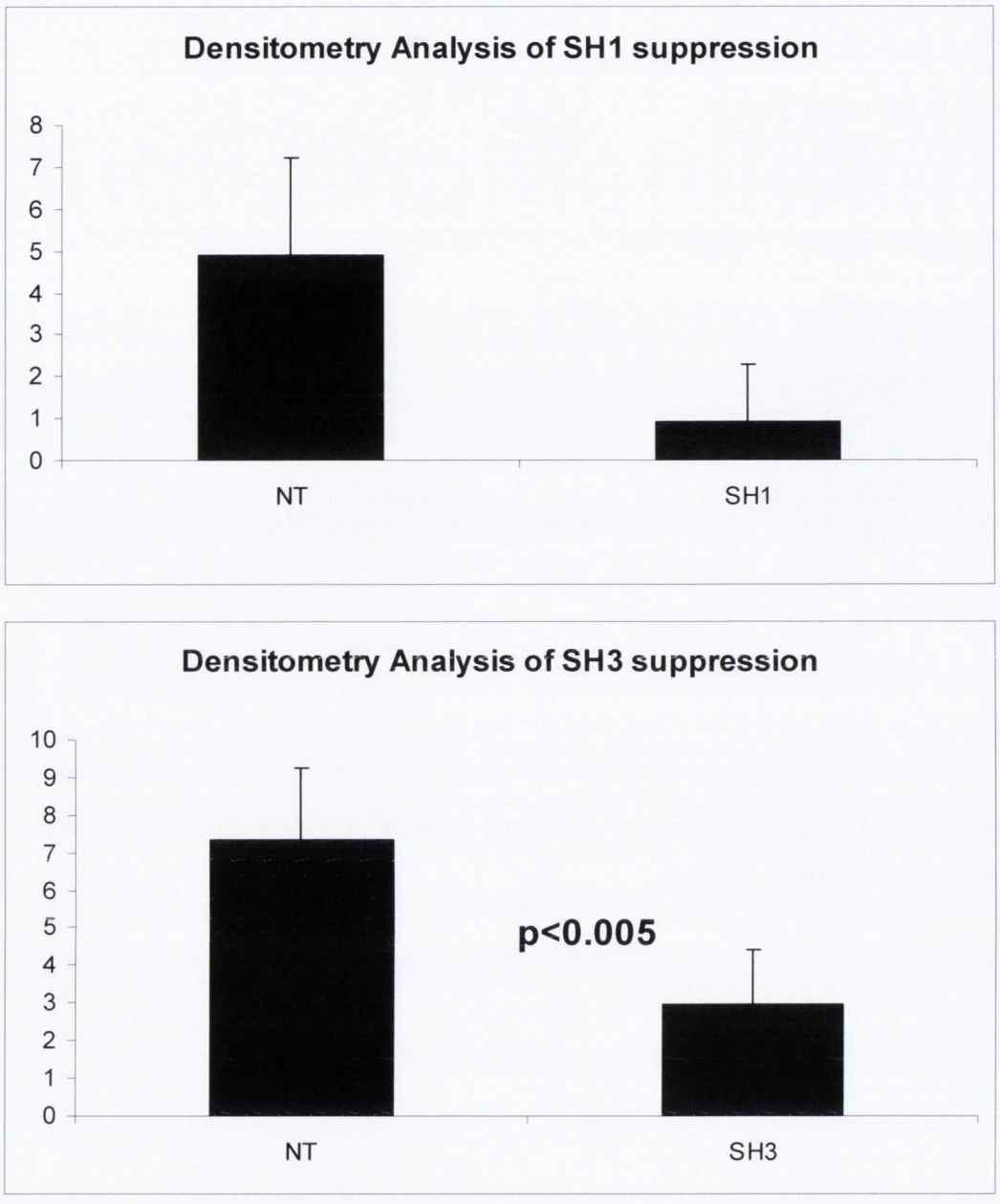

Figure 3.5.25: Densitometry analysis of Rac1 protein suppression *in vivo*

Densitometry analysis was undertaken on the western blot image presented in figure 3.5.24 to quantify the relative levels of Rac1 protein suppression achieved using AAV_shRAC1_1 and 3 (SH1 and SH3). This analysis provided suppression values of 81.14% (±28.4) and 60.0% (±19.5) for SH1 and SH3 respectively. A paired two way student's t-test performed on this data provided P-values of 0.07 and 0.004 for SH1 and SH3 suppression respectively. The analysis shows that both constructs are suppressing expression of Rac1 protein in transduced regions of the retina but that only SH3 mediated suppression of Rac1 has suppressed this expression by a statistically significant amount.

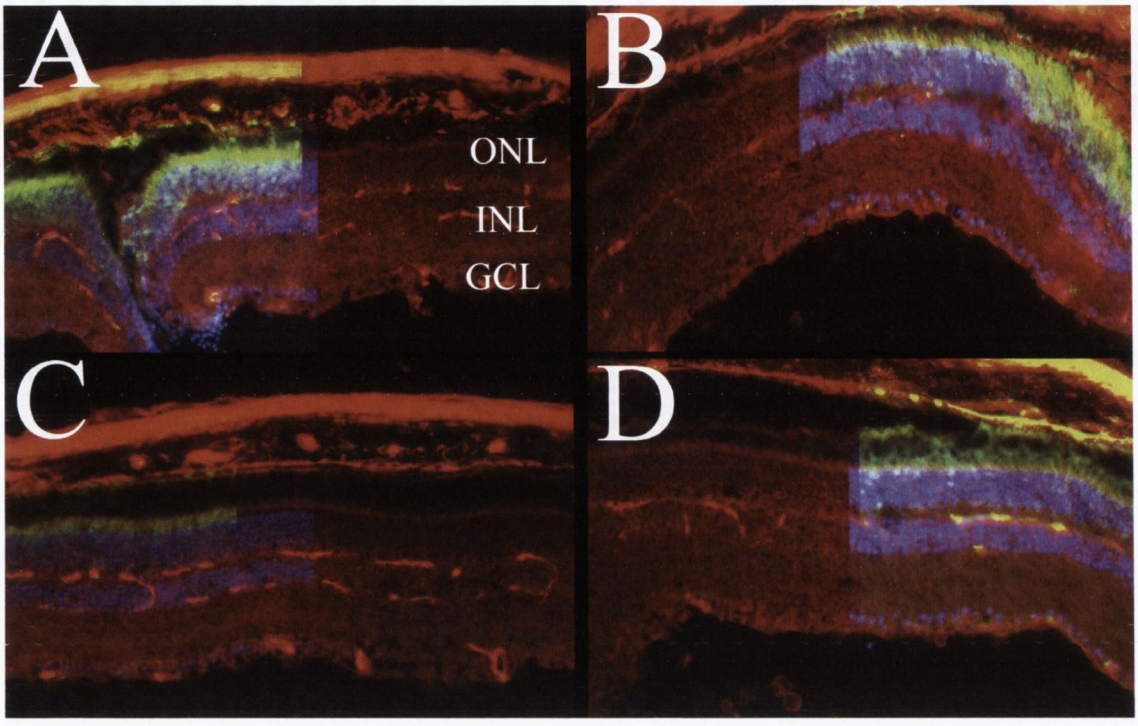

Figure 3.5.26: Retinal histology showing immunofluorescence using a Rac1 specific antibody

Immunohistochemistry was undertaken using a Rac1 specific antibody obtained from Abcam to assess any possible suppression of Rac1 in the ONL of injected retinas. Two wildtype mice of strain 129 were sub-retinally injected with NT20 and Paav_shRAC1_1 in the left and right eyes respectively at P21 and subsequently taken for histology three weeks later. This figure shows Rac1 staining in the left eyes (panels A and C) and contralateral right eyes (panels B and D) of the injected mice. This shows no discernible decrease of Rac1 specific fluorescence in any layers of the neural retina. DAPI staining (blue) of the ONL, INL and GCL as well as EGFP expression (green) of the transduced regions are overlayed on top of the Rac1 antibody staining (red).

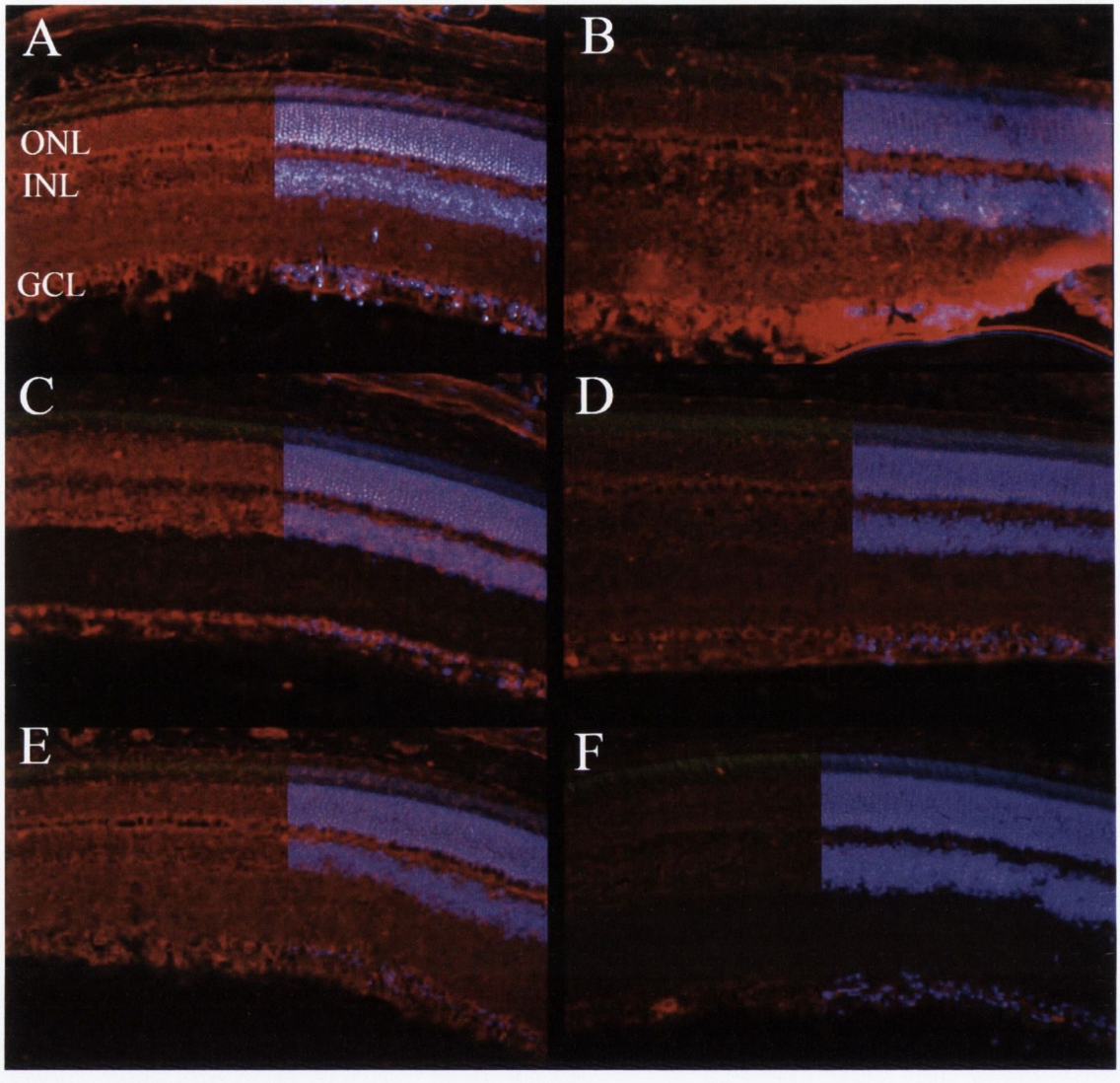

Figure 3.5.27: Retinal Histology showing Rac1 Expression in NT20 and AAV_shRAC1_1 treated eyes.

Immunohistochemistry was undertaken using a Rac1 specific antibody obtained from Millipore. Three mice were injected with NT20 and pAAV_shRAC1_1 in the left and right eyes respectively at P21. These mice were subsequently sacrificed three weeks later and the eyes taken for histology. This figure shows Rac1 antibody staining in the left eyes (panels A, C and E) and right eyes (panels B, D and F) of the three mice. Again no difference in staining pattern is observed between the left and right eyes of these mice. A difference in fluorescent intensity is observable but this seems to be an artefact of staining as the suppression is not limited to the ONL. It should also be noted that these eyes were fixed in 4% paraformaldehyde containing 5% acetic acid which has had the effect of dimming the EGFP signal, making it observable in the outer segments only.

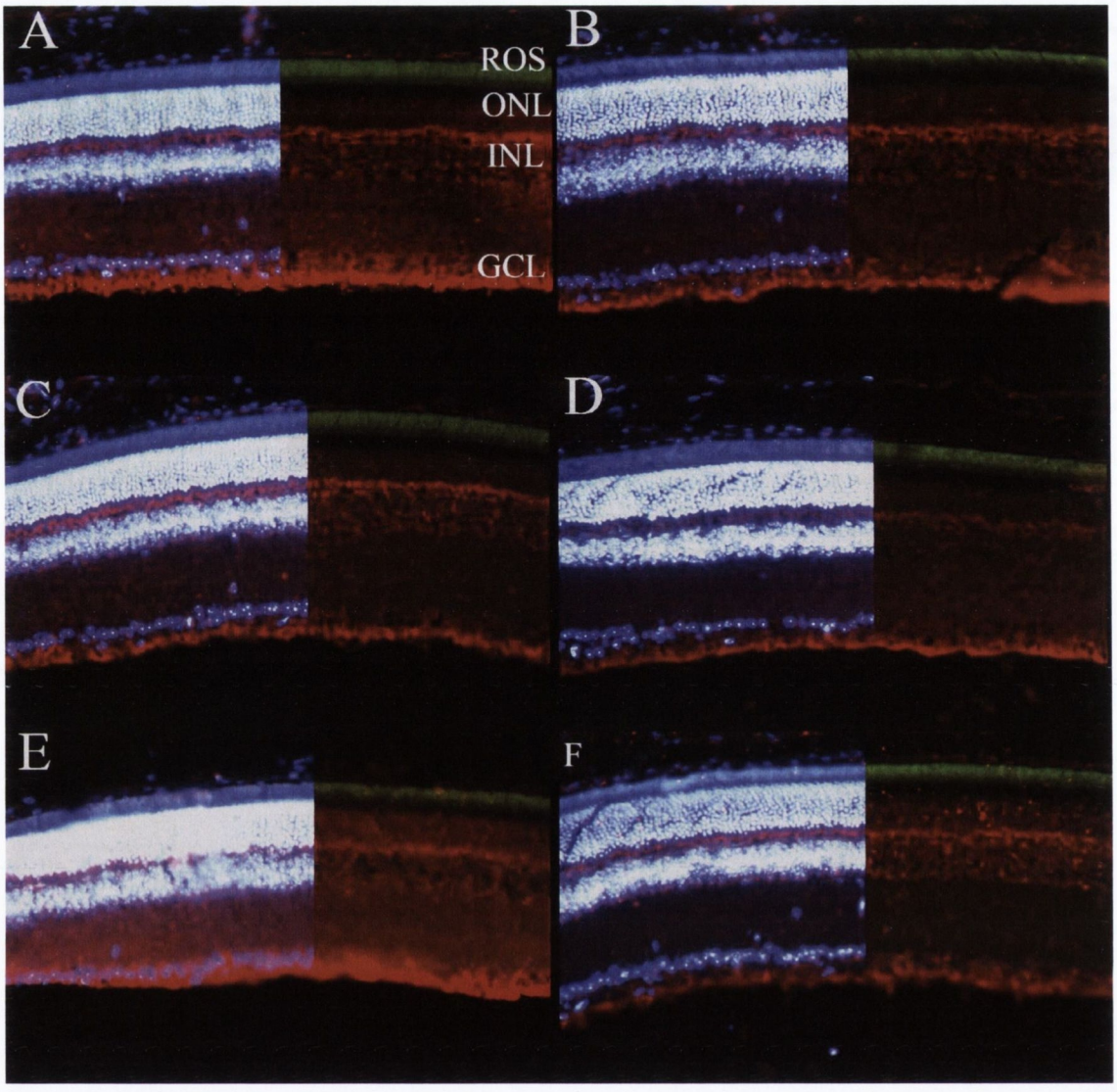

Figure 3.5.28: Retinal Histology showing Rac1 expression in NT20 and AAV_shRAC1_3 treated eyes

Immunohistochemical staining of retinas which had been treated with pAAV_shRAC1_3 and subsequently stained using a Rac1 specific antibody obtained from Millipore. These retinal sections were also fixed using 4% paraformaldehyde with 5% acetic acid. Control left eyes which had been sub-retinally injected at P21 are shown in panels A, C and E while the contralateral right eyes of the same animals received pAAV_shRAC1_3 and are shown in panels B, D and F. All animals were sacrificed and the eyes enucleated for sectioning at three weeks post injection. Again, no discernible decrease of Rac1 antibody staining is observed in the ONL of the Rac1 shRNA treated eyes of these animals. Rac1 antibody staining is shown in red while DAPI staining is shown in blue and EGFP expression marking the transduced regions of the retina is shown in green.

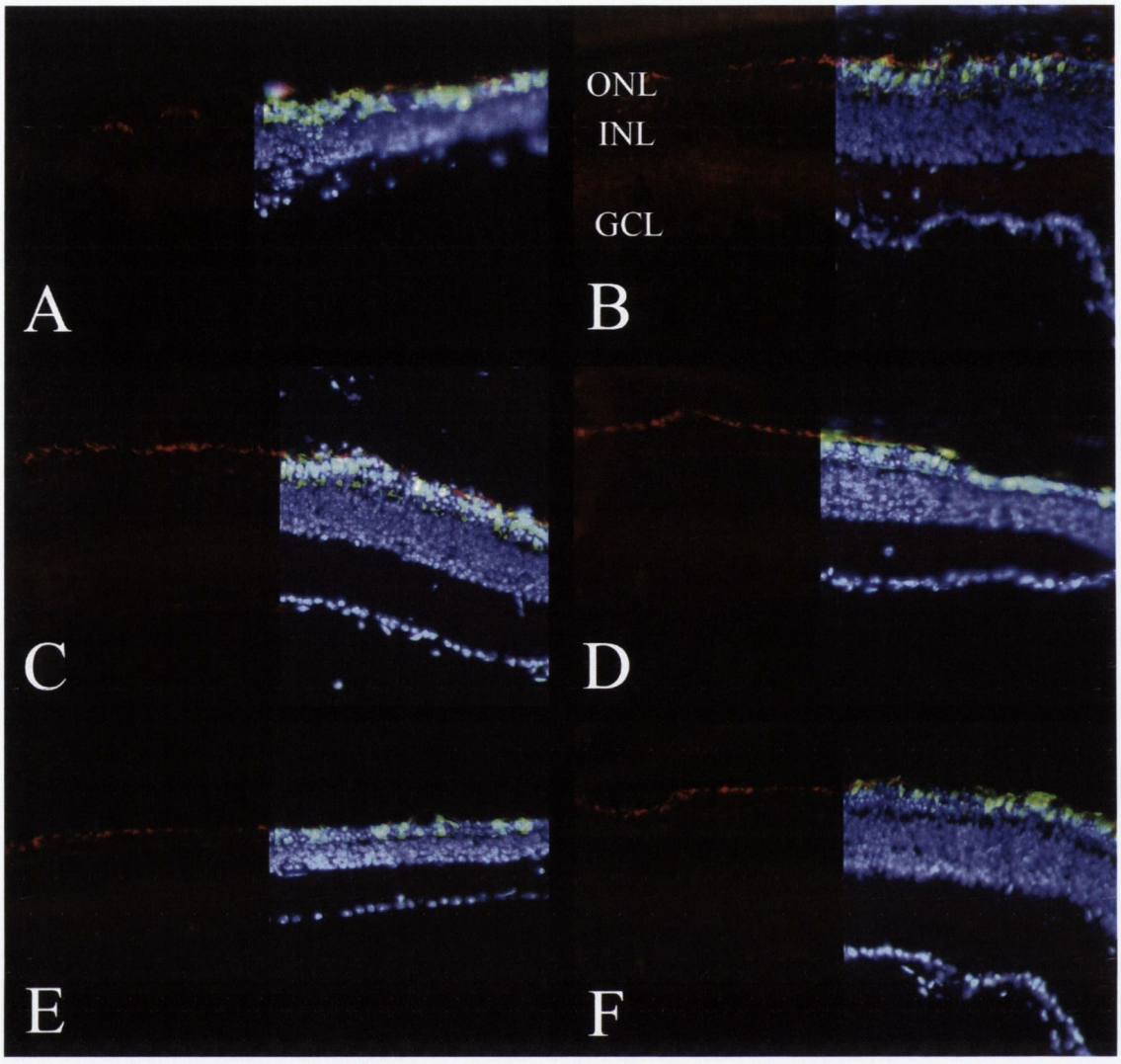

Figure 3.5.29: Retinal histology of hP347S transgenic mice treated with AAV_shRAC1_1 at 4 weeks post injection using a cone specific marker (n=3)

Transgenic mice carrying the hP347S rhodopsin mutation in a heterozygous manner were sub-retinally injected at P21 with NT20 in the control left eye (panels A, C and E) and pAAV_shRAC1_1 in the right eye (panels B, D and F). These mice were sacrificed 4 weeks post injection and the eyes were enucleated for sectioning and antibody staining. The Peanut Agglutinin (PNA) specific antibody was used to stain the cone cells of the retina to assess any effect *Rac1* suppression may have on the survival of this cell type. PNA antibody staining is shown in red while DAPI staining is shown in blue and EGFP expression indicating the transduced region of the retina is shown in green. This figure demonstrates no increase or decrease of cone survival in the Rac1 shRNA treated eyes compared to the contralateral control injected eyes.

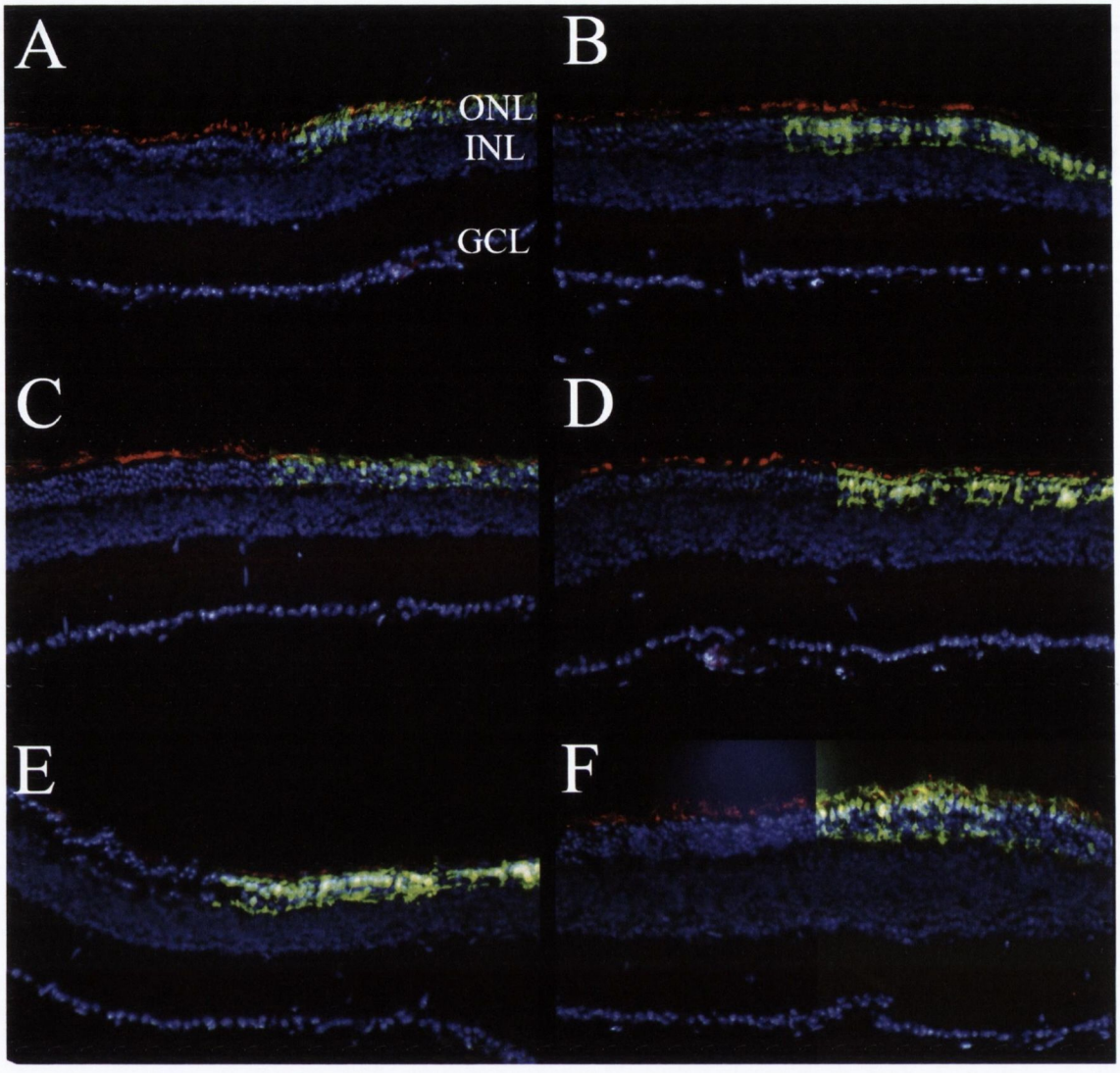

Figure 3.5.30: Retinal Immunohistology of hP347S transgenic mice treated with AAV_shRAC1_3 at 4 weeks post injection using a cone cell specific marker (n=3)

Transgenic mice carrying the hP347S rhodopsin mutation in a heterozygous manner were sub-retinally injected at P21 with NT20 in the control left eye (panels A, C and E) and pAAV_shRAC1_3 in the right eye (panels B, D and F). These mice were sacrificed 4 weeks post injection and the eyes were enucleated for sectioning and antibody staining. The Peanut Agglutinin (PNA) specific antibody was used to stain the cone cells of the retina to assess any effect *Rac1* suppression may have on the survival of this cell type. PNA antibody staining is shown in red while DAPI staining is shown in blue and EGFP expression indicating the transduced region of the retina is shown in green. This figure demonstrates no increase or decrease of cone survival in the Rac1 shRNA treated eyes compared to the contralateral control injected eyes.

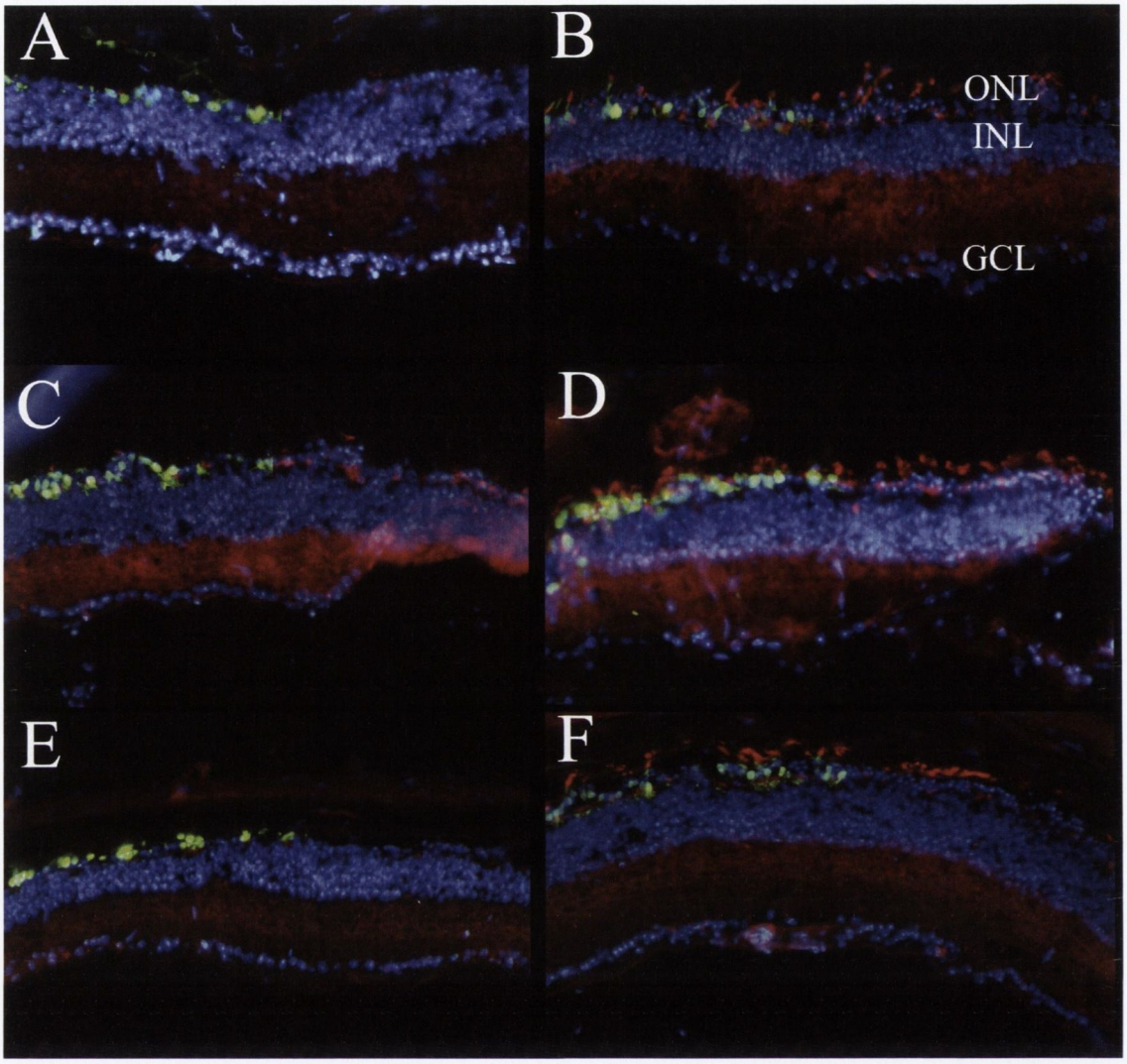

Figure 3.5.31: Retinal Immunohistology of hP347S transgenic mice treated with AAV_shRAC1_3 at 16 weeks post injection using a cone specific marker (n=3)

Cone survival was further assessed in pAAV_shRAC1_3 treated animals at 16 weeks post injection to assess any long term survival of cones which may result from suppression of Rac1 in the retina. Three mice were injected at P21 with NT20 in the left eye (panels A, C and E) and pAAV_shRAC1_3 in the right eye (panels B, D and F). These mice were sacrificed 16 weeks later and the eyes were taken for immunohistochemistry using the PNA specific antibody. PNA staining is shown in red while DAPI staining is shown in blue and EGFP expression indicating the transduced regions of the retina is shown in green. This shows a marginal but discernible increase in PNA staining of the ONL in eyes which received the Rac1 shRNA compared to the left eyes of the same mice which were treated with NT20.

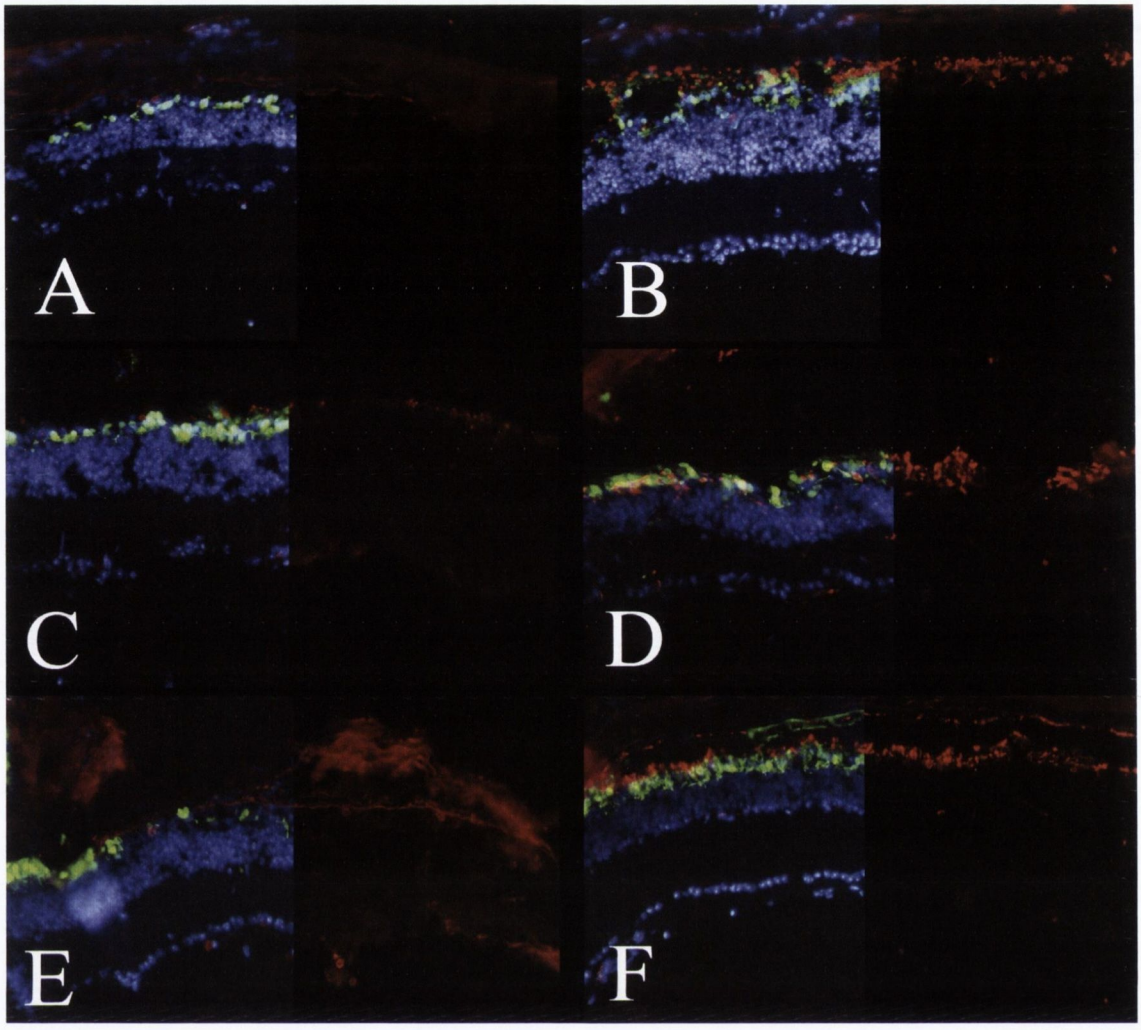

Figure 3.5.32: Retinal Immunohistology of hP347S transgenic mice treated with AAV_shRAC1_3 at 16 weeks post injection using a rod specific antibody (n=3)

Transgenic mice carrying the hP347S rhodopsin mutation in a heterozygous manner were sub-retinally injected at P21 with NT20 in the control left eye (panels A, C and E) and pAAV_shRAC1_3 in the right eye (panels B, D and F). These mice were sacrificed 4 weeks post injection and the eyes were enucleated for sectioning and antibody staining. The Rhodopsin specific antibody was used to stain the rod cells of the retina to assess any effect *Rac1* suppression may have on the survival of this cell type. Rho antibody staining is shown in red while DAPI staining is shown in blue and EGFP expression indicating the transduced region of the retina is shown in green. This figure demonstrates a clearly discernible increase in rod cells in the *Rac1* shRNA treated eyes compared to the contralateral control injected eyes, suggesting that suppression of Rac1 in transduced regions of the retina is preserving rod viability in this mouse model of RP.

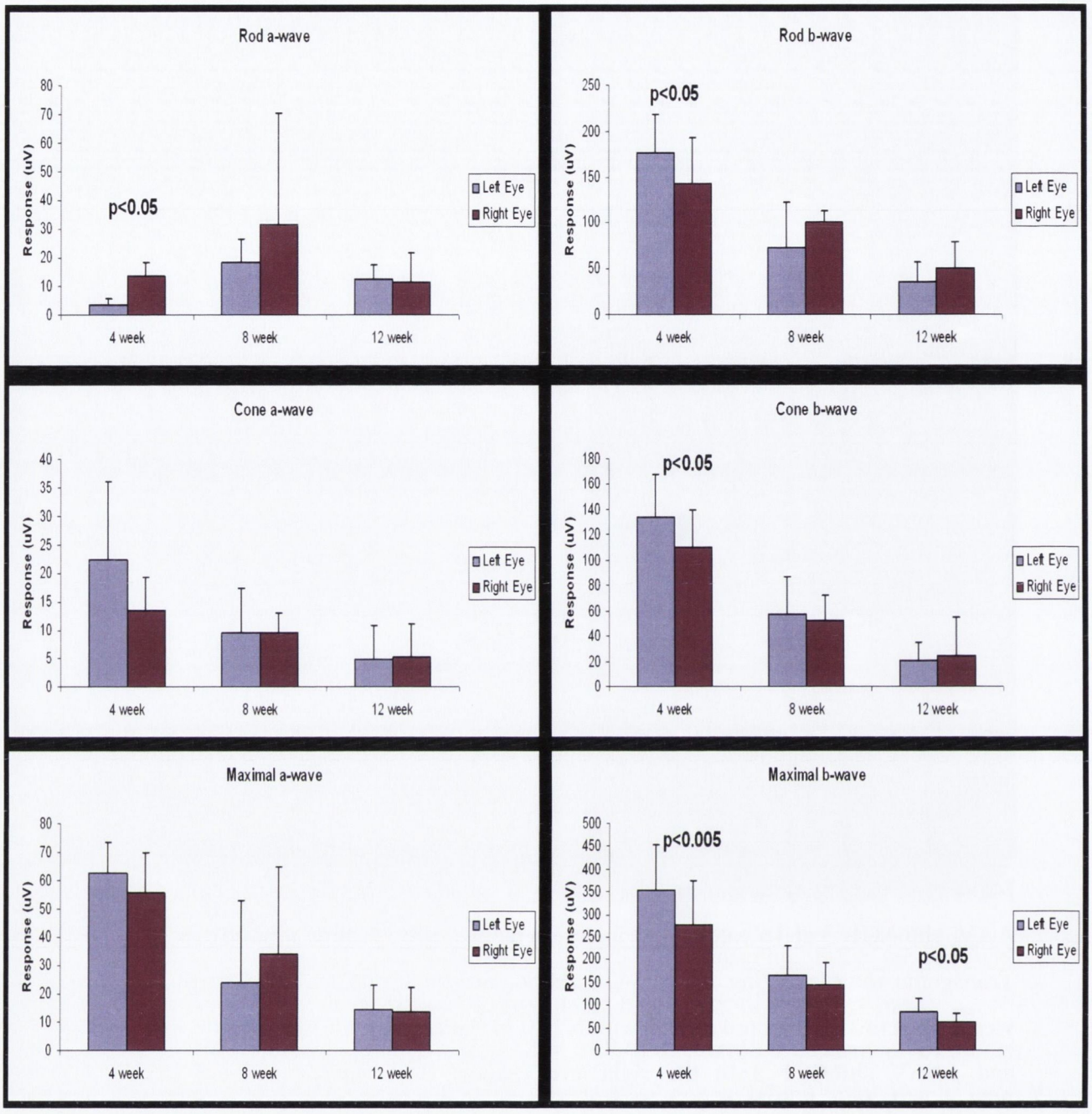

Figure 3.5.33: ERG analysis of AAV_shRAC1_1 injected hP347S transgenic mice at 4-12 weeks post injection (n=4)

Electroretinography was undertaken on four hP347S heterozygous mice sub-retinally injected with NT20 in the left eye and pAAV_shRAC1_1 in the right eye at P21 at three time points post injection; 4 weeks, 8 weeks and 12 weeks. The resulting response amplitude (in μV) for each category of ERG analysis was then averaged across the four mice and a standard deviation was calculated. The resulting data were graphed as a bar chart and a two way paired student's T-test was performed on all data to compare the left and right eye at each time point and in each category. Statistical significant differences are indicated above the bars of any categories which reached a P-value of 0.05 or less. Of

all the a-wave recordings, only the 4 week rod a-wave reached significance. However, for reasons discussed previously, the rod a-wave difference will not be discussed as valid. All b-wave values reached significance at 4 weeks indicating that the left eye had a higher response amplitude, thus suggesting that pAAV_shRAC1_1 is causing further retinal degeneration. Only one other category reached significance, the rod b-wave at 12 weeks. Again this showed a higher response amplitude in the control left eye. Some improvement in rod and cone b-wave was obtained at later time points but this failed to reach statistical significance.

	Left Eye			Right Eye		
	4 week	8 week	12 week	4 week	8 week	12 week
Rod a-wave	3.46±2.08	18.48±8.06	12.43±4.99	13.53±4.94	31.41±39.19	11.29±10.54
Rod b-wave	176±43.31	72.88±49.80	34.92±21.69	143.15±50.13	99.88±13.44	50.68±28.09
Cone a-wave	22.43±13.67	9.60±7.70	4.88±6.00	13.55±5.77	9.55±3.60	5.14±6.04
Cone b-wave	134.15±33.88	58.05±29.22	20.66±14.82	110.08±29.47	52.98±19.45	24.06±30.87
Maximal a-wave	62.53±10.90	23.99±28.86	14.20±9.04	55.53±14.56	33.92±30.87	13.27±8.79
Maximal b-wave	352±103.13	164.75±65.78	83.13±30.59	277.50±96.96	145.15±49.10	61.58±20.53

Table 3.5.3: Showing ERG recordings of SH1 injected hP347S mice

Amplitude responses from ERG analyses of pAAV_shRAC1_1 sub-retinally injected animals were averaged and a standard deviation was calculated for each category and time point. This table gives the amplitude response quantities which have been graphed in figure 3.5.27. All differences in amplitude response between left (control) and right (pAAV_shRAC1_1 treated) eyes which reached statistical significance are highlighted in yellow. The statistically significant P-values, as measured by two way paired student's T-test, attached to these data are as follows;

Rod a-wave 4 week: 0.035

Rod b-wave 4 week: 0.036

Cone b-wave 4 week: 0.006

Max b-wave 4 week: 0.0024

Maxb-wave12week:0.029

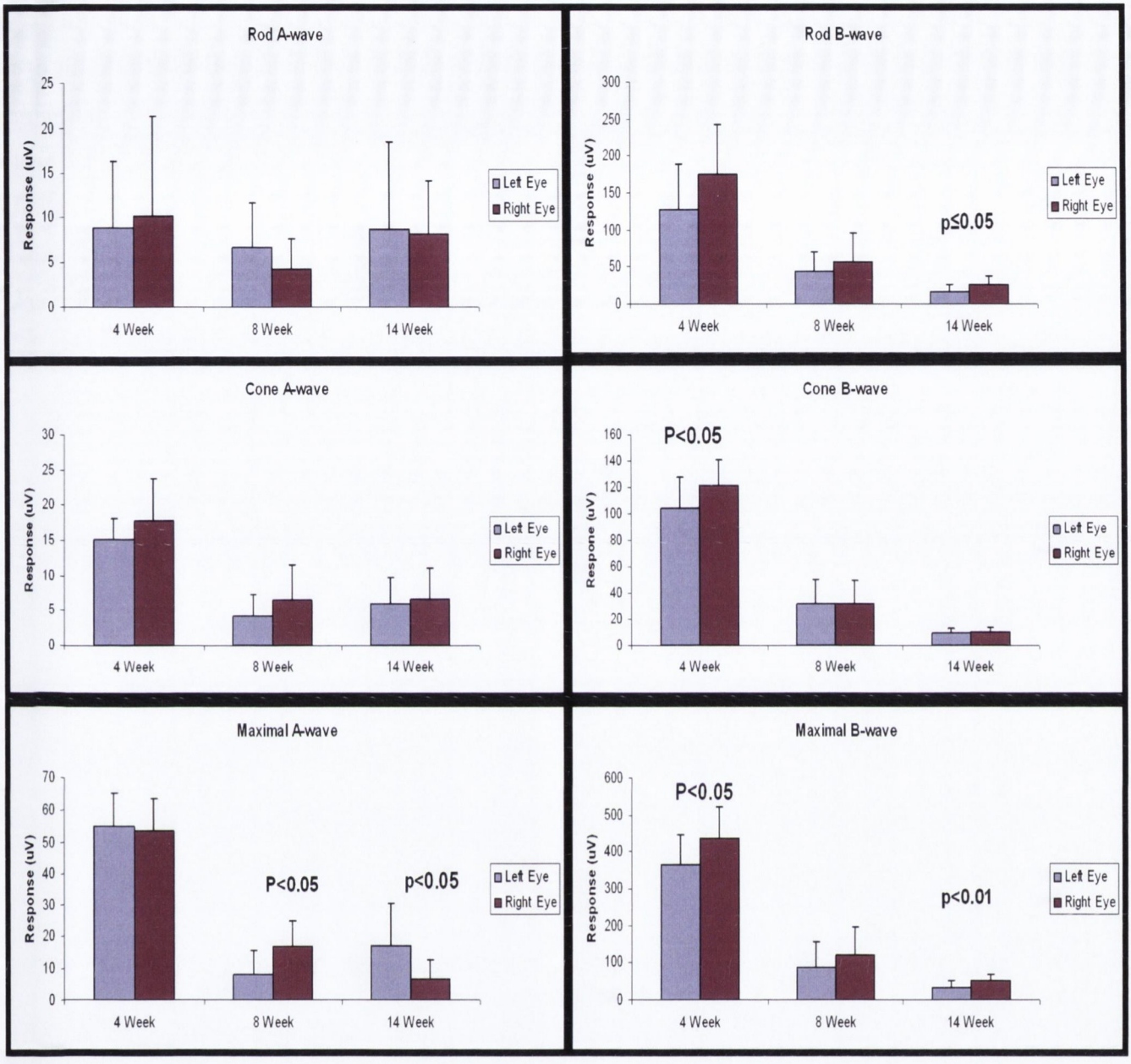

Figure 3.5.34: ERG analysis of AAV_shRAC1_3 injected hP347S mice at 4-14 weeks post injection (n=6)

Electroretinography was undertaken on six hP347S heterozygous transgenic mice which had been injected with NT20 in the left eye and pAAV_shRAC1_3 in the right eye at P21. These mice were subsequently analysed at 4, 8 and 14 weeks post-injection. The resulting amplitude response values (in μV) were averaged across each category and time-point and a standard deviation was calculated for each average value. These data are presented as a series of bar charts in this figure. A two way paired student's T-test was performed on the data to test for statistical significantly differences in amplitude response between left and right eyes. All data sets which reached significance are indicated above the relevant bars in

this figure. Although an increase in ERG response amplitude was recorded for all time points in the cone a-wave category, no data sets reached statistical significance. A statistically significant improvement in maximal a-wave was recorded in the right eye at 8 weeks, however this was lost at 14 weeks post injection and a statistically significant loss of cone a-wave function was observed in the right eye compared to the left eye at this time-point. An increase in right eye function was observed at all time points for each b-wave function except for cone b-wave 8 week. Of these, the data sets which reached statistical significance were rod b-wave 14 week, cone b-wave 4 week, maximal b-wave 4 week and maximal b-wave 14 week.

	Left Eye			Right Eye		
	4 week	8 week	14 week	4 week	8 week	14 week
Rod a-wave	8.85±7.49	6.65±5.10	8.76±9.67	10.26±11.03	4.21±3.39	8.21±5.96
Rod b-wave	126.52±62.69	44.22±25.69	15.79±9.81	174.0±69.11	57.5±38.45	25.5±12.81
Cone a-wave	15.16±2.90	4.17±3.16	6.09±3.65	17.81±6.07	6.48±5.15	6.61±4.55
Cone b-wave	104.14±23.71	31.96±18.50	9.42±3.47	122.0±19.14	32.36±16.83	10.73±3.08
Maximal a-wave	54.72±10.89	7.82±7.65	17.24±13.07	53.34±10.35	16.78±8.05	6.52±6.03
Maximal b-wave	363.80±82.64	87.34±68.37	33.94±17.67	437.60±82.68	121.62±75.46	51.92±14.98

Table 3.5.4: ERG amplitude values of AAV_shRAC1_3 injected hP347S mice.

Amplitude responses obtained from ERG analyses of pAAV_shRAC1_3 injected animals were averaged at each time point and category and a standard deviation was calculated for each data point. The resulting data which were graphed in figure 3.5.28 are presented here as a table. All amplitude differences which reached statistical significance between left (control) and right (pAAV_shRAC1_3 injected) eye are highlighted in yellow. The statistically significant P-values, as measured by two way, paired student's T-test, are as follows;

Rod b-wave 14 week: 0.053

Cone b-wave 4 week: 0.012

Max a-wave 8 week: 0.026

Max a-wave 14 week: 0.032

Max b-wave 4 week: 0.040

Max b-wave 14 week: 0.0097

Chapter 4:Expression of Recombinant Thioredoxin1 *in vitro* and *in vivo*

4.1 Introduction

The role of oxidative stress has become a topic of intense research in many disorders and has become associated with the pathology of Retinitis Pigmentosa over the past decade. As explained in greater detail in section 1.8, this oxidative stress appears to be a by-product of the mutations which cause RP. Therefore a therapeutic which aims to reduce or eliminate this over-abundance of ROS in the retina may result in effective saviour or life prolonging of the cells of the retina. This should in turn delay the onset of blindness in individuals carrying mutations which give rise to Retinitis Pigmentosa. The recent exploration of the pathology of RP and other retinal degenerations has shown that oxidative stress is a common feature of many retinal degenerations, both inherited and non-inherited (Doonan et al, 2012). Therefore, a drug or gene therapy which tackles oxidative stress will be mutation independent in the context of RP and may be applied to many retinal degenerations in which oxidative stress is a contributing factor.

Diabetic Retinopathy (DR) is one such retinal disorder in which oxidative stress has been implicated. Hypergylcaemia caused by diabetes mellitus causes a systemic increase in ROS which in turn causes activation of the transcription factor NFκB (Kowluru et al, 2003). This in turn causes neovascularisation of the choriocapilliaris (the layer of blood vessels closest to the retina) which will cause retinal damage and blindness. Recently, the drug Hesperetin has been shown to reduce the pathology of DR (Kumar et al, 2013). This drug was known to be a free radical scavenger and antioxidant. Treatment of DR induced rats with Hesperetin was shown to reduce caspase mediated cell death and preserve cells in all layers of the retina. A novel drug designed by O' Driscoll et al (2011) named BP3 has also been shown to increase the longevity of retinal cells in three different models of oxidative stress causing retinal degeneration model mice. This drug reduced levels of ROS and preserved photoreceptor morphology in a light induced retinal degeneration, a RP and an induced glaucoma mouse model. Finally, a light ablation mouse model of photo-oxidative induced retinal degeneration was recently treated successfully with a compound derived from rosemary plants called carnosic acid (Rezaie et al, 2012).

The search for drugs which effectively reduce the ROS burden on cells in models of RP has also produced promising results. Mockel et al (2012) have successfully treated retinal explants carrying a Bardet-Biedl syndrome (a form of RP) causing mutation with three drugs which inhibit the Unfolded Protein Response (UPR) pathway. The role of this pathway in the pathology of rhodopsin linked RP is discussed in further detail in section 1.8. Inhibition of the UPR pathway successfully preserved photoreceptor morphology. Unoprostone is a drug which has been tested, with promising results thus far, in a clinical setting for patients suffering from RP (Yamamoto et al, 2012). This too has been shown to act by reducing oxidative stress (Tsuruma et al, 2011). Treatment of the *rd10* mouse model of RP with Zinc–desferrioxamine has been shown to slow the pathogenesis of retinal degeneration of this model (Obolensky et al, 2011). The Zinc-desferrioxamine complex is a chelating agent which chelates ferrous iron molecules and thus sequesters them and reduces fenton reaction mediated O_2^- production in retinal cells, in turn reducing superoxide mediated cell damage and apoptosis. N-acetylcysteine (NAC) is another drug which has been tested in mouse models of RP (Lee et al, 2011). This compound is an orally available antioxidant and was tested in two mouse models of RP, the *rd1* and *rd10* models. Both oral and topical eye administration of NAC was demonstrated to reduce the presence of ROS in the retina and prolong the structure of the retina and the functionality of cones but not rods in these animals, most likely due to the well established role of ROS in the death of cones compared to rods. Finally, treatment of the *rd1* mouse model of RP with 7-nitroindazole has been demonstrated to reduce the number of cone cells from dying in these mice (Komeina et al, 2008). 7-nitroindazole is a specific inhibitor of nNOS which plays a role in the formation of peroxynitrite (see section 1.7). These examples of targeted ROS reduction in the retina illustrate not only the pharmacological approach to ROS mediated retinopathy but also the observation that cone cells are typically the most responsive photoreceptor cells to treatments which aim to reduce oxidative stress in both rods and cones.

Although the examples provided above are all pre-clinical in nature, the progression of free radical scavenging drugs from pre-clical to clinical tests in humans has more recently been demonstrated with the use of MitoQ. This drug accumulates in the mitochondrial inner membrane where it acts as an antioxidant (Smith & Murphy,

2010). Treatment of several human disorders in mouse models (such as ischaemic heart disease, Adlam et al, 2005) later led to three clinical trials of this drug, one of which was terminated due to poor participant recruitment and therefore will not be discussed (NCT00329056, NCT01167088, NCT00433108). Although safety of administration was demonstrated in the two remaining trials, different outcomes were recorded for each. No benefit was observed in a clinical trial of the effect of MitoQ in Parkinson's disease (Snow et al, 2010). However administration of MitoQ reduced liver damage in a study of its effect on patients suffering from Hepatitis C (Gane et al, 2010). These data indicate that antioxidant therapies do have clinical relevance past laboratory studies.

While the search for drugs which ameliorate the symptoms of oxidative stress induced RP has shown promise, these drugs must be administered repeatedly. In cases such as NAC administration, the drug may be administered topically, an un-invasive procedure. However most drugs will require sub-retinal or intravitreal injection; procedures which may cause further damage to the already compromised eye. Therefore a long-lasting therapeutic which requires only one administration over the course of a number of years may hold better promise for the treatment of this disorder. Many gene therapies have been demonstrated to have prolonged expression from a single transduction of cells (DiGiusto et al, 2010). Therefore a single subretinal injection of an antioxidant gene therapy would provide a long term expression of a therapeutic molecule without the need for repeat injections over a long time span.

This approach to treating RP is a relatively new area of research and therefore there is little literature regarding gene therapy for oxidative stress in the retina in comparison to gene therapies which directly address the causative mutation of a disease. Increasing the expression of *catalase* and *SOD1* dismutase had been shown to be protective against oxidative stress related injury in the *rd10* mouse model of RP crossed with *catalase* and *SOD1* over-expressing transgenic mice (Usui et al, 2009). This cross demonstrated greater protection of both cone function and structure. Both *SOD1* and *catalase* are directly involved in the reduction of O_2^- to H_2O_2 and its subsequent reduction to water and molecular oxygen, thus these enzymes play crucial roles in maintaining ROS levels intracellularly. Delivery of

the *catalase* gene by AAV administration to rats which had been subjected to ischaemia/reperfusion injury has been demonstrated to decrease oxidative stress, protect retinal cells from apoptosis and preserve visual function (Chen & Tang, 2011). Adenovirus delivered *catalase* has also been demonstrated to protect cells of the RPE from light exposure induced oxidative stress in mice (Rex et al, 2004). Furthermore, delivery of the *SOD2* dismutase gene to the retina via AAV has been demonstrated to have a neuroprotective effect in the GCL of mice which had been subjected to ischaemia/reperfusion injury (Liu et al, 2012). A third component of this system named *Gpx4* has been demonstrated to reduce oxidative stress in an ischaemia-reperfusion mouse model of oxidative stress in a transgenic model which over-expresses *Gpx4* (Lu et al, 2009). *Gpx4* also plays a role in the reduction of hydrogen peroxide to water and oxygen.

AAV delivery of *γ-Secretase* and *PEDF* (Pigment Epithelium Derived Factor) has resulted in a reduction in the formation of superoxide anion in the retina of laser induced CNV (Choroidal Neovascularisation) mice which form an AMD like phenotype (Qi et al, 2012). This reduction in the levels of superoxide in turn preserved retinal structure by reducing choroidal neovascularisation. Shan et al (2011) were able to save retinal cells *in vitro* by transfecting these cells with XIAP (X-linked Inhibitor of Apoptosis), an anti-apoptopic gene. This gene was able to reduce cell death in cells which had been treated with H_2O_2 and these cells also demonstrated a reduction in oxidative stress. Verma et al (2012) have demonstrated that by introducing *ACEII* into the retina by AAV, it is possible to reduce oxidative stress and thereby reduce neovascularisation in both a mouse and rat model of diabetic retinopathy. ACEII is a component of the renin-angiotensin system which plays a role in vasodilation; reducing vaso-permeability by acting as a ligand for ACE. Components of this system are over-expressed in the eyes of patients suffering from DR and this system contributes to neovascularisation. Therefore the introduction of the ACEII component has had the effect of balancing the ratio of interacting components (ACE and ACEII) of the renin-angiotensin system and reducing oxidative stress associated with overexpression of ACE in the retinas of animal models of DR.

Given the success in treating animal models of RP by reducing oxidative stress, it was decided to introduce an antioxidant gene by AAV delivery in to the Pro23His and Pro347Ser mouse models of RP present in the TCD Ocular Genetics laboratory. The gene that was chosen was *Thioredoxin1*, encoding an antioxidant protein. Thioredoxin (Trx) is a small (105 amino acids) ubiquitously expressed protein which acts to balance the redox environment of the cell. Thioredoxin, Thioredoxin reductase (TrxR) and NADPH were discovered in 1964 as components which act as hydrogen donors for dNTP synthesis in E.coli (Laurent et al, 1964). The kinetics and mechanism of Trx suggest that it is physiologically equivalent to a reducing agent such as dithiothreitol. Trx is a cytoplasmic and extracellular enzyme. Trx2 is an isoform of Trx and is a membrane bound enzyme present in mitochondria. The Trx system serves to act as a protein and other substrate reductase. Electrons are transferred to TrxR which becomes reduced at conserved active sites Cys 32 and Cys35. These electrons are then used to reduce Trx disulfide bonds of cysteine residues (Holmgren and Lu, 2010; Nakamura et al, 2009). Trx subsequently reduces target proteins and other substrates through a hydrophobic surface (see figure 4.5.1).

The major cellular use of the TRX system is in the reduction of the ribonucleotide reductase (RNR) which is involved in the production of dNTPs. This is heavily used during the S phase of cell division when there is a large amount of DNA replication occuring (Holmgren & Lu, 2010). Due to its role in DNA synthesis, TRX proteins are often found to be over-expressed in many cancers; for example, TrxR has become a likely candidate for drug targeting to treat many cancers (Liu et al, 2012). Transgenic mice which over-express *Trx* have been shown to have a longer lifespan and protection from oxidative stress related disease (Holmgren & Lu, 2010). In the cytoplasm, reduced *Trx* acts to inhibit apoptosis by inhibiting apoptosis signal-regulating kinase 1 (*ASK1*, Saitoh et al, 1998) and by activating the Akt pathway by inhibiting PTEN (Meuillet et al, 2004). *Trx1* KO mice are embryonic lethal (Matsui et al, 1996).

Expression of the *Trx* gene is induced by cellular oxidative stress. Its promoter contains an anti-oxidant responsive element (ARE) which is activated by oxidative stress (Tanito et al, 2007). Trx also induces expression of HIF1α which increases

the expression of VEGF which in turn can cause angiogenesis of tumours (Welsh et al, 2002), resulting in Trx being proposed as a target of chemothereapeutics for some forms of cancer. However, the transgenic mouse model overexpressing *Trx* from the β-*actin* promoter shows no sign of sporadic tumour formation (Burke-Gaffney et al, 2005).

Thioredoxin1 (along with the other members of the TRX system) were found to be expressed heavily in the GCL and synaptic layers of the retina (OPL and IPL) with some expression in the ONL, RPE and choriocapiliaris in the wild type rat retina (Aon-Bertolino et al, 2011). Disturbance of the Trx system has been implicated in AMD through increases in oxidative stress in an Aβ amyloid plaque depositing mouse model. These amyloid plaques have been shown to have increased deposition in the retinas of mouse models of AMD (Goldblum et al, 2007). Trx was demonstrated to have reduced activity in these mice compared to wild type animals suggesting a role for Trx in protection against retinal degeneration (Lamoke et al, 2012). Thioredoxin1 seems to play a prominent role in light induced damage to the retina as transgenic mice over-expressing this gene displayed a neuroprotective phenotype in response to light damage compared to wild type mice (Tanito et al, 2002). Further evidence for the role of Trx in retinal degeneration was demonstrated by the protective effect of curcumin induced up-regulation of this gene in a light-induced retinal degeneration rat model (Mandal et al, 2009). This protection is likely induced in wild type animals in response to low levels of light exposure. It has been observed that *Trx* and *TrxR* are up-regulated in light adapted animals and that subsequent neuro-protection against photo-oxidative damage is due to activation of the ARE element in the promoter of *Trx* by Nrf2 (Tanito et al, 2007). Over-expression of *Trx* and *Trx2* in the retinas of mice with induced oxidative stress (due to optic nerve transection) has also been demonstrated to protect the cells of the GCL (Munemasa et al, 2010). Finally, Trx has been shown to protect against ischaemia-reperfusion injury to the retina when rats were pre-treated by systemic injection of recombinant human *TRX1* (Shibuki et al, 2000). Ischaemia-reperfusion is an oxidative stress induced pathology which occurs when tissues are exposed to normoxia after a period of hypoxia (eg. Retinopathy of prematurity in premature babies).

The strongest evidence to suggest a neuroprotective effect of *Trx* in RP was published by Kong et al in 2010. In this publication, a transgenic mouse model which over-expresses *Trx* was crossed with the *Tubby* mouse. The *Tubby* mouse is a mouse model of Usher's syndrome, a ciliopathy which results in sensorineural deafness and retinitis pigmentosa (Noben-Trauth et al, 1996; Kleyn et al, 1996; Mukhopadhyay & Jackson, 2013). The progeny of these mice demonstrated a preservation of over half of the photoreceptors that are lost in the *Tubby* mouse by P34. Furthermore, the progeny displayed a two-fold increase of both cone a-wave and cone b-wave at P34 compared to *Tubby* mice as recorded by electroretinography (ERG). These data indicate that over-expression of *Trx* results in functional benefit in the retina of mice carrying an RP-like mutation.

The objectives of this chapter were to create a novel AAV plasmid containing the *Thioredoxin1* gene downstream of a promoter which would be active in the ONL of the retina. Data were also gathered regarding the expression of this construct *in vitro* before production of high titre AAV 2/5 using this plasmid began. This virus would then be used to evaluate AAV mediated over-expression of the *Thioredoxin1* gene *in vivo*, before examining the effects of *Thioredoxin1* over-expression in two mouse models of RP at both a structural and functional level.

4.2 Materials and Methods

All materials used are listed in section 2.1

4.2.1 Cloning of the Thioredoxin1 Gene

To observe the effects of *Thioredoxin1* over-expression in the retina of mouse models of RP, it was first decided to clone the gene in to the pAAV_MCS plasmid. The mouse *Trx* gene was ordered from a cDNA library housed by Source Bioscience (Clone 4216106). This gene was contained within the pCMV_SPORT6 plasmid and was received to the laboratory as a DNA mini-preparation. It was subsequently transformed in to XL-1 Blue competent *E. coli* cells as outlined in section 2.2.2.11. Based on the sequence of the MCS of the pCMV_SPORT6 and the reference sequence of mouse *Trx* (NM_011660) it was decided to sequence the insert and surrounding regions of the plasmid using the Trx_qF, Trx_qR and M13 primers. The binding sites for these primers were within the *Trx* gene and upstream of the MCS of the pCMV_SPORT6 plasmid. This revealed the presence of *XbaI* and *EcoRI* sites on either end of the *Trx* gene. The sequence of the *Trx* gene was also aligned against the reference sequence of mouse *Trx* which showed 100% homology between the CDS of both sequences. The *XbaI* and *EcoRI* sites were used to clone the *Trx1* CDS in to pAAV_MCS (see figure 4.5.2). The resulting pTrx_AAV plasmid was then mega-prepped for later use in AAV production and transfection of HeLa cells. This plasmid was also restriction digested to ensure the integrity of the plasmid (see figure 4.5.3) and sequenced using the Trx_qF and Trx_qR primers (see appendix).

4.2.2 Transfection and Harvesting of HeLa Cells

HeLa cells were plated in to 24-well plates at a seeding density of $2x10^5$ cells per well. These cells were incubated overnight at 37°C to allow the cells to reach over 90% confluency. At this time the cells were transfected with 0.4µg of DNA per well as outlined in section 2.2.2.6. The cells were then returned to incubation at

37°C for 24 hours before harvesting of RNA or 48 hours before harvesting of protein.

For harvesting for RNA extraction, cells were aspirated of media, washed with 1X PBS and then lysed with 250µl of Tri Reagent per well. The cells were left to lyse for 5 minutes before manual disruption of cell membranes by pipetting up and down. The lysates were collected and quadruplicate cells pooled in to a total of 1ml of lysate. The RNA was then extracted by chloroform extraction, as outlined in section 2.2.3.2. The RNA was DNase treated for one hour at 37°C before heat inactivation of the DNase at 80°C for ten minutes. All samples were assayed for RNA concentration by Nanodrop spectrophotometry.

For harvesting for protein extraction, cells were aspirated of media and washed with 1X PBS. The cells were then lysed with cell lysis buffer. The lysates were collected and quadruplicate wells were pooled in 2ml glass flat bottom specimen tubes. A magnetic stirrer was added to each tube and the lysates were incubated at 4°C for one hour with constant magnetic stirring. After one hour had elapsed, the lysates were transferred to eppendorf tubes, spun at 13,000 for 30 minutes at 4°C and the supernatants collected. The protein concentration in each sample was assayed by BCA assay.

4.2.3 Production of Recombinat AAV_Trx virus

The CMV_EGFP and pTrx_AAV plasmids were used to produce AAV 2/5 by the triple transfection method outlined in section 2.2.6. CMV specific primers were used to titre the resulting virus and these titres are given in section 4.3.

4.2.4 RT-qPCR Analyses

RT-qPCR analysis was undertaken on all RNA samples. RNA was diluted to 2ng/µl for each sample. The standard curve was created by making a 5X serial dilution of a 1/50 dilution of RNA from pTrx_AAV transfected cells or a ½ dilution of RNA from AAV_Trx injected retinas. All RT-qPCR analyses were carried out as outlined

in section 2.2.3.4. All standards were pipetted in to duplicate wells and all unknown samples were pipetted in to triplicate wells. A negative control containing RT mix and nuclease free water was also included. The primers used for this analysis were the Trx_q and ACTB primers.

4.2.5 Western Blotting

Western blotting was carried out as outlined in section 2.2.5. Briefly, all samples were boiled in a 1/5 dilution of 5X Laemmli buffer. The SDS-PAGE gel was then loaded with volumes containing equal amounts of total protein in each volume. Due to the small size of the Thioredoxin1 protein (~12kDa) the transfer of protein from gel to PVDF was carried out at 60mA for one hour to prevent the protein from passing through the PVDF layer completely. The primary antibody used was the Rabbit polyclonal anti-Trx antibody (Abcam). Blots were developed for no longer than 20-30 minutes due to the high expression of the CMV driven *Trx* from pTrx_AAV in HeLa cells and the high expression of endogenous *Trx* expression in HeLa cells. This applied to protein from Trx_AAV injected retinas too as the CMV promoter drives strong expression of *Trx in vivo*. After developing for Trx, all blots were probed for β-Actin using the rabbit anti-β-Actin antibody (Abcam) to ensure equal loading of all samples.

4.2.6 Immunohistochemistry

All immunohistochemistry was carried out as outlined in section 2.2.8. Briefly, virus was injected sub-retinally and incubated in the retina for at least three weeks post-injection before harvesting of tissue. The mice were euthanised and the eyes enucleated. The eyes were then fixed in 4% Pfa before the lens was excised through the cornea of the eye. The eyes were then cryoprotected in sucrose solution before being frozen in OCT and sectioned. All sections were then immunostained. The anti-Trx antibody (Abcam) was diluted 1:200 in antibody solution and the secondary antibody was diluted 1:1000 in antibody solution. The slides were also stained for 5 minutes in DAPI solution to stain the nuclear layers before washing in

1X PBS and mounting of coverslips. The sections were subsequently examined by fluorescence microscopy.

4.3 Results

4.3.1 Cloning of the *Thioredoxin1* Gene into pAAV_MCS

The *Thioredoxin1* gene was ordered as a cDNA library clone from Source Bioscience as an ORF contained in the MCS of the pCMV_SPORT6 plasmid downstream of the CMV promoter. The M13 primer was used to verify the sequence of this plasmid. This demonstrated that the plasmid contained the mouse *Trx* CDS in a reverse orientation relative to the M13 primer binding region. The CDS contained in this plasmid corresponds to nucleotides 202-519 of the mouse *Trx* UniGene reference sequence (NM_011660). Sequencing also revealed an intact *XbaI* restriction site at the 3' end of the gene and an intact *EcoRI* restriction site at the 5' end of the gene. These sites were then used to clone the *Trx1* CDS in to the pAAV_MCS plasmid to create pTrx_AAV (see figure 4.5.2). The plasmid was sequence verified (see appendix) and restriction digested to confirm correct cloning (see figure 4.5.3).

4.3.2 Expression of Exogenous *Thioredoxin1* mRNA in HeLa Cells

HeLa cells were transfected using lipofectamine as outlined in section 2.2.2.6 in a 24-well plate (see table 4.5.1). Each well treated with pTrx_AAV received 0.4μg of plasmid DNA. Cells were transfected in three sets of quadruplicate wells and compared to three sets of untransfected quadruplicate wells. The cells were left for 24 hours post transfection before harvesting using Tri-reagent. This RNA was analysed by RT-qPCR using the mouse *Thioredoxin1* (Trx_q forward and reverse) and human/mouse β-Actin (*ACTB* forward and reverse) specific primers. The standard curve and dissociation curve of *ACTB* primers on HeLa cell derived RNA have previously been discussed in chapter 3 and therefore will not be covered here again. The dissociation curve of the Trx_q primers is presented in figure 4.5.4. This shows a small presence of primer dimers in these samples, however there appears to

be only one main amplicon, indicating specific amplification of *Thioredoxin1* cDNA. The standard curve is shown in figure 4.5.5. This gives an R^2 value of 0.980 and a slope of -2.29. While the R^2 value of this curve is an indication of a reliable quantification of *Trx* cDNA based on detection by the Trx_q primers, the standard curve is well above the ideal slope of -3.33, meaning that any quantities of unknown samples may have a standard error of ±30%. This low slope is due to the large change in expression between un-transfected and transfected cells at the point of analysis (ΔRn). The large difference means that the *Trx* amplicon from cDNA of transfected cell origin is reaching the lag phase of PCR at a low Ct value. This can be observed on the x-axis of the standard curve as the start of the curve begins.

The bar chart detailing the expression of *Trx* expressed from the pAAV CMV promoter is presented in figure 4.5.6. This demonstrates an approximate 16,918 (±6,864)-fold over-expression of *Trx* in transfected cells compared to un-transfected cells. The Trx_q primers will detect only mouse *Trx* which is the version of *Trx* expressed from the pTrx_AAV plasmid. Therefore the level of expression observed here cannot be considered physiologically relevant as the un-transfected cells can be considered to have zero mouse *Trx* transcripts present intracellularly due to their human origin. The point of this experiment however is simply to demonstrate the functionality of the pTrx_AAV plasmid and therefore the relative quantity compared to endogenous levels of *Trx* expression is not as relevant in this setting, as opposed to the testing of siRNAs in HeLa cells whereby the efficacy of the siRNA is evaluated by the relative quantity of mRNA transcripts.

4.3.3 Expression of Exogenous Thioredoxin Protein in HeLa Cells

Over-expression of *Trx* in HeLa cells which were transfected with pTrx_AAV plasmid was further confirmed at the protein level by western blot. Cells were transfected as described previously before the cells were harvested and the total protein extracted. The concentration of each protein sample was recorded by BCA assay before the western gel was loaded with volumes containing the same quantity of total protein. The western blot was probed with anti-Trx antibody and anti-β-Actin antibody to ensure equal loading of samples. Based on the RT-qPCR

analysis, this blot should display bands of very heavy intensity in the lanes loaded with lysate from pTrx_AAV plasmid compared to un-transfected controls. The resulting blot is presented in figure 4.5.7. This blot confirmed the presence of *Thioredoxin1* at the predicted size of 12kDa and these bands appear to be more intense in the transfected cell lanes compared to the untransfected cell lanes. However the change in expression is not as large as what was observed by RT-qPCR of the *Trx* mRNA. This can be explained by the fact that the RT-qPCR primers used to detect *Trx* will amplify mouse cDNA only and therefore will not detect any endogenous human *TRX* mRNA which is human given the origin of HeLa cells from a human cervical carcinoma. The anti-Trx antibody will detect both human and mouse Trx protein and therefore it will detect human Trx in the un-transfected cell lanes. Despite this change in parameters between the two sets of experiments, it is clear that the pTrx_AAV plasmid drives a discernible expression of *Thioredoxin1* at both the mRNA and protein level as evaluated by RT-qPCR and western blot respectively.

4.3.4 Production of Recombinant AAV 2/5

Two recombinant AAV 2/5 viral preparations were generated using the pTrx_AAV plasmid together with a reporter AAV_MCS plasmid containing CMV driven EGFP. This plasmid was used to produce AAV 2/5 viral vector which would act as a functional control for injection in to the contralateral eye to ensure any functional effects produced by expression of exogenous *Trx1 in vivo* are not simply the effects of over-expression from a CMV promoter. All viruses were produced using the triple transfection method as outlined in section 2.2.6. Different fractions of both the resulting Trx_AAV and CMV_EGFP viruses were titred by RT-qPCR using CMV promoter specific primers by the method outlined in section 2.2.6.3. The fractions with the highest titre were then chosen for further experiments *in vivo*. The viral titres for each of the highest titre fractions in vg/ml were as follows; CMV_EGFP: 1.12×10^{12} , Trx_AAV: 9.83×10^{11}.

4.3.5 Expression of Exogenous *Trx* mRNA *in vivo*

In order to confirm the functionality of both the *in vivo* transduction by recombinant AAV and the expression cassette of this virus, Trx_AAV was injected in to the right eye of six wild type strain 129 mice while the left eye was injected with the same volume of PBS. CMV_EGFP was not injected as this was used for later experiments examining the functional effect of *Trx* expression in the retina. The viral load delivered to the sub-retinal space was $2.9x10^9$vg in a 3µl volume. Subsequent to sub-retinal injection, the mice were left for three weeks to allow transduction and spread of the virus and for gene expression to begin. After three weeks had elapsed, the mice were euthanised and the retinas extracted. RNA was extracted from the retinal tissue as outlined in section 2.2.3.3. The percentage change in expression was calculated for each animal by comparison between the left and right eye. The results of this experiment are presented in figure 4.5.8. Figure 4.5.8 demonstrates a relative ~92±10.71-fold increase of *Thioredoxin1* mRNA in the right eye of these mice. A two way paired student's t-test confirmed that this change was statistically significant ($P<0.005$). Unlike earlier experiments *in vitro* which examined only the increase of exogenous mouse *Trx* mRNA in comparison to endogenous expression in HeLa cells (which contain human *Trx* that the *Trx* RT-qPCR primers cannot detect), this RNA analysis in mice includes evaluation of expression of both endogenous and exogenous expression of *Trx*. This is because the sequence of the recombinant *Trx* is of mouse origin and therefore the Trx_q primers will detect both endogenous and exogenous expression. It must also be noted that RNA was extracted from the whole retina which included cells which had not been transduced by Trx_AAV. It is estimated that approximately one third of the retina is transduced following sub-retinal delivery of high titre AAV 2/5 (Palfi et al, 2012). Therefore the expression of *Thioredoxin1* is likely much higher in the regions of the retina which had been effectively transduced.

4.3.6 Expression of Exogenous Trx protein *in vivo*

The expression of *Trx in vivo* was further analysed by western blot analysis of protein extracted from injected retinas of three wild type mice strain 129. These mice received the same titre of virus via sub-retinal injection as used previously for experiments examining mRNA expression ($2.9x10^9$vg). Briefly, mice were

euthanised three weeks post-injection and their retinas removed and placed in tissue lysis buffer. Protein was extracted as outlined in section 2.2.4.2. The concentration of total protein in each sample was assayed by fluorometry and the samples were loaded in to an SDS-PAGE gel in volumes containing equal quantities of total protein. The resulting western blot was probed with anti-Trx antibody and anti-β-Actin antibody. This western blot is presented in figure 4.5.9. The western blot demonstrates over-expression of Trx protein in all three Trx_AAV injected retinas. This over-expression is especially prominent in mice 2 and 3 which show a band of very heavy intensity compared to the band in the lane from the contralateral eye injected with PBS. The over-expression of Trx in mouse 1 however is more difficult to observe as the bands from the left and right eyes are very similar in intensity, with only a slight increase of expression in the right eye. Further investigation revealed that the injection in to the right eye of this mouse was not entirely successful as recorded by Dr Paul Kenna who carried out the sub-retinal injection. Unsuccessful injections are generally caused by a sub-retinal haemorrhage which can prevent efficient spread of the injected virus. It may also be caused by general leakage of the virus. Therefore some virus may have been lost to the surrounding regions of the eye, explaining the lack of retinal Trx expression in the retina of this eye compared to the right eyes of mice 2 and 3.

4.3.7 Immunohistochemical Analysis of Expression of Trx *in vivo*

Eyes from three mice which had been injected with Trx_AAV were taken for immunohistochemistry. This was undertaken to further confirm the functionality of the Trx_AAV virus and to determine the regions of the retina which express both endogenous Trx and exogenous Trx protein. The left eye received 3µl of PBS while the right eye received $2.9x10^9$vg of Trx_AAV within a 3µl volume via sub-retinal injection. Briefly, treated mouse eyes were enucleated, fixed and sectioned as outlined in section 2.2.8. The retinal sections were stained with anti-Trx antibody and DAPI. The resulting sections were examined by fluorescent microscopy and representative images recorded are presented in figure 4.5.10. These images demonstrate that endogenous expression of Trx is largely limited to the inner layers of the retina including the INL, with especially strong expression in the GCL.

Meanwhile, Trx expression in eyes that had been sub-retinally injected with Trx_AAV virus show strong exogenous expression in the ONL and RPE as well as limited endogenous expression in the INL and GCL. The strong over-expression in the ONL and RPE mirrors the tropism of AAV 2/5. A no primary antibody control was also included which was stained with secondary antibody only. This slide acts as a control for unspecific staining. The no antibody control shows no expression of Trx, demonstrating that the primary antibody used is most likely specific to Trx antigen and that the staining pattern observed in the experimental eyes is not a result of background staining by the secondary antibody. These results demonstrate that Trx_AAV is a functional virus which produces full length mouse Trx protein.

4.3.8 Effect of Exogenous Trx Expression in Pro23His RP model Mice

The hP347S mouse model of rhodopsin linked autosomal dominant RP has already been discussed in detail in section 3.3.16 and therefore will not be covered again here. The Pro23His transgenic mouse model of rhodopsin linked autosomal dominant RP was first described by Olsson et al in 1992. This transgenic mouse carries a patient derived rhodopsin transgene containing a missense mutation which manifests as an amino acid substitution of Histidine for Proline at codon position 23. The TCD Ocular Genetics laboratory breeds the P23H E line that was created by Olsson et al. This line shows a completely flat ERG response and one row of ONL nuclei as early as P20 (Olsson et al, 1992), a finding which has also been observed for this line by the TCD Ocular Genetics laboratory (O' Reilly et al, 2007). The genotype of P23H mice used in this study was P23H +/-Rho +/- on a wild type strain 129 background. Therefore these mice carry two rhodopsin alleles, one mutant and one wild type.

4.3.8.1 Immunohistochemical analysis of AAV_Trx retinas of Pro23His Mice

Due to the rapid degradation of the retina of Pro23His transgenic mice, the Trx_AAV construct was sub-retinally delivered to these mice at post natal day zero (P0). These mice also received CMV_EGFP in the left eye as a functional contol as these experiments were carried out with the aim of examining any functional effects

of *Thioredoxin1* expression in a degenerating retina. A smaller volume of virus is also delivered at this stage (due to the smaller size of the mouse eye at P0), containing $7.73x10^8$vg/0.8µl volume compared to the 3µl volume that is usually injected sub-retinally in older mice. Each virus was titre matched prior to injection. Photoreceptor death in this mouse model begins shortly after birth and therefore the potential protective effect of this construct may be negated if eyes were injected at a later stage when there are fewer photoreceptors to be transduced or the pathology of the disease has reached a stage which would not be influenced by a reduction in ROS. However, this also means that no injection record (ie whether the injection has been successful or not) can be observed by the person performing the sub-retinal injection as the eyes of mice at this stage of life are fused closed and the sub-retinal injection must be carried out 'blind' by someone with sufficient expertise and experience. Fortunately, Dr Paul Kenna has many years experience in performing these intricate sub-retinal injections. Two time points for histology were analysed, at P10 and P22. These eyes were enucleated, fixed and sectioned before immunohistochemical staining with anti-Trx antibody and DAPI. Fluorescent microscope images of the retinas harvested at P10 and P22 are presented in figures 4.5.11 and 4.5.12 respectively. It can be observed from figure 4.5.11 that no histological benefit is observed in the ONL of Trx_AAV injected eyes as the thickness of this layer is similar in both the left and right eyes, however some expression of Trx can be observed in the ONL of right eyes compared to the left, thus indicating that Trx expression has begun at ten days post-injection. The ONL of the Trx_AAV injected eye shows a similar thickness to the contralateral eye that had been injected with the control virus CMV_EGFP. However some protection can be observed in the retinas which were harvested at P22 (see figure 4.5.12). This figure suggests that a slower rate of degradation of the ONL is occuring as the Trx_AAV injected eyes display a slightly thicker ONL compared to the contralateral eye which had been injected with the control virus CMV_EGFP. A single row of nuclei is observed in the ONL of the CMV_EGFP injected retinas whereas the Trx_AAV injected retinas display 2-3 rows of intact nuclei in the ONL. This difference in the number of photoreceptors is most pronounced in mice 2 and 3 (panels C-F). Mouse 1 shows little difference in ONL thickness between the left and right eyes (panels A and B). Formal quantification of ONL thickness was undertaken using the ImageJ software to examine if this change in ONL thickness

is statistically significant. For each eye, four micrographs of sections on slides at regular intervals throughout the transduced region of the eye were examined (ie sections were examined from slide 3, 5, 7 and 9 for example). The corresponding contralateral eye was also examined using the same slide numbers in order to measure ONL thickness from similar regions of the retina of each eye to reduce the chance that any decrease or increase in ONL thickness is not an artefact of taking different regions of the retina which may naturally be thicker than other regions. For each micrograph, eight ONL thickness measurements were taken at regular intervals along the length of the retina. The resulting average values of length measurement and standard deviations are presented as a bar chart in figure 4.5.13. This demonstrates an approximate 2.5-fold increase in the thickness of the ONL of eyes which received Trx_AAV compared to CMV_EGFP injected control eyes where n=3 (LE=2.21±1.04μm, RE=5.42±0.9μm). Unfortunately, this increase failed to reach statistical significance as a two way paired student's t-test produced a P-value of 0.061. While this is suggestive of a neuronal protective effect of Trx_AAV within the retina, an increase in n number will be required to validate this observation.

4.3.8.2 ERG analysis of Trx_AAV injected Pro23His Mice

To determine any effect of *Thioredoxin1* over-expression on visual function in the P23H retina, five P23H pups were sub-retinally injected as before at P0 using CMV_EGFP in the left eye and Trx_AAV in the right eye. The viral titre delivered to each sub-retinal space was $7.73x10^8$ vg/0.8μl volume for each virus. These animals were subsequently analysed at P22, the earliest date at which an ERG recording could be carried out. ERG amplitudes were averaged across the five mice for each response recorded, a standard deviation calculated and a paired two way student's t-test was carried out on the amplitude quantities. The result of this analysis is presented in figure 4.5.14. This is suggestive of increases in ERG responses of the Rod a, Rod b and Cone a sets but decreases in the ERG responses of the Rod+Cone (Maximal) a, Rod+Cone b and Cone b sets. None of these changes reached statistical significance, most likely due to the large amount of variance in the ERG recordings, as evidenced by the standard deviation values

presented in table 4.5.2. These data are therefore inconclusive regarding the effect of *Thioredoxin1* over-expression in the retina and likely require an increase in the number of experimental animals used for repeat experiments. Furthermore, the extremely rapid nature of the retinal degeneration in the P23H mouse model results in a small window of time in which functional benefit can be observed.

4.3.9 Effect of Exogenous Trx Expression hP347S RP Model Mice

Given the well documented role which over-production of ROS plays in the death of cone cells (see section 1.8), it was decided to undertake an examination of cone cell survival in hP347S transgenic mice which had been treated with Trx_AAV. Cone cell viability was not assessed in P23H mice as cone cell differentiation ends and pedicle formation begins at P10 only and therefore it was deemed that experiments aimed at assessing the density of these cells are better suited to later time-points of mouse development (Fei, 2003).

4.3.9.1 Immunohistochemical analysis of Trx_AAV injected hP347S mice

The Trx_AAV construct was delivered by sub-retinal injection to hP347S heterozygous mice. The first set of mice which were examined was three mice which were treated with CMV_EGFP in the left eye and Trx_AAV at a titre of in the right eye of $2.9x10^9$vg/3µl volume via sub-retinal injection at P21. These mice were subsequently euthanised at 4 weeks post-injection and the eyes were harvested for immunohistochemistry. The PNA stain was used to evaluate the presence or absence of cone photoreceptors in the retinas of these mice. Representative micrographs of the left and right eyes of these mice are presented in figure 4.5.15. This figure demonstrates that no change in cone cell density is observed between the CMV_EGFP treated retinas and the Trx_AAV treated retinas. A PNA stain was also undertaken to assess the viability of cones at 16 weeks post-injections. Three mice were sub-retinally injected at P21 with 2.9vg/3µl of CMV_EGFP in the left eye and Trx_AAV in the right eye. At 16 weeks post-injection the animals were sacrificed and the eyes harvested for immunohistochemistry. Representative micrographs of the transduced regions of these retinas are presented in figure

4.5.16. This demonstrates no difference in cone cell density between the left and right eyes of these mice, with little or no PNA staining observed in any of the retinas examined. These data suggest that Trx_AAV has no beneficial effect on cone survival in the hP347S transgenic mouse model of RP at a histological level.

4.3.9.2 ERG analysis of Trx_AAV injected hP347S mice

A set of three hP347S heterozygous transgenic mice were analysed by electroretinography at 4, 8, 12 and 16 week post injection time points. All three mice were sub-retinally injected at P21 with $2.9x10^9$ vg/3µl injection of each virus. The resulting data were averaged and a standard deviation was calculated for each category of ERG undertaken. A p-value was then calculated for each category using a paired two way student's t-test. The resulting data are presented as a bar chart in figure 4.5.17. Of the four time points taken, only two sets of data reached statistical significance; the 16 week post injection Cone b-wave response and the 16 week maximal a-wave response. The 16 week cone b response reached significance showing that the left eye (injected with CMV_EGFP) elicited a higher cone b response than the right eye, suggesting that the Trx_AAV construct is detrimental to the eyesight of these animals. Conversely the 16 week post injection maximal a-wave response demonstrated that the Trx_AAV injected eye elicited a higher response than the contralateral eye injected with CMV_EGFP. Unfortunately these data exhibit a very large degree of variance, making it difficult to correctly interpret any data. However a general trend across all responses at 12 weeks is an improvement in elicited response in the Trx_AAV injected eye. Although none of these data points reached statistical significance, this may be an indication that the Trx_AAV is partially beneficial at the later stages of the retinal degeneration. Unfortunately this trend of possible preservation of photoreceptor function does not continue at 16 weeks post injection. It must be noted that the n number used to record ERG response in these animals was quite low and produced a large degree of variance in the amplitude data. Therefore an increase in n number will be required to further validate the results obtained here.

It was thought that the failure of Trx_AAV to produce satisfactory ERG results and histological benefit may be due to pathological overexpression of *Trx* as this construct produces an approximately 80-fold expression level of *Trx* compared to control injected eyes in whole retinal extracts (see figure 4.5.8). Therefore ERG analysis was carried out on hP347S heterozygous mice which had been sub-retinally injected at P21 with a ½ dilution or 1/10 dilution of Trx_AAV in the right eye and a titre matched viral load of NT20 delivered via sub-retinal injection to the left eye. These dilutions result in a delivery of $1.48x10^9$ and $2.95x10^8$ viral genomes per sub-retinal injection for the ½ and 1/10 dilutions of viral vector respectively. Reducing the delivered viral load should result in reduced expression of *Trx* and therefore may reach a dose which is beneficial to the visual function of these mice. The resulting data are presented in figures 4.5.18, 4.5.19 and 4.5.20. Two time-points of the ½ Trx_AAV (n=3) and one time-point of the 1/10 Trx_AAV injected mice (n=4) were taken at 4 and 12 weeks and 6 weeks respectively. This reduction in viral load failed to produce any statistically significant changes in ERG amplitude between the left and right eye however. Some improvement in cone and maximal responses were observed in the right eye compared to left eye at the ½ dilution at 12 weeks compared to 4 weeks but these changes in ERG amplitude did not reach statistical significance.

4.3.10 ERG analysis of Thioredoxin1 over-expression in wild type mice

Due to the lack of functional benefit provided by the Trx_AAV virus in either of the transgenic mouse models examined, it was decided to examine the functional effect of this virus in wild type mice. A range of dilutions of this virus were injected sub-retinally in to the right eyes of wild type mice at P21 and titre matched CMV_EGFP was injected in to the left eye. The dilutions used were ½, 1/10, 1/100 and 1/1000 to deliver a viral load of $1.47x10^9$, $2.95x10^8$, $2.95x10^7$ and $2.95x10^6$ vg in a 3µl volume where n=2 for each dilution. ERG analysis was undertaken at 4 weeks post-injection and the resulting data are presented in figure 4.5.21. A two way paired student's t-test performed on the data between left and right eye provided a statistically significant p-value for two of the rod a-wave responses (Trx 1/100 and Trx 1/1000). However for reasons discussed already, the rod a-wave was

dismissed as non-reliable. The cone a-wave produced a statistically significant p-value between the left and right eye at a dilution of ½, suggesting that over-expression of *Trx* is detrimental to vision at this high titre. Bonferroni multiple comparison ANOVA was also undertaken on each set of data within a wave data set. This analysis provided no statistically significant p-values except for the cone a-wave which had six statistically significant p-values. Four had a p-value less than 0.05; ½ LE vs 1/1000 RE, ½ LE vs 1/100 RE, 1/10 LE vs 1/1000 LE and 1/10 RE vs 1/1000 RE. Two p-values were equal to or less than 0.01; 1/10 LE vs 1/1000 LE and 1/10 LE vs 1/1000 RE. These data seem to indicate that lowering the dose of Trx_AAV is having a negative effect on the visual function of wild type mice. However this trend is not observed for any of the other responses. Furthermore an increase in visual function is observed from Trx ½ to Trx 1/10, a data set which displays the largest ERG response in all waves recorded, suggesting that these data may be the result of inter-animal variance. In addition, the dilution seems to be virus independent as the left eye which received CMV_EGFP has also declined as the dilution has increased, again suggesting that the change in ERG response is inter-animal variance. Therefore the n number would have to be increased in a repeat of this experiment. However, this experiment has shown that dilution of the injected Trx_AAV has had little effect on visual function.

4.4 Discussion

The use of gene therapy to deliver coding sequences to a tissue of interest has long been established. However, the treatment of human Leber Congenital Amaurosis using a virally delivered wild type copy of the *RPE65* gene provided clear evidence that this method of treating inherited disease is both safe and efficient (Bainbridge et al, 2008; Maguire et al, 2008; Hauswirth et al, 2008). Follow up studies of treated LCA patients has demonstrated that there are no adverse effects of subretinal AAV delivery of this *RPE65* vector (Simonelli et al, 2010; Testa et al, 2013) or of re-administration of this therapy (Bennett et al, 2012). The best preservation of visual function was observed in younger patients (Maguire et al, 2009). Furthermore, treatment of LCA patients with this therapy preserves cortical visual pathways in treated eyes (Ashtari et al, 2011). Delivery of a gene coding sequence under the control of an appropriate promoter also avoids many of the pitfalls associated with RNAi based therapies such as sequence based off-target effects and saturation of the RNAi pathway (Davidson & McCray Jr, 2011). More recently, the use of RNAi has come under scrutiny due to its possibly pathological effect on the retina (Kleinman et al, 2012). The issues of RNAi and its use in human therapies can in principle be avoided if a genetic disease phenotype does not require suppression of a mutant allele (ie. dominant diseases). During the course of the studies detailed in this chapter, two mouse models of autosomal dominant RP were examined for any potential functional benefit which may result from treatment of the retina with an AAV 2/5 vector containing an expression cassette which drives expression of *Thioredoxin1*. The hypothesis driving the rationale of treatment with this gene for a dominant disease was that *Thioredoxin1* would act on a secondary effect of the primary mutation which causes the disease; in particular it was introduced with the aim of reducing oxidative stress rather than addressing the underlying causative mutation; based on prior publications which detailed the protective effect of over-expression of this gene for retinal degeneration *in vivo* (Kong et al, 2010).

The coding sequence for mouse *Trx* was obtained commercially and cloned in to the pAAV_MCS plasmid for further studies both *in vitro* and *in vivo*. To our

knowledge this is the first time that this gene has been used to generate a recombinant AAV vector. Subsequent to selection of a successful clone and production of this plasmid in XL1-blue E. coli cells, pTrx_AAV was transfected in to HeLa cells to confirm that this plasmid was functioning to produce *Trx* mRNA. This experiment revealed a substantial increase in expression of *Trx* in pTrx_AAV treated cells compared to NT20 treated control cells (figure 4.5.6). Confirmation of this increase in expression was performed by western blot analysis using a Trx specific antibody to determine if over-expression of *Trx* mRNA was leading to an over-expression of Trx protein (figure 4.5.7). This set of experiments also revealed an increase in Trx expression in HeLa cells but not to the large extent observed by RT-qPCR. The discrepancy in expression quantities can be explained by the fact that the primers used to amplify *Thioredoxin1* mRNA are mouse specific and therefore will only detect transcripts produced by the pTrx_AAV plasmid. In contrast, the antibody used to detect Thioredoxin protein will detect both human and mouse protein and therefore will detect both pTrx_AAV produced mouse Thioredoxin and endogenous human TRX protein expressed by HeLa cells. The western blot analysis of HeLa cells reveals a relatively high expression of endogenous TRX, which would be expected in these cells owing to their quick rate of division and the role which TRX plays in the S phase of mammalian cell division (Zahedi Awal & Holmgren, 2009; Deiss & Kimchi, 1991).

After successful demonstration of *Trx* expression from the pTrx_AAV plasmid *in vitro*, this plasmid was used to produce high titre recombinant AAV containing pTrx_AAV as the genome. A control virus was also produced using the CMV_EGFP plasmid obtained from another member of the laboratory. This plasmid was created by cloning the EGFP gene in to the MCS of the pAAV_MCS plasmid downstream of the CMV promoter. The resulting CMV_EGFP virus was then employed as a control vector for over-expression induced phenotype as strong over-expression of many genes is known to be toxic to the cell (Sopko et al, 2006). Titre matched sub-retinal injection of each virus was then carried out in wild type mice to examine the efficacy of *Trx* over-expression *in vivo*. RT-qPCR analysis of injected animals confirmed that eyes which received the Trx_AAV injection displayed a ~80-fold over expression of *Trx* mRNA (figure 4.5.8). This level of expression is far less than what was observed *in vitro*. However, this experiment

was carried out using mouse specific primers which will detect endogenous *Trx* expression as well as Trx_AAV driven expression. Furthermore, for these experiments, whole retinal RNA extractions were carried out and therefore no selection of virally transduced regions of the retina was performed. The Trx_AAV vector contains no reporter gene, making selection of EGFP positive regions of the retina impossible, although it was anticipated that over-expression of *Trx* would be easily observable based on prior results *in vitro* which demonstrated the strength of the CMV promoter used to drive expression of *Trx*. It is also known that sub-retinal injection of AAV vector will typically transduce about one third of the retina (Palfi et al, 2012) and therefore extracting RNA from the entire retina will mask the true extent of over-expression achieved with this virus.

The expression of *Trx in vivo* was also examined by western blot analysis (figure 4.5.9). This experiment revealed a clear increase in Trx protein expression in Trx_AAV treated retinas compared to CMV_EGFP treated retinas. One mouse of the three treated mice demonstrated a smaller increase in expression. This was likely due to a sub-retinal haemorrhage which occurred during injection and which adversely affected AAV transduction of the retina (Martin et al, 2002). Finally, immunohistochemical analysis of Trx_AAV treated eyes was undertaken to observe any changes in Trx expression which occurred following sub-retinal injection. This revealed a clear and distinct increase in expression of Trx in the ONL and RPE of retinas treated with Trx_AAV compared with CMV_EGFP treated retinas (figure 4.5.10). Control injected eyes revealed retinal layers which endogenously express Trx, most notably in the INL and GCL. Tanito et al, previously published immunohistochemistry results suggesting expression of Trx in the GCL only, with transient expression of Trx in the ONL and INL after light adaptation (Tanito et al, 2002). However Munemasa et al reported endogenous Trx expression in only the INL and GCL, results which closely mirror the expression data gathered in the present study (Munemasa et al, 2008). The emerging hypothesis of Thioredoxin1 function in the retina is that this gene is generally expressed most heavily in the GCL as this is the most metabolically active layer of the retina and is therefore subject to considerable oxidative stress. However, expression of *Thioredoxin1* (or other members of the thioredoxin system such as *TrxR* and *TXNIP*) is up-regulated in other layers of the retina such as the ONL in

response to oxidative stress which is observed in a number of retinal degenerations such as glaucoma and AMD (Lamoke et al, 2012), light induced damage (Tanito et al, 2002 and 2005), glaucoma (Munemasa et al, 2008), diabetic retinopathy (Devi et al, 2013) and ischaemia-reperfusion injury (Chen et al, 2013).

Once a recombinant AAV vector which provided over-expression of *Trx in vitro* and *in vivo* had been developed and characterised, the effect of *Thioredoxin1* over-expression was examined in the rhodopsin mutant P23H mouse model of adRP. Two time points were evaluated, at P10 and P22 (when there are little or no photoreceptors remaining in the P23H retina). These time points were used for immunohistochemistry to ensure that AAV delivered *Trx* is being expressed adequately and to determine any beneficial effects that this over-expression may exert on the course of retinal degeneration. No histological benefit to ONL thickness was observed between the control NT20 treated eyes and the Trx_AAV treated eyes at P10 (figure 4.5.11). However, a small but discernible increase in expression of Trx was observed in the ONL of these mice, suggesting that the Trx_AAV vector is functioning to produce Thioredoxin1 protein as early as ten days post injection. Transgene expression from AAV cassettes is known to increase with time as the AAV continues to transduce cells of the retina. At P10, the transduction rate of photoreceptors by sub-retinal injection of AAV 2/5 has been observed to be between 15-40% (Sarra et al, 2002) however a degree of variability of the rate of transduction is present, depending on the mouse strain and genotype injected, developmental time of injection and the nature of the delivered transgene. At P22, a much greater increase in expression of Trx was observed in the diminished ONL of Trx_AAV injected P23H mice compared to CMV_EGFP injected retinas (figure 4.5.12). Of the three mice examined, two appeared to have a thicker ONL thickness in the treated eye compared to the control contralateral left eye, suggesting that Trx is slightly protective at the later stages of retinal degeneration. Formal quantification of this increase revealed an approximately 2.5-fold increase in ONL thickness in the Trx_AAV treated eyes at P22, suggesting that Trx is acting as a late stage therapeutic of photoreceptors (figure 4.5.13). However this analysis failed to reach statistical significance, with a two way paired student's T-test producing a p-value of 0.06. It is likely that an increase in n number would validate this result as the standard deviations of these data do not overlap and a

marked average increase was recorded in all three animals examined. Therefore the failure of the p-value to reach significance is likely due to the low n number used (n=3).

The effect of *Thioredoxin1* over-expression in the P23H mouse was further evaluated by ERG analysis of treated animals. In this case, a single time point was evaluated at P22 as ERG analysis was not possible to carry out at an earlier time point in young pups and no ERG response would be expected at later time points due to the rapid retinal degradation of the P23H mouse model of adRP. In this set of experiments, ERG analysis revealed no functional effect of *Thioredoxin1* over-expression in the P23H mouse (figure 4.5.14). The ERG and histology results indicate that treatment of this model with Trx_AAV confers no functional protection to photoreceptor cells but may preserve the longevity of photoreceptor cells. The P23H mouse model of adRP has proved to be difficult to treat due to the extremely rapid nature of retinal degeneration. It is likely that disease progression may occur too quickly for an AAV mediated gene therapy to provide significant functional benefit. Previous studies of this model using a rhodopsin suppression and replacement strategy (discussed in section 1.16) have demonstrated no functional benefit as assayed by ERG but preservation of ~33% of ONL thickness at P10 (O' Reilly et al, 2007). Furthermore, the difficulty inherent in sub-retinal injection at P0 also results in a fewer number of successful surgeries compared to injection of adult mice, whereby the sub-retinal injection is observable by the person administering it.

The effect of *Thioredoxin1* over-expression was then examined in the hP347S transgenic mouse model of adRP. The pace of retinal degeneration in this model is known to occur much at a much slower rate than that observed in the P23H model, with photoreceptor cell death beginning shortly after birth and almost a complete loss of photoreceptors at 4 months of age in the P23H mouse (Li et al, 1996). Histological analysis was carried out using the PNA stain for cones as this cell type is known to be particularly affected by retinal oxidative stress (Shen et al, 2005; Usui et al, 2009; Usui et al, 2009b; Yang et al, 2009). Retinal sections from mice which had been treated with Trx_AAV vector were examined at 4 and 16 weeks post injection. This revealed no change in cone cell density at either 4 or 16 weeks post injection (figures 4.5.15 and 4.5.16). At 16 weeks post injection, no PNA

staining was observed in either Trx_AAV or CMV_EGFP treated eyes. These data suggest that no beneficial effect is exerted upon cone cell longevity by over-expression of *Trx* in the ONL.

ERG analysis was also carried out on hP347S transgenic animals treated with Trx_AAV vector to determine if any functional effects of *Thioredoxin1* over-expression could be observed in this model. ERG analysis revealed no statistically significant change in ERG response between the control and Trx_AAV treated eyes at any time points taken except for two time-points (figure 4.5.17). The two time points which reached significance were the 16 week maximal a-wave (suggesting functional preservation of Trx_AAV injected retinas) and the 16 week cone b-wave (suggesting functional degradation of Trx_AAV injected retinas). A trend towards preservation of visual benefit was observed at 12 weeks post injection in all wave responses; however these data points failed to reach significance. In a similar manner to the experiments examining the effects of Trx_AAV vector administration to P23H mouse models of RP, an increase in the n number of these experiments will be required in the future to confirm the findings presented in this study.

A review of the literature which has detailed over-expression of *Thioredoxin1* and its effect on ERG response has been undertaken. Tanito et al, demonstrated that *Thioredoxin1* over-expression in either a transgenic *Trx* over-expressing mouse or a long-term light adapted wild type mouse preserves ERG function after light ablation of these animals (Tanito et al, 2002 & 2007). This protection of ERG response ranged from a ~33% increase in maximal b-wave in *Trx* over-expressing mice to a 5-fold increase in both maximal a-wave and b-wave response in light adapted mice twelve hours after exposure to light ablation. Kong et al have also shown that crossing a transgenic mouse which over-expresses *Thioredoxin1* with the *Tubby* transgenic mouse (a genetic mouse model of Usher's syndrome, discussed in more detail in section 4.1) results in a two-fold increase in ERG response of both cone a and b-wave amplitudes (Kong et al, 2010). Finally Mandal et al have demonstrated a 1.5 fold increase in rod and cone b-wave ERG amplitude responses after light ablation was carried out on curcumin fed rats (Mandal et al, 2009). Curcumin was shown to protect photoreceptors from photo-oxidative stress

by up-regulating *Thioredoxin1* expression amongst other anti-oxidant genes. Therefore, prior publications concerning the over-expression of *Thioredoxin1* in the degenerating retina has suggested that over-expression of *Thioredoxin1* in the mouse models of RP examined within the course of this study should have produced a beneficial outcome in visual function.

The failure of *Thioredoxin1* over-expression to adequately protect photoreceptor cell function in two transgenic mouse models of RP is somewhat surprising given the protective role this gene has been shown to provide in other models of oxidative stress induced retinal degeneration. Much of the research investigating the protective effects of *Thioredoxin1* has focused on the role that this gene plays in the protection of retinal ganglion cells (Munemasa, 2009; Caprioli, 2009; Munemasa 2008; Inomata, 2006) suggesting that this layer of retinal cells is more amenable to *Trx* mediated neuronal protection against oxidative stress. However a limited number of papers have explored the protective effects of *Thioredoxin1* in photoreceptor cells. Kong et al, have shown that crossing a *Trx* over-expressing transgenic mouse (with Trx under the control of the β-Actin promoter) with the *tubby* mouse model of Ushers syndrome preserves the longevity of photoreceptors (Kong et al, 2010). In addition, Tanito et al have shown that up-regulation of Trx occurs after photo-oxidative damage to photoreceptors in vivo (Tanito et al, 2002) and in photoreceptor derived 661W cells (Tanito et al, 2007). A notable exclusion from the literature presented here is the presence of quantitative data of *Trx* expression in any of the models examined, including *Trx* over-expressing transgenic mice, recombinant *Trx* injected mice and *Trx* expression induced mice (by oxidative stress, optic nerve transaction or pharamacologically induced). The studies detailed in these papers demonstrate up-regulation of *Trx* expression by western blot or immunohistochemistry. However, immunohistochemistry tends not to be amenable to quantitative analysis and while western blot results can be quantified (by pixel intensity analysis), this method of quantification is highly variable and heavily depends on the experimental conditions under which the western blot is carried out (ie protein concentration, the antibody used and its dilution and the length of exposure of the western blot to X-ray film to name just four). The lack of published quantitative expression data of *Trx* hinders any attempt to compare the results obtained during the course of the studies detailed within this

chapter to those previously published. One possibility to explain the lack of functional benefit observed in the experiments detailed in this chapter is that the significant over-expression of *Thioredoxin1* demonstrated *in vivo* may have become toxic to the cells of the ONL and therefore may have conferred no functional or structural benefit to the transgenic animals treated with Trx_AAV. Therefore two dilutions of Trx_AAV were used for two sets of animals to examine any difference in functional effect that this may have. The two dilutions used were a ½ (where n=3) and a 1/10 (where n=4) dilution of the Trx_AAV concentration, initially tested in hP347S heterozygous mice. Two time points of the ½ dilution and one time point of the 1/10 dilution of Trx_AAV treated animals were examined. However, the reduction in viral titre administered failed to produce any statistically significant changes in ERG response in any wave response at any time point recorded suggesting that over-expression of *Thioredoxin1* in the mouse ONL has no beneficial effect on the pathology of Retinitis Pigmentosa in the mouse models of this disease examined during the course of this study (figures 4.5.18, 4.5.19 and 4.5.20). In order to determine if over-expression of *Trx* is having a toxic effect on the cells of the retina, a range of dilutions of Trx_AAV were also tested in wild type animals. All animals received Trx_AAV in the right eye at a dilution ranging from ½ to 1/1000 where n=2 for each group. The left eye received titre matched CMV_EGFP. This resulted in no statistically significant change in ERG response for any of the wave responses examined (figure 4.5.21). A student's t-test and ANOVA statistical test suggested that dilution of Trx_AAV may have a detrimental effect on the cone a-wave. However this is likely due to inter-animal variance as the average amplitude response elicited by animals in the Trx 1/10 group were higher in all response sets examined. Furthermore, if dilution of Trx_AAV was resulting in toxicity to the wild type retina then this would immediately eliminate the hypothesis that over-expression of *Trx* is causing detriment to the cellular viability of the photoreceptors. No histology of these animals was undertaken as histology demonstrating the *Trx* expression of the neat virus in wild type animals *in vivo* had already demonstrated that over-expression of *Trx* in the ONL of the retina caused no observable reduction in the thickness of the ONL (figure 4.5.10).

A second possibility which may explain the lack of functional benefit achieved with *Trx* over-expression is the effect of rate limitation on the reducing power of

exogenous Trx caused by a lower expression of Thioredoxin reductase (TrxR). This protein is required to reduce Trx. Therefore a high level of Trx expression may have no functional biochemical effect if there is little TrxR expression in comparison. Little data could be found in the scientific literature regarding TrxR expression in the retina. It is known that there is expression of this protein in the retina and that the expression profile of TrxR is likley to be similar to that of endogenous Trx given the presence of AREs in the promoters of both genes (Tanito et al, 2007). Furthermore, expression of TrxR does not change in cells lines derived from a patient carrying a NARP (Neurogenic Ataxia Retinitis Pigmentosa) mutation compared to wildtype cells (Wojewoda et al, 2010) suggesting that there is no larger pool of TrxR in RP model mice from which exogenous Trx may be reduced. The introduction of exogenous Trx in this study was carried out based on previous results by other laboratories and the hypothesis that exogenous Trx expression would at least be partially reduced by the endogenous TrxR system. The activity of this exogenous Trx in vivo is something which must be addressed in future studies to determine if the over-expressed protein is funcctional.

The data presented in this chapter detail the successful cloning of the mouse *Thioredoxin1* gene in to the pAAV plasmid and the subsequent success of expression of both *Trx* mRNA and protein from this plasmid *in vitro*. High titre AAV 2/5 was then produced using this plasmid to create the Trx_AAV vector, a virus which produces high copy numbers of *Trx* mRNA and protein within the ONL and RPE following sub-retinal injection (figure 4.5.10). The effect of over-expression of this gene was examined at both the histological and functional level in two mouse models of RP. The data generated suggest that *Trx* over-expression is not protective of photoreceptor viability or function throughout the course of rhodopsin mutation induced mouse models of retinal degeneration. Although a possible increase in photoreceptor cell number was observed at the later stage of P23H induced retinal degeneration, a repeat of this experiment using more animals would be desirable as quantification of this increase failed to reach statistical significance. To better understand the effects that *Trx* over-expression has had on levels of reactive oxygen species in the same mouse models of RP, DHE staining was undertaken to evaluate the presence of superoxide in these animals. This evaluation is the focus of the experiments detailed in chapter 5, together with the

effects of *Rac1* suppression on the production of reactive oxygen species in the hP347S transgenic mouse model of RP.

4.5 Tables and Figures

Untransfected 1	Untransfected 2	Untransfected 3	pAAV_Trx 1	pAAV_Trx 2	pAAV_Trx 3
1	1	1	1	1	
2	2	2	2	2	
3	3	3	3	3	
4	4	4	4	4	

Table 4.5.1: Schematic of transfection of 24-well plate of HeLa cells

This schematic shows the layout of HeLa cells in a 24 well plate that had been transfected with pTrx_AAV. This layout was used to test the functionality of the pTrx_AAVplasmid *in vitro* for both mRNA and protein analysis.

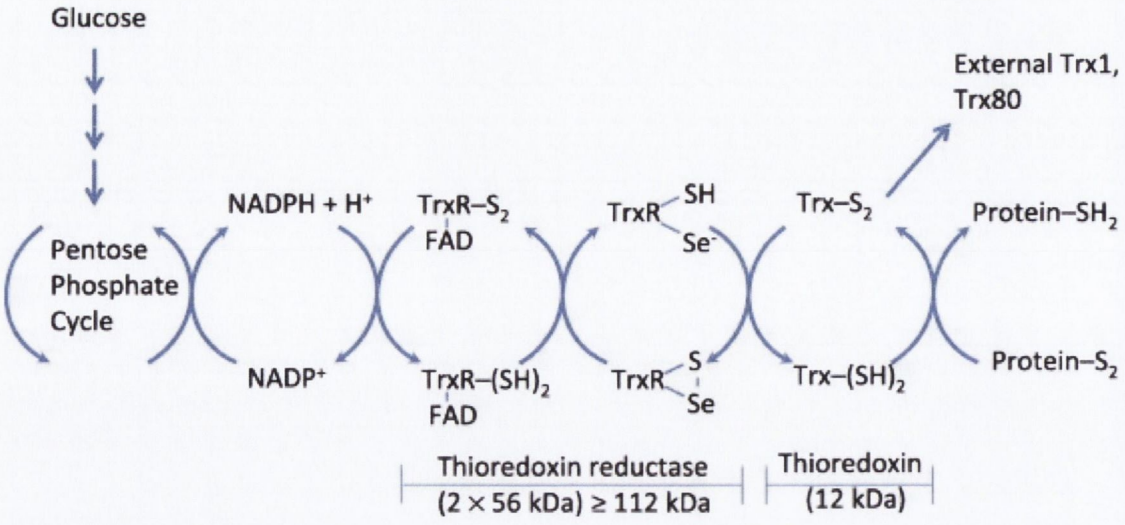

Figure 4.5.1: Biochemical pathway showing the generation of reduced Trx by TrxR.

This simplified biochemical pathway shows that reduction of a disulfide bond within the Thioredoxin reductase (TrxR) protein structure by NADPH allows TrxR to further reduce a thioredoxin (Trx) disulfide bridge, creating reactive sulfhydryl groups on specific amino acid sites of thioredoxin. These sites are then used a general reducing agent upon non-specific target proteins which become oxidised by reactive oxygen species (ROS).

Figure adapted from Holgren &Lu (2010).

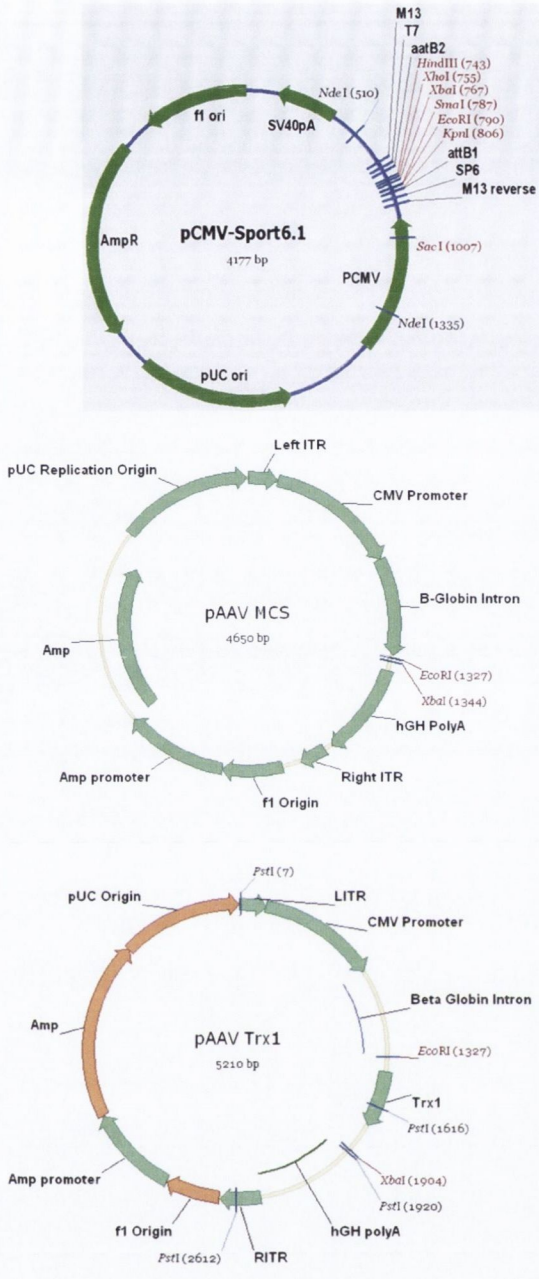

Figure 4.5.2: Vector Maps used for Thioredoxin Cloning

Vector maps showing the layout of the pCMV_SPORT6, pAAV_MCS and pTrx_AAV (named pAAV Trx1 in this figure) plasmids. The *Trx* CDS was excised from the pCMV_SPORT6 plasmid using the *EcoRI* and *XbaI* restriction enzymes. This fragment was then ligated in to the pAAV_MCS plasmid using the same restriction sites (marked on vector map). The resulting plasmid, the pTrx_AAV plasmid, is shown with the cloning sites marked along with the *PstI* sites which were used to ensure recombination had not occurred between the two ITR sites.

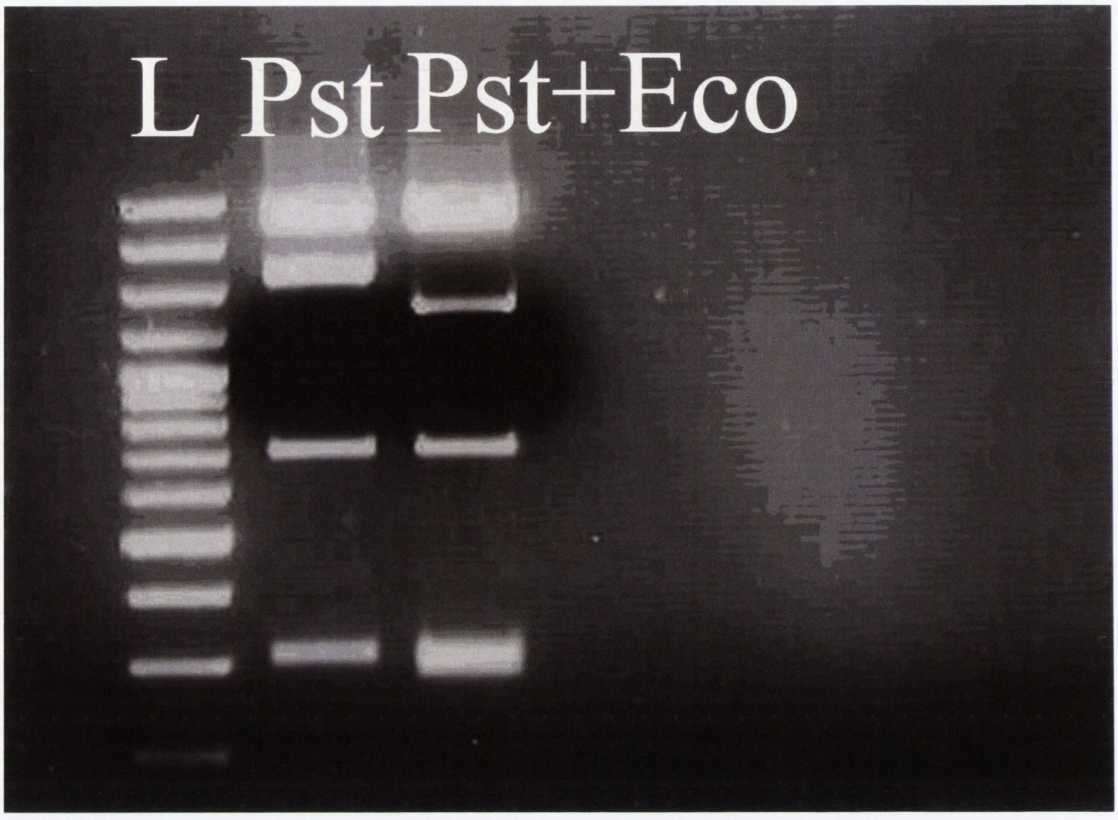

Figure 4.5.3: Agarose gel showing restriction digest of pTrx_AAV

To ensure that no recombination has occurred between the inverted terminal repeats (ITRs) of the pTrx_AAV plasmid during the course of cloning, the megaprepped plasmid which was used for production of recombinant AAV 2/5 was restriction digested with either *PstI* or *PstI* and *EcoRI*. The resulting DNA fragements were run on an agarose gel to examine if these fragments are the expected size based on the sequence maps of the plasmid. This figure demonstrates that digestion with *PstI* produces fragments of the expected lengths of 2605, 1609, 692 and 312 nucleotides. Digestion with PstI and EcoRI produces fragments of the expected lengths of 2605, 1320, 692, 312 and 289 nucleotides in length. In the lane which was loaded with DNA digested with PstI and EcoRI, the fragments of 312 and 289 have not separated due to their similar sizes. Therefore this fragment is observed as a doublet.

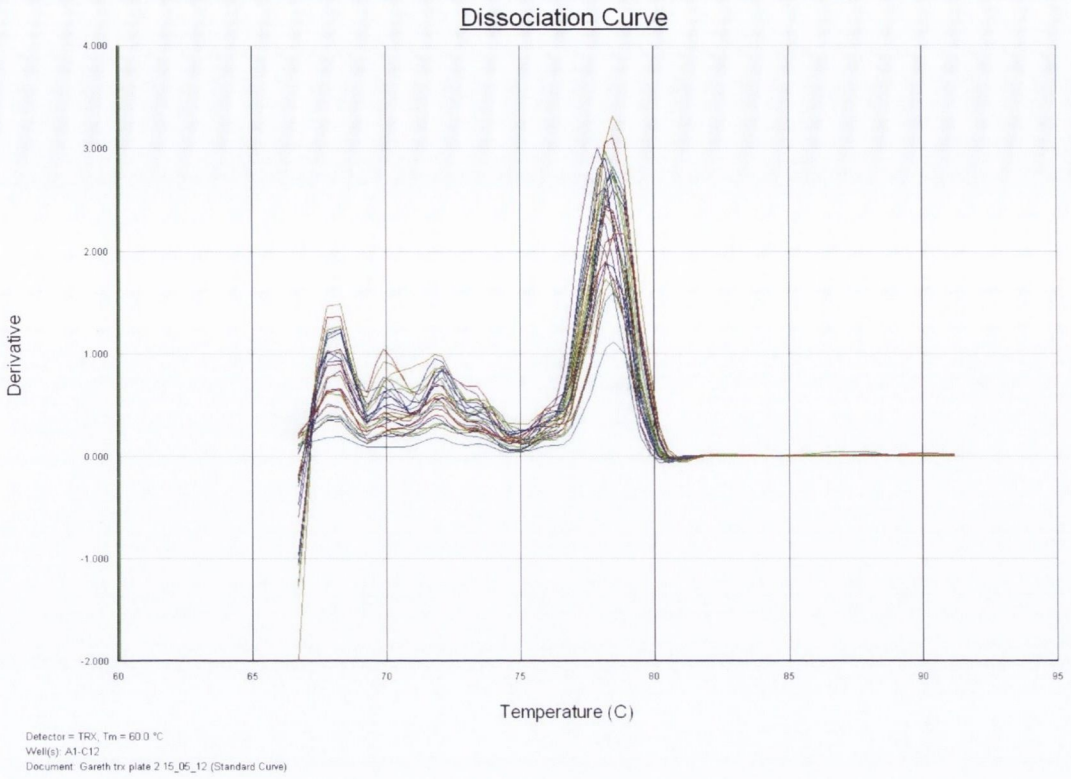

Figure 4.5.4: Trx Dissociation Curve

The dissociation curve achieved using the Trx_qF and Trx_qR primers. This shows one main amplicon produced using these primers at 78°C. However there appears to be a second amplicon present at 68°C. Given the low melting temperature of this amplicon, the peak is more than likely an indication of the presence of primer dimers.

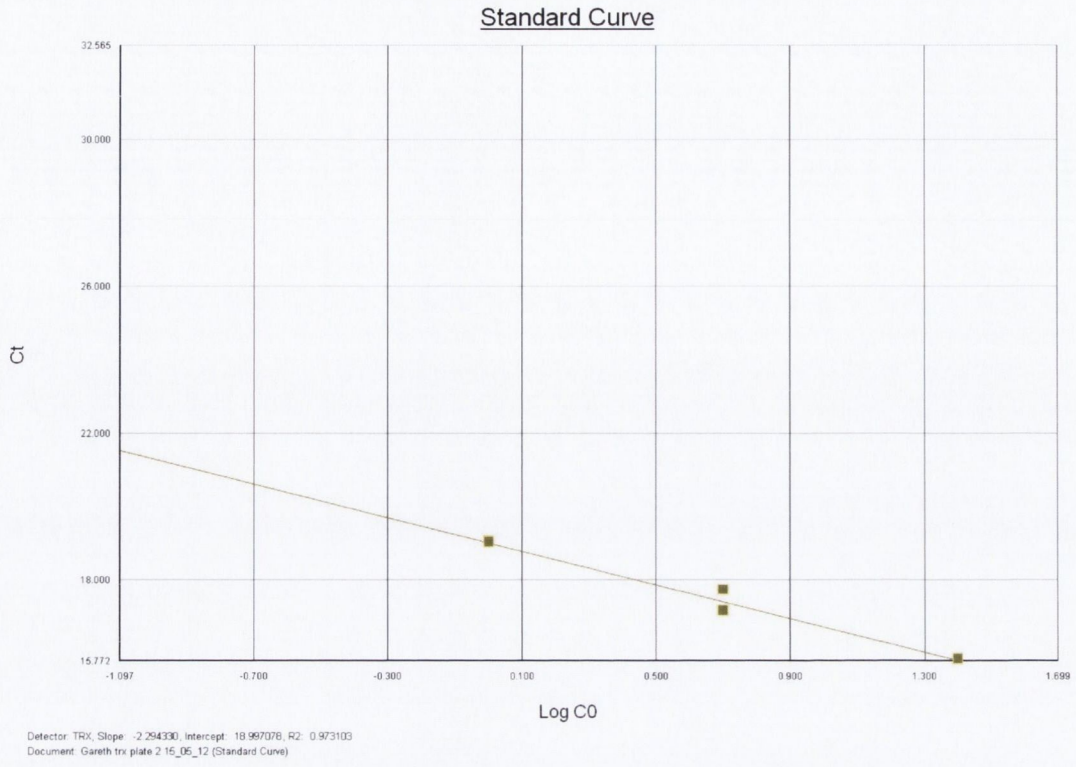

Figure 4.5.5: Trx Standard Curve

The standard curve used to assign quantities to unknown samples of cDNA using the Trx_q primers. This standard curve is not ideal due to high slope of -2.29. This is due to the low Ct value at which the point of analysis (ΔRn) was taken. A low Ct value indicates high expression of the locus of interest which is what has happened due to the high expression of *Trx* from the CMV promoter.

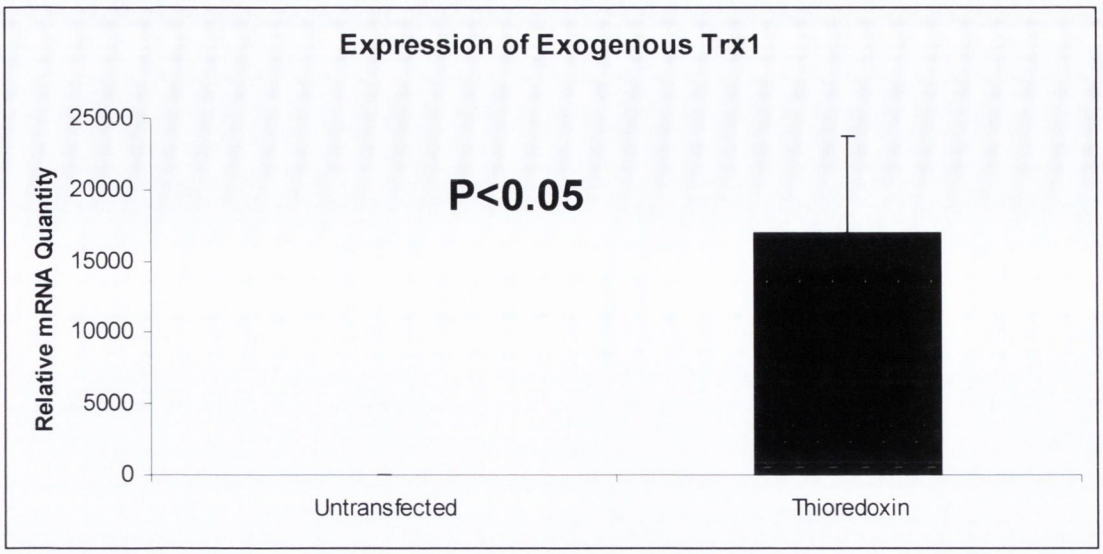

Figure 4.5.6: CMV driven Expression of Thioredoxin in HeLa cells.

Bar chart showing the expression of *Trx* mRNA from the CMV promoter of pTrx_AAV in HeLa cells transfected with this plasmid. This demonstrates a 16,918-fold (±6,864) over-expression of mouse *Trx* compared to untransfected HeLa cells. A two way unpaired student's t-test performed on the this data produced a P-value of 0.026.

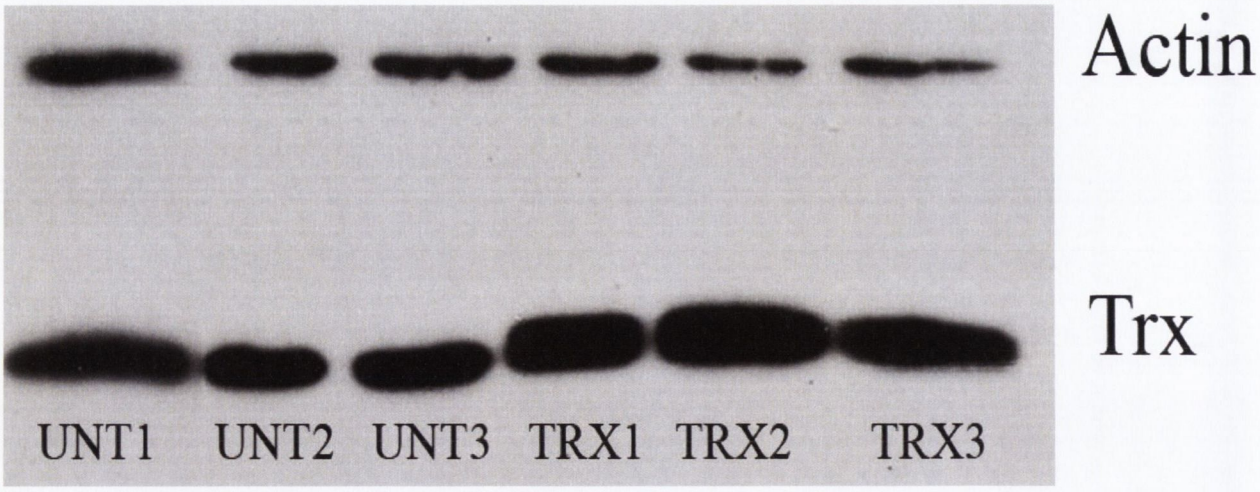

Figure 4.5.7: Overexpression of Trx in HeLa Cells

Western Blot showing overexpression of Trx protein in lanes 4-6 (TRX1-3) compared to lanes 1-3 (UNT1-3) loaded with protein from cells that had been transfected with pTrx_AAV or had been left untransfected respectively. The blot was probed with anti-Trx and anti-β-Actin antibodies which show bands at 12kDa and 46kDa respectively. β-Actin was probed to show equal loading. This demonstrates an increase in Trx protein expression in transfected cells.

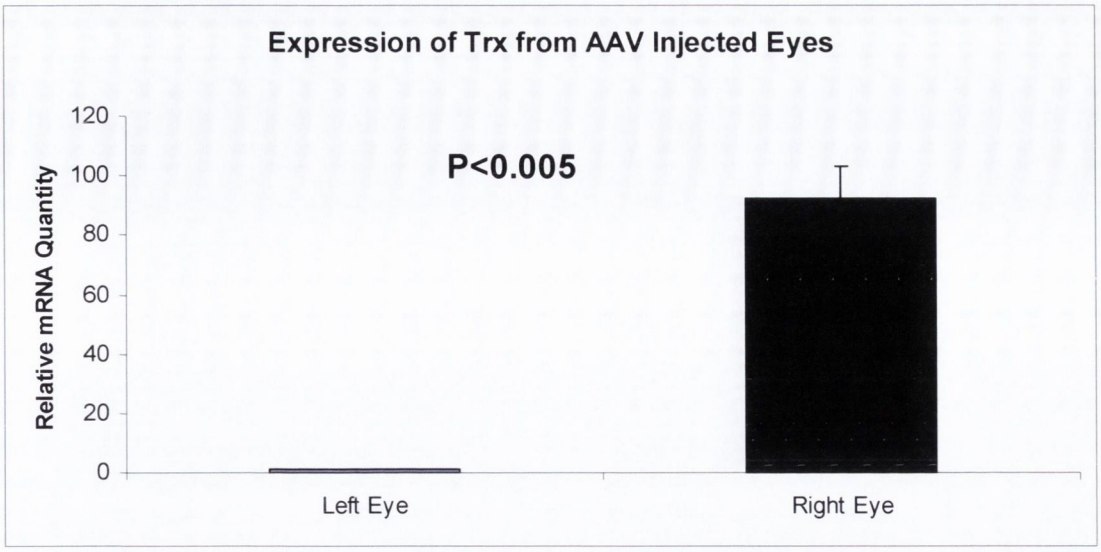

Figure 4.5.8: Overexpression of Trx in Injected Whole Retina where n=5

Bar chart showing the expression of *Trx* mRNA in the retinas of wild type mice sub-retinally injected with PBS in the left eye and Trx_AAV in the right eye. Whole retinas were taken for RNA analysis as no EGFP marker gene was present in the Trx_AAV virus and *in vitro* results suggested a high enough expression of *Trx* from this construct to easily ascertain *in vivo* expression. The RT-qPCR analysis confirms the *in vitro* findings which indicated the functionality of the pTrx_AAV plasmid as an expression agent of *Trx1*. This shows a 92.13-fold (±10.71) over-expression of *Trx* mRNA in the right eye compared to the left eye. A paired two way student's T-test of these data produced a P-value of 0.0023.

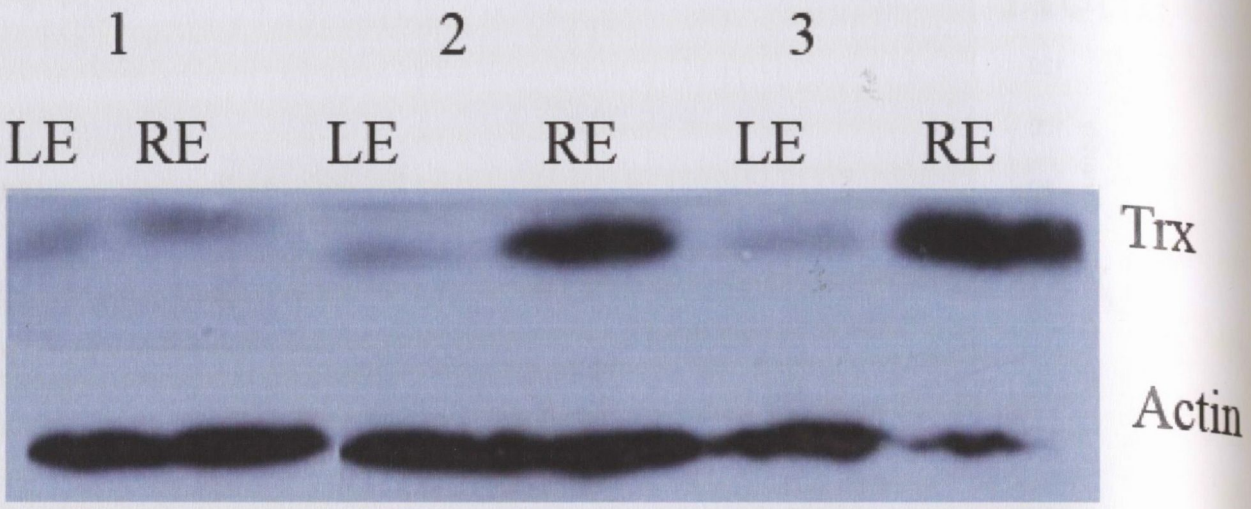

Figure 4.5.9: Western Blot showing overexpression of Trx *in vivo* where n=3

Protein samples extracted from retinal lysates were probed with anti-Trx and anti-β-Actin antibodies. This demonstrated over-expression of Trx in the right eyes of all three animals. Mice 2 and 3 show the greatest change in expression whereas mouse 1 shows a much smaller increase. This was due to an unsuccessful sub-retinal injection likely resulting in less efficient retinal transduction by AAV. This western blot confirms that the Trx_AAV viral vector produces Thioredoxin1 protein in retinal cells *in vivo*.

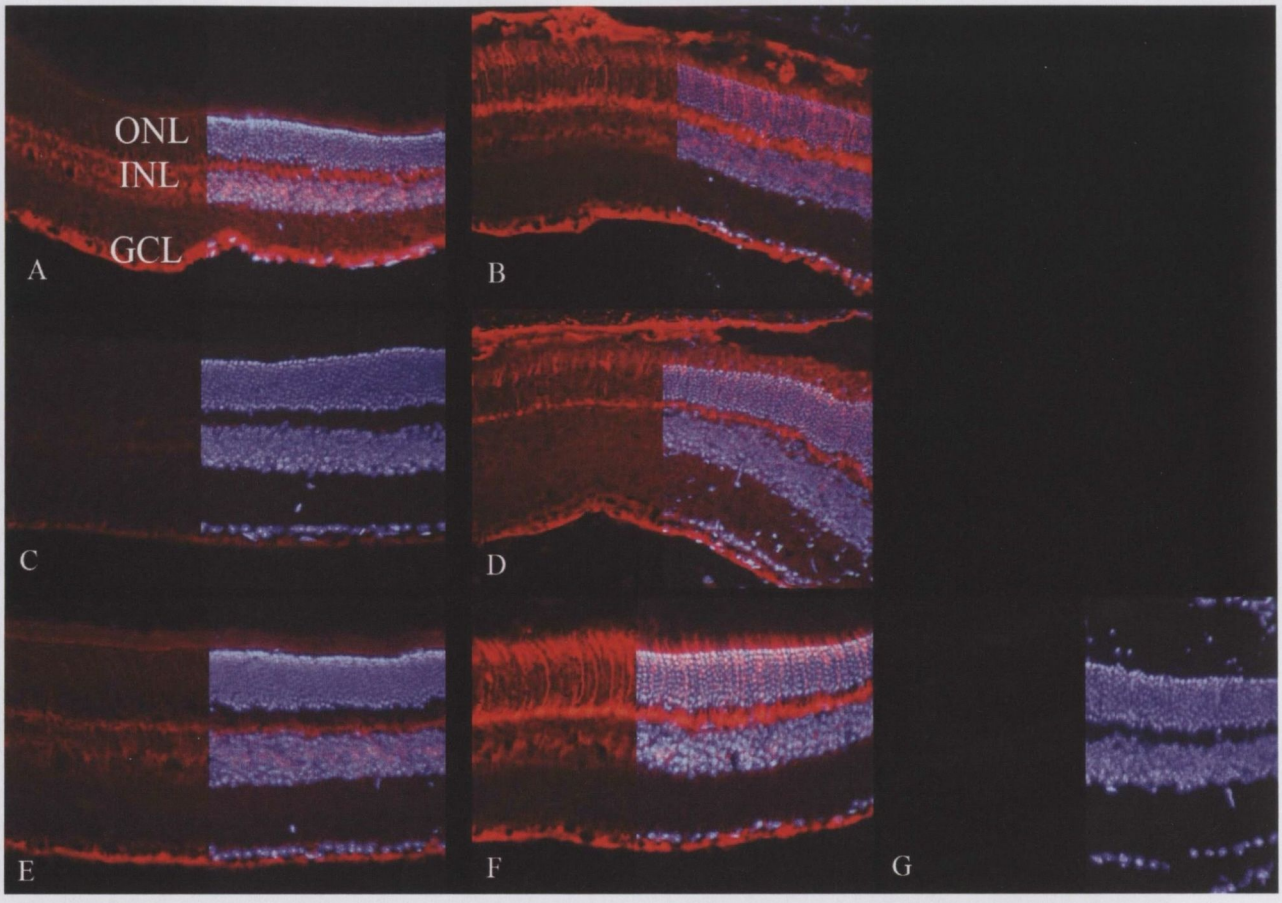

Figure 4.5.10: Immunohistochemistry of Trx_AAV Injected Wildtype Retinas where n=3

Over-expression of Trx in Trx_AAV injected retinas was further confirmed by immunohistochemistry. Images A, C and E show expression of Trx (in red) in the left eyes of mice 1, 2 and 3 respectively; which had received a sub-retinal injection of PBS. This demonstrates expression in the INL and GCL. Images B, D and F show Trx expression in the right eyes of mice 1, 2 and 3 respectively. These show expression in the INL and GCL as well as heavy expression in the ONL and RPE, the cell layers transduced by the Trx_AAV virus. Image G shows a no primary antibody control which was stained with secondary antibody but without primary antibody. This was performed to act as a control for unspecific staining. This image shows no Trx expression, illustrating the specificity of the anti-Trx antibody.

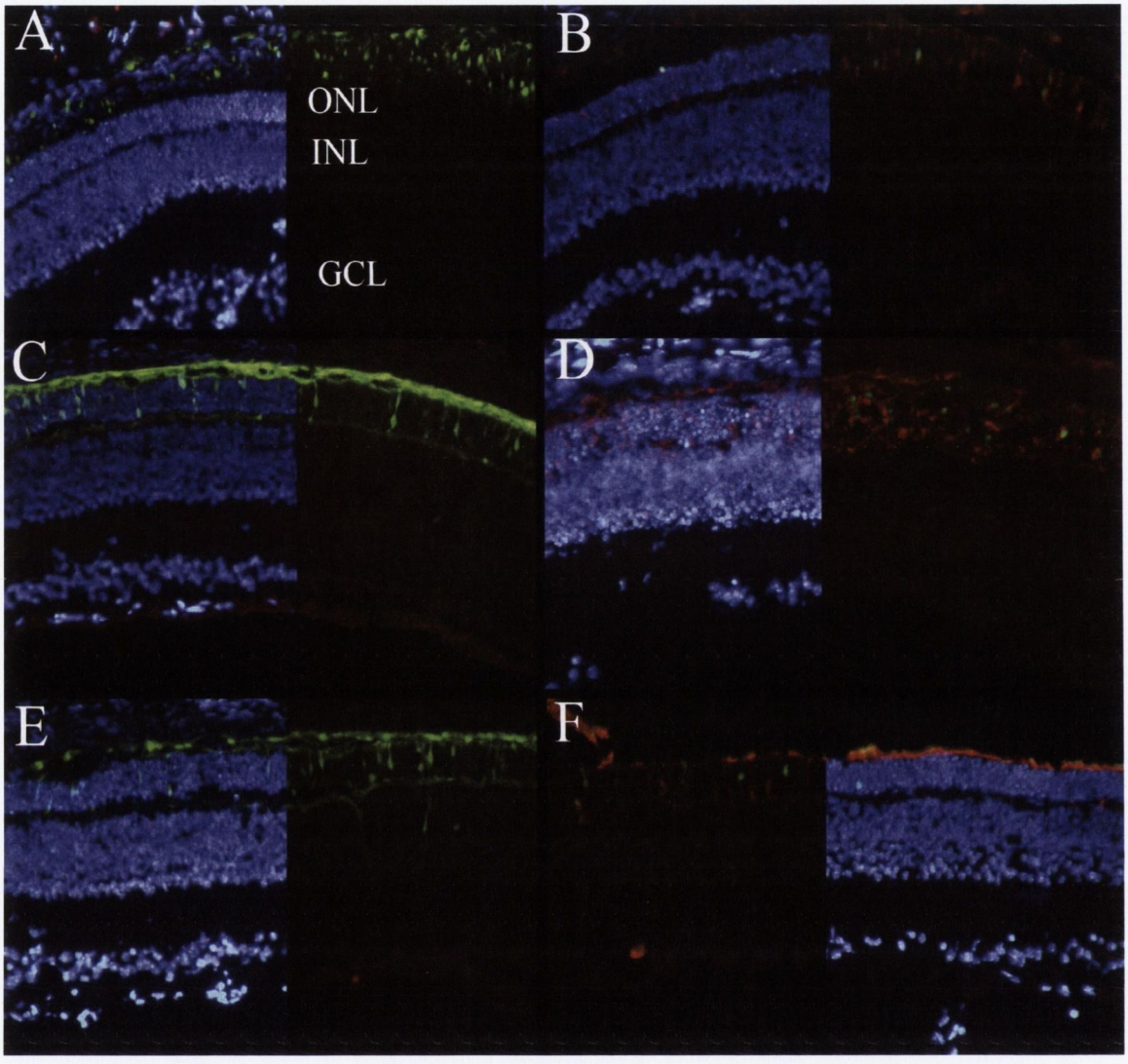

Figure 4.5.11: Immunohistochemistry of Trx_AAV injected P23H Mice at P10 where n=3

Immunohistochemical sections demonstrating expression of Trx in the Trx_AAV injected right eyes of P23H mice. These mice were injected at P0 and the retinas harvested at P10. Panels A, C and E display retinal sections of the left eyes which were injected with CMV_EGFP and panels B, D and F display retinal sections of the right eyes which were injected with Trx_AAV. This shows exogenous expression of Trx in the right eyes compared to no expression of Trx in the ONL of the left eyes. The exogenous expression of Trx in the right eyes provides no histological benefit to the ONL of these mice as the thickness of the ONL is similar in both the left and right eyes.

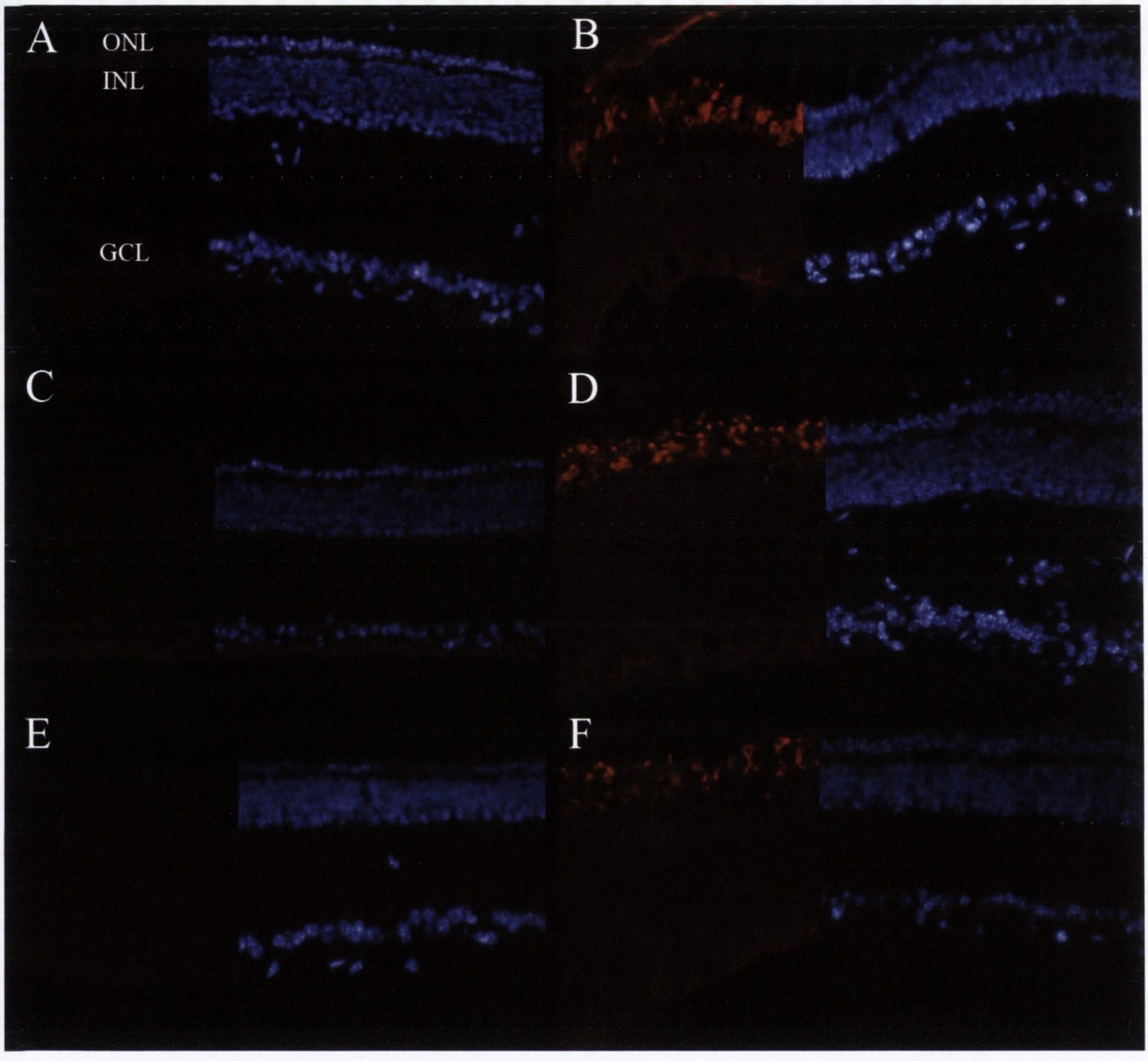

Figure 4.5.12: Immunohistochemistry of Trx_AAV injected P23H Mice at P22 where n=3

Immunohistochemical sections showing Trx expression in the right eyes of three Pro23His mice. These mice were injected with CMV_EGFP in the left eye and Trx_AAV in the right eye on P0 and euthanised for histology on P22. Images A, C and E show Trx expression in the left eyes of mice 1, 2 and 3 respectively. This demonstrates some expression of Trx in the GCL but little expression in the INL. Images B, D and F show Trx expression in the right eyes of mice 1, 2 and 3 respectively. These show strong viral-mediated expression of Trx in the ONL. The expression of Trx in the ONL in these mice also seems to have preserved some layers of the ONL. This is especially apparent in images D and F which display 2-3 layers of ONL compared to the one layer that remains in the left eye of these mice.

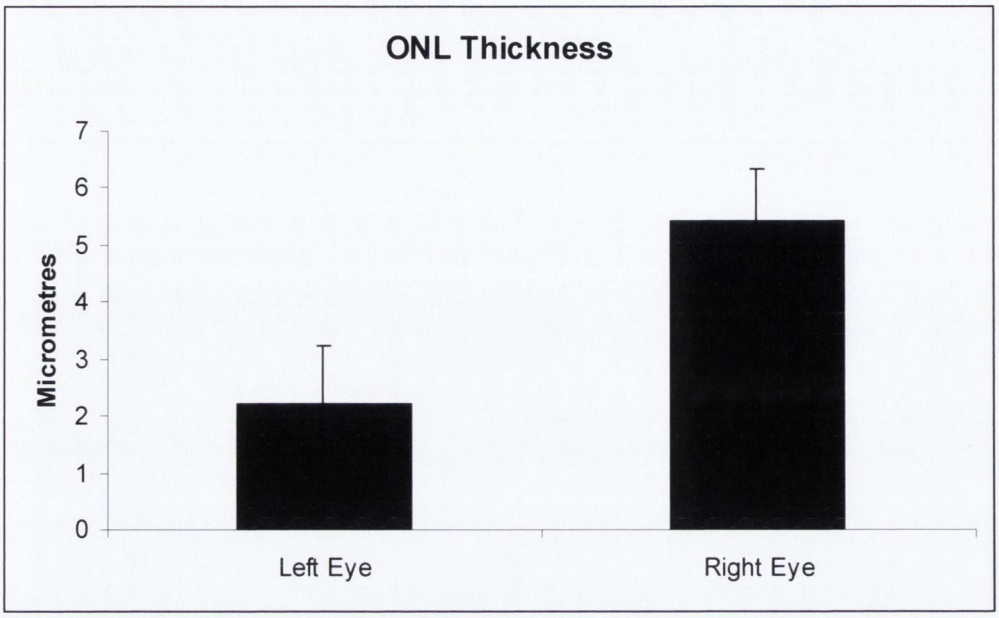

Figure 4.5.13: ONL thickness of P23H mouse left eyes and right eyes at 22 days post-injection of CMV_EGFP and Trx_AAV respectively where n=3

Outer nuclear layer (ONL) thickness was assayed in the Trx_AAV injected retinas of P23H transgenic mice at P22 by taking measurements of the ONL at eight separate points along the length of a micrograph. For each eye, four micrographs were examined. These data were averaged and a standard deviation was calculated to produce the figure presented above. This figure indicates that the ONL of Trx_AAV injected retinas are approximately 2.5 times thicker than control retinas treated with CMV_EGFP. A two way paired student's t-test failed to reach statistical significance, producing a p-value of 0.061.

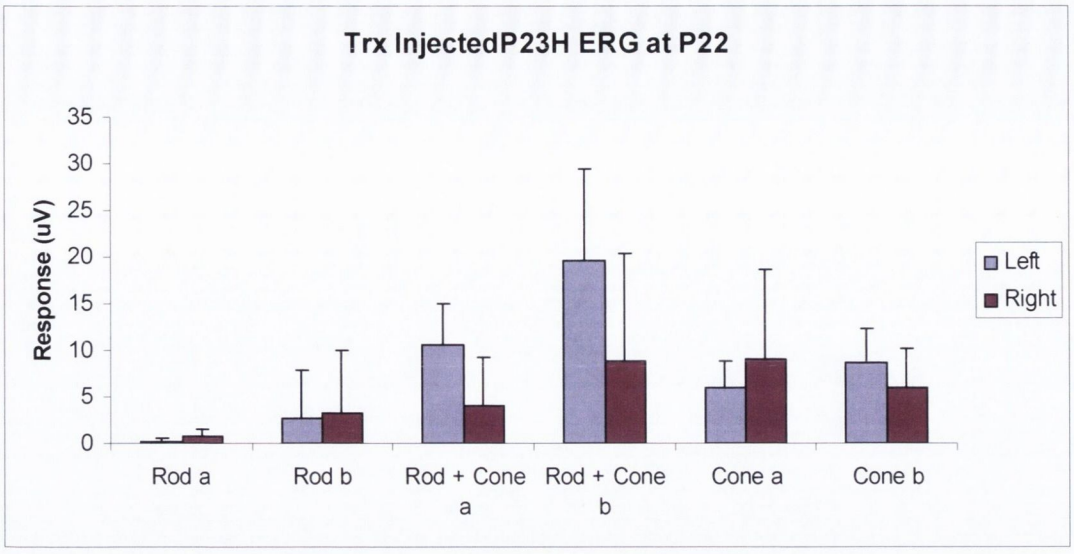

Figure 4.5.14: Electroretinographic Analysis of Trx_AAV injected P23H Mice at P22 where n=5

Bar chart showing the ERG response of mice sub-retinally injected in the right eye with Trx_AAV and the left eye with CMV_EGFP at P0 and analysed at P22. This demonstrates a slight increase of Rod a, Rod B and Cone a responses. However the right eye shows a decrease of Rod+Cone a, Rod+Cone b and Cone a. None of these changes between left and right eye reached statistical significance with P values of 0.2, 0.4, 0.06, 0.1, 0.6 and 0.2 for Rod a, Rod b, Rod+Cone a, Rod+Cone b, Cone a and Cone b respectively.

	Average		Standard Deviation		
	Left Eye	Right Eye	Left Eye	Right Eye	P-Value
Rod a	0.22	0.75	0.44	0.87	0.20
Rod b	2.6	3.35	5.2	6.7	0.39
Rod+Cone a	10.61	4.01	4.37	5.23	0.06
Rod+Cone b	19.56	8.85	9.84	11.51	0.11
Cone a	5.98	9.0	2.93	9.57	0.58
Cone b	8.63	6.03	3.67	4.14	0.23

Table 4.5.2: ERG amplitudes of the left and right eyes P23H P22

The ERG amplitudes which are presented as a bar chart in figure 4.5.12 are presented here in a table which also lists the corresponding standard deviations of each average amplitude value. The p-values of each set of data are also presented. These values were calculated by two way paired student's t-test. No data sets reached statistical significance; the set with a P-value closest to significance is the

Rod+Cone (maximal) data set which suggests that Trx_AAV may be detrimental to visual function.

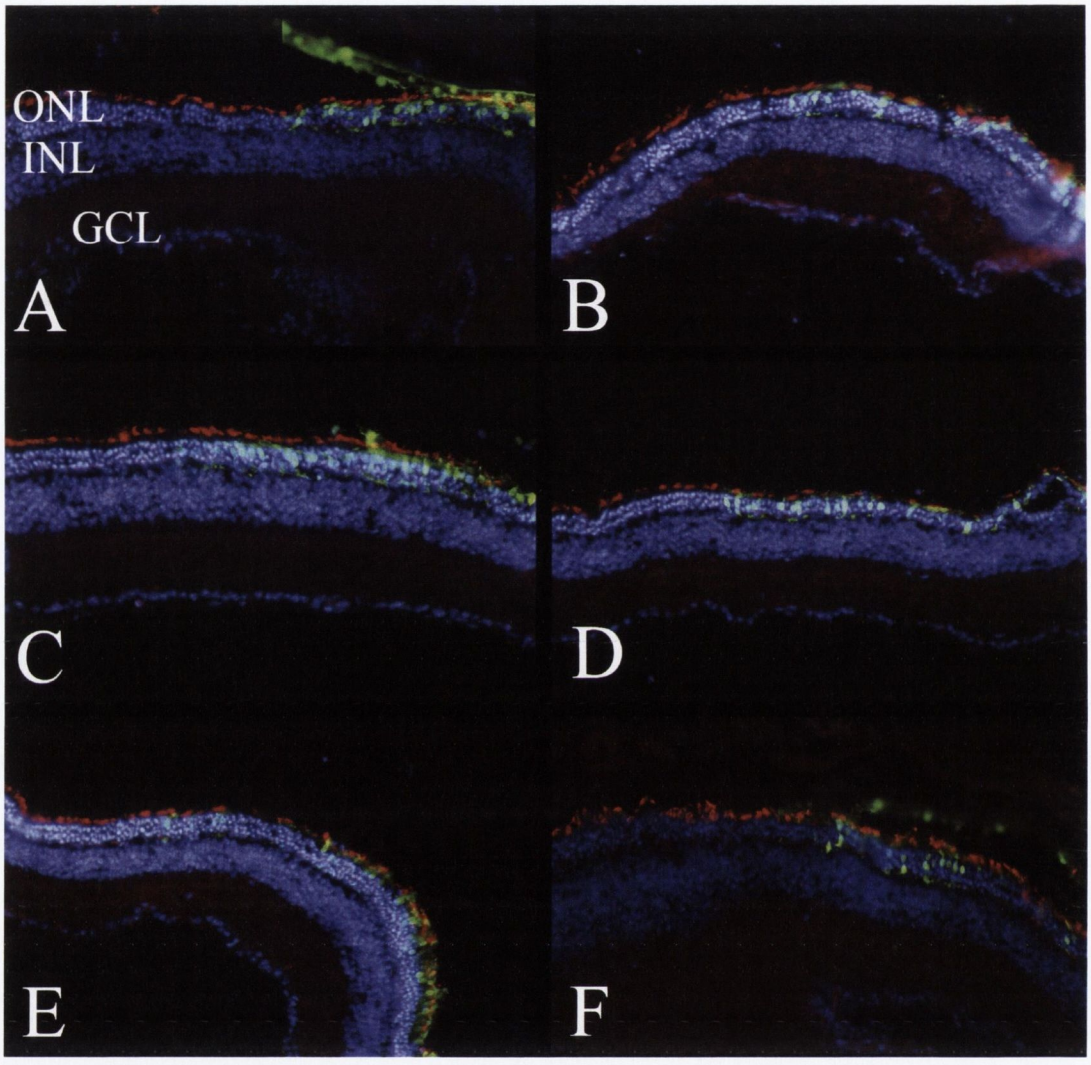

Figure 4.5.15: PNA staining of hP347S mice treated with Trx_AAV at 4 weeks post-injection where n=3

Immunohistochemical staining of retinal sections taken from hP347S transgenic mice using the PNA differential stain for cones at 4 weeks post-injection. This figure demonstrates no observable difference in the density of cones between the left (NT20 injected, panels A, C and E) and right (Trx_AAV injected) eyes (panels B, D and F). Transduced regions of the retina were determined by examining the EGFP expression in the ONL of the retina. In the right eye this EGFP expression is a result of a 1/10 dilution on CMV_EGFP in the Trx_AAV injection volume. This figure demonstrates that Trx_AAV has no positive effect on cone survival at 4 weeks post-injection.

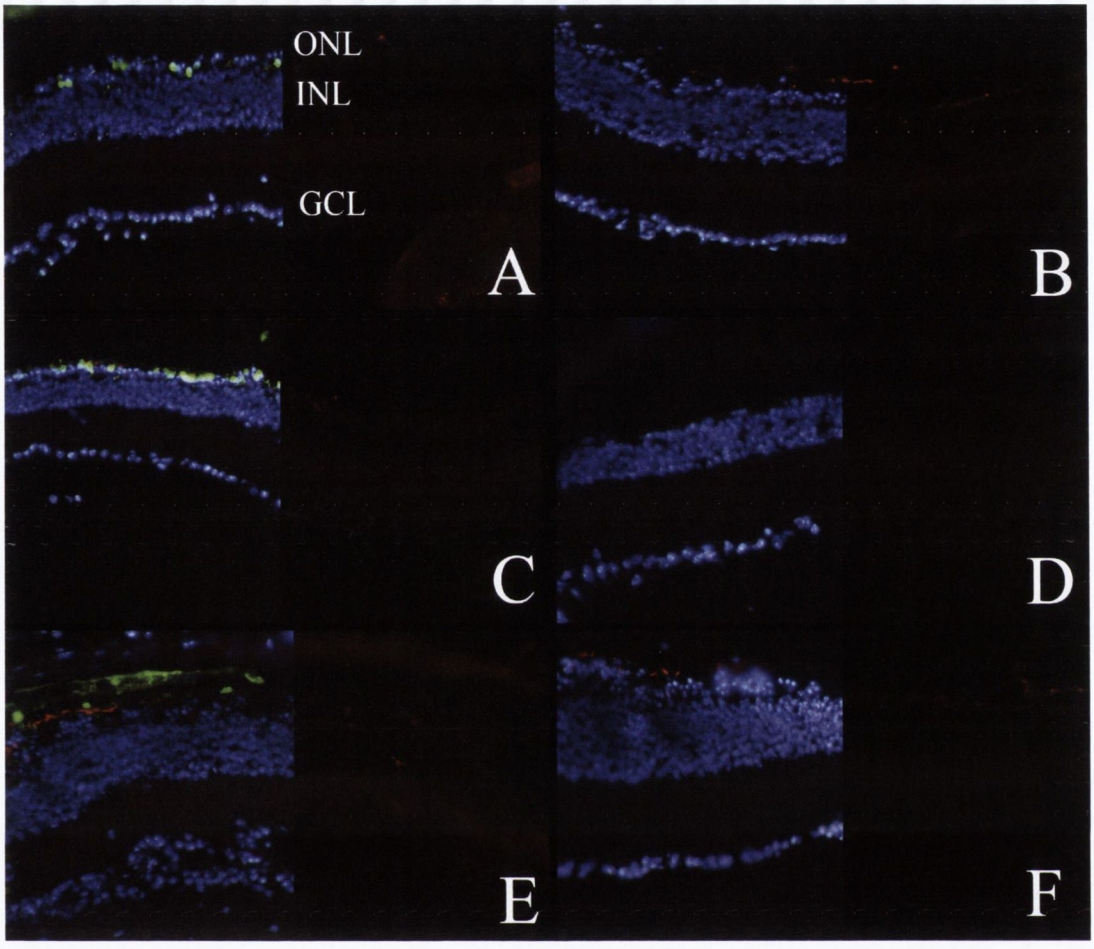

Figure 4.5.16: PNA staining of hP347S mice treated with Trx_AAV at 16 weeks post-injection where n=3

Immunohistochemical staining of retinal sections taken from hP347S transgenic mice using the PNA differential stain for cones at 16 weeks post-injection. This figure demonstrates an almost complete loss of cones in both the left (NT20 injected, panels A, C and E) and right (Trx_AAV injected) eyes (panels B, D and F). Some staining is observed in panel B but this failed to be replicated in other right eyes in panels D and F. At this time, the CMV_EGFP expression has been completely lost in Trx_AAV treated eyes compared to the EGFP expression observed in figure 4.5.15 at 4 weeks post-injection (as CMV_EGFP was used as a tracer of transduction by diluting 1/10 in the initial volume sub-retinally injected in to the right eyes).This figure demonstrates that Trx_AAV has no positive effect on cone survival at 16 weeks post-injection.

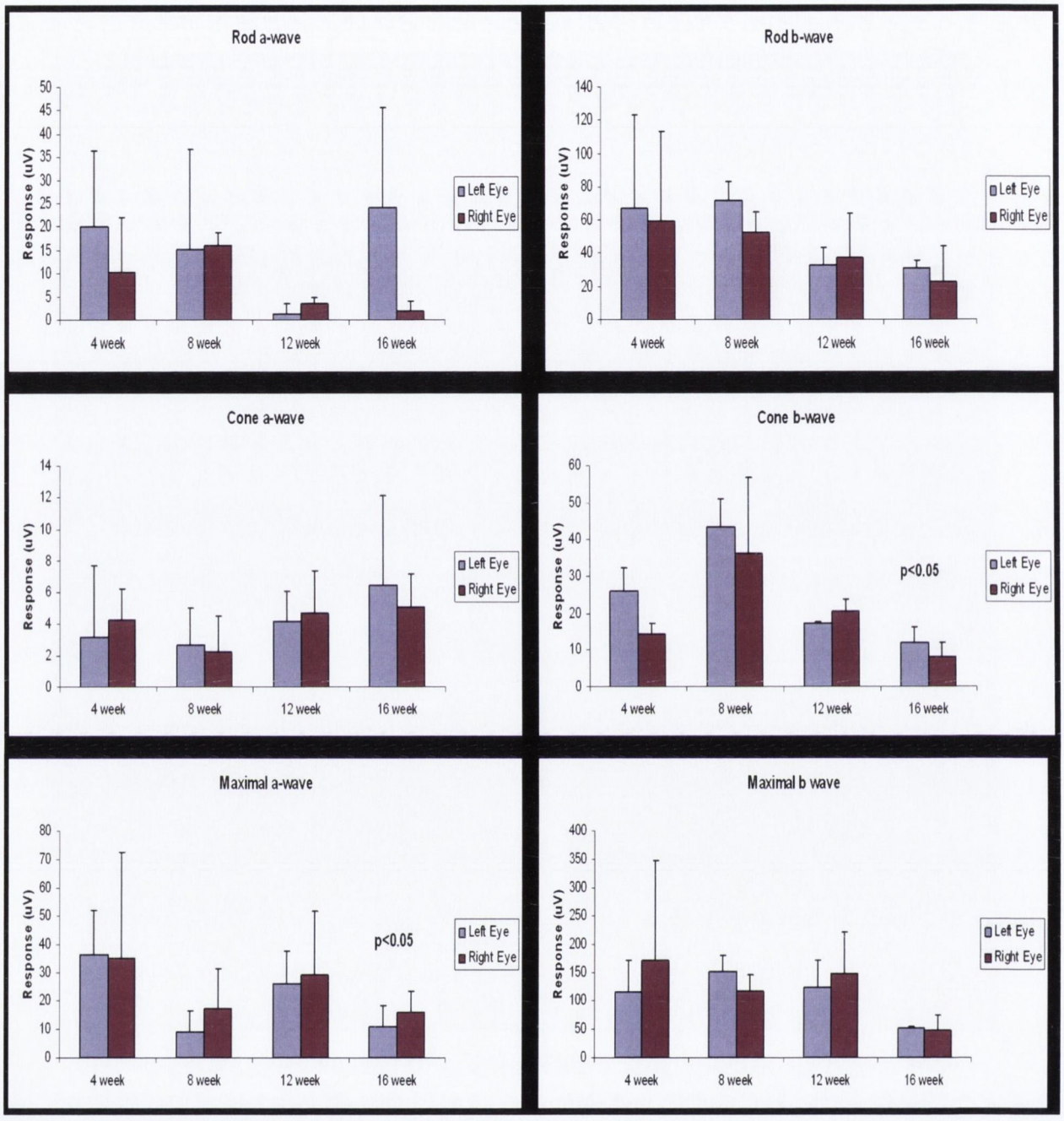

Figure 4.5.17: ERG analysis of Trx_AAV injected hP347S mice 4-16 weeks post injection where n=3

Bar chart showing the average ERG amplitudes for hP347S heterozygous mice injected sub-retinally with NT20 in the left eye and Trx_AAV in the right eye. The average quantities are shown at four time-points from 4 weeks to 16 weeks post-injection in 4 week intervals. It can be observed that Trx_AAV has had no statistically significant positive effect on visual function except for the 16 weeks maximal a-wave time-point. However at 16 weeks post-injection, Trx_AAV appears to be detrimental to the cone b-wave. These

two time-points are the only data sets which reached statistical significance as measured by two way paired student's t-test.

	Left Eye				Right Eye			
	4 week	8 week	12 week	16 week	4 week	8 week	12 week	16 week
Rod a-wave	20.05±16.42	15.11±21.64	1.44±1.96	24.05±21.69	10.37±11.67	16.03±2.81	3.59±1.30	1.80±2.20
Rod b-wave	66.70±56.70	71.40±11.79	32.70±10.74	31.26±4.63	59.43±53.57	52.83±12.19	37.40±26.24	23.13±20.62
Cone a-wave	3.21±4.51	2.70±2.29	4.18±1.91	6.47±5.64	4.23±2.03	2.23±2.28	4.73±2.64	5.13±2.03
Cone b-wave	26.25±6.01	43.30±7.56	17.43±0.15	11.96±4.50	14.50±2.83	36.17±20.54	20.43±3.36	8.03±4.08
Max a-wave	36.67±15.31	9.22±7.46	26.17±11.87	10.87±7.59	35.29±37.53	17.52±13.62	29.30±22.46	16.00±7.44
Max b-wave	116.27±55.75	152.00±27.51	124.93±46.92	52.27±3.04	172.53±176.21	117.30±27.59	147.30±73.56	47.63±27.09

Table 4.4.3: ERG recordings of Trx_AAV injected hP347S heterozygous mice (n=3)

Average values were recorded for each of the three mice analysed by electroretinography and a standard deviation was calculated for each average. These data were presented as a bar chart in figure 4.5.15. The left and right eye ERG values which provided a statistically significant p-value are highlighted in red and yellow. These two data points suggest that Trx_AAV is having a positive effect on maximal a-wave at 16 weeks but a detrimental effect on cone b-wave.

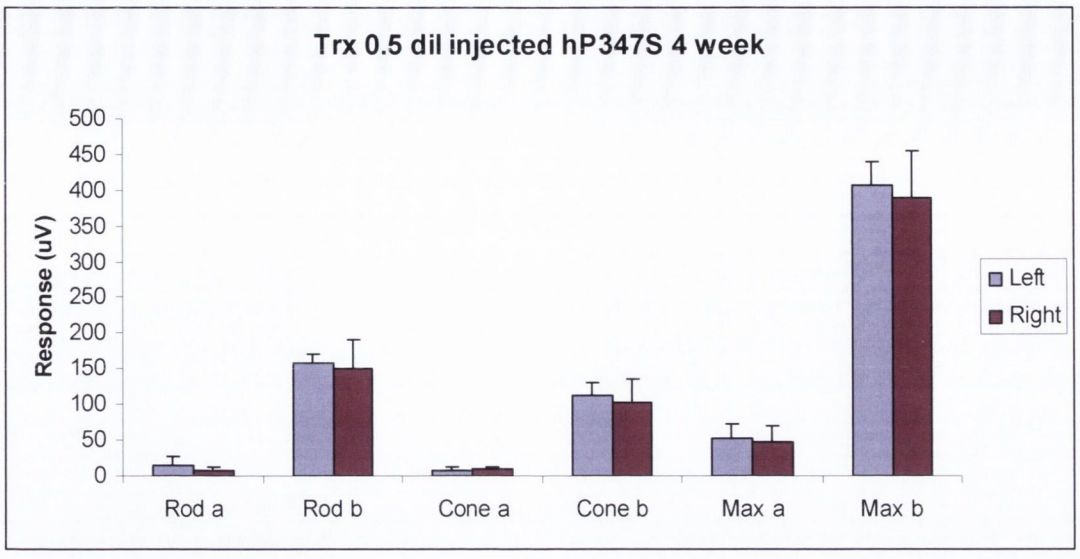

Figure 4.5.18: ERG analysis of Trx_AAV (1/2 dilution) injected hP347S mice 4 weeks post injection where n=3

Three hP347S heterozygous mice which had been sub-retinally injected with CMV_EGFP in the left eye and Trx_AAV in the right eye at P21 were analysed by ERG at 4 weeks post injection. The resulting average and standard deviation data are shown graphically in this figure. This shows no statistically significant change in ERG amplitudes between the left and right eye for any of the six responses recorded.

	Average		Standard Deviation		
	Left Eye	Right Eye	Left Eye	Right Eye	P-value
Rod a	16.24667	6.330667	12.44531	5.245978	0.432801
Rod b	157.3333	150.6667	13.01281	39.80368	0.819622
Cone a	6.306667	10.12333	6.911507	2.798291	0.510308
Cone b	113.6667	103.6667	15.82193	31.89566	0.664548
Max a	52.9	47.83333	20.72462	21.61165	0.716824
Max b	406.3333	388.3333	32.86842	65.65313	0.754551

Table 4.5.4: ERG recordings of Trx_AAV (1/2 dilution) injected hP347S heterozygous mice at 4 weeks post injection where n=3

Average values were recorded for each of the three mice analysed by electroretinography and a standard deviation was calculated for each average. These data were presented as a bar chart in figure 4.5.18. The p-values of each set

of data are provided. This indicates that a 1 in 2 dilution of the Trx_AAV virus has no effect of visual function at 4 weeks post injection.

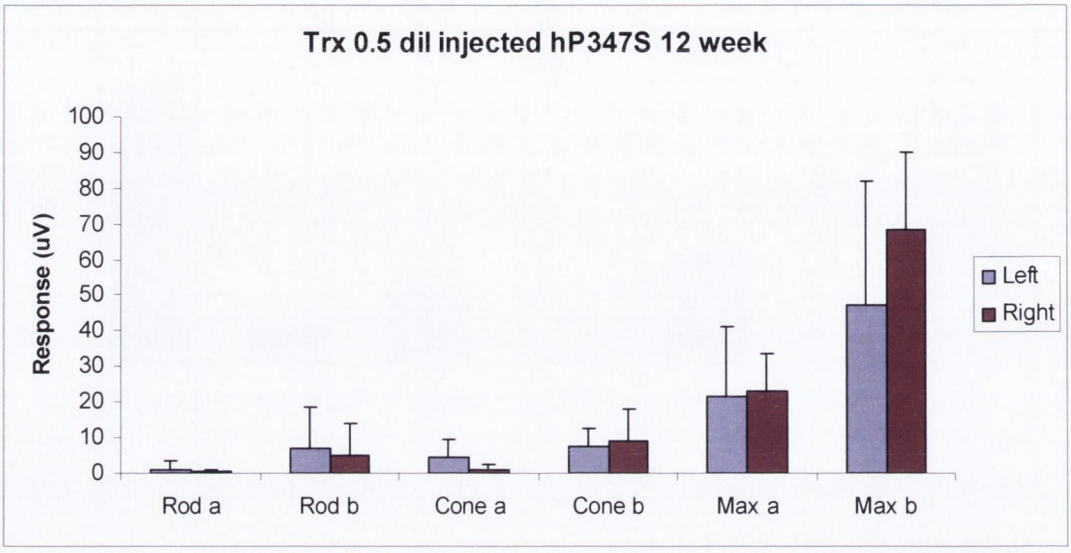

Figure 4.5.19: ERG analysis of Trx_AAV (1/2 dilution) injected hP347S mice 12 weeks post injection where n=3

Three hP347S heterozygous mice which had been sub-retinally injected with CMV_EGFP in the left eye and Trx_AAV in the right eye at P21 were analysed by ERG at 12 weeks post injection. The resulting average and standard deviation data are shown graphically in this figure. This shows no statistically significant change in ERG amplitudes between the left and right eye for any of the six responses recorded.

	Average		Standard Deviation		
	Left Eye	Right Eye	Left Eye	Right Eye	P-Value
Rod a	1.20	0.51	2.08	0.50	0.63
Rod b	6.80	5.13	11.77	8.89	0.42
Cone a	4.74	1.25	4.82	1.30	0.24
Cone b	7.74	9.12	4.99	8.91	0.87
Max a	21.74	22.97	19.71	10.81	0.92
Max b	47.13	68.57	34.64	21.33	0.19

Table 4.5.5: ERG recordings of Trx_AAV (1/2 dilution) injected hP347S heterozygous mice at 12 weeks post injection where n=3

Average values were recorded for each of the three mice analysed by electroretinography and a standard deviation was calculated for each average.

These data were presented as a bar chart in figure 4.5.19. The p-values of each set of data are provided. This indicates that a 1 in 2 dilution of the Trx_AAV virus has no effect of visual function at 12 weeks post injection.

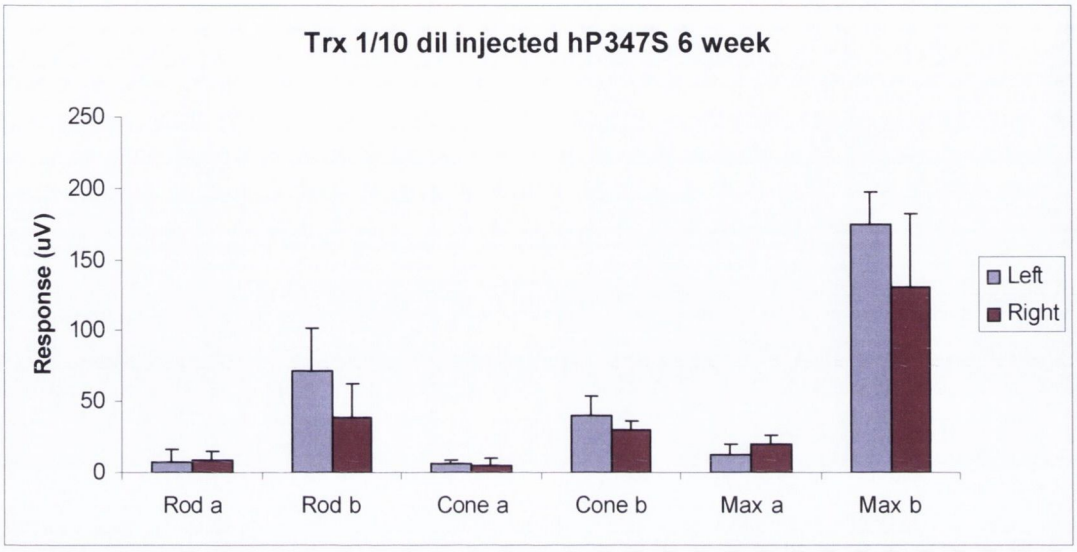

Figure 4.5.20: ERG analysis of 1/10 dilution of Trx_AAV injected hP347S at 6 weeks post injection where n=4

Four hP347S heterozygous mice which had been sub-retinally injected with CMV_EGFP in the left eye and Trx_AAV in the right eye at P21 were analysed by ERG at 6 weeks post injection. The resulting average and standard deviation data are shown graphically in this figure. This shows no statistically significant change in ERG amplitudes between the left and right eye for any of the six responses recorded.

	Left Eye	Right Eye	Left Eye	Right Eye	P-Value
Rod a	7.52	9.31	8.44	6.16	0.51
Rod b	71.60	39.04	30.30	23.60	0.09
Cone a	5.92	5.13	2.42	4.67	0.82
Cone b	40.13	29.60	14.20	6.98	0.13
Max a	12.35	20.20	8.31	5.85	0.17
Max b	174.75	130.53	22.07	51.22	0.22

Table 4.5.6: ERG recordings of Trx_AAV (1/10 dilution) injected hP347S heterozygous mice at 6 weeks post injection where n=3

Average values were recorded for each of the three mice analysed by electroretinography and a standard deviation was calculated for each average. These data were presented as a bar chart in figure 4.5.20. The p-values of each set of data are provided. This indicates that a 1 in 10 dilution of the Trx_AAV virus has no effect of visual function at 6 weeks post injection.

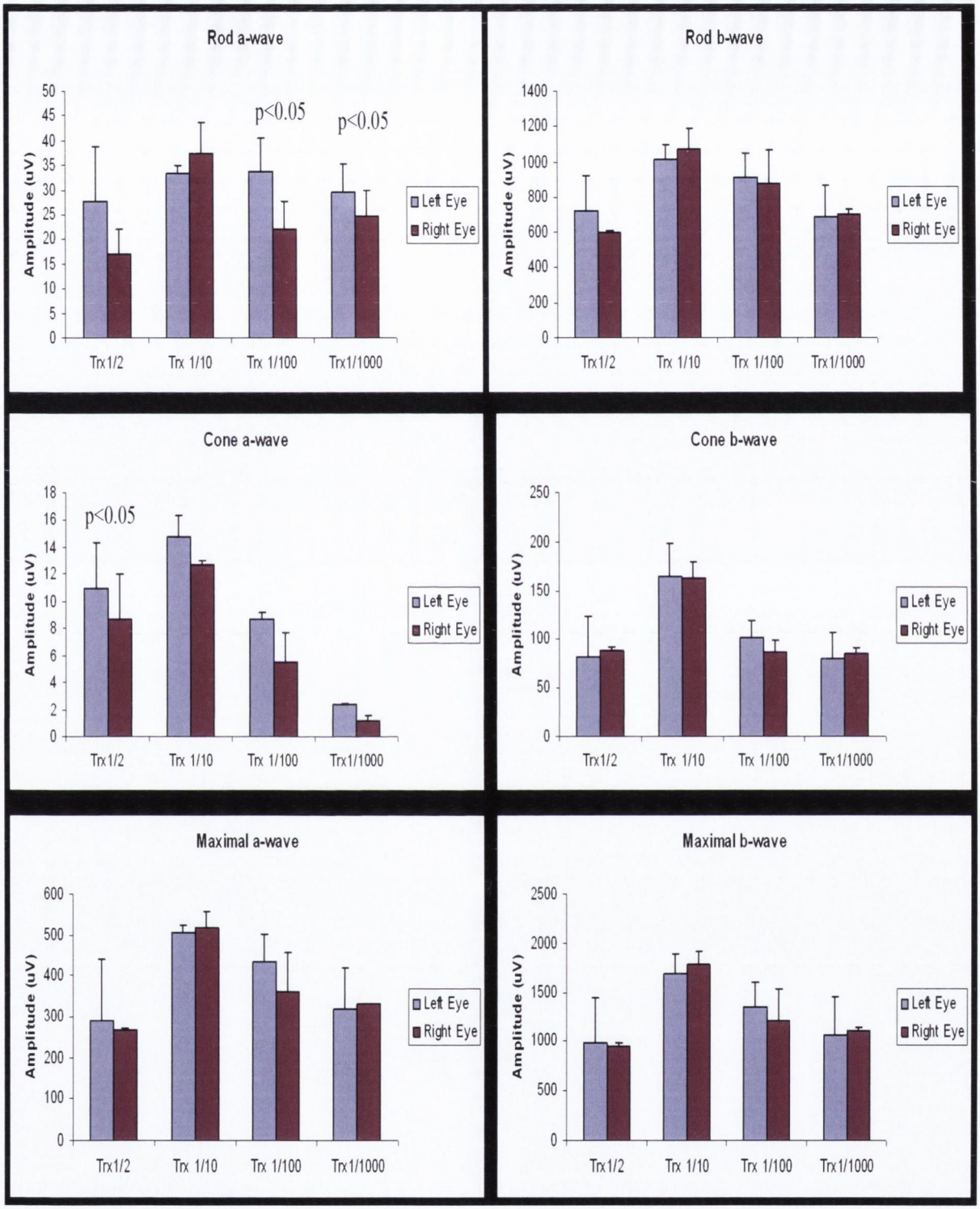

Figure 4.5.21: ERG responses of a range of Trx_AAV dilutions in wild type mice.

Mice which had been injected with a range of dilutions of Trx_AAV and CMV_EGFP were analysed by ERG at 4 weeks post injection to determine if the Trx_AAV virus is toxic at higher concentrations. This figure details the responses of these animals for each dilution where n=2 for each dilution. A two way paired student's t-test performed to compare left and right eyes resulted in a statistically

significant p-value for the cone a-wave at 4 weeks post-injection. The results of the rod a-wave were dismissed. ANOVA statistical analysis determined that many of the cone a-wave responses are significantly different to suggest that Trx_AAV may be toxic at lower doses. However ANOVA analysis demonstrated non significance for all other wave responses.

Chapter 5: Investigation of Dihydroethidium as a Retinal Marker of Oxidative Stress

5.1 Introduction

The primary objective of this PhD was the AAV-mediated delivery of DNA based therapies of genetic elements which have previously been demonstrated to have a role in the protection of mammalian retinal cells through a reduction in the levels of reactive oxygen species (ROS, Doonan et al, 2012). ROS can cause cellular damage and subsequent death in several models of retinal degeneration. In order to assess these levels of ROS in the transgenic models of retinal degeneration present in the TCD Ocular Genetics laboratory, the nuclear stain dihydroethidium (DHE) was chosen based on its success as a marker of retinal oxidative stress in previously published papers (Stevenson et al, 2010; Al-Shabrawey et al, 2008; Sasaki et al, 2010; Tan et al, 2013). Dihydoethidium is the reduced form of the regularly used DNA stain ethidium bromide. When DHE becomes oxidised, the resulting ethidium molecule becomes positively charged and allows intercalation in to DNA and fluorescence at a wavelength of 567nm which can be visualised by fluorescent microscopy (Zhao et al, 2003, Figure 5.1.1). DHE was first used as a general nuclear stain due to its relatively small size and its inherent ease of access in to cells, where it was assumed that DHE was oxidised by a cellular dehydrogenase (Bucana et al, 1986). However, it was not until 1990 that the DHE stain was used as a marker of ROS, in particular as a marker of the phagocytic respiratory burst used to kill invading bacteria (Rothe & Valet, 1990). Since then, DHE has proven to be an effective marker of intracellular superoxide anions in many tissues including endothelial cells of the aorta (Damiano et al, 2013), hair cells of the cochlea (Fetoni et al, 2013) and neurons of the hippocampus (Choi et al, 2012) amongst many other examples. The broad application of this stain is also related to its relative ease of use on cultured cells, cells *in vivo* and tissue explants due to its ease of passage through the cell membrane.

To date, DHE has been used to assess several models of oxidative stress induced retinal damage, as many of these animal models produce excess quantities of superoxide (O_2^-) which specifically reacts with DHE to form ethidium (Punzo et al, 2012; Chrysostomou et al, 2013; Trifunovic et al, 2012). Rogers et al used DHE to show an increase in staining of the photoreceptor inner segments subsequent to

$FeSO_4$ mediated damage to the retina (Rogers et al, 2007). Peng et al have shown that the rod cells of *shaker* mice (a genetic mouse model of Usher's syndrome) accumulate 3.5 times the levels of superoxide compared to wild type mice of the same background strain and age using DHE (Peng et al, 2011). DHE has also been used to characterise the increase in superoxide production in the retinas of eyes which had been intravitreally injected with paraquat, a herbicide which induces oxidative damage by acting as an electron acceptor to molecular oxygen to form superoxide (Cingolani et al, 2006). This study also highlighted the differences in DHE staining observed across strains by comparing retinal sections of BALB/c and C57BL/6, demonstrating that BALB/c mice exhibit a higher level of oxidative stress than the C57BL/6 mice.

More recently DHE has been used to evaluate oxidative stress in the retina of the *Gpx1* (an antioxidant protein) knockout mouse which was subjected to retinopathy of prematurity via an oxygen induced retinopathy (OIR) protocol. OIR treatment exposes mice to hyperoxia which induces retinal neovascularisation when the mice are returned to normoxia (Smith et al, 1993). This study demonstrated an almost two-fold increase in DHE staining intensity in *Gpx1* KO mice compared to wild type mice which were also OIR treated, particularly in the GCL (Tan et al, 2013). The DHE stain has also been used to characterise the levels of oxidative stress in all three neuronal layers of the retina of the db/db mouse, a model of diabetic retinopathy. Quantification of the intensity of DHE staining demonstrated over a two-fold increase in the levels of superoxide in these mice compared to wild type mice of the same genetic background (He et al, 2013). These are two examples of almost fifty publications released in 2013 featuring DHE staining of the retina as of June 2013.

DHE has also been used in research of models of RP, many of which have increased levels of ROS, particularly in the photoreceptors (Padnick-Silver et al, 2006). Usui et al employed the DHE stain to exhibit increased production of superoxide in the ONL of the *rd10* mouse model of RP. The intensity of DHE staining was decreased after crossing *rd10* mice with *SOD1* (a detoxifying enzyme which converts superoxide to H_2O_2) overexpressing transgenic mice (Usui et al, 2011). Additionally, O' Driscoll et al demonstrated an increased level of superoxide

in the *rd10* mouse model of RP. This group showed that treatment of *rd10* mice with a free radical scavenger decreased DHE staining intensity in the ONL (O' Driscoll et al, 2011).

Dihyrdoethidium has proven itself to be a reliable and reproducible stain for superoxide in many tissues and animal models of oxidative stress. However a number of other stains are available to researchers in the field of oxidative stress related biology. A number of examples of these markers are discussed below with a focus on their use in models of RP.

Nitrotyrosine is a byproduct of oxidative stress caused by nitration of tyrosine residues of proteins. This nitration frequently occurs through the action of peroxynitrite, a highly reactive species formed by the reaction of NO and superoxide discussed in section 1.7. Therefore measuring the relative level of nitrotyrosine in a tissue of interest gives an indication of the overall level of oxidative damage to proteins. Roddy et al have demonstrated that treatment of the RCS rat with stanniocalcin-1 (a gene whose protein product is known to decrease oxidative stress) decreases levels of nitrotyrosine as measured by ELISA (Roddy et al, 2012). The RCS rat is a model of RP which carries a mutation in the *MERTK* gene, resulting in impaired phagocytosis of the photoreceptor outer segments by the RPE (Gal et al, 2000). Komeina et al have also used nitrotyrosine as a marker of oxidative stress in the *rd1* mouse model of RP which displayed an increase in the presence of nitrotyrosine in the INL of the *rd1* mouse compared to wild type mice as measured by immunohistochemistry (Komeina et al, 2008). Shen et al have observed increased levels of nitrotyrosine in the retinas of P347L transgenic RP model pigs compared to age matched wild type animals (Shen et al, 2005).

An alternative assay for oxidative stress is the antibody detection of 8-oxo-2'-deoxyguanosine (8-OH-dG), a product of guanine oxidation in nuclear DNA. In the publication by Shen et al which detailed the oxidative stress associated with the P347L transgenic pig, the authors noted increased 8-OH-dG staining in the ONL and the outer segments of the photoreceptors of these animals (Shen et al, 2005). The anti-8-OH-dG antibody stain has also been used by Obolensky et al to evaluate oxidative stress in the *rd10* RP mouse model, demonstrating an increase in the

number of stained cells of these mice compared to their wild type counterparts (Oboloensky et al, 2011).

One of the most reliable approaches to measurement of oxidative stress is the assaying of products of lipid peroxidation as this process has been directly linked to cellular apoptosis (Wu et al, 2012, Sugano et al, 2013). Therefore measuring the relative levels of lipid peroxidation occurring in a tissue of interest gives a reliable indication of the state of stress that the tissue is in. Two of the most common methods of quantifying lipid peroxidation are the antibody detections of 4-Hydroxynonenal (4-HNE) or Acrolein. 4-HNE is the end product of a free radical propagated chain reaction initiated by the reaction of an n-6-poly-unsaturated fatty acid (PUFA, with a double bond between carbons 6 and 7 of the fatty acid chain) with peroxynitrite, hydroxyl radical, superoxide or nitric oxide. Of these ROS, peroxynitrite is heavily implicated as the most prevalent initiator of this chain reaction (Mattson, 2009). Both of these stains were used by Shen et al to show a marked increase in HNE staining, initially in the inner segments of the cones but spreading to the cone cell bodies with time (Shen et al, 2005). This pattern of staining was also observed using the anti-acrolein antibody stain. Acrolein is another by-product of PUFA lipid peroxidation, with increasing yield of acrolein produced as the number of double bonds increases in the aliphatic chain of the fatty acid (Onyango, 2012). Acroelin was used in the characterisation of oxidative stress of the *rd1* RP mouse model, demonstrating a progressive increase in acrolein staining of retinal sections with time (Komeina et al, 2006). This staining co-localised with a stain for PNA, a marker of cones, showing that these cells were most heavily stressed by ROS; results which agree with the current model of RP retinal degeneration which suggests that the initial loss of rod cells causes further oxidative stress to cones from choroidal blood supply (Yu et al, 2004). Staining of acrolein was also used to characterise lipid peroxidation in the *rd10* mouse model which showed a large increase of acrolein staining in all layers of the retina as early as P32 compared to wild type mice (Corrochano et al, 2008). The use of 4-HNE as a stain of lipid peroxidation in the retina has been largely limited to studies of light induced retinal oxidative stress and AMD (Tanito et al, 2005; Ethen et al, 2007), both of which demonstrate an increase in 4-HNE staining compared to control animals.

Although a wide range of assays and stains for the measurement of ROS are available to the researcher, the DHE stain was chosen over others for a number of reasons. Firstly, this stain has been used extensively in the investigation of oxidative stress in the eye (see above) and therefore has been validated by other laboratories as a suitable marker of ROS in the retina. This would also allow a more direct comparison of data regarding a change in the occurrence of ROS in this study compared to studies carried out in other laboratories. The second reason this stain was chosen was due to the ease of use of the stain. Antibody stains (such as the 8-OH-dG) require fixation of the samples and long incubation periods. They are also more expensive than the DHE stain. Finally, this chapter has largely focused on assays of ROS which are largely examined by histology. A large range of assays are available which would allow for biochemical or FACS based analysis of ROS. These types of assays were not chosen as they often require live cells which may be diffuclt to isolate and experiment upon satisfactorily after removal from the retina. Furthermore, histological examination is a skill which is heavily employed successfully in this laboratory and therefore it was felt that the DHE stain was best suited to our needs and skills. Another dye which may be employed to detect superoxide is the MitoSox Red indicator (Life Technologies). Although this stain was considered when deciding which assay to choose, further investigation revealed the mechanism of action to be the same as that of DHE and the MitoSox core chemical structure is almost the exact same as that of DHE. Additionally, MitoSox appears to be selective for mitochondrial derived ROS and therefore would be unsuitable for experiments examining cytosolic ROS production (Mukhopadhyay et al, 2007).

The aim of the research undertaken in this chapter was to evaluate the levels of retinal oxidative stress in several mouse models of retinal degeneration using the dihydroethidium stain of superoxide radicals. The DHE stain was chosen due to its relative ease of use and analysis and its success in detection of retinal superoxide by other laboratories. This stain was used to quantify differences in superoxide levels present in the retina in wildtype mice compared to Pro23His and human Pro347Ser rhodopsin mutant transgenic mice models of RP and a mouse model of Leber's Hereditary Optic Neuropathy (LHON). Subsequent to the characterisation of

superoxide levels in these mouse models of retinal degeneration, this stain was utilised to measure any changes in superoxide levels of the retina of mice which received a *Rac1* shRNA (chapter 3) or the *Thioredoxin1* gene (chapter 4) by AAV delivery.

5.2 Materials and Methods

All materials used are listed in section 2.1.8.

5.2.1 Preparation of DHE solution

Dihydroethidium was purchased from Invitrogen as a powdered solid. This was immediately dissolved in 100% DMSO (Sigma Aldrich) to a concentration of 3.17mM and stored for up to 6 months at -20°C in the dark to prevent photo-oxidation. Working solutions of DHE solution were diluted to 5µM in DMSO in 1ml aliquots and were wrapped in aluminium foil to prevent photo-oxidation. These working stocks were kept frozen at 4°C (due to the high melting temperature of DMSO) for up to two weeks. For direct administration to mice via intraperitoneal injection, DHE powder was dissolved in DMSO to a concentration of 10µg/µl before dilution to a working concentration of 1µg/µl in PBS in a protocol modified from Behrens et al, 2007. Due to the potential mutagenic effects of ethidium, all work with powdered DHE was carried out in a fume hood and all waste DHE was disposed of in the same manner as ethidium bromide.

5.2.2 Administration of DHE by intraperitoneal injection

DHE solution was freshly prepared to a concentration of 1µg/µl immediately prior to administration and incubated to room temperature. Each mouse was then firmly scruffed and a volume of 200µl was administered via i.p. injection to the left side of the mouse. Thirty minutes after the initial injection, a second i.p. injection of 200µl of DHE solution was administered to the right side of the mouse. The mice were then returned to their cages for 18 hours before euthanisation and harvesting of the eyes. These eyes were fixed in 4% paraformaldehyde (see section 2.2.8.1) before cryo-sectioning the eyes to a width of 12µm per section. The sections were DAPI stained to allow examination of the retinal structure. Sections were then examined by fluorescence microscopy.

5.2.3 *Ex vivo* staining of the retina using DHE

Mice were sacrificed and the eyes enucleated using forceps before the eyes were briefly washed in 1X PBS. The eyes were then placed into casts containing OCT compound and the casts frozen. The unfixed eyes were sectioned into 12µm sections and placed onto Poly-D Lysine glass slides. For sections from eyes which had been injected with NT20, pAAV_shRAC1_1 or pAAV_shRAC1_3, the slides were examined by fluorescence microscopy to identify EGFP positive sections. These sections were chosen to be stained with DHE as EGFP expressing cells must also express *Rac1* specific shRNA or a non-targeting shRNA as both constructs are present in the same viral vector as the CMV promoter driven EGFP. In experiments using sections from eyes which had been injected with CMV_EGFP or Trx_AAV, a 1/10 dilution of CMV_EGFP was added to the Trx_AAV viral preparation prior to injection. This allows EGFP positive sections to be identified as both viruses will have significant overlap in the areas of the retina which they transduce. The borders of the sections were then marked with PAP pen (Sigma-Aldrich) which leaves a hydrophobic mark at the edge of the sections. This mark helps contain the DHE solution which will be placed over the sections. DHE stain (5µM) was then pipetted onto the sections and the sections were covered in aluminium foil. The slides were placed into a dark incubator at 37°C for 30 minutes. The slides were briefly and gently washed with 1X PBS and stained with DAPI solution. The slides were then

washed twice with 1X PBS. Slides were covered with mounting solution before coverslips were placed over the eye sections. The slides were then immediately examined by fluorescent microscopy.

5.2.4 Data Interpretation and Statistical Analysis

All fluorescent micrographs of sections stained with DHE solution were examined using the ImageJ imaging software (available free online at http://rsbweb.nih.gov/ij/)
This program allows the intensity of brightness of a given area within an image to be quantified in arbitrary units. The trace tool of the ImageJ program was used to create an area containing the ONL and INL of each micrograph image and the fluorescence of DHE in this region was then quantified. A background area of equal area size (containing no regions of the retina) of the same micrograph was also fluorescence quantified. The fluorescence quantity of this background region was then subtracted from the value produced from quantification of the retinal area to provide a normalised quantity which was then used in further data analysis.

The normalised values from each set in an experiment (for example wild type vs transgenic, left vs right) were averaged and a standard deviation was calculated for each set which was averaged. These data were then graphed by bar chart to allow for a direct comparison in DHE staining intensity between sets of experimental retinas. For all experiments comparing the retinal DHE staining intensity between wild type and disease model mice a two tailed unpaired student's t-test was performed using all normalised values in each set. For all experiments comparing DHE staining intensity between left and right eyes a two tailed paired student's T-test was performed using the average staining intensity values for each eye as described in section 2.2.9.

5.3 Results

5.3.1 Evaluation of DHE as a marker of Oxidative Stress *in vivo*

The DHE stain was initially tested as an *in vivo* marker of superoxide through systemic injection of the stain in to live animals. The animals chosen were mice which had been intravitreally injected 5 months prior with 0.5µl of 1.5mM rotenone which induces a Leber's Hereditary Optic Neuropathy (LHON) like phenotype (discussed in more detail in section 5.4). This disease has been shown to result in an increase in retinal ROS and therefore should exhibit high fluorescence when stained with DHE. DHE solution was prepared as outlined in section 5.2.1 and i.p. injected in a volume of 400µl at a concentration of 1µg/µl in to four mice in a protocol modified from Behrens et al, 2007. The injection of DHE solution was not well tolerated however and of the four mice injected, only two survived to the 18 hour post injection time point at which it had been intended to sacrifice all injected mice. The two remaining live mice were immediately euthanised as clear indications of stress such as shivering, failure to respond to stimuli and piloerection (hair standing up) were observed (Wolfensohn & Lloyd, 2003). The eyes from all four animals were then harvested for sectioning. Representative fluorescent micrographs of a region of the retina of one of these mice are presented in figure 5.3.2. No specific staining was observed in panel A of this figure, taken using the '20' filter of the microscope which filters observable fluorescence to wavelengths of 575-640nm, a range which should detect any DHE staining as the oxidised DHE fluoresces at a wavelength of ~605nm. Furthermore, a similar staining pattern is observed using all available filters which filter light to optimal wavelengths of 540nm, 615nm and 510nm, presented in panels B, C and D respectively. This suggests that the faint staining observed in panel A may be an auto-fluorescent artefact and not a result of reaction between DHE and superoxide. Panel E shows the cellular structure of the same area of the retina by DAPI staining of the nuclei in the ONL, INL and GCL. Due to the distress caused to the injected mice and the unspecific nature of the DHE stain *in vivo*, i.p. injections of DHE solution were not performed again during the course of this PhD study.

5.3.2 Evaluation of DHE as a marker of Oxidative Stress *ex vivo*

The DHE stain was next used to stain sectioned retinas from rotenone injected mice as well as transgenic hP347S and P23H heterozygous RP model mice. An increase in retinal oxidative stress is known to occur in RP (see section 1.8) and LHON (see section 5.4) and therefore an increase in DHE staining intensity would likely be expected in the retinas of these animals.

The first set of animals which were stained with DHE *ex vivo* was four hP347S +/- transgenic mice and four wild type mice of the same genetic background. Briefly, these mice were euthanised at age P28 and the eyes were enucleated, sectioned and stained with DHE. The resulting stained sections were examined by fluorescence microscopy and the results of this are presented in figures 5.5.3 and 5.5.4. Figure 5.5.3 presents representative micrographs comparing the retinal DHE staining of the wild type and hP347S transgenic mouse eyes. It can be observed that the wild type retina has retained much of its total cellular volume compared to the thin layer of retina observed in the transgenic mouse. Secondly, a slight increase in DHE staining intensity is observed in the transgenic hP347S retina. However, subsequent quantitative analysis of the staining intensity using the ImageJ program revealed no statistically significant increase in staining between the two sets of animals, suggesting that oxidative stress is not increased in the retinas of hP347S mice at P28 as evaluated by this assay.

The second set of animals which were stained with DHE was three P23H +/- transgenic mice. Due to the rapid retinal degeneration which occurs in this mouse model, the mice were sacrificed at P5. Three wild type mice of the same genetic background were sacrificed at the same time point and both sets of eyes were sectioned and DHE stained at the same time. Representative micrographs of the wild type and P23H mouse retinas are presented in figure 5.5.5. This demonstrates a large increase in DHE staining intensity in the transgenic mouse retinas suggesting a large increase in superoxide levels present in the retinas of these animals at this time-point. This increase was further validated by quantification of DHE staining intensity in both sets of animals using the ImageJ program. The results of this analysis are graphed as a bar chart in figure 5.5.6, showing a

statistically significant (P=0.00014) two-fold increase of DHE staining intensity in the P23H transgenic mouse retinas compared to the wild type mice as measured using a two-way unpaired student's t-test. This data suggests that even at an early stage of post natal development, the P23H mouse model undergoes high exposure to potentially pathological levels of ROS in the retina.

The final animal model which was examined using the DHE stain *ex vivo* was the rotenone injected mouse model of LHON. Five wildtype strain 129 mice were intravitreally injected with DMSO in the left eye and rotenone dissolved in DMSO to a concentration of 2.5mM in the right eye at P28. The injected mice were sacrificed 14 days after injection and the eyes were harvested for sectioning and staining with 5μM DHE. Representative fluorescent micrographs of the DHE stained left and right eyes of each of the five mice are presented in figure 5.5.7. A slight increase in staining intensity can be observed in the right eyes of these mice, especially in mouse 4 and mouse 5 (panels G-J). Quantitative analysis was undertaken using ImageJ software which revealed an approximately 25% increase in staining in the right eyes of these mice (Figure 5.5.8). A two way paired student's t-test performed on these data indicated that the data are just approaching statistical significance with a p-value of 0.052. These data suggest that the LHON model mice exhibit a slight but non negligible increase in potentially damaging retinal ROS at 14 days post-injection of rotenone. Although the retinopathy associated with LHON primarily occurs in cells of the GCL, the cells of the ganglion cells were not clearly visible after staining with DHE. It is possible that the introduction of rotenone has induced cell death in this layer in the two weeks between injection of rotenone and harvesting of the eyes. Nonetheless, DHE measurements were obtained from the ONL and INL as it is possible for superoxide molecules to be effluxed from the cell in which they were produced (Mumbengegwi et al, 2008).

5.3.3 Examination of changes in retinal superoxide levels in disease model mice injected with recombinant *Thioredoxin*

Transgenic mouse models of RP carrying either the P23H and hP347S mutations of human rhodopsin were sub-retinally injected with the Trx_AAV vector (the generation of which is discussed in section 4.3.4) and subsequently analysed using the DHE stain. It should be noted that all retinal sections examined were chosen based on the fluorescence of EGFP positive cells as these cells are positive for viral transduction and therefore the phenotype mediated by the delivery of either the *Rac1* shRNA or *Trx* cDNA will be most notable in these regions. However, treatment of the sections with DHE dissolved in DMSO had the effect of removing this EGFP signal for reasons not yet understood. Therefore the representative micrographs presented in the rest of this chapter have no overlay images of the retina taken using the EGFP filter of the microscope. All sections were viewed before treatment with DHE solution to select slides containing EGFP positive retinal cells.

DHE analysis was carried out with a set of experiments examining the effect of *Thioredoxin* overexpression in the P23H retina at P22. Three P23H mouse pups were sub-retinally injected with CMV_EGFP viral vector in the left eye and Trx_AAV viral vector in the right eye at P0 and these mice were sacrificed at P22. The final titre of each virus delivered to the retina was $7.9x10^8$vg in a volume of 0.8µl. The eyes were enucleated, sectioned and stained with DHE. The results of this experiment are presented in figures 5.5.9 and 5.5.10. It can be observed from figure 5.5.9 that there appears to be a large decrease in DHE staining observed in the right eye of all three injected mice. This reduction in staining was quantified using the ImageJ program, resulting in the data presented in figure 5.5.10. This bar chart reveals a small decrease of 13% in DHE staining intensity in the retinas which received Trx_AAV. However the large variance in DHE staining (likely due to n=3) of both sets of eyes resulted in a non-significant p-value of 0.55, calculated using a two way paired student's t-test.

The Trx_AAV 2/5 viral prep was also sub-retinally injected in to hP347S heterozygote mice of the same genotype which was used in chapters 3 and 4. However these mice were injected at P21 and therefore a larger volume of virus ($3x10^9$ vg in a volume of 3µl) could be administered by sub-retinal injection. Again, CMV_EGFP and Trx_AAV were sub-retinally injected to the left and right eyes

respectively of all hP347S mice injected. The first set of injected animals examined was sacrificed at 4 weeks post injection. The results of this experiment are presented in figures 5.5.11 and 5.5.12. A decrease in DHE staining intensity is discernible in only one of the three mice (panels C and D) in figure 5.5.11. Of the remaining two mice, one has a very small decrease in DHE staining intensity in the right eye (panels A and B) while no reduction in staining can be observed in the other mouse (panels E and F). Any changes between the left and right eyes were quantified and are presented as a bar chart in figure 5.5.12. From figure 5.5.12, a reduction of approximately 12% in DHE staining intensity in the right eyes was calculated from the ImageJ data. In a similar manner to the reduction in DHE staining in P23H mice however, this change in staining intensity failed to reach significance, with a paired student's t-test producing a p-value of 0.34.

Finally, the DHE staining intensity was examined in the left and right eyes of hP347S heterozygous transgenic mice 16 weeks post injection of $3x10^9$ vg of CMV_EGFP and Trx_AAV in the left and right eyes respectively. A total of three mice were injected at P21 and sacrificed 16 weeks later. The resulting sections of enucleated eyes were stained with 5μM DHE. Representative retinal micrographs of all three mice injected are presented in figure 5.5.13. Although the ONL is hardly visible due to apoptosis of the photoreceptors, a slight reduction in staining intensity is visible in the INL of all three right eyes. This reduction was quantified and the resulting data are presented as a bar chart in figure 5.5.14. A negligible reduction in DHE staining of approximately 3% was observed in the right eyes of the three injected mice. This small reduction in staining coupled with a large degree of variance, especially evident in the right eye, resulted in a non significant p-value of 0.74.

5.3.4 Examination of changes in superoxide levels of RP disease model mice injected with shRNAs targeting *Rac1*

The hP347S transgenic mouse model of adRP was used to evaluate any possible changes in DHE staining which may occur following sub-retinal delivery of pAAV_shRAC1_1 or pAAV_shRAC1_3. The first group of mice injected was a set

of three hP347S heterozygous transgenic mice with a sub-retinal injection of $1.08vgx10^9vg$ in a volume of 3µl of NT20 and pAAV_shRAC1_1 in the left and right eye respectively. The mice were injected at P21 and sacrificed 4 weeks later. The eyes were enucleated, sectioned to a thickness of 12µm and stained with 5µM DHE solution. Slides were examined by fluorescence microscopy and representative micrographs of the retinas from the left and right eyes of all three mice are presented in figure 5.5.15. This figure shows a reduction in DHE staining intensity in the right eye of all three mice injected. This reduction was formally quantified using the ImageJ program to produce a bar chart detailing the DHE staining intensity quantities of both the left and right eyes which is presented in figure 5.5.16. Although a clear reduction in staining intensity is observed in figure 5.5.15, quantification of this change in figure 5.5.16 revealed only a ~6% reduction in staining in the right eye. This change failed to reach significance with a two way paired student's t-test producing a p-value of 0.085.

A further four hP347S heterozygous mice were injected at P21 with NT20 and pAAV_shRAC1_1 in the left and right eye respectively. These mice were left for 16 weeks before sacrificing and harvesting of the eyes for sectioning and staining with DHE solution. Representative micrographs displaying the DHE staining intensity of each of the eyes from the four mice are presented in figure 5.5.17. This figure reveals a distinct reduction in staining in the right eyes of each of the four mice, however a greater degree of inter-animal variance is observed between the mice in this group than what has been observed in previous experiments. Quantification of the staining intensity of all eyes was undertaken using the ImageJ program and the resulting data are presented as a bar chart in figure 5.5.18. Quantitative analysis of the data produced by ImageJ showed that treatment with pAAV_shRAC1_1 reduced DHE staining by approximately 14% compared to the NT20 treated eye. However statistical analysis of these data produced a P-value of 0.087, resulting in non-significance for this change in staining between left and right eye.

The second virus containing a different *Rac1* specific shRNA (pAAV_shRAC1_3) was also utilised to examine any effects this may exert on the levels of retinal superoxide in the hP347S transgenic mouse. In the first set of experiments

examining the effect of this virus *in vivo*, a group of six hP347S heterozygous mice (age P21) were sub-retinally injected with $1.16x10^9$vg in a volume of 3µl of NT20 and pAAV_shRAC1_3 in the left and right respectively. These mice were sacrificed 4 weeks post injection and the eyes were harvested for DHE staining. Micrographs detailing the DHE staining of each eye are presented in figure 5.5.19. This figure suggests that treatment with pAAV_shRAC1_3 clearly reduces DHE staining intensity in all right eyes compared to the left eyes which received NT20. Formal quantification of this change in staining was undertaken using the ImageJ program to produce a bar chart presented in figure 5.5.20. The data produced by ImageJ indicate that DHE staining intensity in the right eye is approximately 34% lower than the control left eye. A two way paired student's t-test confirmed that this change is statistically significant, producing a p-value of 0.0046. DHE staining of three AAV_shRAC1_3 injected animals was also undertaken at 16 weeks post-injection. Representative micrographs of DHE stained retinas from this experiment are presented in figure 5.5.21. This figure displays a large variance in the intensity of DHE staining, with no clear indication of a reduction in staining in the right eyes of these mice. Formal quantification of the DHE staining intensity revealed no change in DHE staining intensity between the left and right eyes of these mice. A very slight increase in DHE staining was observed in the right eye although a paired student's t-test on the data produced by ImageJ resulted in a p-value of 0.97. A bar chart detailing the intensity quantities is presented in figure 5.5.22.

5.4 Discussion

In recent years the study of retinal degeneration has begun to focus, in part, on the role that oxidative stress plays in the pathology of many diseases of the retina including Age-Related Macular Degeneration, Diabetic Retinopathy and Retinitis Pigmentosa. Although increased oxidative damage has been documented in many disease model animals and patient post-mortem eyes (Nag et al, 2011), strategies aimed at saving eye sight in patients with antioxidants have failed to produce satisfactory results in patients of AMD (Age-Related Eye Disease Study 2 Research Group 2, 2013) with some success in patients of neovascular AMD (Chew et al, 2013). Supplementing the diet of RP patients with the anti-oxidant vitamin A has been shown to preserve central visual acuity and slow the rate of decline of ERG response in these patients (Berson et al, 2012; Berson et al, 1993). However the method of action of this supplement remains unclear as Vitamin A is also an essential precursor of the synthesis of retinal which is utilised by photoreceptors to detect light and the overall beneficial effect is small (Bates, 1995). Unlike conventional gene therapies which attempt to correct a pathological mutation of a well characterised gene, the *Rac1* and *Thioredoxin1* AAV based therapies were developed with the aim of reducing a specific metabolite (superoxide) in the retina. Therefore, any possible reduction in the production of superoxide should be characterised in mouse models treated with these therapies in order to understand any changes which these therapies may have on visual response. To study superoxide levels, dihydroethidium was utilised as a marker of superoxide in three different disease model mice present in the TCD Ocular Genetics laboratory in order to evaluate the state of oxidative stress in the retinas of these animals. DHE was then employed to measure any changes in superoxide in the retinas of RP disease model mice treated with virally delivered *Thioredoxin1* cDNA or *Rac1* shRNA.

The animal models chosen to evaluate retinal oxidative stress were the rotenone induced Leber's Hereditary Optic Neuropathy (LHON) mouse model and the rhodopsin mutant P23H and hP347S mouse models of autosomal dominant Retinitis Pigmentosa. The rotenone induced LHON mouse model was first described by Zhang et al who demonstrated that intravitreal injection of rotenone

significantly reduced the thickness of the GCL (Zhang et al, 2002). Rotenone is a complex I inhibitor which specifically binds to the ND1 subunit of mitochondrial complex 1, causing de-coupling of mitochondrial oxidative phosphorylation (Singer & Ramsay, 1994). The intravitreal injection of rotenone causes no changes in the thickness of the ONL or INL as the GCL is closer to the vitreous of the eye and is the most metabolically active cell layer of the retina, a property which contributes to GCL cell death in inherited LHON. Thus injection of rotenone closely mirrors the pathology of human LHON which can be caused by mutation of the *ND1* gene amongst other subunits. It has been suggested that oxidative stress plays a role in the pathology of LHON as primary cell lines carrying an LHON mutation show a 57% increase in oxidative stress (Park et al, 2007). Furthermore, this increase was dramatically reduced and cell viability increased when the cells were transfected with wild type yeast *NDI1*, suggesting that oxidative stress was the main effector of pathology in this mutant cell lines. Further confirmation of the role of oxidative stress in the pathology of LHON was provided by Lin et al who created a transgenic mouse model of LHON and demonstrated that increased oxidative stress and not depletion of cellular ATP caused cell death (Lin et al, 2012). Oxidative stress was assessed by measuring the rate of H_2O_2 production from the mitochondria using the commercially available Amplex Red reagent (Invitrogen). The fact that superoxide production is likely to arise from the GCL presents a problem for the experimental approach undertaken in the experiments detailed in this chapter as the outer and inner nuclear layers were examined for increased DHE staining. Superoxide is known to have low permeability across cell membranes as it is anionic (Lynch and Fridovich, 1978). However, it has been shown that superoxide can be effluxed from cells by a number of anion channels (Mumbengegwi et al, 2008). Furthermore, superoxide is readily converted to hydroperoxyl which can easily pass through cell membranes and cause oxidative damage in proximal cells to the site of superoxide production (Salvador et al, 2001).

Given the prominent role which overproduction of ROS plays in LHON, it was decided to stain the rotenone induced mouse model with DHE. This was first performed using DHE as a systemic stain *in vivo* using a protocol published by Behrens et al (2007). The resulting discomfort and death experienced by the injected animals immediately excluded this method of DHE staining from future

studies. Furthermore, no specific staining was observed using this stain *in vivo* (figure 5.5.2). The reasons for this adverse reaction to the DHE stain can only be speculated upon as no post mortem analysis was undertaken. DHE is most likely highly mutagenic based on its similarity in structure to Ethidium Bromide but this is unlikely to be the cause of death as much longer exposure would be required to cause death. No further information regarding the toxicity of DHE could be found. The best source of any data on the toxicity of this compound is available on the MSDS sheet (http://www.sigmaaldrich.com/MSDS/MSDS/DisplayMSDSPage.do?country=IE&language=en&productNumber=D7008&brand=SIAL&PageToGoToURL=http%3A%2F%2Fwww.sigmaaldrich.com%2Fcatalog%2Fproduct%2Fsial%2Fd7008%3Flang%3Den) which claims that no studies have been undertaken to examine the possible toxic effects of DHE, with some indication that DHE is non-carcionogenic. No adverse reaction was noted in the publication by Behrens et al from which this protocol was taken. The concentration of DHE delivered to these animals was also lower than what was used by Behrens et al who used two i.p. injections to deliver a total quantity of 27mg of DHE per kg of mouse weight. Based on the average weights of this strain of mouse at this age (18.18g for females and 21.72g for males; Jackson Laboratories), the injected mass of DHE previously published by Behrens et al would equate to 490.86-586.44µg, far higher than the 400µg delivered to the mice in experiments detailed in this chapter. Death may also have been caused by the 40µl of DMSO within the 400µl of total volume delivered to each mouse by i.p. injection. DMSO is known to be toxic to several organ systems including the kidneys and liver, both of which would have been in direct contact with the injected material (DMSO MSDS sheet: http://www.sciencelab.com/msds.php?msdsId=9927347). However the LD50 (lethal dose for 50% of animals injected) for mice by i.p. injection ranges from 267.25mg to 369.24mg based on the average weights of mice this age (DMSO toxicity sheet compiled by the Gaylord Chemical company; http://www.gaylordchemical.com/uploads/images/pdfs/literature/106B.pdf). This is far above the 44mg administration (based on the density of DMSO at 1.1g/ml) of DMSO which has been detailed here. Therefore the reasons for death and distress in these animals remain unclear.

To overcome the toxicity related problems associated with direct injection of the DHE stain, an alternative staining protocol requiring no *in vivo* staining was undertaken. This protocol was derived from a protocol utilised by Sasaki et al to measure retinal ROS in the streptozocin induced mouse model of diabetes and quantify this DHE staining intensity using the ImageJ program *ex vivo* (Sasaki et al, 2010). This staining protocol proved to require less time as no injection of the stain or fixing of the eyes were required. More importantly, however, the use of DHE as an *ex vivo* stain demonstrated an increase in retinal superoxide levels in the P23H and LHON mouse models of retinal degeneration (figures 5.5.6 and 5.5.8), suggesting its viability as a marker of oxidative stress given the evidence within the scientific literature regarding oxidative stress in these models (Tanito et al, 2006; Lin et al 2012). No evidence was found for an increase in DHE staining intensity in the one month old hP347S mouse model (figure 5.5.4). However only one time point was taken (at P28) and the visual degeneration of this model is known to occur much later than the P23H mouse model (Li et al, 1996; Chadderton et al, 2009). Therefore, any possible increases in oxidative stress which would be associated with photoreceptor cell death may not have manifested at this stage of retinal degeneration. Further time-points were not undertaken as the functionality of the DHE stain had already been attained in the P23H and LHON mouse models of retinal degeneration. In addition, the oxidative stress associated with the P347L mutation of rhodopsin has been studied in detail by Shen et al (2005) who used 4 different assays to measure the generation of ROS in a P347S transgenic pig. Therefore it was decided to make use of the hP347S mouse model of RP in studies examining the effect of *Rac1* suppression or over-expression of *Trx* in this mouse model of RP at later time-points. Searches of the scientific literature provide little information regarding the retinal oxidative stress levels of the P347S or P23H mouse models of RP, although oxidative stress is known to be increased in the retina of the P23H rat (Kaur et al, 2011). This finding has been confirmed in the current study using the DHE stain which demonstrated a two-fold increase in staining intensity as early as P5 compared to wild type mice at the same age and genetic background (figure 5.5.6). Previous findings by Lin et al demonstrating that oxidative stress is increased in the LHON transgenic mouse model have also been confirmed using the DHE stain, which demonstrated a 25% increase in retinal staining using the rotenone induced LHON model (figure 5.5.8). These findings

validated the use of DHE as a marker of oxidative stress *ex vivo* and allowed for further experiments detailing the pattern of oxidative stress in *Thioredoxin1* cDNA and *Rac1* shRNA treated eyes to be carried out.

The first construct to be tested for its potential effect on reduction of superoxide production in the retina was the Trx_AAV viral vector containing the *Thioredoxin1* coding sequence downstream of the CMV promoter. This construct was tested in both the P23H and hP347S mouse models whereas the *Rac1* shRNA viruses were tested only in the hP347S mouse models. The reasoning behind this decision lay with the mechanism of action of *Trx* which is a direct reducing agent of ROS and oxidised proteins as opposed to the indirect action of *Rac1* which is an activator of the NADPH Oxidase complex (see sections 3.1 and 4.1). Since the P23H mice have a rapid degeneration and a large load of retinal superoxide, it was deemed that the *Rac1* shRNA may be too slow to exert a physiological effect in these mice and so the shRNA constructs were initially tested only in the hP347S mouse model of RP. Analysis of the P23H mouse model was carried out at P22 after sub-retinal injection at P0. Any earlier time points were deemed irrelevant as the transduced virus takes up to 2 weeks to express CMV driven transgene cassettes within the AAV vector at approximately 40% efficiency (Sarra et al, 2002).

Analysis of P22 P23H mice treated with Trx_AAV revealed no statistically significant change in DHE staining between the left and right eyes (figure 5.5.10). Interestingly an increase in ONL thickness was observed in the treated eyes (figure 5.5.9); a result which was also obtained in figure 4.5.12 of chapter 4 which demonstrated increased thickness of the ONL in treated eyes compared to CMV_EGFP treated eyes. However this cannot be taken as further proof of therapeutic benefit as the DHE staining is carried out on unfixed sections and therefore the increased ONL thickness may be an artefact of sectioning. Treatment of hP347S transgenic mice with Trx_AAV also had no effect on DHE staining intensity at either 4 weeks (figure 5.5.11) or 16 weeks post injection (figure 5.5.13). A small decrease in staining was observed in the treated eye at 4 weeks post injection but this failed to reach statistical significance. The failure of Trx_AAV to reduce superoxide production is concomitant with the failure of this virus to

preserve ERG function at P22 in the P23H mouse and at similar time points in the hP347S mouse, results which were detailed in chapter 4.

The *Rac1* shRNA constructs (AAV_shRAC1_1 and AAV_shRAC1_3) were also tested to determine any possible effect they may have in DHE staining intensity in the hP347S mouse model. Unfortunately, no statistically significant changes were observed between AAV_shRAC1_1 and NT20 treated eyes (figures 5.5.16 and 5.5.18). However, slight decreases observed between the left and right eyes in these experiments approached statistical significance much more readily than experiments detailing the DHE staining changes using Trx_AAV. At 4 weeks post injection the p-values attached to the DHE staining changes of Trx_AAV and AAV_shRAC1_1 treated eyes were 0.34 and 0.085 respectively. A similar trend is observed at the 16 week time point with P-values for Trx and AAV_shRAC1_1 treated eyes of 0.74 and 0.087 respectively. The discrepancy in P-values between the two time-points cannot be explained by n numbers as the n number was three for all experiments except the 16 week post AAV_shRAC1_1 treatment (n=4). This change in p-values suggests that the experiments examining AAV_shRAC1_1 mediated change in DHE staining may require more animals to reach a statistically significant difference between treated and control eyes. A larger cohort of experimental animals should theoretically decrease the variance in DHE staining (which ranged from 10.3% (4 week, SH1 treated eye) to 18% (16 week, NT20 treated eye) of the total quantity) and therefore may validate the changes in DHE staining observed by decreasing the p-value to below 0.05. A significantly larger change in DHE staining between control and shRNA treated eyes may also result from injection at an earlier time-point. The injections detailed here were performed at P21, a stage when oxidative stress may have already accumulated to levels which would be unaffected by suppression of *Rac1* and in turn decreased activation of the NADPH Oxidase complex.

The largest change in DHE staining was obtained using the AAV_shRAC1_3 virus to treat hP347S mice. Examination of the DHE staining intensity in these mice at 4 weeks post injection demonstrated a statistically significant ~34% decrease in DHE staining of the treated eyes compared to NT20 treated eyes (figure 5.5.20). This decrease corresponds to an improvement in ERG b-wave responses at the same

time point using this virus to treat the same transgenic mouse strain (see figure 3.5.29). These data together suggest that a significant reduction in production of superoxide mediated oxidative stress may lead to an improvement in the visual response of these animals. Unfortunately no change in DHE staining was observed in AAV_shRAC1_3 treated retinas at 16 weeks post-injection (figure 5.5.22). A possible explanation for this lack of change may be a loss of absorption of oxygen from the choroid as the cells of the ONL have largely degenerated at this stage of the disease progression. Oxygen from the choroid is known to pass to the retina which is a tissue of lower oxygen partial pressure. In the RCS rat (a model of RP) it has been demonstrated that oxygen concentration in the ONL drops as the photoreceptors die but oxygen concentrations remain the same in other layers of the retina (Yu & Cringle, 2000). Therefore the generation of superoxide will also decrease as oxygen supply decreases. It was observed in figure 3.5.27 that while AAV_shRAC1_3 improves visual function and preserves photoreceptor viability, no overall thickness in ONL was evident in animals treated with this virus. Therefore the decrease in oxygen load at this stage of disease progression will be comparable in both eyes. The decrease in DHE staining at 4 weeks was most likely mediated by *Rac1* suppression induced inhibition of the NADPH oxidase (which is estimated to contribute to ~10% of cellular superoxide) at a stage in disease progression when oxygen load to the photoreceptors from the choroid had not decreased. At 16 weeks, *Rac1* suppression is likely having little effect on production of superoxide as there are less cells from which NADPH oxidase is active and the decrease in oxygen load has masked any small decrease in NADPH oxidase produced superoxide.

The discrepancy in phenotype observed between shRAC1_1 and shRAC1_3 treated animals has again become apparent in the experiments detailed in this chapter, as a difference in visual function was also observed in chapter 3. The possible reasons for this have been discussed in section 3.4. To gain a clearer picture of the relevance of the preliminary data detailed in this chapter, a two-three fold increase in the number of animals injected and examined would have to be undertaken. As DHE analysis had not been undertaken by any members of the TCD Ocular Genetics laboratory previously, it was difficult to anticipate the expected variance in DHE staining and therefore to adequately predict the statistical power of this

study. Furthermore, in all cases involving the use of animals for research, the "Three R's" principle has been applied throughout this thesis. This principle refers to Replacement, Reduction and Refinement an approach which aims to limit the total number of animals used for research purposes to a minimum. This ethical approach to animal testing is a requisite of any ethical approval of a study and is part of Irish law governing the use of animals in research. However, an indication has been provided of which of the three viruses reduces retinal ROS most effectively as measured by DHE staining. This chapter has shown that AAV_shRAC1_3 is an efficient effector of a reduction in retinal DHE staining in the hP347S mouse model of RP. AAV_shRAC1_1 has also been shown to reduce DHE staining but this reduction failed to reach statistical significance and the change in DHE staining was minimal. More animals would be required to examine if a change in n number would affect the p-value obtained in the current study. Therefore, any further experiments examining the effect of AAV mediated RNAi suppression of *Rac1* should concentrate efforts on AAV_shRAC1_3. Surprisingly, no reduction in DHE staining was observed in animals treated with Trx_AAV. This recombinant virus had been shown to drive strong expression of *Thioredoxin1* (see chapter 4) and therefore a decrease in DHE staining had been expected in mouse retinas treated with this preparation. There are a number of possible explanations as to why Trx_AAV failed to produce a satisfactory decrease in DHE staining. The first explanation is that over-expression of *Trx* may have caused increased stress in the cells of the retina and therefore resulted in no net decrease of ROS production. This would be caused by saturation of the endoplasmic reticulum which ensures that proteins are folded correctly before exiting. Saturation of this pathway induces the unfolded protein response (UPR) pathway and an increase in oxidative stress (Raden et al, 2005). Interestingly, an approach to treating the P23H model of RP has involved the introduction of BiP, a chaperone protein which enhances ER mediated folding of aberrant proteins, to the retina in order to increase folding of mutant rhodopsin and preventing UPR pathway activation (Gorbatyuk et al, 2010). However, the hypothesis of over-expression of Trx causing cellular toxicity was explored in the experiments detailed in chapter 4 and is not considered to be a contributory factor to the failure of Trx_AAV to produce a functional benefit in these disease model mice. A second possibility as to why Trx_AAV failed to reduce DHE staining is the fact that Thioredoxin1 protein is a general reducing

agent of other proteins and therefore will not directly interact with superoxide or react specifically with superoxide, unlike Rac1 which specifically produces superoxide through its interaction with other members of the NADPH oxidase complex. Therefore the DHE stain may not detect any Trx induced changes in ROS as it is a superoxide specific stain. However Trx1 is known to reduce excess cellular H_2O_2 which is a downstream product of superoxide and therefore a reduction in DHE staining would in principle be expected after treatment with Trx_AAV by shifting the cellular chemical equilibrium of superoxide and hydrogen peroxide (Nakamura et al, 2009). If this is indeed the case, then an antibody stain for 4-HNE would be a desirable assay as the formation of 4-HNE can be initiated by lipid peroxidation by ROS such as superoxide and hydroxyl free radicals or reactive nitrogen species (RNS) such as nitric oxide and peroxynitrite (Mattson, 2009).

The aims of this chapter were to validate the functionality of DHE as a stain of oxidative stress in a number of mouse models of retinal degeneration and to observe any changes in DHE staining which may arise as a result of treatment of transgenic mouse models of retinal degeneration with gene therapies aimed at reducing oxidative stress. DHE has been demonstrated to be an effective stain for oxidative stress in two of the three mouse models examined: the P23H mouse model of rhodopsin linked adRP and the rotenone induced mouse model of LHON. The DHE stain also confers a degree of indirect quantification of tissue superoxide levels which may be of use when attempting to link a vision loss phenotype with an increase in retinal oxidative stress. To our knowledge this is the first use of DHE to characterise superoxide production in these animal models. Furthermore, the DHE stain has been successfully used to characterise the effects of AAV 2/5 delivered *Thioredoxin1* cDNA and *Rac1* shRNA treatment of mouse models of adRP. The studies detailed in this chapter suggest that treatment of hP347S transgenic mice with AAV_shRAC1_3 results in a statistically significant decrease in retinal superoxide load at 4 weeks post injection, a result which closely mirrors the ERG results detailed in chapter 3. Given its reliability and ease of use, the DHE stain has proved to be a reliable marker of oxidative stress which in the future may be used in other studies of retinal degeneration in mouse models.

5.5 Figures

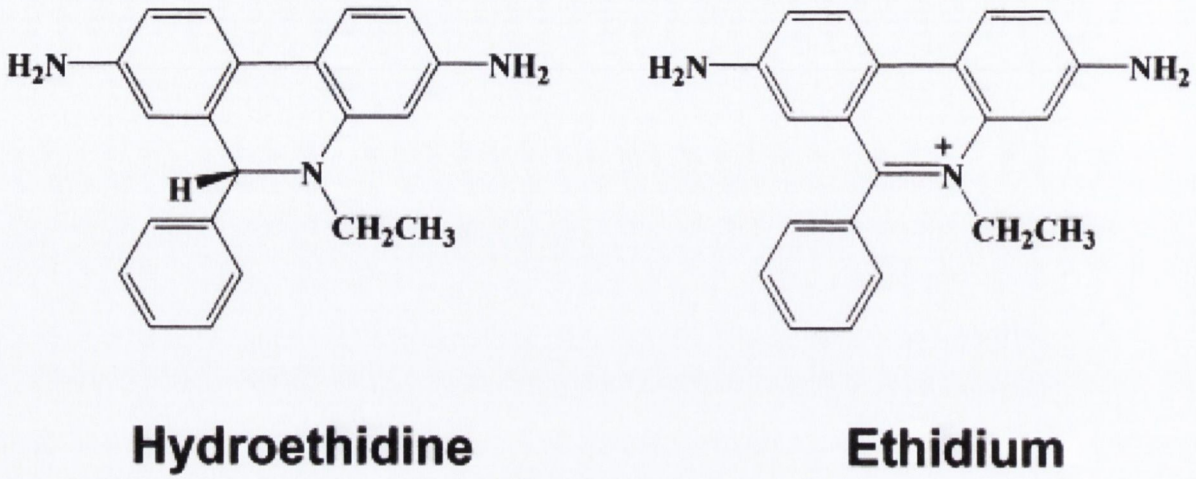

Figure 5.5.1: Molecular Structures of DHE and ethidium

The structure of DHE (labelled as hydroethidine) presented in this figure can be observed to have no net ionic charge and is therefore unable to bind to DNA. However upon oxidation, a specific hydrogen atom is chemically removed from DHE, resulting in cationic ethidium which can then bind to DNA and fluoresce. Figure adapted from Zhao et al, 2003.

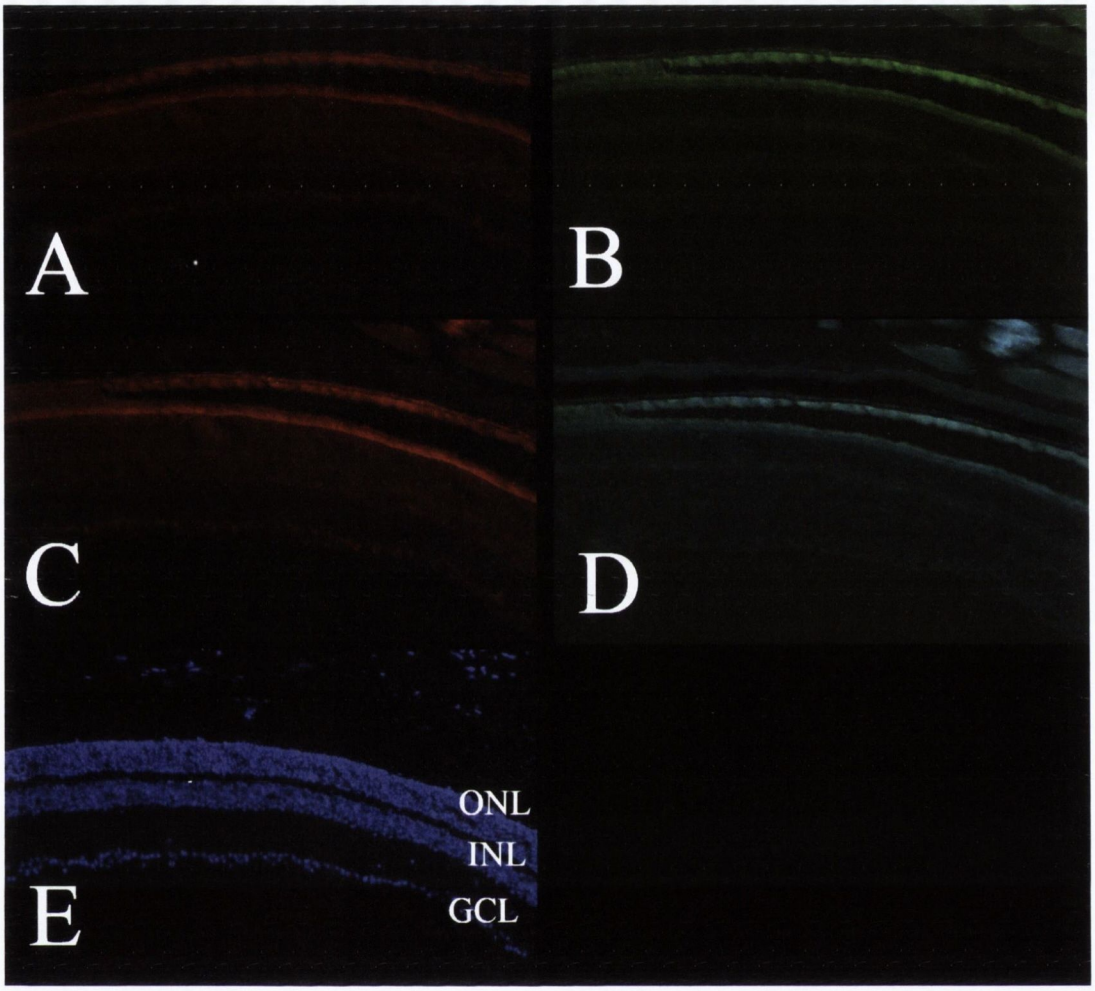

Figure 5.5.2: *In vivo* DHE staining of the retinas of Rotenone Injected Eyes

Four mice were intravitreally injected with 0.5µl 1.5mM rotenone in DMSO and were subsequently i.p. injected with a total of 400µl 1µg/µl DHE five months later, before harvesting of the eyes and sectioning. The DHE stain fluoresces at ~605nm and therefore should be observed using the '20' filter of the fluorescent microscope (panel A). However this staining pattern was uncharacteristically weak at a camera exposure of 200ms and the same staining pattern was observed using all filters (panels B-D) suggesting non-specific autofluorescence. Panel E shows the retinal structure of the eye by DAPI staining.

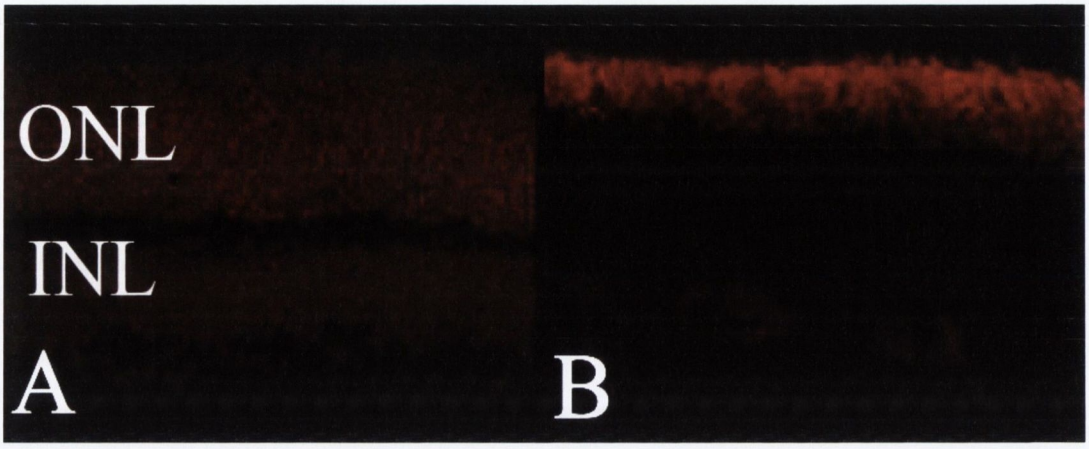

Figure 5.5.3: *Ex vivo* DHE staining of retinal sections of wild type and hP347S mice

Four mice were euthanised of both wildtype and hP347S transgenic strains of the same background at P28 and the eyes were enucleated, sectioned and stained with 5μM DHE dissolved in DMSO before micrographs were taken at 100ms exposure. Representative retinal images from the wildtype (panel A) and transgenic (panel B) mouse eyes are shown above. This shows little difference between the wild type and transgenic mice in DHE staining.

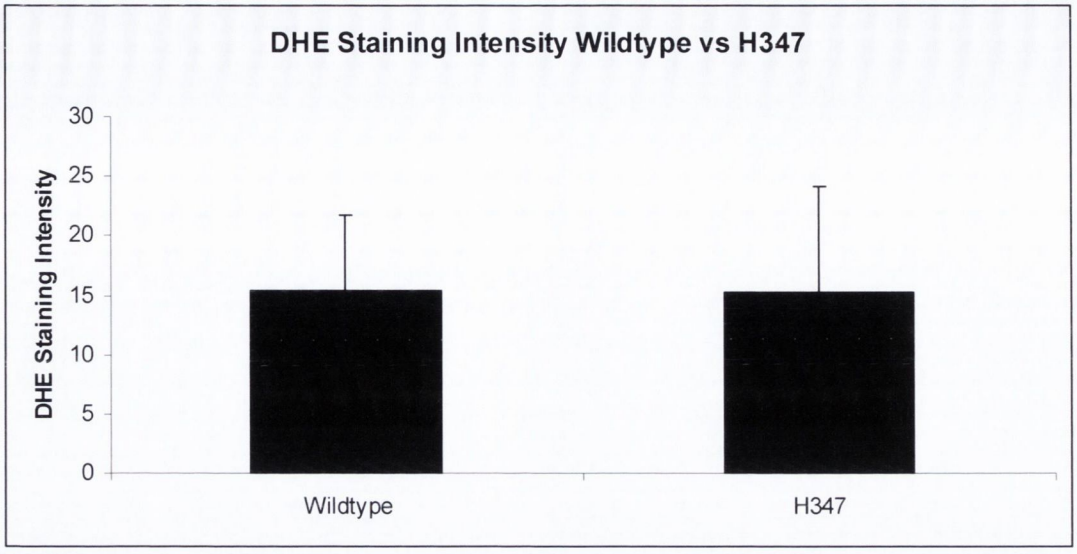

Figure 5.5.4: Quantification of DHE staining intensity of wild type and hP347 retinas (n=4)

Staining intensity was quantified using ImageJ software. Three slides mounted with retinal sections from each animal were examined by fluorescence microscopy and three micrographs were taken of different sections of each slide to give a total of 36 micrographs for each set of animals. Staining intensity of the ONL and INL was then recorded as an arbitrary unit for each micrograph and the average and standard deviation calculated for each group. This data was graphed as a bar chart showing the following data; Wild type average: 15.33±6.41, hP347: 15.30±8.86. An unpaired two way student's t-test resulted in a P value of 0.986.

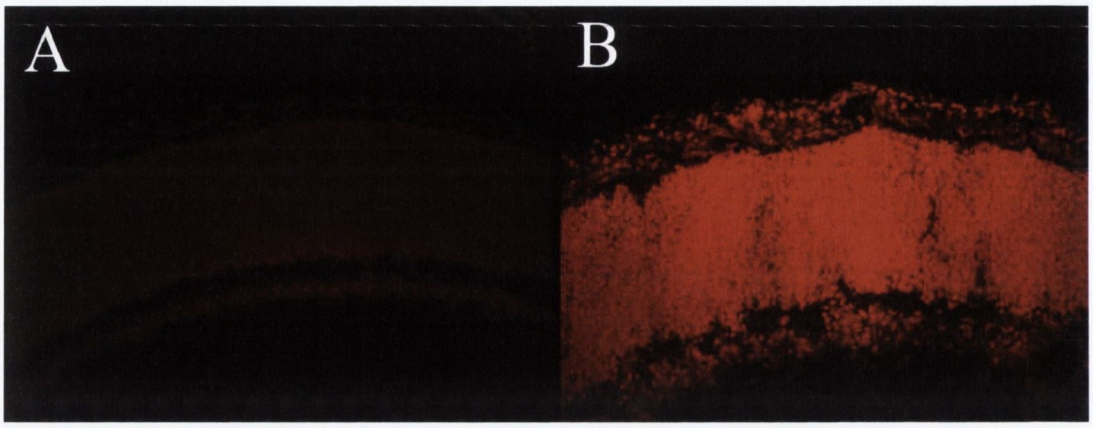

Figure 5.5.5: *Ex vivo* DHE staining of retinal sections of wild type and P23H mice

Three mice were euthanised from both wild type and P23H transgenic stocks of mice at P5. The eyes were enucleated and subsequently sectioned before staining with 5μM DHE dissolved in DMSO. All micrographs were taken at an exposure time of 100ms. Representative images are shown of wild type (panel A) and P23H (panel B) above. A large increase in DHE staining intensity in P23H animals is observed, suggesting high levels of superoxide in the retinas of these mice.

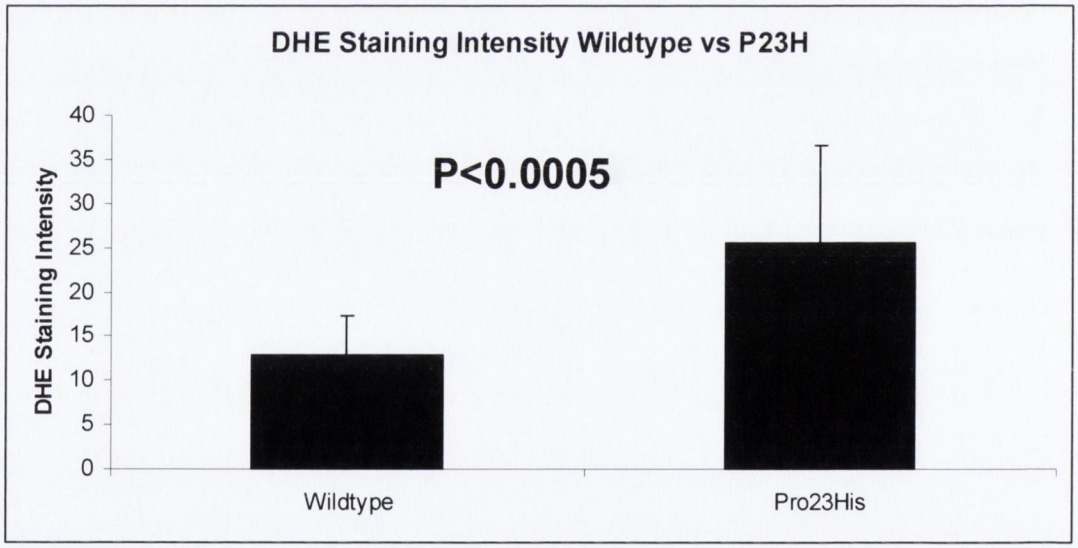

Figure 5.5.6: Quantification of DHE staining intensity of wild type and P23H retinas

Staining intensity was measured using the ImageJ software. A total of 18 images were taken for each group by fluorescence microscopy. The resulting data were averaged and a standard deviation was recorded for each group. The data graphed above show the following intensity values; Wild type: 12.78±4.579, Pro23His: 25.49±11.18. An unpaired two-way student's t-test resulted in a statistically significant P value of 0.00014.

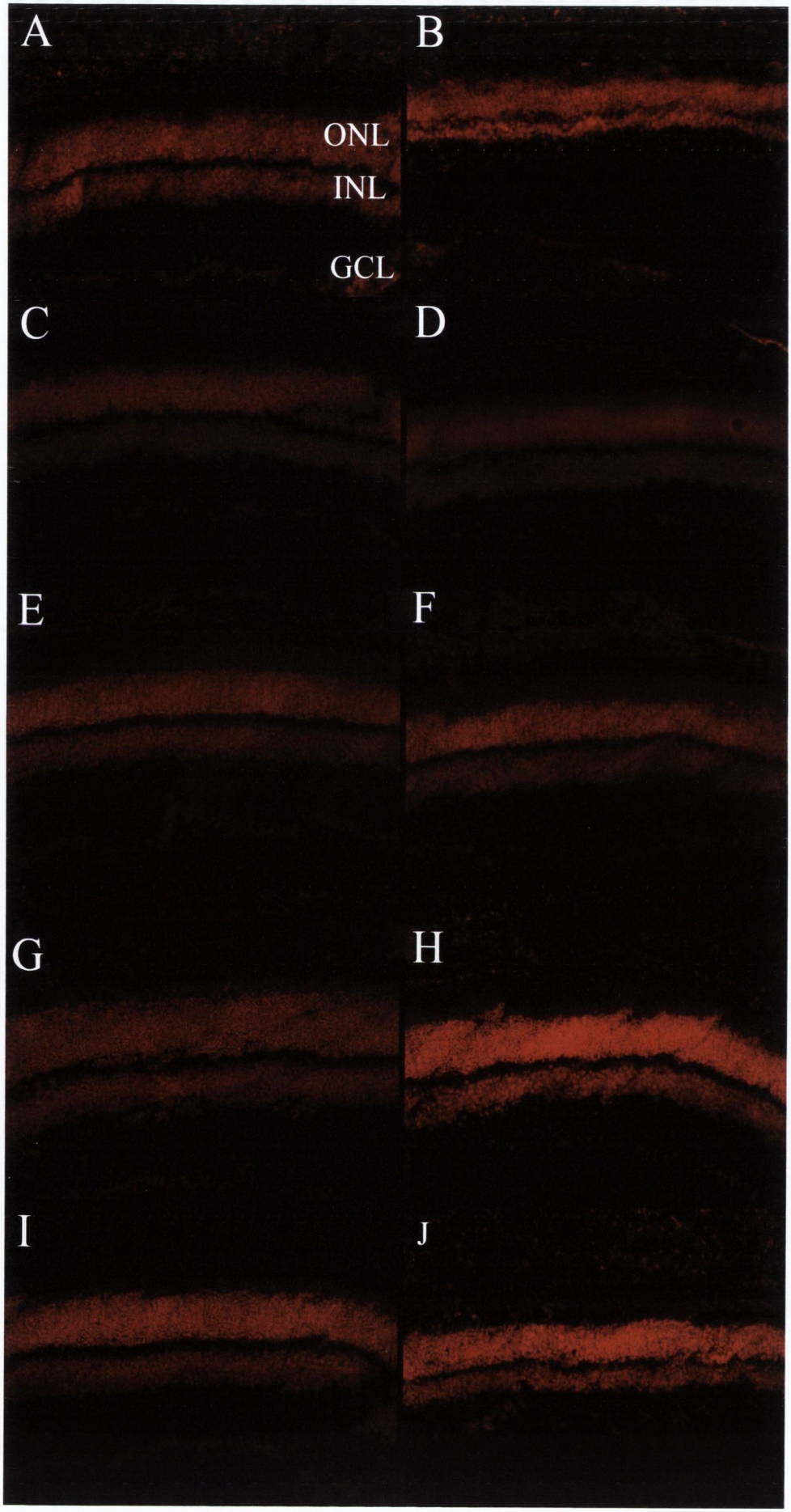
A
ONL
INL
GCL
B
C
D
E
F
G
H
I
J

Figure 5.5.7: *Ex vivo* DHE staining of retinal sections of LHON model mice

Five one month old wild type mice were intravitreally injected in the right eye with 0.5µl 12mM rotenone dissolved in DMSO which induces an LHON phenotype. The left eye was injected with the same volume of DMSO to act as a control. These mice were euthanised 14 days later and the eyes were enucleated, immediately frozen in OCT compound and sectioned before being stained with 5µM DHE. The resulting sections were examined by fluorescence microscopy at an exposure time of 100ms. Representative images from all five animals are shown above with panels A, C, E, G and I showing the left eyes and panels B, D, F, H and J showing the contralateral right eyes. A marginal increase in DHE staining was observed which is especially evident in panels H and J.

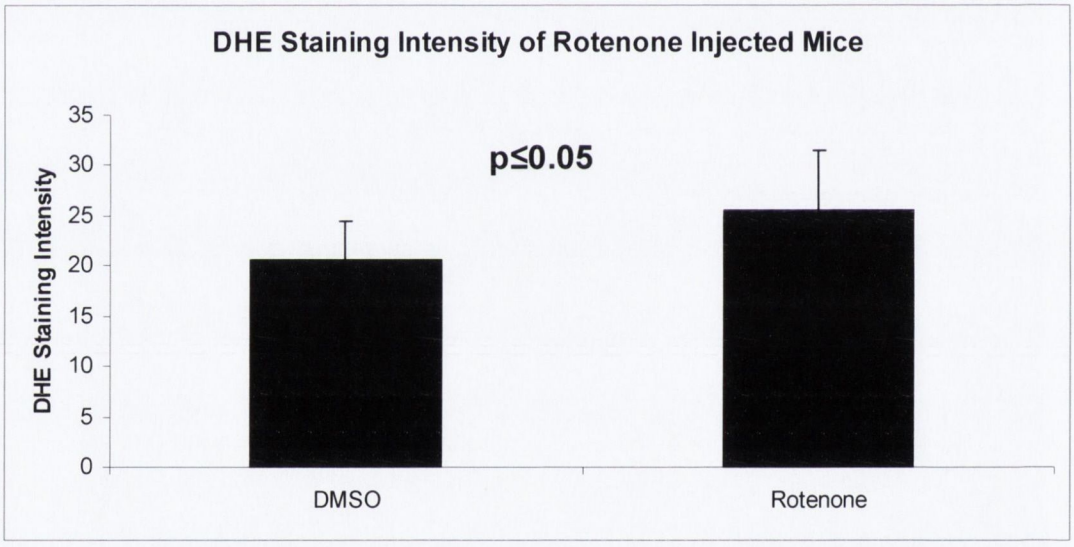

Figure 5.5.8: Quantification of DHE staining intensity of LHON mouse model retinas

Staining intensity of the rotenone and DMSO injected retinas were measured using ImageJ software. Two slides of each eye were taken and three fluorescent micrographs of each slide were taken to give a total of 30 images for each group. The DHE staining intensity of the ONL and INL was then measured in arbitrary units using the ImageJ program. The average and standard deviation were calculated for each group to give the following details; DMSO: 20.58 ±3.83, Rotenone: 25.45±5.95. Averages were also calculated for each individual retina. This allowed for a paired two way student's t-test to be calculated, resulting in a statistically significant P-value of 0.0516.

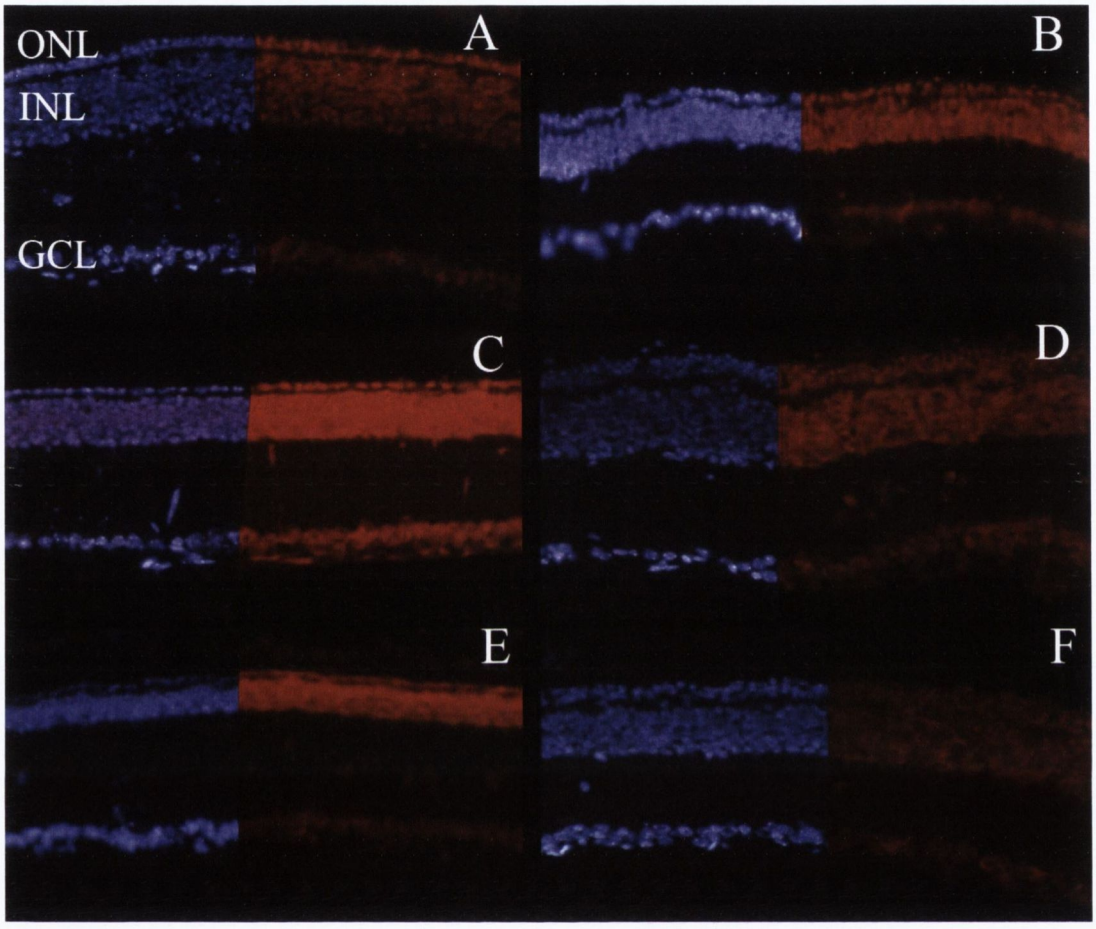

Figure 5.5.9: *Ex vivo* DHE staining of P22 P23H mice treated with Trx_AAV

Three P23H mice were sub-retinally injected at P0 with CMV_EGFP in the left eye and Trx_AAV in the right eye. These mice were euthanised at P22 and the eyes were enucleated, immediately frozen in OCT compound and sectioned. The sections were stained with 5μM DHE in DMSO and examined by fluorescence microscopy. Representative micrographs are shown above. Retinas from the left eyes are shown in panels A, C and E while the contralateral right eyes from the same animals are shown in panels B, D and F. A visible decrease in DHE staining is observed in the eyes which received thioredoxin compared to the control eyes.

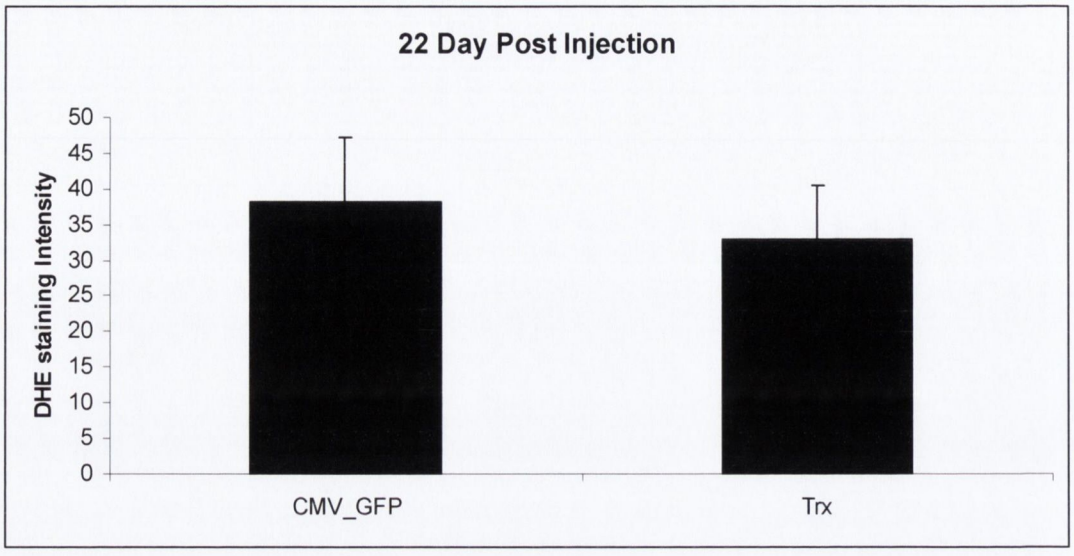

Figure 5.5.10: Quantification of DHE staining intensity of P23H mice treated with Trx_AAV

Three slides from each eye were examined by fluorescent microscopy and three images were taken from each slide to give a total of 27 images for each group. The images were analysed using ImageJ software to give DHE staining intensity quantities. These were averaged and a standard deviation was calculated for each group to give the following quantities which were graphed as a bar chart; CMV_EGFP: 38.08±9.18, Trx: 33.03±7.35. Average values for each retina were also calculated to allow a paired two way student's T-test to be calculated. This resulted in a P value of 0.55 which is non-significant.

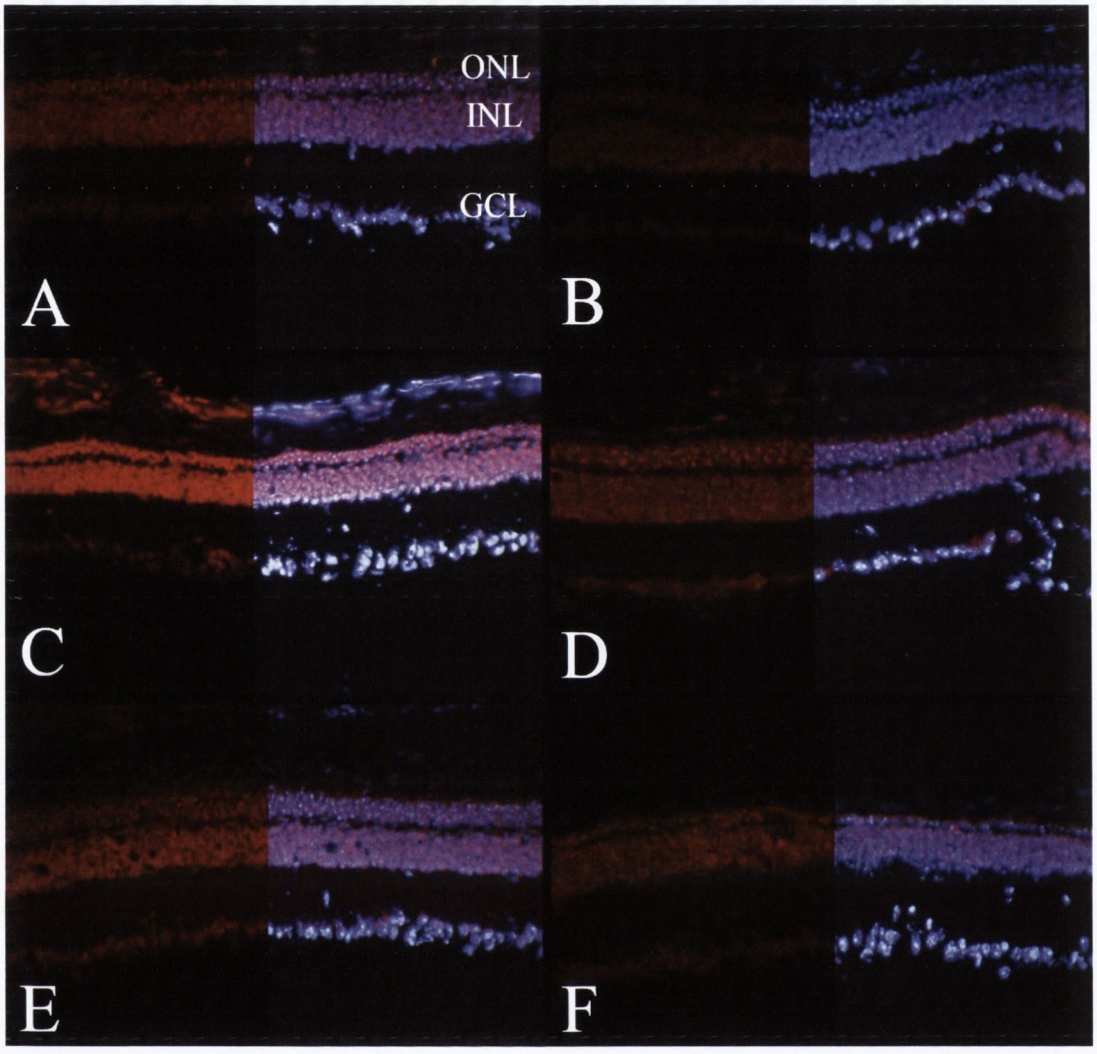

Figure 5.5.11: *Ex vivo* DHE staining of hP347S mice treated with Trx_AAV 4 week post injection

Three hP347S mice were sub-retinally injected at P21 with CMV_EGFP in the left eye and Trx_AAV in the right eye. The mice were euthanised 4 weeks post injection, the eyes were enucleated and immediately frozen in OCT before sectioning and staining with 5μM DHE. Representative micrographs are shown from the left (panels A, C and E) and right eyes (panels B, D and F) of each animal. A slight decrease in DHE staining intensity is observed in the right eyes of these animals, a pattern especially evident between panels C and D.

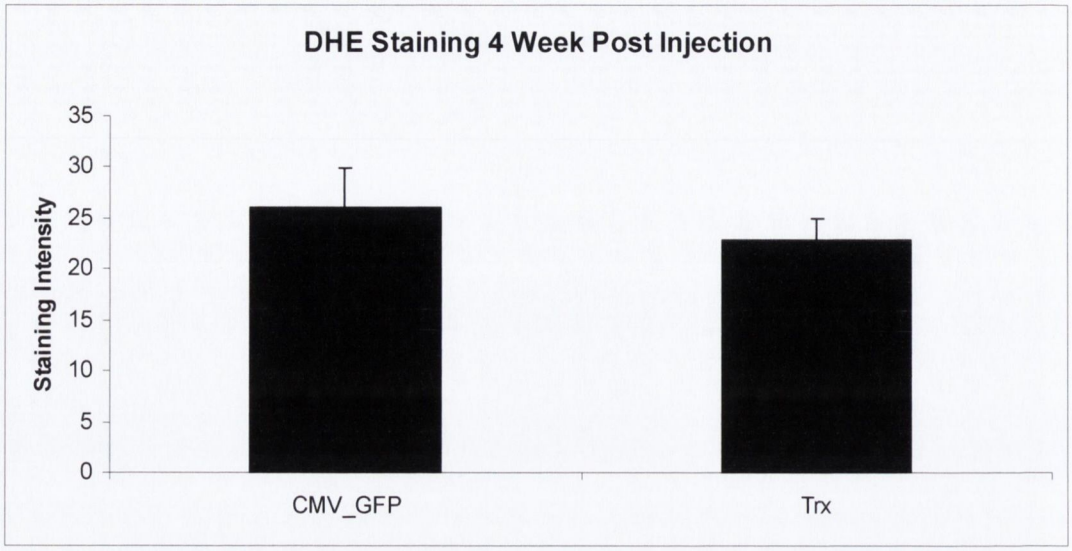

Figure 5.5.12: Quantification of DHE staining intensity of hP347S mice treated with Trx_AAV 4 week post injection

Three slides from each eye were examined by fluorescence microscopy and three images of each slide were taken to give a total of 27 images for each set of eyes. DHE staining values were assigned using the ImageJ software and these values were averaged and a standard deviation calculated for each group. This gave the following data which is graphed by bar chart above; CMV_EGFP: 25.97±3.96, Trx: 22.94±1.97. Average values for each individual eye were also recorded and used to calculate a P value of 0.34 by paired two way student's T-test.

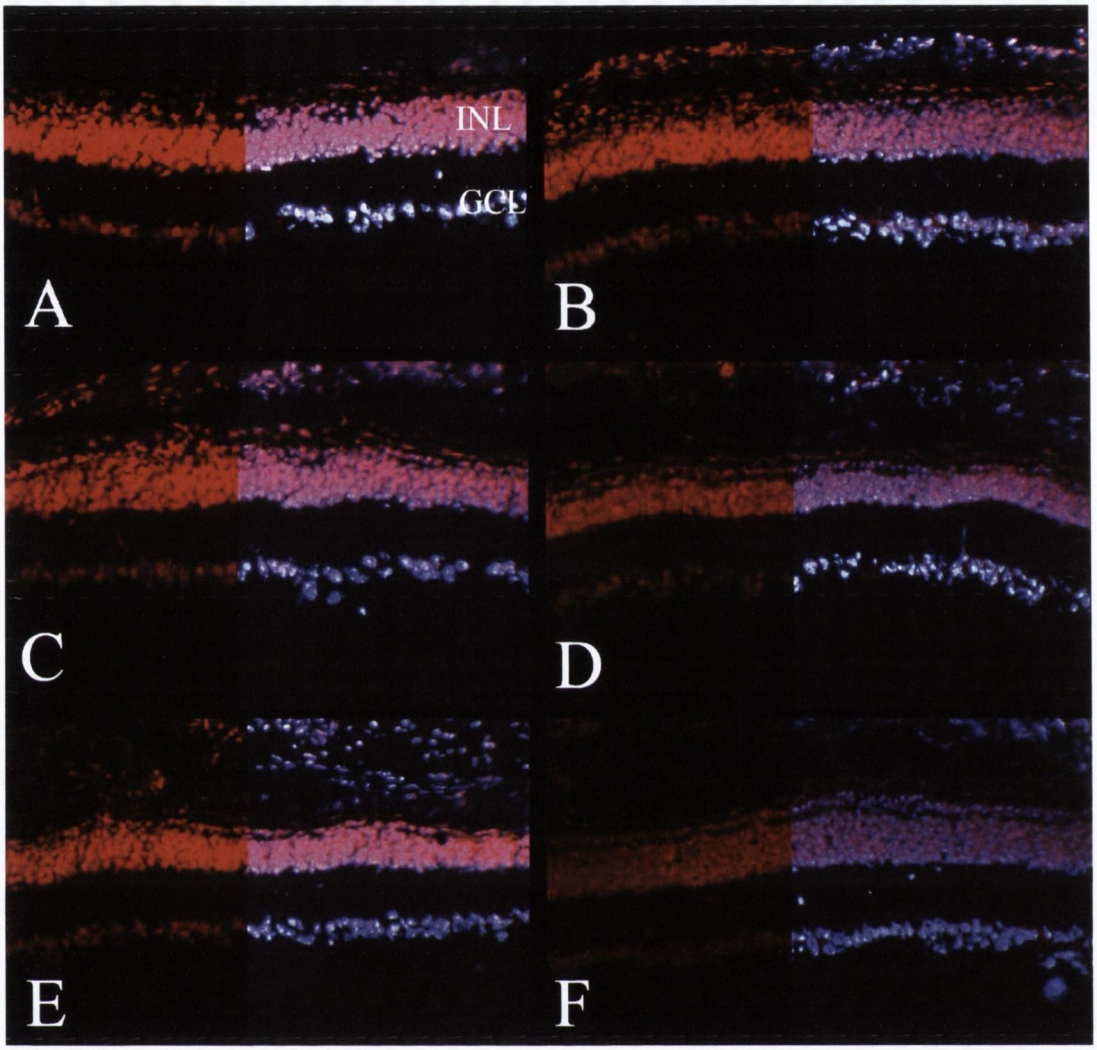

Figure 5.5.13: *Ex vivo* DHE staining of hP347S mice treated with Trx_AAV 16 week post injection

Three hP347S mice were injected sub-retinally with CMV_EGFP in the left eye and Trx_AAV in the right eye at P21 and were euthanised at 16 weeks post injection. The eyes were enucleated and placed directly in to OCT, sectioned and stained with 5μM DHE in DMSO. Representative micrographs are shown from the left eyes (panels A, C and E) and the contralateral right eyes (panels B, D and F) of these three mice. This shows a slight decrease in staining of the right eyes of these mice.

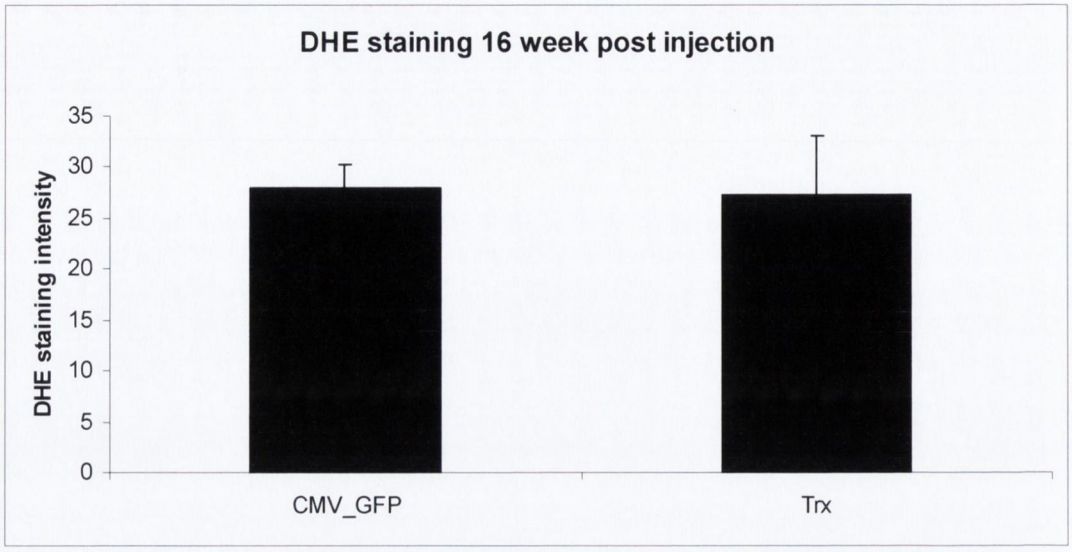

Figure 5.5.14: Quantification of DHE staining intensity of hP347S mice treated with Trx_AAV 16 week post injection

Three slides from each eye were examined and three images were taken of different sections from each slide to give a total of 27 images for each set of either left or right eyes. ImageJ software was used to assign DHE staining values of the ONL and INL of each eye based on pixel intensity and the average and standard deviation was calculated for each set of eyes. This data was graphed as a bar chart (above) to give the following pixel intensity quantities; CMV_EGFP: 28.04±2.16, Trx: 27.20±5.88. A paired two way student's T test performed on these quantities resulted in a P-value of 0.74 indicating no statistical significance in the slight decrease on DHE staining in the right eye.

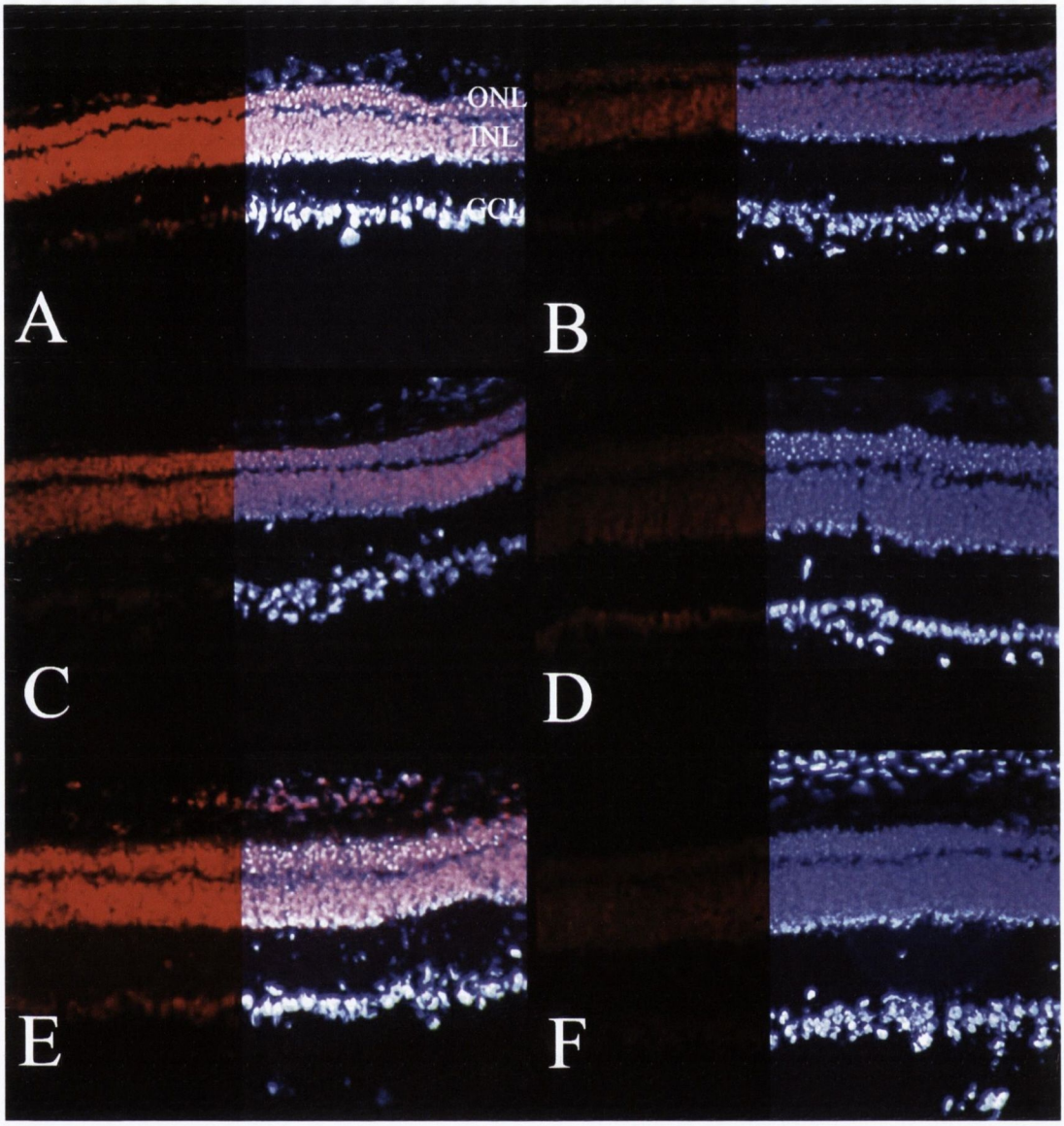

Figure 5.5.15: *Ex vivo* DHE staining of hP347S mice treated with AAV_shRAC1_1 4 week post injection

Three hP347S mice were sub-retinally injected with NT20 in the left eye and AAV_shRAC1_1 in the right eye at P21. These mice were subsequently euthanised 28 days post-injection; the eyes were enucleated, sectioned and stained with 5μM DHE. Representative micrographs are shown of the retinas of the left eye of each mouse (panels A, C and E) and the contralateral right eye of each mouse (panels B, D and F). A decrease in DHE staining is observed in the ONL and INL of the right eye of each mouse.

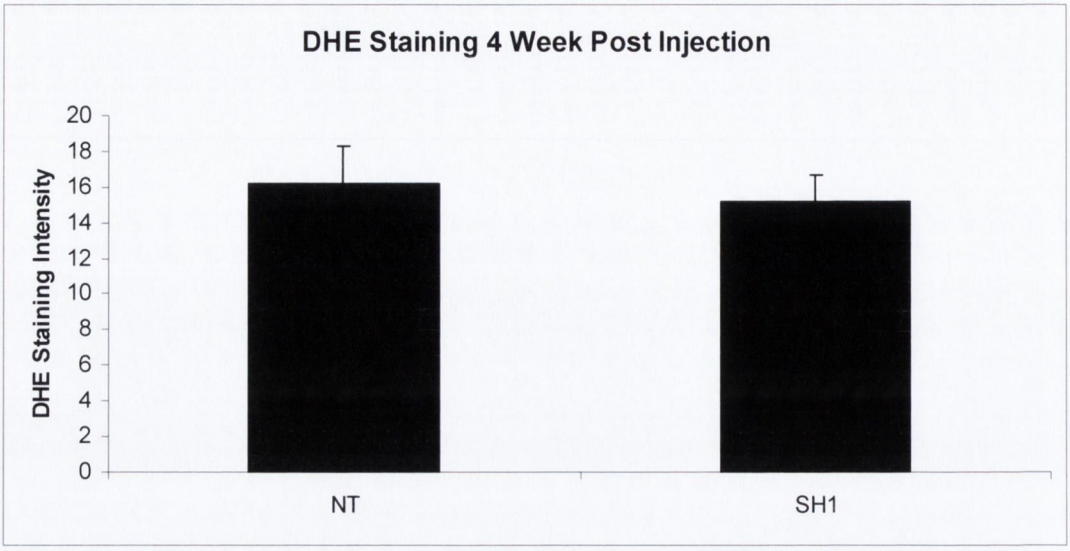

Figure 5.5.16: Quantification of DHE staining of hP347S mice treated with AAV_shRAC1_1 4 week post injection

Three slides of each eye were examined by fluorescence microscopy and three micrograph images were taken of each slide to give a total of 27 images for each set of eyes. These images were subsequently analysed for DHE staining intensity using the ImageJ software to assign quantities of pixel intensity to the ONL and INL of each image. The average and standard deviation was calculated for each set of data to give the following quantities which are graphed above; NT: 16.21±2.05, SH1: 15.17±1.56. This showed a slight decrease in DHE in the pAAV_shRAC1_1 treated eye but a paired two student's T test performed on the average values for each experimental eye failed to reach significance (P=0.085).

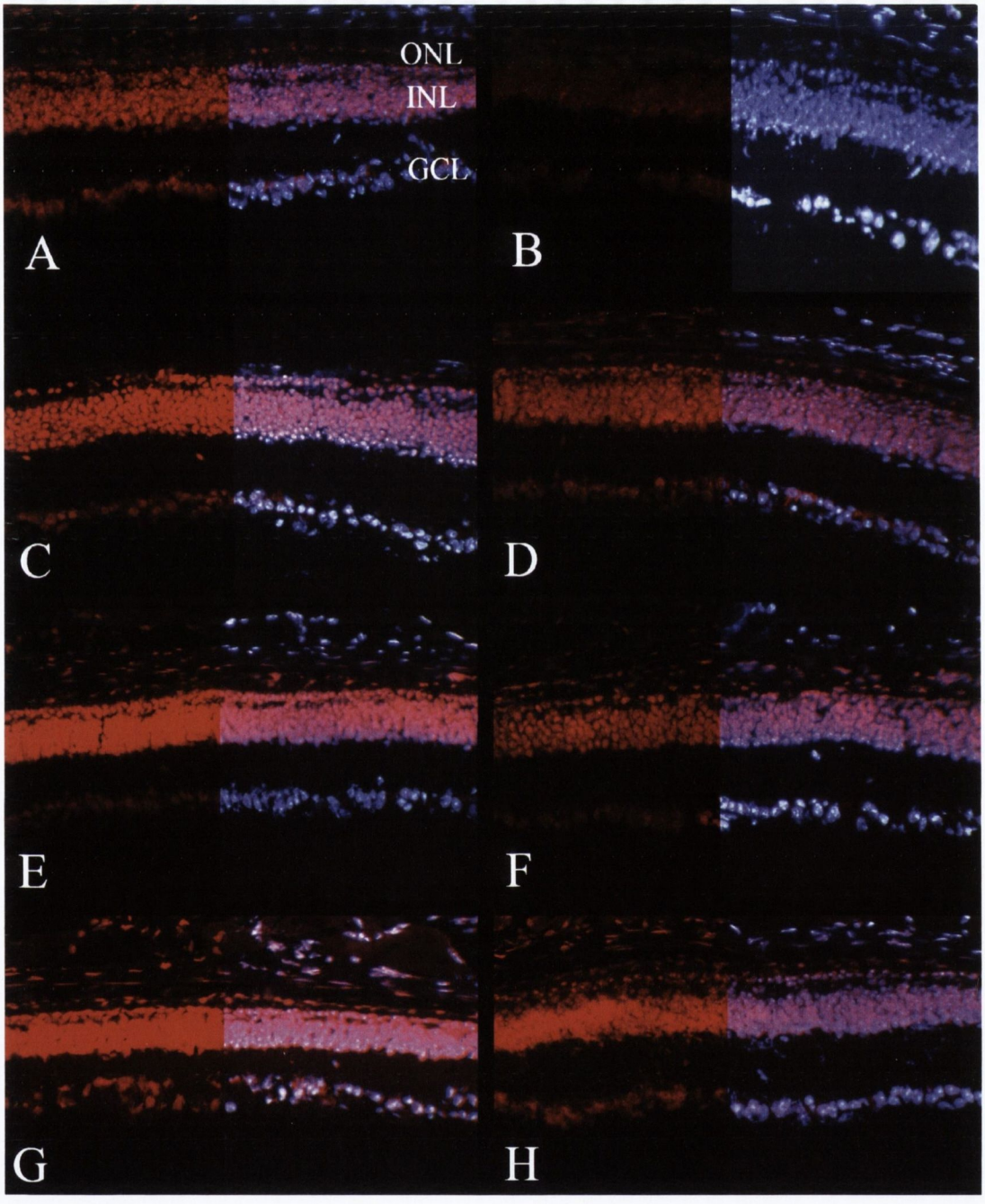

Figure 5.5.17: *Ex vivo* DHE staining of hP347S mice treated AAV_shRAC1_1 16 week post injection

Four hP347S were injected at P21 with AAV_shRAC1_1 in the right eye and NT20 in the left eye. Injected mice were sacrificed 16 weeks post injection, the eyes were enucleated, sectioned and stained with DHE solution. Representative retinal micrographs are shown of the left (panels A, C, E and G) and right (B, D, F and G) eyes of each of the four mice. A slight decrease in DHE staining can be observed in the right eye of all four mice.

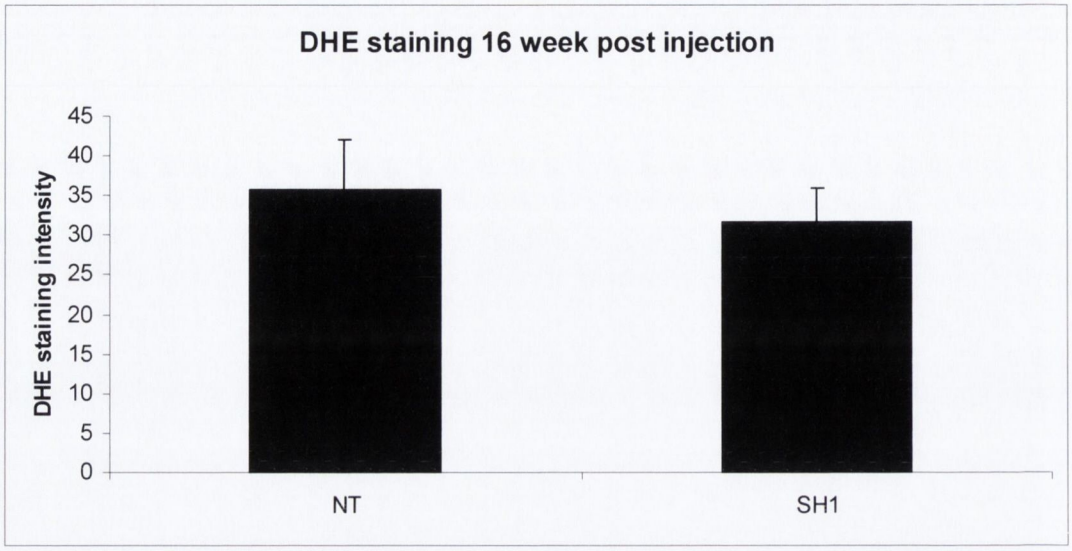

Figure 5.5.18: Quantification of DHE staining intensity of hP347S mice treated with AAV_shRAC1_1 16 week post injection

Two slides of each eye were examined by fluorescence microscopy and three images were taken of different sections from each slide. The DHE staining intensity of the ONL and INL was recorded for each image using the ImageJ program. These quantitative data were averaged and the standard deviation calculated for each set of eyes. The resulting data are graphed above using the following quantities; NT: 35.71±6.46, SH1: 30.82±4.09. This slight decrease in staining failed to reach significance with a two way paired student's T-test, producing a P-value of 0.087.

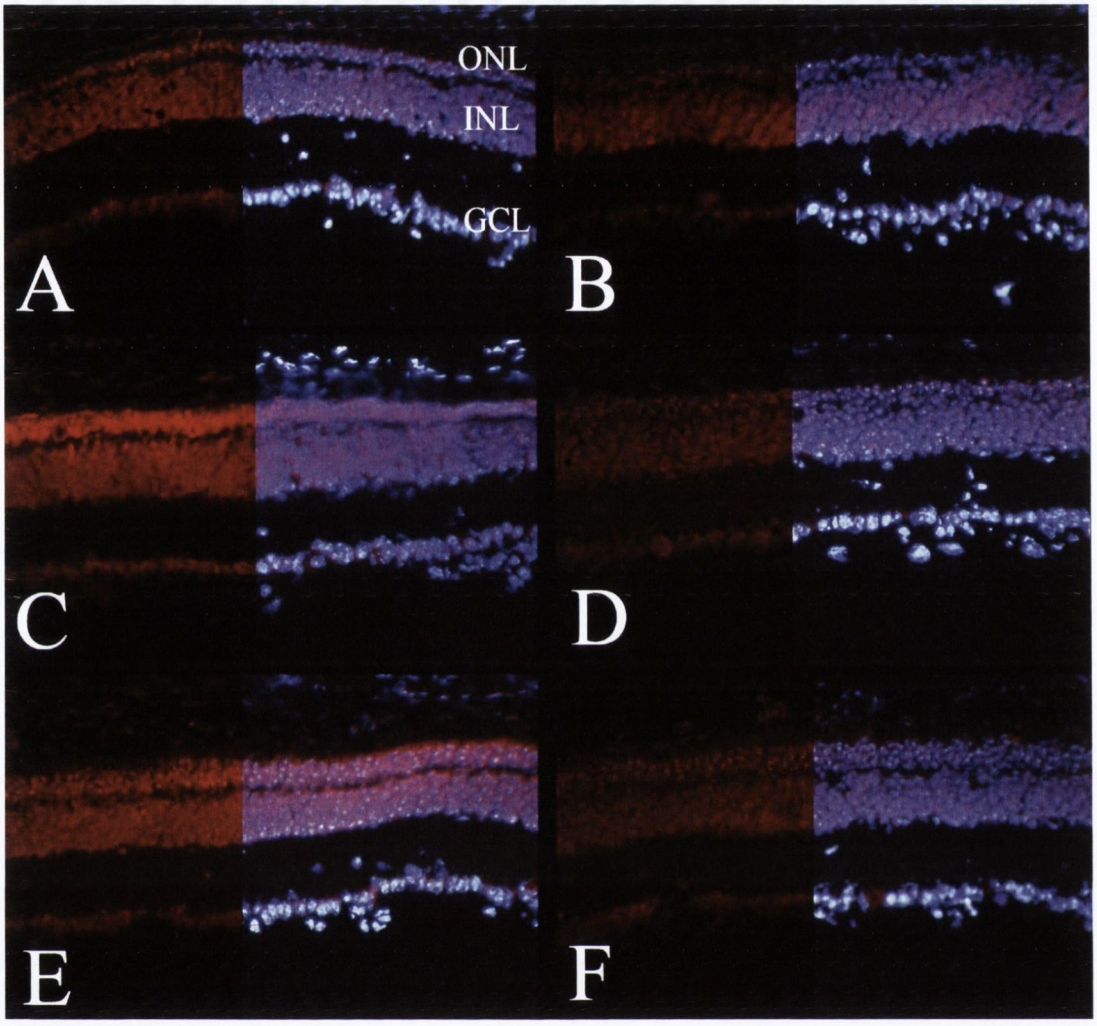

Figure 5.5.19: *Ex vivo* DHE staining of hP347S mice treated with AAV_shRAC1_3 4 week post injection (n=6)

Six hP347S mice were injected in the left eye with NT20 and in the right eye with AAV_shRAC1_3 at P21. These mice were euthanised 28 days post-injection, the eyes were enucleated and placed directly in OCT compound, sectioned and stained with 5μM DHE. Representative micrographs are shown of the retinas of the left eye of three of these mice (panels A, C and E) and the contralateral right eye (panels B, D and F). A clearly discernible decrease in DHE staining is observed in the right eyes of these mice.

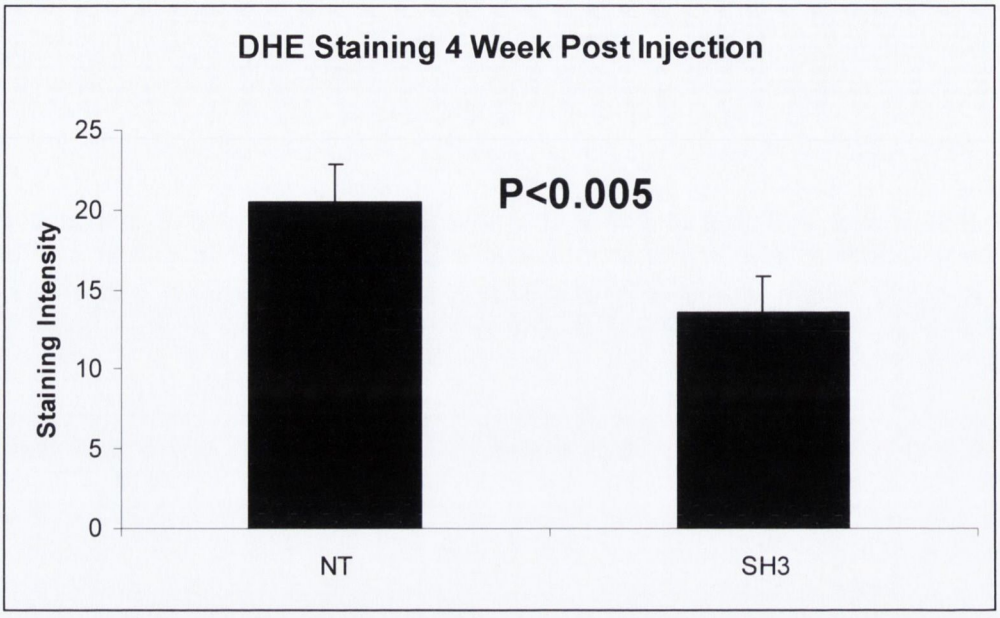

Figure 5.5.20: Quantification of DHE staining intensity of hP347S mice treated with AAV_shRAC1_3 4 week post injection (n=6)

Three slides of each eye were examined by fluorescence microscopy and three micrographs were taken from each slide to give a total of 27 images for each set of eyes. The pixel intensity of the ONL and INL regions of the micrographs was then analysed using the ImageJ program to assign quantities of intensity to each image. The average and standard deviation was calculated for each set of eyes and graphed as a bar chart (above) showing the following results; NT: 20.49±2.38, SH3: 13.58±2.20. A paired two student's T test performed on the average quantities of each eye resulted in a P value of 0.0046, indicating statistical significance.

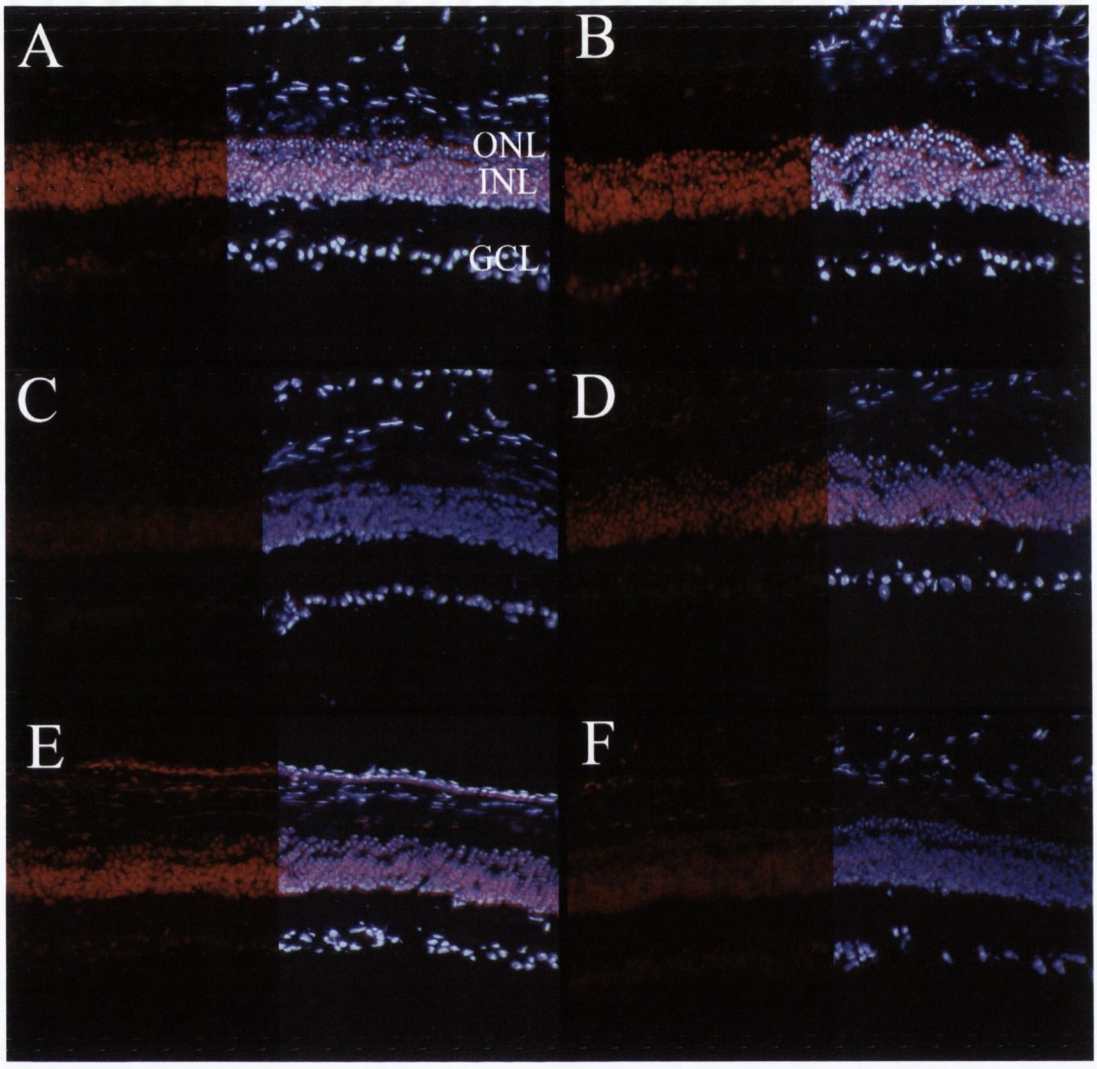

Figure 5.5.21: *Ex vivo* DHE staining of hP347S mice treated with AAV_shRAC1_3 16 week post injection

Three hP347S transgenic mice were sub-retinally injected at P21 with NT20 in the left eye and AAV_shRAC1_3 in the right eye. These mice were euthanised 16 weeks post-injection, the eyes were enucleated, sectioned and stained with DHE solution. Representative micrographs are presented showing the left eyes (panels A, C and E) and the corresponding right eyes (panels B, D and F) of each mouse. No pattern of reduction in DHE staining is observed across all three animals examined.

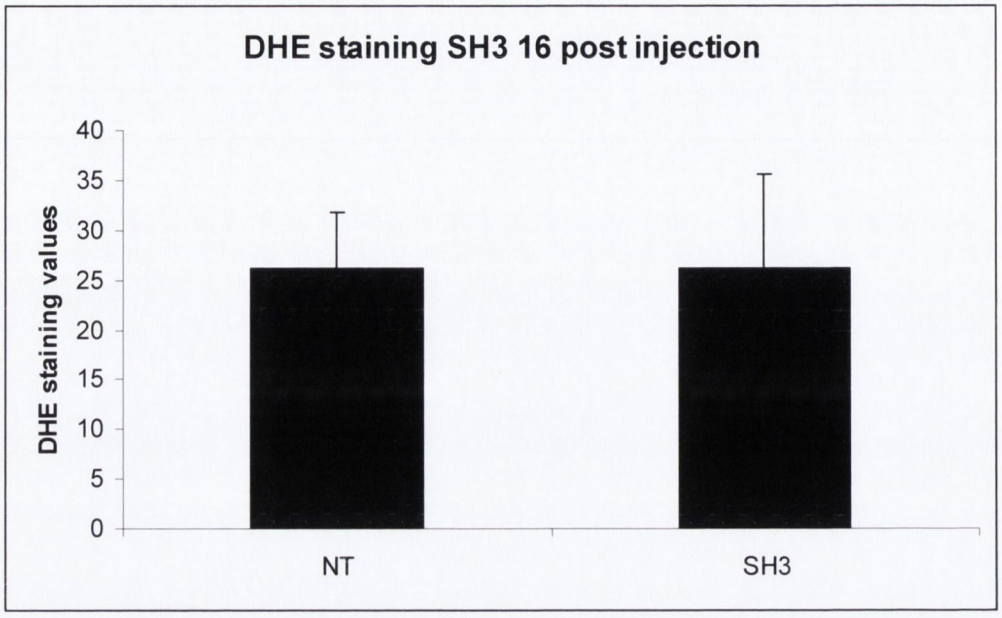

Figure 5.5.22: Quantification of DHE staining intensity of hP347S mice treated with AAV_shRAC1_3 16 week post injection

Three slides of each eye were examined by fluorescence microscopy and three micrographs were taken from each slide to give a total of 27 images for each set of eyes. The pixel intensity of the ONL and INL regions of the micrographs was then analysed using the ImageJ program to assign quantities of intensity to each image. The average and standard deviation was calculated for each set of eyes and graphed as a bar chart (above) showing the following results; NT: 26.10±5.63, SH3: 26.22±9.41. A paired two student's T test performed on the average quantities of each eye resulted in a P value of 0.975, indicating no statistical significant change in DHE staining intensity between the two sets of eyes.

Chapter 6: General Discussion

The severely debilitating effect of inherited retinal degeneration on the sufferers of these diseases has driven the international research community to focus much energy over many years to understanding the pathology of these disorders and to the exploration of a wide range of therapeutic approaches for such diseases. This sub-set of eye disorders includes many non-inherited disorders (such as Diabetic Retinopathy and Age-related Macular Degeneration) and inherited disorders (such as Retinitis Pigmentosa, Leber's Hereditary Optic Neuropathy and Leber Congenital Amaurosis) to name just a few. The range of therapies that have been pursued include gene therapy, pharmacological treatment and stem cell treatment (reviewed in McClements &MacLarem, 2013; Agosta et al, 2012 (for treatment of AMD) and Ramsden et al, 2013 respectively). Of particular note has been the recent successful pre-clinical integration of embryonic stem cell (ESC) derived photoreceptor cells in to several mouse models of retinal degeneration and the successful formation of synaptic connections from these transplanted cells (Gonzalez-Cordaro et al, 2013). The use of optogenetic approaches (discussed in section 1.13) for treating retinal disorders has also become a promising area of research (Jacobson et al, 2013). This type of therapeutic involves the introduction of light sensing molecules to the retina which cause hyperpolarisation of a cell, allowing these proteins to be expressed in layers of the retina other than the photoreceptors which may have degenerated past the point of use of conventional gene therapies. In addition to these molecular approaches to treating retinal disorders, much research has also been employed in the field of visual prostheses (Weiland et al, 2011). Retinal prostheses function by electrically stimulating areas of the degenerating retina in response to light. (Garg & Federman, 2013). For patients of RP, the ArgusII model of retinal prosthesis has been tested in detail. A clinical trial carried out in patients with end stage RP (ie completely blind) has demonstrated an ability to detect motion when these patients were epiretinally implanted with the ArgusII device on to the surface of the macular retina (Dorn et al, 2013). The authors noted that patients implanted with this device could detect the motion of a 1.4" moving bar on a 19" computer screen from 12" away. Furthermore, in most cases, the patients could also determine the direction of movement. In a separate study of the effect of this device in patients of RP, implantation allowed patients to correctly read large letters on a computer screen from 30cm away (daCruz et al, 2013). In addition, the ArgusII prosthesis allows

patients of RP to guide hand movements, as assessed by a patient's ability to trace a pathway through an image of a maze on a touchscreen (Barry et al, 2012).

The focus of the TCD Ocular Genetics laboratory has for many years been the inherited retinal disorder Retinitis Pigmentosa (RP). This laboratory initially explored the genetic basis of inherited RP by pedigree linkage analysis (Farrar et al, 1991; Farrar et al, 1990; Farrar et al, 1988) and subsequently created a rhodopsin knockout mouse model (Humphries et al, 1997). In recent years, the objectives of the laboratory have begun to concentrate on the use of suppression and replacement gene therapy in murine models of autosomal dominant RP (Palfi et al, 2012; Millington-Ward et al, 2011; Chadderton et al, 2009; O' Reilly et al, 2007). This use of RNAi mediated suppression and delivery of a genetic coding sequence has been utilised separately within this current study for two different genes; *Rac1* and *Thioredoxin1* in an attempt to slow the rate of degeneration in two mouse models of RP. The exploration of secondary gene therapies which aim to reduce the retinal burden of reactive oxygen species was borne out of a relatively recent interest in the potential role which oxidative stress plays in the pathology of retinopathy (reviewed in Doonan et al, 2012 and Wilkinson-Berka, 2013). In particular, the work of Peter Campochiaro's laboratory (amongst others) which has published many papers detailing the role which oxidative stress plays in retinal degeneration, including Retinitis Pigmentosa (Usui et al, 2011; Lee et al, 2011; Oveson et al, 2011; Usui et al, 2009 and Usui et al, 2009b). The choice of *Rac1* for targeted RNAi mediated suppression was made after the publication of two papers which demonstrated a functional benefit in RP mouse models after administration to the retina of apocynin, an inhibitor of the NADPH Oxidase complex (Usui et al, 2009), and partial knockout of *Rac1* in a conditional knockout (by engineering opsin promoter expressed Cre recombinase expression to restrict knockout to the rods) cross with a RP mouse model (Haruta et al, 2009). These papers demonstrated a beneficial effect to the cone and rod photoreceptors respectively; suggesting *Rac1*as an ideal target for AAV delivered RNAi mediated suppression, a molecular tool which has already been optimised and used routinely in the TCD Ocular Genetics laboratory. The use of delivery of the *Trx* coding sequence as a therapeutic was spurred by the discovery of the role that over-expression of this gene plays in the protection of photoreceptor cells in the *Tubby* mouse model of retinal degeneration (Kong et al,

2010) as well as the protective role that this gene plays in retinal ganglion cells (Caprioloi et al, 2009; Munemasa et al, 2010). Given that the TCD Ocular Genetics laboratory also has much experience in the AAV mediated delivery of a replacement gene, delivery of *Trx* also became a potentially viable therapeutic approach to explore in mouse models of RP.

The design of siRNAs and generation of shRNAs which target *Rac1* mRNA was explored in chapter 3 of the thesis. Initially three siRNAs were designed and tested *in vitro* using HeLa cells. These experiments provided evidence of suppression of approximately 75% of endogenous *Rac1* expression and approximately 50-70% of endogenous and exogenous CMV promoter driven *Rac1* expression (figures 3.5.11 & 3.5.14). Evidence was also provided of suppression of Rac1 protein using two siRNAs; RAC1_1 and RAC1_3 (figure 3.5.15). To create an expression vector which would produce RNAi agents which target *Rac1*, the RAC1_1 and RAC1_3 sequences were used to generate shRNA constructs which were subsequently cloned in to an AAV plasmid. This was performed by sub-cloning the shRNAs from the pSuper shRNA expression vector characterised by Brummelkamp et al (2002). The shRNAs were also tested *in vitro* to confirm that these new constructs were functional, resulting in suppression values of approximately 35% (figure 3.5.18). These data indicated that discernible suppression of *Rac1* in HeLa cells expression was achievable and allowed the study to continue from *in vitro* experiments to *in vivo* experiments.

Subsequent to the production of recombinant AAV 2/5 created using the pAAV_shRAC1 plasmid vectors and sub-retinal injection of these viruses in to wild type mice, a series of experiments were undertaken to evaluate *Rac1* expression after delivery of these *Rac1* shRNAs to the retina. These data provided conflicting reports of the efficacy of *Rac1* suppression. Notably, *Rac1* suppression of approximately 55-70% was evident at the mRNA level as evaluated by RT-qPCR (figures 3.5.22 & 3.5.23). However when confirmation of suppression was undertaken by western blot, it appeared that a second Rac1 specific band was appearing in the lanes loaded with retinal lysate from eyes which received *Rac1* shRNA. Although reduced levels of protein were observed at 21kDa (the size of

Rac1), a large band appeared at approximately 25kDa and was recognised by the Rac1 specific antibody (figure 3.5.24). The possible identity of this band has been discussed in section 3.5 yet the presence of this band has never been adequately explained. It is clear that the possible identities of this band are very wide-ranging given the integrated position of Rac1 within several signalling pathways.However, the remit of this study was to identify genetic components which would provide a functional benefit to the retina in mouse models of RP and therefore further studies pursued this goal rather than focusing on identification of this extra band. Should *Rac1* suppression be carried forward in to large animal models, the identity of the extra band must be elucidated. Li et al (2012) have also examined the use of *Rac1* shRNA in the retina using a lipid based delivery method to introduce *Rac1* specific shRNA in a pSuper vector to the retinas of rat models of choroidal neovascularisation. However no quantitative data were assessed *in vivo* while only RT-qPCR analysis was performed *in vitro*. Therefore a reasonable approach to identifying this extra band observed in this study may be to perform a microarray analysis to determine if the introduction of this shRNA is causing up-regulation of a related gene. If suppression of Rac1 is causing the remaining Rac1 to bind to another protein (such a RhoGDI) then purification of this complex by affinity chromatography using the same Rac1 antibody could aid in its identification. Mass spectrometry may then be used to identify this binding partner. Fluorescence microscopy using two separate Rac1 specific antibodies also failed to demonstrate a decrease of Rac1 expression in the retina. However this would be expected if these antibodies are detecting the extra band observed on the western blot. Of note, the extra band was observed in lysates from *in vivo* experiments only, reflecting the different transcriptomes of human derived cell cultures *in vitro* and mouse retinal cells *in vivo*.

Following the demonstration that AAV_shRAC1 mediated suppression is occurring in the retina, it was decided to introduce these viral preparations to the retina of the hP347S transgenic mouse model of RP via sub-retinal delivery. This transgenic mouse model has been used repeatedly by other members of the TCD Ocular Genetics laboratory in the past to assess the functional efficacy of pre-clinical gene therapies (Millington-Ward et al, 2011; Loscher et al, 2007; Chadderton et al, 2009) and by other laboratories worldwide (Brill et al, 2007, Bramall et al, 2013).

Delivery of the first shRNA virus, AAV_shRAC1_1, resulted in no preservation of cone cell density at 4 weeks post-injection (figure 3.5.28). Furthermore, this virus seemed to have a negative effect on visual function as assayed by electroretinography (figure 3.5.32). The second shRNA virus to be examined, AAV_shRAC1_3, also had no effect on cone cell density at 4 weeks post-injection (figure 3.5.29). However at 16 weeks post-injection, a clear increase of both rods and cones was observed in the retinas of treated eyes compared to non-targeting treated control eyes (figure 3.5.30). Furthermore, this beneficial effect was observed at the functional level as recorded by ERG. The discrepancy in outcome of the two shRNA viruses has been discussed in section 3.5; briefly it is believed that AAV_shRAC1_1 may have elicited a TLR mediated immune response due to the presence of immunostimulatory motifs on the siRNA sequence. Further work to characterise the expression change of interferons by RT-qPCR must be carried out to validate this hypothesis. However, the experimental work presented in chapter 3 has highlighted the potential beneficial effects of AAV_shRAC1_3 mediated *Rac1* suppression in the retina of the hP347S transgenic mouse model of RP.

In the present study, an alternative strategy to RNAi mediated suppression of Rac1 was employed in an attempt to reduce retinal oxidative stress, that is, the over-expression of *Thioredoxin1*. The effect of *Thioredoxin1* over-expression was examined in chapter 4. While a clear increase in *Trx* expression was observed both *in vitro* and *in vivo* (figures 4.5.6-10), this over-expression failed to produce any functional effect on visual function when delivered to the retina of either the P23H or hP347S mouse models of RP (figures 4.5.11-17). Some benefit was observed at a histological level in the P23H at P22 (figure 4.5.13), however this failed to reach statistical significance, most likely due to the small n number (n=3) as all animals examined demonstrated a clear increase in ONL thickness. Although no functional benefit was observed by ERG in the hP347S mouse model it was thought that Trx_AAV may provide a late stage beneficial effect akin to what was casually observed in the P23H mouse model. The P23H mouse model has previously been treated with a rhodopsin suppression and replacement AAV therapy which resulted in no functional benefit but a preservation of ONL thickness (O' Reilly et al, 2007). However no increase in ONL thickness or the preservation of cone cell density was observed in the hP347S mouse model at 4 or 16 weeks post injection of Trx_AAV

(figures 4.5.15 & 4.5.16). Initially it was thought that the over-expression of *Trx* in the retina may be having a detrimental effect on visual function which may have explained the lack of any positive data in the hP347S mouse model. To address this possibility, visual function was examined by ERG analysis in hP347S mice which received either a ½ or 1/10 dilution of Trx_AAV. Dilution of the virus had no effect on visual function in these mice (figures 5.5.18-20). These data suggest that the lack of functional benefit provided by over-expression of *Thioredoxin1* was dose independent and instead is a result of a lack of functional benefit exerted by the function of the protein itself. Furthermore, analysis of wild type animals which received a range of Trx_AAV dilutions from ½ to 1/1000 provided no difference in visual function compared to CMV_EGFP injected contralateral eyes (figure 4.5.21). These data indicate that although Trx has a well documented role as an antioxidant protein with a beneficial effect in other models of retinal degeneration (Kong et al, 2010; Munemasa et al, 2010; Caprioli et al, 2010) delivery of this gene to the retina provides no beneficial effect in two mouse models of RP.

In order to assess the biochemical effect of introduction of either *Rac1* targeting shRNA or *Trx* cDNA, the effect that introduction of these constructs to the retina on the generation of superoxide molecules was determined through the use of the DHE stain. In addition, the DHE stain was employed to assess the levels of retinal superoxide in three models of retinal degeneration compared to wild type mice of the same age and genetic background. These models emulate the disease phenotype of Leber's Hereditary Optic Neuropathy (LHON), Rho P23H mutation induced adRP and Rho P347S induced adRP. These analyses demonstrated an increase in DHE staining in the LHON and P23H models of retinal degeneration (figures 5.5.6 and 5.5.8). No increase was observed in the P347S model, however only one relatively early time-point of this mouse model was examined (figure 5.5.4). Of all three constructs examined, only one (AAV_shRAC1_3) produced a statistically significant decrease in staining, of approximately 34% at 4 weeks post injection (figure 5.5.20). This decrease in staining was initially observed in a set of only three animals, producing a p-value of less than 0.05 and a reduction of 37%. The n number was subsequently increased to six by examining three different mice of the same genotype and treated with AAV_shRAC1_3 resulting in a similar reduction (34%) to what had been observed previously and a reduced p-value of less than

0.005, strongly indicating that suppression of *Rac1* with this construct is reducing the superoxide output of the NADPH Oxidase complex. Furthermore, the decrease in DHE staining coincides with an increase of ERG b-wave response at 4 weeks (figure 3.5.33). However the reduction of DHE staining was not maintained at 16 weeks post injection (figure 5.5.22). These data suggest that suppression of *Rac1* using AAV_shRAC1_3 is reducing the levels of ROS within the retina and that this reduction may be preserving visual function and the longevity of both rods and cones at later time-points. The lack of a decrease in DHE staining at 16 weeks post injection is likely the result of a NADPH oxidase independent production of ROS which has dwarfed any decreases that may be a result of suppression of *Rac1*. Although suppression of *Rac1* seems only to have had a transient effect on the levels of superoxide, this initial decrease seems to have preserved functional photoreceptors up to 16 weeks post-injection as examined by ERG analysis and immunohistochemistry.

As mentioned previously, a number of hurdles would have to be overcome for the AAV_shRAC1_3 construct to ever proceed in to large animal models, non human primates or indeed humans. Firstly, the discrepancy in phenotype between the two *Rac1* suppressors has highlighted the need for an examination of both the immunostimulatory effects of these shRNAs and the possible off target effects which these shRNAs may produce. The siRNA mediated stimulation of the immune response by a TLR was first shown to occur through Toll Like Receptor 3 (TLR3) (Kariko et al, 2004). Stimulation of the innate immune response by siRNAs has shown to be sequence independent when recognised by TLR3 but the main stimulation occurs through the recognition of UGU sequence motifs in RNAs by TLR7 and TLR8 resulting in a production of pro-inflammatory cytokines and interferon α (IFNα), (Jackson & Linsey, 2010). Although these studies have focused on the siRNA mediated immunostimulation, it must be remembered that shRNAs are processed to siRNAs in the cell. Furthermore, shRNA has been shown to be equally immunostimulatory when compared to an siRNA containing the same 19 nucleotide target sequence (Hornung et al, 2005), suggesting that shRNA mediated toxicity occurs through the same TLR mediated immunostimulation pathway as siRNAs. Therefore the ability of both AAV_shRAC1_1 and AAV_shRAC1_3 to induce the up-regulation of these factors should be addressed

in the future as inflammation of retinal tissue would be detrimental to the normal functioning of this tissue (Kleinman et al, 2012). For this, RT-qPCR analysis and enzyme linked immunosorbent assay (ELISA) may be employed to determine the increase in these factors in the retina following delivery of these shRNAs. Determination of the increase in such factors may not be possible by a blood test as Judge & MacLachlan (2008) have shown that many of these effects are local and cannot be detected in the blood. Off target effects can occur through the saturation of the RNAi pathway or by targeting of siRNAs to 3' UTR sequences through the seed region of the siRNA. This phenomenon was first demonstrated by Jackson et al who used microarray analysis to demonstrate a large swathe of genes whose regulation was inadvertedly affected by RNAi mediated suppression (Jackson et al, 2003). Saturation of the RNAi pathway occurs when the concentration of siRNA in the cell is at a high dose and interferes with the normal miRNA machinery of the cell. This saturation primarily occurs to the Argonaute protein, a key part of the RISC, although Exportin-5 is believed to play a role in saturation as well (Grimm et al, 2010). Addressing the problem of saturation is an important factor when deciding on the promoter of the RNAi vector delivered to the tissue of choice, a reason why miRNA mimics are now more widely used in pre-clinical studies as they are longer than shRNAs and are therefore amenable to expression from a larger range of promoters (Boudreau et al, 2009). In addition, miRNA mimics are more closely related to endogenous miRNAs and therefore exert less processing related toxicity. The degree of miRNA like off-targeting (off targeting caused by binding to the 3' UTR of transcripts) is more difficult to address as this would involve changing the sequence of the shRNA itself and therefore changing the possible efficacy of the RNAi agent. However, it is imperative that a shRNA which is brought forward for pre-clinical trials in large animal models is examined for these off target effects. It has already been observed by western blot that suppression of Rac1 induced over-expression of an unknown protein in the retina (figure 3.5.24) although this is likely not due to miRNA like off target effects as it occurred when retinas treated with either AAV_shRAC1_1 or AAV_shRAC1_3. Again, the use of microarray profiling would be of great use in examining this type of off target effect. In order to address these issues, the use of a miRNA vector to deliver a *Rac1* targeted RNAi agent to the retina may be a useful next step to be undertaken in the exploration of *Rac1* suppression and its potentially beneficial role

within the retina. miRNA vectors have already been used in this fashion to treat a wide variety of disorders in a pre-clinical setting including Huntington's disease (Fiszer et al, 2012), spinal and bulbar muscular atrophy (Miyazaki et al, 2012) and leukaemia (Kaser et al, 2012). Furthermore, AAV mediated delivery of targeted miRNA constructs to the retina has been used in several pre-clinical settings *in vivo* (Pihlmann et al, 2012; Georgiadis et al, 2010).

A second consideration which must be addressed should any RNAi based therapy be brought forward to a clinical setting is the use of AAV to deliver this agent to the retina. Although discernible suppression of *Rac1* was observed with both shRNAs tested, the efficacy of these molecules *in vivo* is less than what has previously been achieved by the TCD Ocular Genetics laboratory using shRNA based vectors targeted against Rhodopsin (Millington-Ward et al, 2011). Recently, the use of AAV 2/8 has been proposed as a more potent AAV serotype due to its increased range of transduction of layers of the retina and higher rate of transduction of the photoreceptors (Natkunarajah et al, 2008). A higher efficacy of transduction has also been observed by the TCD Ocular Genetics laboratory (unpublished results). More recently this serotype of AAV was used in the delivery of a shRNA to the retina to treat a murine model of inherited rod cone dystrophy (Jiang et al, 2013). A comparison of the efficacy of AAV 2/5 and AAV 2/8 in pigs has also confirmed the increased efficacy obtained using AAV 2/8 (Mussolino et al, 2011). Therefore employing this serotype as a method of transduction may be a preferable route of administration of *Rac1* shRNA to the retina in the future. However the increased range of tropism of this serotype of AAV in the mammalian retina may produce unknown results as it is not clear what the effect of *Rac1* suppression may be in layers other than the ONL and RPE which were the layers transduced in this study by AAV 2/5. Immunohistochemical analysis of the expression of Rac1 in the retina (figure 3.5.6) demonstrated that expression of this gene appears to be ubiquitous in all layers examined, with stronger expression in the nuclear layers. In addition, much research has been carried out regarding suppression of *Rac1* in the photoreceptors of the ONL (Haruta et al, 2009) and the RPE (Mizutani et al, 2013). In both of these cases, the suppression of *Rac1* was shown to be beneficial; in a mouse model of light induced damage (Haruta et al, 2009) and a mouse model of choroidal neovascularisation (CNV, a hallmark of many retinopathies including

AMD, Mizutani et al, 2013). However, the role of *Rac1* in other layers of the retina remains unclear and therefore delivery of this RNAi agent via AAV2/8 may have unexpected results.

The safety of AAV mediated delivery to the retina has been the subject of many clinical and pre-clinical studies. The safety of AAV2 serotype to deliver a transgene was examined in cynomolgus monkeys which had been treated with this virus via intravitreal injection (Mac Lachlan et al, 2011). This study demonstrated that AAV2 induced some local AAV mediated inflammation of the vitreous in a high dose group (which received a viral dose of $2.4x10^{10}$vg) however this tended to gradually resolve. Furthermore, no negative effects on the histology or ERG response were recorded in any of these animals. In addition to these studies, many follow up studies have been performed on patients who received RPE65 transgene via AAV2 delivery for the treatment of LCA, the safety of which has been discussed in section 4.4 (Bennett et al, 2012; Simonelli et al, 2010; Maguire et al, 2009). For AAV 2/5 delivery, Stieger et al have demonstrated that viral particles remain localised within the retina for up to four years post-injection of dogs (Stieger et al, 2009). In the pig retina following sub-retinal injection of AAV 2/5, no adverse effects were recorded by ERG analysis, histology or TUNEL (Terminal deoxynucleotidyl transferase dUTP nick end labelling) staining of the retina (a stain for apoptopic cells). Furthermore, neutralising antibodies against AAV were observed in the serum of only 3 out of 21 animals (Mussolino et al, 2011). However, sub-retinal injection in one of the animals caused a retinal detachment which completely ablated visual function as assessed by ERG and induced cell death in the retina, highlighting the danger inherent in a sub-retinal injection which usually induces a transient retinal degeneration which normally resolves within days of injection (Johnson et al, 2008). However, the various publications mentioned here provide data which demonstrates the relative safety of AAV mediated delivery of a therapeutic to the retina should the *Rac1* shRNA be chosen for further work in large animal models. While much data has been gathered over the years, additional data regarding the optimal viral dose and viral serotype in large animal models is still required.

The data presented in this thesis detail the RNAi mediated suppression of *Rac1* and the over-expression of *Thioredoxin1* in the retina of mice carrying a mutation which causes a rhodopsin-linked adRP like phenotype. These studies have demonstrated that although over-expression of *Trx* in the retina of a mouse model of RP has been achieved, this has failed to produce a functional benefit in these mice, contrary to expectations given the protective role which over-expression of this gene plays in the retina of the *Tubby* mouse (Kong et al, 2010). In addition, a protective effect of visual function in the hP347S transgenic mouse model of RP has been achieved with one of two RNAi agents tested which target *Rac1*. This discrepancy in outcome highlights the need to investigate the effects of several siRNAs against a gene of interest, an approach which has begun to be implemented given the potential for off-target effects (Mohr & Perriman, 2012). Nonetheless, the AAV_shRAC1_3 virus has been demonstrated to reduce production of potentially damaging ROS, increase the cell viability of both rods and cones and increase the visual function of a transgenic mouse model of RP, making it a clear candidate for the further studies suggested in this discussion. Although only one of three constructs has succeeded in completing the aims of this thesis (ie to develop an antioxidant gene therapy which preserves visual function in mouse models of RP) it must be noted that further characterisation of the oxidative stress associated with various mutations which cause different forms of retinal degeneration is required.

Although the use of suppression of *Rac1* as a potential therapeutic for retinal degenerations would be uncommon as it does not address the primary mutation or encode a neurotrophic factor, the increased understanding of the pathology underlying retinal degeneration has provided the research community with new avenues with which to explore novel routes of therapeutic development. Therefore a combinatorial approach which addresses the primary mutation and the secondary pathology associated with the retinal degeneration may be the most feasible approach to the future treatment of Retinitis Pigmentosa amongst other retinal degenerations. It is hoped that patients who present with a retinopathy may in the future have a range of potential therapies available which may be chosen based on a clinical and genetic examination. For those with the early hallmarks of disease progression, or those with a genetic predisposition to a given retinopathy, the use of gene therapy in combination with a pharmacological therapy (such as N-

Acetylcysteine, an orally and topically available anti-oxidant which has been studied in a pre-clinical setting, discussed in chapter 4; Lee et al, 2011) may prove to be the most viable option to preserve eyesight. This would likely be of use at a stage when photoreceptors are still viable within the retina and therefore amenable to a DNA or RNA based therapy. Treatment using an AAV delivered DNA based therapy has already been demonstrated to adequately treat patients of LCA (Bennett et al, 2012; Simonelli et al, 2010; Maguire et al, 2009). For those patients for whom there is no known inherited factor causing the disease, a secondary gene therapy such as the delivery of neurotrophic factors or the delivery of a genetic component which alters the retinal levels of oxidative stress may be the most feasible option. It is anticipated that a *Rac1* RNAi suppression agent may be of most use for patients who fall within this category. A *Rac1* RNAi suppression therapy would also have the advantage of potential benefit in more than one disorder, given the role which oxidative stress plays in several retinopathies (Doonan et al, 2012). For those patients presenting with a later stage of retinopathy, in which the photoreceptors have already undergone apoptosis, an optogenetic, retinal prosthetic or stem cell therapy may be of greater use. The purpose the studies detailed in this thesis was to identify a genetic based therapy which provided a functional benefit in a mouse model of RP. Of three AAV based constructs tested, the AAV_shRAC1_3 therapy has thus far emerged as holding the most promise for patients with this disease. Although there are many hurdles to be overcome before a treatment such as this becomes a feasible therapeutic in humans, it is hoped that future work will address the issues presented here and examine the potential beneficial effects that *Rac1* suppression may have in other retinal degenerations.

Chapter 7: Appendix

Figure 8.1: Sequence of *RAC1* coding sequence in expression plasmid

The human *RAC1* coding sequence was present in an expression vector already present in the library. Sequencing revealed that this gene was intact from start to stop codon (denoted above) and downstream of the Rhodopsin promoter (not shown). This gene contained the exons of the gene only.

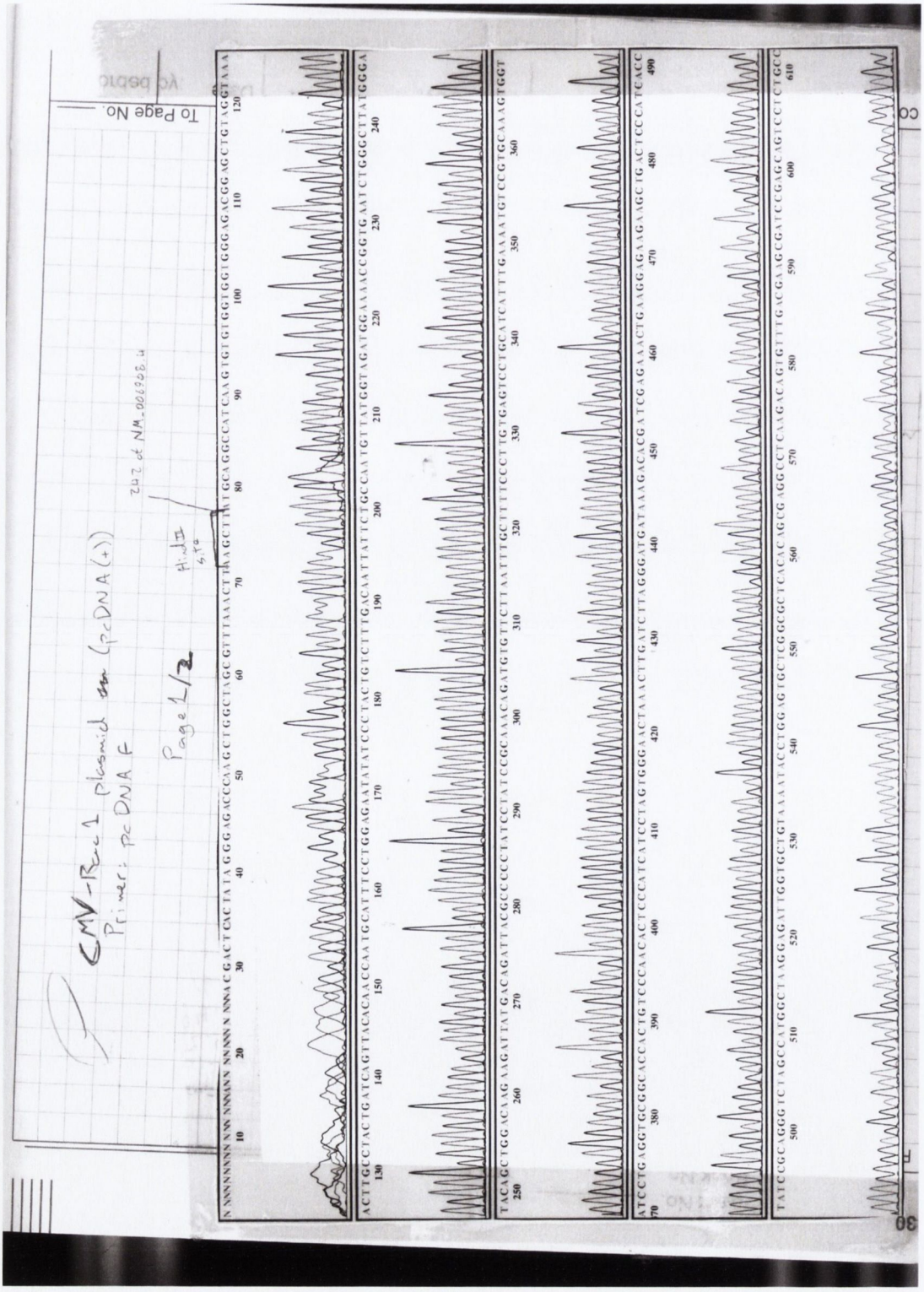

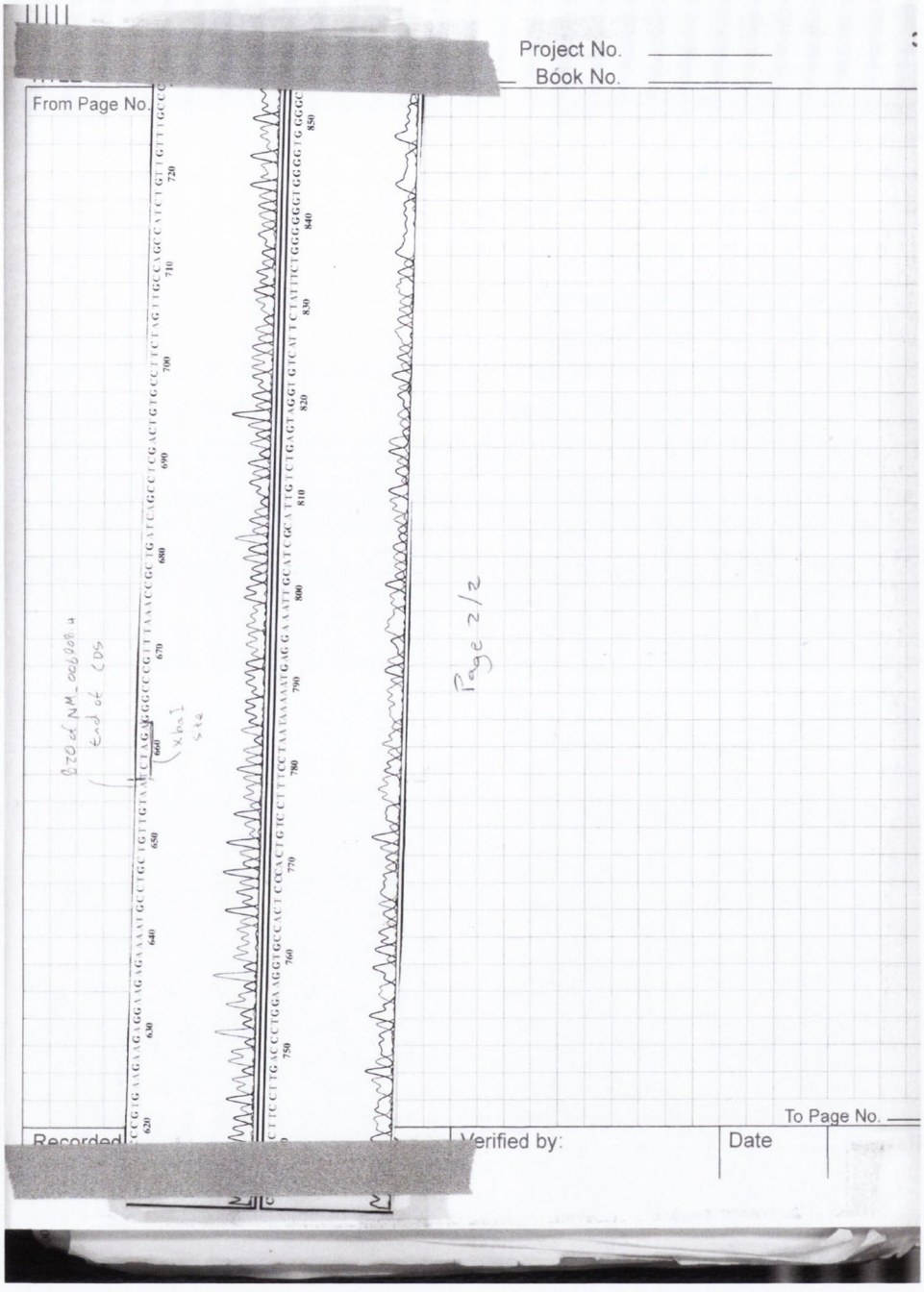

Figures 8.2 & 8.3: The sequence of the *RAC1* coding sequence demonstrating successful cloning of this gene in to the pcDNA expression vector

The coding sequence of *RAC1* which had PCR amplified from the plasmid shown in figure 8.1 was cloned in to the pcDNA+ expression vector. Successful cloning was confirmed by the sequence shown in figures 8.2 and 8.3. The restriction sites used for cloning (*HindIII* and *XbaI*) are marked at the flanking ends of the *RAC1* coding

sequence as are the start and stop codons of the *RAC1* gene.

AAV_Sh1 with CMV-EGFP

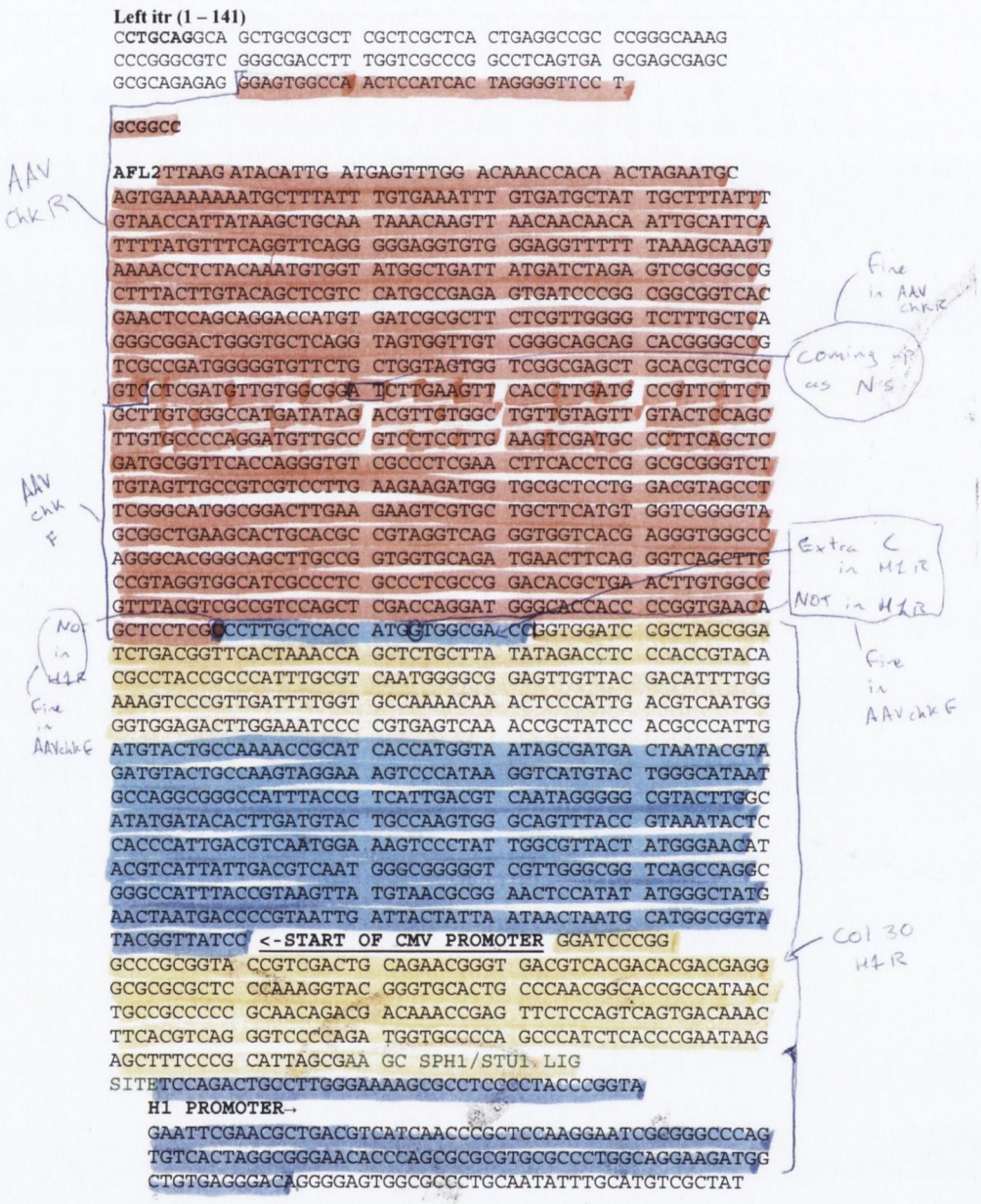

H1-149C PROMOTER GTGTTCTGGGAAATCACC

ATAAACGTGAAATGTCTTTGGATTTGGGAATCTTATAAGTTCTGTATGAG
ACCAC

BGL2 SITE AGATCT

CCCGTGTCCGTGCAAAGTGGTATTTCAAGAGAATACCACTTTGCACGGAC
ATTTTTTCTA GAGGAAA

HIND3 SITE AAGCT

GGCC GC

Right itr (1913 - 2053)

AGGAACCC CTAGTGATGG AGTTGGCCAC TCCCTCTCTG
CGCGCTCGCT CGCTCACTGA GGCCGGGCGA CCAAAGGTCG CCCGACGCCC
GGGCTTTGCC CGGGCGGCCT CAGTGAGCGA GCGAGCGCGC AGCTGCCTGC
AGG
GGCGCCT GATGCGGTAT TTTCTCCTTA CGCATCTGTG CGGTATTTCA
CACCGCATAC GTCAAAGCAA CCATAGTACG CGCCCTGTAG CGGC

f1 origin (2145 - 2451)

GCATTA
AGCGCGGCGG GTGTGGTGGT TACGCGCAGC GTGACCGCTA CACTTGCCAG
CGCCCTAGCG CCCGCTCCTT TCGCTTTCTT CCCTTCCTTT CTCGCCACGT
TCGCCGGCTT TCCCCGTCAA GCTCTAAATC GGGGGCTCCC TTTAGGGTTC
CGATTTAGTG CTTTACGGCA CCTCGACCCC AAAAAACTTG ATTTGGGTGA
TGGTTCACGT AGTGGGCCAT CGCCCTGATA GACGGTTTTT CGCCCTTTGA
CGTTGGAGTC CACGTTCTTT AATAGTGGAC TCTTGTTCCA AACTGGAACA
A

Amp^r promoter (2452 - 3829)

CACTCAACC CTATCTCGGG CTATTCTTTT GATTTATAAG GGATTTTGCC
GATTTCGGCC TATTGGTTAA AAAATGAGCT GATTTAACAA AAATTTAACG
CGAATTTTAA CAAAATATTA ACGTTTACAA TTTTATGGTG CACTCTCAGT
ACAATCTGCT CTGATGCCGC ATAGTTAAGC CAGCCCCGAC ACCCGCCAAC
ACCCGCTGAC GCGCCCTGAC GGGCTTGTCT GCTCCCGGCA TCCGCTTACA
GACAAGCTGT GACCGTCTCC GGGAGCTGCA TGTGTCAGAG GTTTTCACCG
TCATCACCGA AACGCGCGAG ACGAAAGGGC CTCGTGATAC GCCTATTTTT
ATAGGTTAAT GTCATGATAA TAATGGTTTC TTAGACGTCA GGTGGCACTT
TTCGGGGAAA TGTGCGCGGA ACCCCTATTT GTTTATTTTT CTAAATACAT
TCAAATATGT ATCCGCTCAT GAGACAATAA CCCTGATAAA TGCTTCAATA
ATATTGAAAA AGGAAGAGT

Amp resistance (2970 - 3830)

A TGAGTATTCA ACATTTCCGT GTCGCCCTTA
TTCCCTTTTT TGCGGCATTT TGCCTTCCTG TTTTTGCTCA CCCAGAAACG
CTGGTGAAAG TAAAAGATGC TGAAGATCAG TTGGGTGCAC GAGTGGGTTA
CATCGAACTG GATCTCAACA GCGGTAAGAT CCTTGAGAGT TTTCGCCCCG
AAGAACGTTT TCCAATGATG AGCACTTTTA AAGTTCTGCT ATGTGGCGCG
GTATTATCCC GTATTGACGC CGGGCAAGAG CAACTCGGTC GCCGCATACA
CTATTCTCAG AATGACTTGG TTGAGTACTC ACCAGTCACA GAAAAGCATC
TTACGGATGG CATGACAGTA AGAGAATTAT GCAGTGCTGC CATAACCATG

Figures 8.4 & 8.5: The sequence of the pAAV_shRAC1_1 plasmid showing successful cloning of this plasmid

Subsequent to successful cloning of the RAC1_1 shRNA in to the initial AAV_shRAC1_1 plasmid, the PGK promoter and EGFP coding region of DNA was excised and replaced by CMV promoter driven EGFP. Sequence verification of successful cloning is shown in this figure. Hand written notes describe loss of

sequence read at some regions of the plasmid. However these regions were later verified using overlapping sequence of the same region using different reads produced by different primers. The different reads are displayed as different coloured highlights of the sequence.

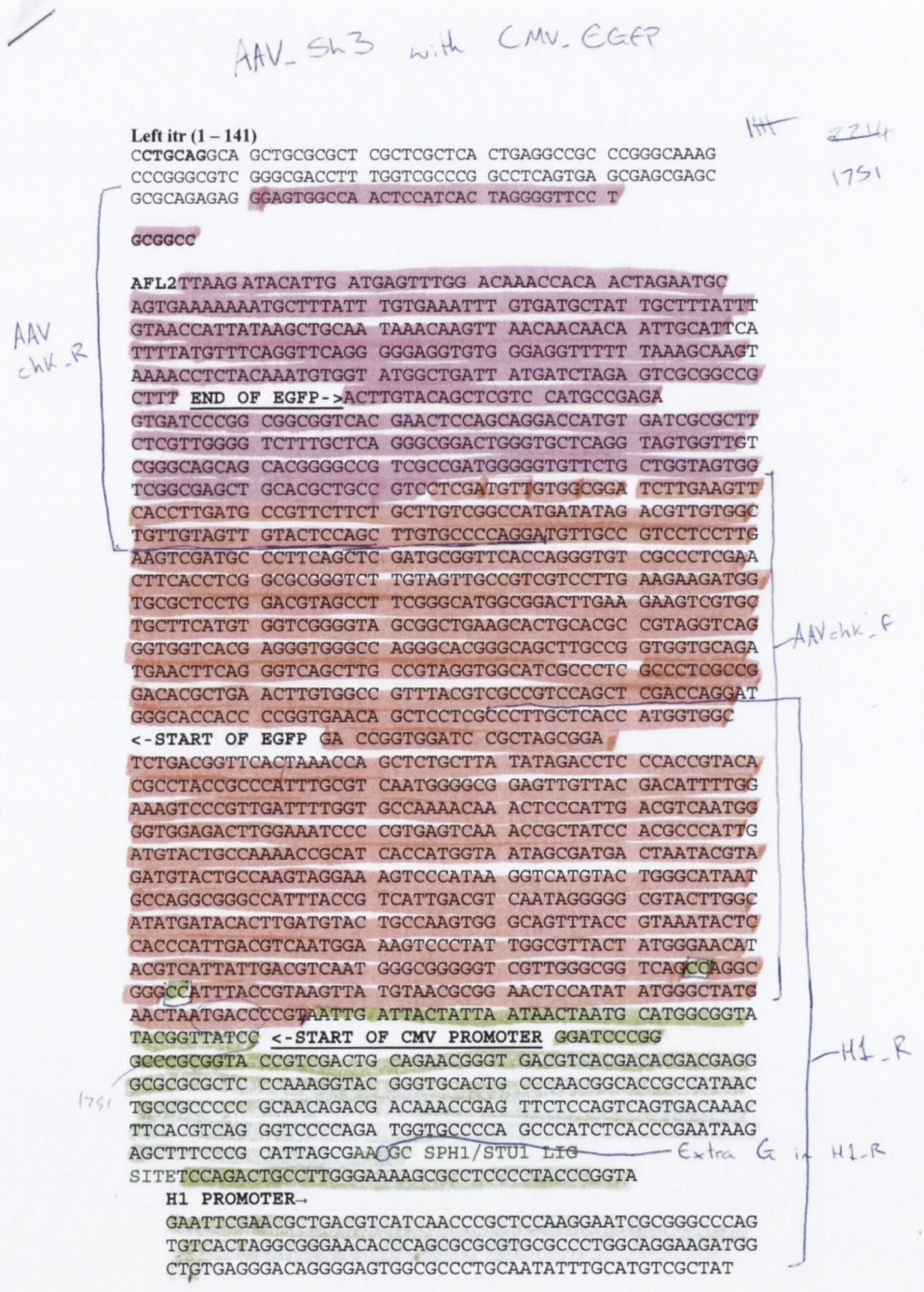

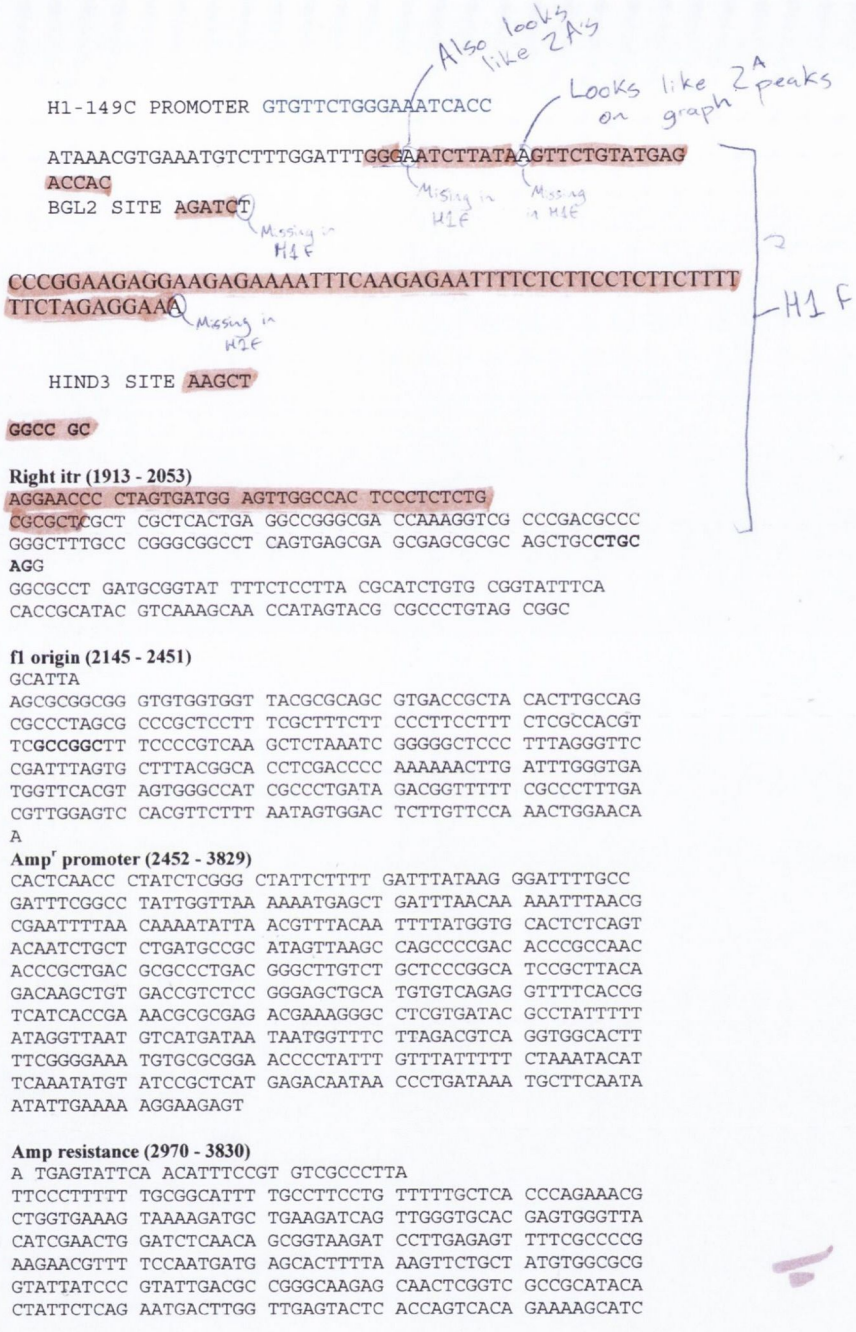

Figures 8.6 & 8.7: The sequence of the pAAV_shRAC1_3 plasmid showing successful cloning of this plasmid

Subsequent to successful cloning the RAC1_3 shRNA in to the initial AAV_shRAC1_3 plasmid, the PGK promoter and EGFP coding region of DNA was excised and replaced by CMV promoter driven EGFP. Sequence verification of successful cloning is shown in this figure. Hand written notes describe loss of

sequence read at some regions of the plasmid. However these regions were later verified using overlapping sequence of the same region using different reads produced by different primers. The different reads are displayed as different coloured highlights of the sequence.

TRX QR (Rev comp)

GCCGCGCTTAATGCGCCGCTACAGGGCGCGTCCCATTCGCCATTCAGGC
TGCGCAACTGTTGGGAAGGGCGATCGGTGCGGGCCTCTTCGCTATTACG
CCAGCCAATACGCAAACCGCCTCTCCCCGCGCGTTGGCCGATTCATTNA
ANNGCAGGATCGATCCAGACATGATAAGATACATTGATGAGTTTGGAC
AAACCACAACTAGAATGCAGTGAAAAAAATGCTTTATTTGTGAAATTTG
TGATGCTATTGCTTTATTTGTAACCATTATAAGCTGCAATAAACAAGTTA
ACAACAACAATTGCATTCATTTTATGTTTCAGGTTCAGGGGGAGGTGTG
GGAGGTTTTTTAAAGCAAGTAAAACCTCTACAAATGTGGTATGGCTGAT
TATGATCATGAACAGACTGTGAGGACTGAGGGGCCTGAAATGAGCCTT
GGGACTGTGAATCTAAAATACACAAACAATTAGAATCACTAGCTCCTGT
GTATAATATTTTCATAAATCATACTCAGTAAGCAAAACTCTCAAGCAGC
AAGCATATGCAGCTAGTTTAACACATTATACACTTAAAAATTTTATATTT
ACCTTAGAGCTTTAAATCTCTGTAGGTAGTTTGTCCAATTATGTCACACC
ACAGAAGTAAGGTTCCTTCACAAAGATCCCAAGCTAGCAGTTTTCCCAG
TCACGACGTTGTAAAACGACGGCCAGTGCCTAGCTTATAATACGACTCA
CTATAGGGACCACTTTGTACAAGAAAGCTGGGTACGCGTAAGCTTGGGC
CCCTCGAGGGATAC**TCTAGA (XbaI Site)**
GCGGCCGCCCTTTTTTTTTTTTTTTTAAAA
M13
GGGTAGAATTAATATTTTATTGTCATTTATAATCAGATGGCAGTTGGGT
ATAGACTCTCCACACTTCATAGTTTTTTGCAAATTAAAAAAGGTACAGG
TTTTAAACAGCTGGTAGCTGGTTACACTTTTCAGAGCATG**ATT (Stop Codon)**AGGCATATTCAGTAATAGAGGCTTCAAGCTTTTCCTTGTTAGCAC
CGGAGAACTCCCCCACCTTTTGACCCTTTTTATAAAACTGGAAGGTCGG
CATGCATTTGACTTCACAGTCTGCAG
TRX QF
CAACATCCTGGCAGTCATCCACATCCACTTCAAGGAACACCACATTGGA
ATACTTGTCACAGAGGGAATGGAAGAAGGGCTTGATCATTTTGCAAGGT
CCACACCACGTAGCAGAGAAGTCCACCACGACAAGCTTGTCTCCCGCGG
CGGCCAGGGCCTCCTGAAAAGCTTCCTTGCTCTCGATCAGCTTCAC**CAT (Start Codon)**
TTTGGCTGTTGCGGGGAGGGAGCCACACGCGTCTCAGCAGAACCAGAT
GGAAATGGCGGACGCGTGGGTCGACGATATCCCGG**GAATTC (EcoRI Site)**CGGACCGGTACCAGCCTGCTTTTTTGTACAAACTTGTTCTATAGTGT
CACCTAAATAGGCCTAATGGTCATAGCTGTTTCCTGTGTGAAATTGTTAT
CCGTCCCGCGGCCTAGGCTAGAGTCCGGAGGCTGGATCGGTCCCGGTGT
CTTCTATGGAGGTCAAAACAGCGTGGATGGCGTCTCCAGGCGATCTGAC
GGTTCACTAAACGAGCTCTGCTTATATAGACCTCCCACCGTACACGCCT
ACCGCCCATTTGCGTCAATGGGGCGGAGTTGTTACGACATTTTGGAAAG
TCCCGTTGATTTTGGTGCCAAAACAAACTCCCATTGACGTCAATGGGGT
GGAGACTTGGAAATCCCCGTGAGTCAAACCGCTATCCACGCCCATTGAT

GTACTGCCAAAACCGCATCACCATGGTAATAGCGATGACTAATACGTAG
ATGTACTGCCAAGTAGGAAAGTCCCATAAGGTCATGTACTGGGCATAAT
GCCAGGCGGGCCATTTACCGTCATTGACGTCAATAGGGGGCGTACTTGG
CATATGATACACTTGATGTACTGCCAAGTGGGCAGTTTACCGTAAATAC
TCCACCCATTGACGTCAATGGAAAGTCCCTATTGGNGTTACTATGGGAA
CATACGTCATTATTGACGTCAATGGGCGGGGGTC

Figure 8.8: Sequence of Thioredoxin Clone

Figure showing the sequence of the *Trx* clone obtained commercially from Source Bioscience, sequenced using the Trxq_F, Trxq_R and M13 primers. The regions of the plasmid which have been sequenced with these primers are highlighted in red, green and blue. Also shown here are the CDS of *Trx* along with the restriction sites used to clone this CDS in to the pAAV_MCS plasmid. The *Trx1* CDS is highlighted in red.

pAAV.MCS with Trx insert (in green) col1

Left itr (1 – 141)

CCTGCAGGCA GCTGCGCGCT CGCTCGCTCA CTGAGGCCGC CCGGGCAAAG
CCCGGGCGTC GGGCGACCTT TGGTCGCCCG GCCTCAGTGA GCGAGCGAGC
GCGCAGAGAG GGAGTGGCCA ACTCCATCAC TAGGGGTTCC T

GCGGCCGC

CMV promoter (150 - 812)

A
CGCGTGGAGC TAGTTATTAA TAGTAATCAA TTACGGGGTC ATTAGTTCAT
AGCCCATATA TGGAGTTCCG CGTTACATAA CTTACGGTAA ATGGCCCGCC
TGGCTGACCG CCCAACGACC CCCGCCCATT GACGTCAATA ATGACGTATG
TTCCCATAGT AACGTCAATA GGGACTTTCC ATTGACGTCA ATGGGTGGAG
TATTTACGGT AAACTGCCCA CTTGGCAGTA CATCAAGTGT ATCATATGCC
AAGTACGCCC CCTATTGACG TCAATGACGG TAAATGGCCC GCCTGGCATT
ATGCCCAGTA CATGACCTTA TGGGACTTTC CTACTTGGCA GTACATCTAC
GTATTAGTCA TCGCTATTAC CATGGTGATG CGGTTTTGGC AGTACATCAA
TGGGCGTGGA TAGCGGTTTG ACTCACGGGG ATTTCCAAGT CTCCACCCCA
TTGACGTCAA TGGGAGTTTG TTTTGGCACCA AAATCAACGG GACTTTCCAA
AATGTCGTAA CAACTCCGCC CCATTGACGC AAATGGGCGG TAGGCGTGTA
CGGTGGGAGG TCTATATAAG CAGAGCTCGT TTAGTGAACC GTCAGATCGC
CTGGAGACGC CATCCACGCT GTTTTGACCT CCATAGAAGA CACCGGGACC
GATCCAGCCT CC

GCGGATT

Extra N in sequence

Extra G in sequence

N in sequence

Trx qF

660

β-globin intron (820 - 1312)

C GAATCCCGGC CGGGAACGGT GCATTGGAAC
GCGGATTCCC CGTGCCAAGA GTGACGTAAG TACCGCCTAT AGAGTCTATA
GGCCCACAAA AAATGCTTTC TTCTTTTAAT ATACTTTTTT GTTTATCTTA
TTTCTAATAC TTTCCCTAAT CTCTTTCTTT CAGGGCAATA ATGATACAAT
GTATCATGCC TCTTTGCACC ATTCTAAAGA ATAACAGTGA TAATTTCTGG
GTTAAGGCAA TAGCAATATT TCTGCATATA AATATTTCTG CATATAAATT
GTAACTGATG TAAGAGGTTT CATATTGCTA ATAGCAGCTA CAATCCAGCT
ACCATTCTGC TTTTATTTTA TGGTTGGGAT AAGGCTGGAT TATTCTGAGT
CCAAGCTAGG CCCTTTTGCT AATCATGTTC ATACCTCTTA TCTTCCTCCC
ACAGCTCCTG GGCAACGTGC TGGTCTGTGT GCTGGCCCAT CACTTTGGCA
AAGAATTGGG AT

TCGAAC

MCS

AT CGATTGAATT
CCCGGGATATCGTCGACCCACGCGTCCGCCATTTCCATCTGGTTCTGCTGAGACGCGTGTGG
CTCCCTCCCCGCAACAGCCAAAATGGTGAAGCTGATCGAGAGCAAGGAAGCTTTTCAGGAGG
CCCTGGCCGCCGCGGGAGACAAGCTTGTCGTGGTGGACTTCTCTGCTACGTGGTGTGGACCT
TGCAAAATGATCAAGCCCTTCTTCCATTCCCTCTGTGACAAGTATTCCAATGTGGTGTTCCT
TGAAGTGGATGTGGATGACTGCCAGGATGTTGCTGCAGACTGTGAAGTCAAATGCATGCCGA
CCTTCCAGTTTTATAAAAAGGGTCAAAAGGTGGGGGAGTTCTCCGGTGCTAACAAGGAAAAG
CTTGAAGCCTCTATTACTGAATATGCCTTAATCATGCTCTGAAAAGTGTAACCAGCTACCAGC
TGTTTAAAACCTGTACCTTTTTTAATTTGCAAAAAACTATGAAGTGTGGAGAGTCTATACGC
AACTGCCATCTGATTATAAATGACAATAAAATATTAATTCTACCCTTTAAAAAAAAAAAAA
AAAAGGGCGGCCGCTCTAGAGTATCCCTCGAGGGGCCC AAGCTTGCCT CGAGCAGCGC
TGCTCGAGAG ATCT

EcoRI

Start codon

Stop codon

TrxqR

Hind III

1936

hGH polyA (1395 - 1873)

ACGGGT
GGCATCCCTG TGACCCCTCC CCAGTGCCTC TCCTGGCCCT GGAAGTTGCC
ACTCCAGTGC CCACCAGCCT TGTCCTAATA AAATTAAGTT GCATCATTTT
GTCTGACTAG GTGTCCTTCT ATAATATTAT GGGGTGGAGG GGGGTGGTAT
GGAGCAAGGG GCAAGTTGGG AAGACAACCT GTAGGGCCTG CGGGGTCTAT
TGGGAACCAA GCTGGAGTGC AGTGGCACAA TCTTGGCTCA CTGCAATCTC
CGCCTCCTGG GTTCAAGCGA TTCTCCTGCC TCAGCCTCCC GAGTTGTTGG
GATTCCAGGC **ATGCAT**GACC AGGCTCAGCT AATTTTTGTT TTTTGGTAG
AGACGGGGTT TCACCATATT GGCCAGGCTG GTCTCCAACT CCTAATCTCA
GGTGATCTAC CCACCTTGGC CTCCCAAATT GCTGGGATTA CAGGCGTGAA
CCACTGCTCC CTTCCCTGTC CTT

CTGATTT TGTAGGTAAC CACGTGCGGA
CCGA**GCGGCC GC**

Right itr (1913 - 2053)

AGGAACCC CTAGTGATGG AGTTGGCCAC TCCCTCTCTG
CGCGCTCGCT CGCTCACTGA GGCCGGGCGA CCAAAGGTCG CCCGACGCCC
GGGCTTTGCC CGGGCGGCCT CAGTGAGCGA GCGAGCGCGC AGCTGC**CTGC**
AGG

GGCGCCT GATGCGGTAT TTTCTCCTTA CGCATCTGTG CGGTATTTCA
CACCGCATAC GTCAAAGCAA CCATAGTACG CGCCCTGTAG CGGC

f1 origin (2145 - 2451)

GCATTA
AGCGCGGCGG GTGTGGTGGT TACGCGCAGC GTGACCGCTA CACTTGCCAG
CGCCCTAGCG CCCGCTCCTT TCGCTTTCTT CCCTTCCTTT CTCGCCACGT
TC**GCCGGC**TT TCCCCGTCAA GCTCTAAATC GGGGGCTCCC TTTAGGGTTC
CGATTTAGTG CTTTACGGCA CCTCGACCCC AAAAAACTTG ATTTGGGTGA
TGGTTCACGT AGTGGGCCAT CGCCCTGATA GACGGTTTTT CGCCCTTTGA
CGTTGGAGTC CACGTTCTTT AATAGTGGAC TCTTGTTCCA AACTGGAACA
A

Amp^r promoter (2452 - 3829)

CACTCAACC CTATCTCGGG CTATTCTTTT GATTTATAAG GGATTTTGCC
GATTTCGGCC TATTGGTTAA AAAATGAGCT GATTTAACAA AAATTTAACG
CGAATTTTAA CAAAATATTA ACGTTTACAA TTTTATGGTG CACTCTCAGT
ACAATCTGCT CTGATGCCGC ATAGTTAAGC CAGCCCCGAC ACCCGCCAAC
ACCCGCTGAC GCGCCCTGAC GGGCTTGTCT GCTCCCGGCA TCCGCTTACA
GACAAGCTGT GACCGTCTCC GGGAGCTGCA TGTGTCAGAG GTTTTCACCG
TCATCACCGA AACGCGCGAG ACGAAAGGGC CTCGTGATAC GCCTATTTTT
ATAGGTTAAT GTCATGATAA TAATGGTTTC TTAGACGTCA GGTGGCACTT
TTCGGGGAAA TGTGCGCGGA ACCCCTATTT GTTTATTTTT CTAAATACAT
TCAAATATGT ATCCGCTCAT GAGACAATAA CCCTGATAAA TGCTTCAATA
ATATTGAAAA AGGAAGAGT

Amp resistance (2970 - 3830)

A TGAGTATTCA ACATTTCCGT GTCGCCCTTA
TTCCCTTTTT TGCGGCATTT TGCCTTCCTG TTTTTGCTCA CCCAGAAACG
CTGGTGAAAG TAAAAGATGC TGAAGATCAG TTGGGTGCAC GAGTGGGTTA
CATCGAACTG GATCTCAACA GCGGTAAGAT CCTTGAGAGT TTTCGCCCCG
AAGAACGTTT TCCAATGATG AGCACTTTTA AAGTTCTGCT ATGTGGCGCG
GTATTATCCC GTATTGACGC CGGGCAAGAG CAACTCGGTC GCCGCATACA

Figures 8.9 & 8.10: Sequence of the Trx_AAV plasmid showing successful cloning

The *HindIII* and *EcoRI* sites were used to excise the *Trx* coding sequence from the original expression plasmid (presented in figure 8.8) and ligate this segment of DNA in to the pAAV_MCS plasmid. Confirmation of successful cloning was verified by sequence analysis (presented above). The restriction sites are marked and separate reads of this plasmid using different primers (Trx_qF and Trx_qR) are shown highlighted in different colours.

Bibliography

Gomperts B, Kramer IM, Tatham PER (2009). *Signal Transduction*: Chapter 6 The Regulation of Visual Transduction and Olfaction 159-183.

Niewhohner J, Tannert C (2006). *Gene Therapy: Prospective Technology Assessment in its Societal Context.*

Ryan SJ, Ogden TE, Hinton DR, Schachat AP (2001). *Retina: Volume 1.*

Wolfensohn S, Lloyd M (2003). Handbook of Laboratory Animal Management and Welfare 3rd edition.

References

Acland GM, Aguirre GD, Ray J, Zhang Q, Aleman TS, Cideciyan AV, Pearce-Kelling SE, Anand V, Zeng Y, Maguire AM, Jacobson SG, Hauswirth WW, Bennett J (2001). Gene therapy restores vision in a canine model of childhood blindness. *Nature Genetics* **28**: 92-95.

Adlam VJ, Harrison JC, Porteous CM, James AM, Smith RA, Murphy MP, Sammut IA (2005). Targeting an antioxidant to mitochondria decreases cardiac ischemia-reperfusion injury. *FASEB Journal* **19**: 1088-1095.

Age-Related Eye Disease Study 2 Research Group (2013). Lutein + zeaxanthin and omega-3 fatty acids for age-related macular degeneration: the Age-Related Eye Disease Study 2 (AREDS2) randomized clinical trial. *Journal of American Medical Association* **309**: 2005-2015.

Agosta E, Lazzeri S, Orlandi P, Figus M, Fioravanti A, Di Desidero T, Sartini MS, Nardi M, Danesi R, Bocci G (2012). Pharmacogenetics of antiangiogenic and antineovascular therapies of age-related macular degeneration. *Pharmacogenomics* **13**: 1037-1053.

Ahmad I, Del Debbio CB, Das AV, Parameswaran S (2011). Müller glia: a promising target for therapeutic regeneration. *Investigative Ophthalmology and Visual Science* **52**: 5758-5764.

Al-Shabrawey M, Bartoli M, El-Remessy AB, Ma G, Matragoon S, Lemtalsi T, Caldwell RW, Caldwell RB (2008). Role of NADPH oxidase and Stat3 in statin-mediated protection against diabetic retinopathy. *Investigative Ophthalmology and Visual Science* **49**: 3231-3238.

Anasagasti A, Irigoyen C, Barandika O, de Munain AL, Ruiz-Ederra J (2012). Current mutation discovery approaches in Retinitis Pigmentosa. *Vision Research* http://dx.doi.org/10.1016/j.visres.2012.09.012.

Aon-Bertolino ML, Romero JI, Galeano P, Holubiec M, Badorrey MS, Saraceno GE, Hanschmann EM, Lillig CH, Capani F (2011). Thioredoxin and glutaredoxin system proteins-immunolocalization in the rat central nervous system. *Biochima et Biophysica acta* **1810**: 93-110.

Ashtari M, Cyckowski LL, Monroe JF, Marshall KA, Chung DC, Auricchio A, Simonelli F, Leroy BP, Maguire AM, Shindler KS, Bennett J (2011). The human visual cortex responds to gene therapy-mediated recovery of retinal function. *Journal of Clinical Investigation* **121**: 2160-2168.

Asi H, Perlman I (1992). Relationships between the electroretinogram a-wave, b-wave and oscillatory potentials and their application to clinical diagnosis. *Documenta Ophthalmologica* **79**: 125-139.

Asokan A, Schaffer DV, Samulski RJ (2012). The AAV vector toolkit: poised at the clinical crossroads. *Molecular Therapy* **20**: 699-708.

Assari T (2006). Chronic Granulomatous Disease; fundamental stages in our understanding of CGD. *Medical Immunology* **5**: 4.

Babior BM, Lambeth JD, Nauseef W (2002). The neutrophil NADPH Oxidase. *Archives of Biochemistry and Biophysics* **397**: 342-344.

Bainbridge JW, Smith AJ, Barker SS, Robbie S, Henderson R, Balaggan K, Viswanathan A, Holder GE, Stockman A, Tyler N, Petersen-Jones S, Bhattacharya SS, Thrasher AJ, Fitzke FW, Carter BJ, Rubin GS, Moore AT, Ali RR (2008). Effect of gene therapy on visual function in Leber's congenital amaurosis. *New England Journal of Medicine* **358**: 2231-2239.

Balasubramanian N, Slepak VZ (2003). Light mediated activation of Rac-1 in photoreceptor outer segments. *Current Biology* **13**: 1306-1310.

Balaggan KS, Duran Y, Georgiadis A, Thaung C, Barker SE, Buch PK, MacNeil A, Robbie S, Bainbridge JW, Smith AJ, Ali RR (2012). Absence of ocular malignant transformation after sub-retinal delivery of rAAV2/2 or integrating lentiviral vectors in p53-deficient mice. *Gene Therapy* **19**: 182-188.

Banasik MB, McCray PB Jr (2010). Integrase-defective lentiviral vectors: progress and applications. *Gene Therapy* **17**: 150-157.

Barry MP, Dagnelie G; Argus II Study Group (2012). Use of the Argus II retinal prosthesis to improve visual guidance of fine hand movements. *Investigative Ophthalmology and Visual Science* **53**: 5095-5101.

Bates CJ (1995). Vitamin A. *The Lancet* **345**: 31-35.

Batten ML, Imanishi Y, Tu DC, Doan T, Zhu L, Pang J, Glushakova L, Moise AR, Baehr W, Van Gelder RN, Hauswirth WW, Rieke F, Palczewski K (2005). Pharmacological and rAAV gene therapy rescue of visual functions in a blind mouse model of Leber congenital amaurosis. *PLoS Medicine* **2**: e333.

Bedard K, Krause K-H (2007). The NOX Family of ROS-Generating NADPH Oxidases: Physiology and Pathophysiology. *Physiological Reviews* **87**: 245-313.

Behrens MM, Ali SS, Dao DN, Lucero J, Shekhtman G, Quick KL, Dugan LL (2007). Ketamine-induced loss of phenotype of fast-spiking interneurons is mediated by NADPH-oxidase. *Science* **318**: 1645-1647.

Belmonte MA, Santos MF, Kihara AH, Yan CY, Hamassaki DE (2006). Light-Induced photoreceptor degeneration in the mouse involves activation of the small GTPase Rac1. *Investigative Ophthalmology and Visual Science* **47**: 1193-1200.

Bennett J, Ashtari M, Wellman J, Marshall KA, Cyckowski LL, Chung DC, McCague S, Pierce EA, Chen Y, Bennicelli JL, Zhu X, Ying GS, Sun J, Wright JF, Auricchio A, Simonelli F, Shindler KS, Mingozzi F, High KA, Maguire AM (2012). AAV2 gene therapy readministration in three adults with congenital blindness. *Science Translational Medicine* **4**: 120ra15.

Berson EL, Rosner B, Sandberg MA, Hayes KC, Nicholson BW, Weigel-DiFranco C, Willett W (1993). A randomized trial of vitamin A and vitamin E supplementation for retinitis pigmentosa. *Archives of Ophthalmology* **111**: 761-772.

Berson EL, Rosner B, Sandberg MA, Weigel-DiFranco C, Willett WC (2012). ω-3 intake and visual acuity in patients with retinitis pigmentosa receiving vitamin A. *Archives of Ophthalmology* **130**: 707-711.

Birmingham A, Anderson E, Sullivan K, Reynolds A, Boese Q, Leake D, Karpilow J, Khvorova A (2007). A protocol for designing siRNAs with high functionality and specificity. *Nature Protocols* **2**: 2068-2078.

Blaese RM, Culver KW, Miller AD, Carter CS, Fleisher T, Clerici M, Shearer G, Chang L, Chiang Y, Tolstoshev P, Greenblatt JJ, Rosenberg SA, Klein H, Berger M, Mullen CA, Ramsey WJ, Muul L, Morgan RA, Anderson WF (1995). T

lymphocyte-directed gene therapy for ADA- SCID: initial trial results after 4 years. *Science* **270**: 475-480.

Bochot A, Fattal E, Boutet V, Deverre JR, Jeanny JC, Chacun H, Couvreur P (2002). Intravitreal delivery of oligonucleotides by sterically stabilized liposomes. *Investigative Ophthalmology and Visual Science* **43**: 253-259.

Bosco EE, Mulloy JC, Zheng Y (2009). Rac1 GTPase: a "Rac" of All Trades. *Cellular and Molecular Life Sciences* **66**: 370-374.

Boudreau RL, Rodriguez-Lebron E, Davidson BL (2011). RNAi medicine for the brain: progresses and challenges. *Human Molecular Genetics* **20**: R21-R27.

Boudreau RL, Martins I, Davidson BL (2009). Artificial microRNAs as siRNA shuttles: improved safety as compared to shRNA *in vitro* and *in vivo*. *Molecular Therapy* **17**: 169-175.

Bramall AN, Szego MJ, Pacione LR, Chang I, Diez E, D'Orleans-Juste P, Stewart DJ, Hauswirth WW, Yanagisawa M, McInnes RR (2013). Endothelin-2-mediated protection of mutant photoreceptors in inherited photoreceptor degeneration. *PLoS One* **8**: e58023.

Bridges CDB (1981). Lectin receptors of rods and cones. Visualization by fluorescent label. *Investigative Ophthalmology and Visual Science* **20**: 8-16.

Brill E, Malanson KM, Radu RA, Boukharov NV, Wang Z, Chung HY, Lloyd MB, Bok D, Travis GH, Obin M, Lem J (2007). A novel form of transducin-dependent retinal degeneration: accelerated retinal degeneration in the absence of rod transducin. *Investigative Ophthalmology and Visual Science* **48**: 5445-5453.

Bromberg Y, Shani E, Joseph G, Gorzalczany Y, Sperling O, Pick E (1994). The GDP-bound form of the small G protein Rac1 p21 is a potent activator of the superoxide-forming NADPH oxidase of macrophages. *Journal of Biological Chemistry* **269**: 7055-7058.

Brown BD, Naldini L (2009). Exploiting and antagonizing microRNA regulation for therapeutic and experimental applications. *Nature Reviews Genetics* **10**: 578-585.

Brummelkamp TR, Bernards R, Agami R (2002). A system for stable expression of short interfering RNAs in mammalian cells. Science 296: 550-553.

Bucana C, Saiki I, Nayar R (1986). Uptake and accumulation of the vital dye hydroethidine in neoplastic cells. Journal of Histochemistry and Cytochemistry 34: 1109-1115.

Buchlis G, Podsakoff GM, Radu A, Hawk SM, Flake AW, Mingozzi F, High KA (2012). Factor IX expression in skeletal muscle of a severe hemophilia B patient 10 years after AAV-mediated gene transfer. *Blood* **119**: 3038-3041.

Burke-Gaffney A, Callister ME, Nakamura H (2005). Thioredoxin: friend or foe in human disease? *Trends in Pharmacological Sciences* **26**: 398-404.

Busskamp V, Duebel J, Balya D, Fradot M, Viney TJ, Siegert S, Groner AC, Cabuy E, Forster V, Seeliger M, Biel M, Humphries P, Paques M, Mohand-Said S, Trono D, Deisseroth K, Sahel JA, Picaud S, Roska B (2010). Genetic reactivation of cone photoreceptors restores visual responses in retinitis pigmentosa. *Science* **329**: 413-417.

Cao S, Walker GB, Wang X, Cui JZ, Matsubara JA (2013). Altered cytokine profiles of human retinal pigment epithelium: oxidant injury and replicative senescence. *Molecular Vision* **19**: 718-728.

Caprioli J, Munemasa Y, Kwong JM, Piri N (2009). Overexpression of thioredoxins 1 and 2 increases retinal ganglion cell survival after pharmacologically induced oxidative stress, optic nerve transection, and in experimental glaucoma. *Transactions of the American Ophthalmological Society* **107**: 161-165.

Cepko CL (2012). Emerging Gene Therapies for Retinal Degenerations. *The Journal of Neuroscience* **32**: 6415-6420.

Chadderton N, Millington-Ward S, Palfi A, O'Reilly M, Tuohy G, Humphries MM, Li T, Humphries P, Kenna PF, Farrar GJ (2009). Improved retinal function in a mouse model of dominant retinitis pigmentosa following AAV-delivered gene therapy. *Molecular Therapy* **17**: 593-599.

Chang K, Elledge SJ, Hannon GJ (2006). Lessons from Nature: microRNA-based shRNA libraries. *Nature Methods* **3**: 707-714.

Charbel Issa P, MacLaren RE (2012). Non-viral retinal gene therapy: a review. *Clinical and Experimental Ophthalmology* **40**: 39-47.

Chen FT, Yang CM, Yang CH (2013). The protective effects of the proteasome inhibitor bortezomib (velcade) on ischemia-reperfusion injury in the rat retina. *PLoS One* **8**: e64262.

Chen AF, Chen DD, Daiber A, Faraci FM, Li H, Rembold CM, Laher I (2012). Free radical biology of the cardiovascular system. *Clinical Science* **123**: 73-91.

Chen B, Tang L (2011). Protective effects of catalase on retinal ischemia/reperfusion injury in rats. *Experimental Eye Research* **93**: 599-606.

Chen Q, Vazquez EJ, Moghaddas S, Hoppel C, Lesnefsky EJ (2003). Production of reactive oxygen species by mitochondria: central role of complex III. *The Journal of Biological Chemistry* **278**: 36027-36031.

Chew EY, Clemons TE, Agrón E, Sperduto RD, Sangiovanni JP, Kurinij N, Davis MD; Age-Related Eye Disease Study Research Group (2013). Long-Term Effects of Vitamins C and E, β-Carotene, and Zinc on Age-Related Macular Degeneration: AREDS Report No. 35. Ophthalmology: http://dx.doi.org/10.1016/j.ophtha.2013.01.021.

Choi BY, Jang BG, Kim JH, Lee BE, Sohn M, Song HK, Suh SW (2012). Prevention of traumatic brain injury-induced neuronal death by inhibition of NADPH oxidase activation. *Brain Research* **1481**: 49-58.

Chrysostomou V, Rezania F, Trounce IA, Crowston JG (2013). Oxidative stress and mitochondrial dysfunction in glaucoma. *Current Opinion in Pharmacology* **13**: 12-15.

Cingolani C, Rogers B, Lu L, Kachi S, Shen J, Campochiaro PA (2006). Retinal degeneration from oxidative damage. *Free Radical Biology and Medicine* **40**: 660-669.

Corrochano S, Barhoum R, Boya P, Arroba AI, Rodríguez-Muela N, Gómez-Vicente V, Bosch F, de Pablo F, de la Villa P, de la Rosa EJ (2008). Attenuation of vision loss and delay in apoptosis of photoreceptors induced by proinsulin in a mouse model of retinitis pigmentosa. *Investigative Ophthalmology and Visual Science* **49**: 4188-4194.

Couto LB, High KA (2010). Viral vector-mediated RNA interference. *Current Opinion in Pharmacology* **10**: 534-542.

Cronin T, Raffelsberger W, Lee-Rivera I, Jaillard C, Niepon ML, Kinzel B, Clérin E, Petrosian A, Picaud S, Poch O, Sahel JA, Léveillard T (2010). The disruption of the rod-derived cone viability gene leads to photoreceptor dysfunction and susceptibility to oxidative stress. *Cell Death and Differentiation* **17**: 1199-1210.

da Cruz L, Coley BF, Dorn J, Merlini F, Filley E, Christopher P, Chen FK, Wuyyuru V, Sahel J, Stanga P, Humayun M, Greenberg RJ, Dagnelie G; Argus II Study Group (2013). The Argus II epiretinal prosthesis system allows letter and word reading and long-term function in patients with profound vision loss. *British Journal of Ophthalmology* **97**: 632-636.

Dalkara D, Byrne LC, Klimczak RR, Visel M, Yin L, Merigan WH, Flannery JG, Schaffer DV (2013). In vivo-directed evolution of a new adeno-associated virus for

therapeutic outer retinal gene delivery from the vitreous. *Science Translational Medicine* **5**: 189ra76.

Damiano S, Trepiccione F, Ciarcia R, Scanni R, Spagnuolo M, Manco L, Borrelli A, Capasso C, Mancini R, Schiattarella A, Iervolino A, Zacchia E, Bata-Csere A, Florio S, Anastasio P, Pollastro R, Mancini A, Capasso G (2013). A new recombinant MnSOD prevents the Cyclosporine A-induced renal impairment. *Nephrology, Dialysis, Transplantation* **doi**: 10.1093/ndt/gft020.

Davidson BL, McCray Jr PB (2011). Current prospects for RNA interference-based therapies. *Nature Reviews Genetics* **12**: 329-340.

Davis ME, Zuckerman JE, Choi CH, Seligson D, Tolcher A, Alabi CA, Yen Y, Heidel JD, Ribas A (2010). Evidence of RNAi in humans from systemically administered siRNA via targeted nanoparticles. *Nature* **464**: 1067-1070.

de Curtis I (2008). Functions of Rac GTPases during neuronal development. *Developmental Neuroscience* **30**: 47-58.

de Fougerolles A, Vornlocher HP, Maraganore J, Lieberman J (2007). Interfering with disease: a progress report on siRNA-based therapeutics. *Nature Reviews Drug Discovery* **6**: 443-453.

Deiss LP, Kimchi A (2009). A genetic tool used to identify thioredoxin as a mediator of a growth inhibitory signal. *Science* **252**: 117-120.

Delorme-Walker VD, Peterson JR, Chernoff J, Waterman CM, Danuser G, DerMardirossian C, Bokoch GM (2011). Pak1 regulates focal adhesion strength, myosin IIA distribution, and actin dynamics to optimize cell migration. *Journal of Cell Biology* **193**: 1289-1303.

DerMardirossian C, Schnelzer A, Bokoch GM (2004). Phosphorylation of RhoGDI by Pak1 mediates dissociation of Rac GTPase. *Molecular Cell* **15**: 117-127.

Devi TS, Hosoya K, Terasaki T, Singh LP (2013). Critical role of TXNIP in oxidative stress, DNA damage and retinal pericyte apoptosis under high glucose: implications for diabetic retinopathy. *Experimental Eye Research* **319**: 1001-1012.

DiGiusto DL, Krishnan A, Li L, Li H, Li S, Rao A, Mi S, Yam P, Stinson S, Kalos M, Alvarnas J, Lacey SF, Yee JK, Li M, Couture L, Hsu D, Forman SJ, Rossi JJ, Zaia JA (2010). RNA-based gene therapy for HIV with lentiviral vector-modified CD34(+) cells in patients undergoing transplantation for AIDS-related lymphoma. *Science Translational Medicine* **2**: 36ra43.

Dong A, Shen J, Krause M, Hackett SF, Campochiaro PA (2007). Increased expression of glial cell line-derived neurotrophic factor protects against oxidative damage-induced retinal degeneration. *Journal of Neurochemistry* **103**: 1041-1052.

Doonan F, Groeger G, Cotter TG (2012). Preventing retinal apoptosis--is there a common therapeutic theme? *Experimental Eye Research* **318**: 1278-1284.

Dorn JD, Ahuja AK, Caspi A, da Cruz L, Dagnelie G, Sahel JA, Greenberg RJ, McMahon MJ; Argus II Study Group (2013). The Detection of Motion by Blind Subjects With the Epiretinal 60-Electrode (Argus II) Retinal Prosthesis. *JAMA Ophthalmology* **131**: 183-189.

Doroudchi MM, Greenberg KP, Liu J, Silka KA, Boyden ES, Lockridge JA, Arman AC, Janani R, Boye SE, Boye SL, Gordon GM, Matteo BC, Sampath AP, Hauswirth WW, Horsager A (2011). Virally delivered channelrhodopsin-2 safely and effectively restores visual function in multiple mouse models of blindness. *Molecular Therapy* **19**: 1220-1229.

Drittanti L, Jenny C, Poulard K, Samba A, Manceau P, Soria N, Vincent N, Danos O, Vega M (2001). Optimised helper virus-free production of high-quality adeno-associated virus vectors. *Journal of Gene Medicine* **3**: 59-71.

Duarte S, Carle G, Faneca H, de Lima MC, Pierrefite-Carle V (2012). Suicide gene therapy in cancer: where do we stand now? *Cancer Letters* **324**: 160-170.

Dudus L, Anand V, Acland GM, Chen SJ, Wilson JM, Fisher KJ, Maguire AM, Bennett J (1999). Persistent transgene product in retina, optic nerve and brain after intraocular injection of rAAV. *Vision Research* **39**: 2545-2553.

Elbashir SM, Harborth J, Lendeckel W, Yalcin A, Weber K, Tuschl T (2001). Duplexes of 21-nucleotide RNAs mediate RNA interference in cultured mammalian cells. *Nature* **411**: 494-498.

Emerit J, Edeas M, Bricaire F (2004).Neurodegenrative diseases and oxidative stress. *Biomedicine & Pharmocotherapy* **58**: 39-46.

Ethen CM, Reilly C, Feng X, Olsen TW, Ferrington DA (2007). Age-related macular degeneration and retinal protein modification by 4-hydroxy-2-nonenal. *Investigative Ophthalmology and Visual Science* **48**: 3469-3479.

Fan LM, Teng L, Li JM (2009). Knockout of p47 phox uncovers a critical role of p40 phox in reactive oxygen species production in microvascular endothelial cells. Arterioslerosis, *Thrombosis and Vascular Biology* **29**: 1651-1656.

Farjo R, Skaggs J, Quiambao AB, Cooper MJ, Naash MI (2006). Efficient non-viral ocular gene transfer with compacted DNA nanoparticles. *PLoS One* **20**: e38.

Farrar GJ, Geraghty MT, Moloney JM, McConnell DJ, Humphries P (1988). Linkage analysis of X linked retinitis pigmentosa in the Irish population. *Journal of Medical Genetics* **25**: 222-226.

Farrar GJ, McWilliam P, Bradley DG, Kenna P, Lawler M, Sharp EM, Humphries MM, Eiberg H, Conneally PM, Trofatter JA, Humphries P (1990). Autosomal dominant retinitis pigmentosa: linkage to rhodopsin and evidence for genetic heterogeneity. *Genomics* **8**: 35-40.

Farrar GJ, Kenna P, Jordan SA, Kumar-Singh R, Humphries MM, Sharp EM, Sheils DM, Humphries P (1991). A three-base-pair deletion in the peripherin-RDS gene in one form of retinitis pigmentosa. *Nature* **354**: 478-480.

Farrar GJ, Kenna PF, Humphries P (2002). On the genetics of retinitis pigmentosa and on mutation-independent approaches to therapeutic intervention. *EMBO Journal* **21**: 857-864.

Farrar GJ, Millington-Ward S, Chadderton N, Humphries P, Kenna PF (2012). Gene-based therapies for dominantly inherited retinopathies. *Gene Therapy* **19**: 137-144.

Fei Y (2003). Development of the cone photoreceptor mosaic in the mouse retina revealed by fluorescent cones in transgenic mice. *Molecular Vision* **9**: 31-42.

Fernández D, Horrillo A, Alquezar C, González-Manchón C, Parrilla R, Ayuso MS (2013). Control of cell adhesion and migration by podocalyxin. Implication of Rac1 and Cdc42. *Biochemical and Biophysical Research Communications* **432**: 302-307.

Ferrari S, Di Iorio E, Barbaro V, Ponzin D, Sorrentino FS, Parmeggiani F (2011). Retinitis pigmentosa: genes and disease mechanisms. *Current Genomics* **12**: 238-249.

Fetoni AR, De Bartolo P, Eramo SL, Rolesi R, Paciello F, Bergamini C, Fato R, Paludetti G, Petrosini L, Troiani D (2013). Noise-induced hearing loss (NIHL) as a target of oxidative stress-mediated damage: cochlear and cortical responses after an increase in antioxidant defense. *The Journal of Neuroscience* **33**: 4011-4023.

Fire A, Albertson D, Harrison SW, Moerman DG (1991). Production of antisense RNA leads to effective and specific inhibition of gene expression in *Caenorhabditis elegans muscle*. *Development* **113**: 503-514.

Fire A, Xu S, Montgomery MK, Kostas SA, Driver SE, Mello CC (1998). Potent and specific genetic interference by double stranded RNA in *Caenorhabditis elegans*. *Nature* **391**: 806-811.

Ford KJ, Feller MB (2012). Assembly and disassembly of a retinal cholinergic network. *Visual Neuroscience* **29**: 61-71.

Fukai T, Ushio-Fukai M (2011). Superoxide dismutases: role in redox signaling, vascular function, and diseases. *Antioxidants and Redox Signalling* **15**: 1583-1606.

Gal A, Li Y, Thompson DA, Weir J, Orth U, Jacobson SG, Apfelstedt-Sylla E, Vollrath D (2000). Mutations in MERTK, the human orthologue of the RCS rat retinal dystrophy gene, cause retinitis pigmentosa. *Nature Genetics* **26**: 270-271.

Gane EJ, Weilert F, Orr DW, Keogh GF, Gibson M, Lockhart MM, Frampton CM, Taylor KM, Smith RA, Murphy MP (2010). The mitochondria-targeted anti-oxidant mitoquinone decreases liver damage in a phase II study of hepatitis C patients. *Liver International* **30**: 1019-1026.

Garg SJ, Federman J (2013). Optogenetics, visual prosthesis and electrostimulation for retinal dystrophies. *Current Opinion in Ophthalmology* **24**: 407-414.

Glaus E, Schmid F, Da Costa R, Berger W, Neidhardt J (2011). Gene therapeutic approach using mutation-adapted U1 snRNA to correct a RPGR splice defect in patient-derived cells. *Molecular Therapy* **19**: 936-941.

Godinho BM, Ogier JR, Darcy R, O'Driscoll CM, Cryan JF (2013). Self-assembling modified β-cyclodextrin nanoparticles as neuronal siRNA delivery vectors: focus on Huntington's disease. *Molecular Pharmaceutics* **10**: 640-649.

Goldblum D, Kipfer-Kauer A, Sarra GM, Wolf S, Frueh BE (2007).Distribution of Amyloid precursor protein and Amyloid-beta Immunoreactivity in DBA/2J Glaucomatous Mouse Retinas. *Investigative Ophthalmology and Visual Science* **11**: 5085–5090.

Gonzalez-Cordero A, West EL, Pearson RA, Duran Y, Carvalho LS, Chu CJ, Naeem A, Blackford SJ, Georgiadis A, Lakowski J, Hubank M, Smith AJ, Bainbridge JW, Sowden JC, Ali RR (2013). Photoreceptor precursors derived from three-dimensional embryonic stem cell cultures integrate and mature within adult degenerate retina. *Nature Biotechnology* **31**: 741-747.

Gorbatyuk M, Justilien V, Liu J, Hauswirth WW, Lewin AS (2007). Suppression of mouse rhodopsin expression in vivo by AAV mediated siRNA delivery. *Vision Research* **47**: 1202-1208.

Gorbatyuk MS, Knox T, LaVail MM, Gorbatyuk OS, Noorwez SM, Hauswirth WW, Lin JH, Muzyczka N, Lewin AS (2010). Restoration of visual function in P23H rhodopsin transgenic rats by gene delivery of BiP/Grp78. *Proceedings of the National Academy of Sciences* USA **107**: 5961-5966.

Grimm D, Wang L, Lee JS, Schürmann N, Gu S, Börner K, Storm TA, Kay MA (2010). Argonaute proteins are key determinants of RNAi efficacy, toxicity, and persistence in the adult mouse liver. *The Journal of Clinical Investigation* **120**: 3106-3119.

Groeger G, Mackey AM, Pettigrew CA, Bhatt L, Cotter TG (2009). Stress-induced activation of Nox contributes to cell survival signalling via production of hydrogen peroxide. *Journal of Neurochemistry* **109**: 1544-1554.

Grüter O, Kostic C, Crippa SV, Perez MT, Zografos L, Schorderet DF, Munier FL, Arsenijevic Y (2010). Lentiviral vector-mediated gene transfer in adult mouse photoreceptors is impaired by the presence of a physical barrier. *Gene Therapy* **12**: 942-947.

Guilluy C, Garcia-Mata R, Burridge K (2011). Rho protein crosstalk: another social network? *Trends in Cell Biology 21*: 718-726.

Hamel C (2006). Retinitis Pigmentosa. *Orphanet Journal of Rare Diseases* **1**: 40-52.

Harper SQ, Staber PD, He X, Eliason SL, Martins IH, Mao Q, Yang L, Kotin RM, Paulson HL, Davidson BL (2005). RNA interference improves motor and neuropathological abnormalities in a Huntington's disease mouse model. *Proceedings of the National Academy of Sciences USA* **102**: 5820-5825.

Hartong DT, Berson EL, Dryja TP (2006). Retinitis Pigmentosa. *Lancet* **368**: 1795-1809.

Haruta M, Bush RA, Kjellstrom S, Vijayasarathy C, Zeng Y, Le YZ, Sieving PA (2009). Depleting Rac1 in mouse rod photoreceptors protects them from photo-oxidative stress without affecting their structure or function. *Proceedings of the National Academy of Sciences of the USA* **106**: 9397-9402.

Harzand A, Tamariz L, Hare JM (2012). Uric acid, heart failure survival, and the impact of xanthine oxidase inhibition. *Congestive Heart Failure* **18**: 179-182.

Hashimoto T, Gibbs D, Lillo C, Azarian SM, Legacki E, Zhang XM, Yang XJ, Williams DS (2007). Lentiviral gene replacement therapy of retinas in a mouse model for Usher syndrome type 1B. *Gene Therapy* **14**: 584-594.

Hauswirth WW, Aleman TS, Kaushal S, Cideciyan AV, Schwartz SB, Wang L, Conlon TJ, Boye SL, Flotte TR, Byrne BJ, Jacobson SG (2008). Treatment of leber congenital amaurosis due to RPE65 mutations by ocular subretinal injection of adeno-associated virus gene vector: short-term results of a phase I trial. *Human Gene Therapy* **19**: 979-990.

He M, Pan H, Xiao C, Pu M (2013). Roles for redox signaling by NADPH oxidase in hyperglycemia-induced heme oxygenase-1 expression in the diabetic retina. *Investigative Ophthalmology and Visual Science* doi: 10.1167.

Heynen SR, Tanimoto N, Joly S, Seeliger MW, Samardzija M, Grimm C (2011). Retinal degeneration modulates intracellular localization of CDC42 in photoreceptors. *Molecular Vision* **17**: 2934-2946.

Hicks D, Molday RS (1986). Differential immunogold-dextran labeling of bovine and frog rod and cone cells using monoclonal antibodies against bovine rhodopsin. *Experimental Eye Research* **42**: 55-71.

Hoggan MD, Blacklow NR, Rowe WP (1966). Studies of small DNA viruses found in various adenovirus preparations: physical, biological, and immunological characteristics. *Proceedings of the National Academy of Sciences USA* **55**: 1467-1474.

Holmgren A, Lu J (2010). Thioredoxin and thioredoxin reductase: current research with special reference to human disease. *Biochemical and Biophysical Research Communications* **21**: 120-124.

Hornung V, Guenthner-Biller M, Bourquin C, Ablasser A, Schlee M, Uematsu S, Noronha A, Manoharan M, Akira S, de Fougerolles A, Endres S, Hartmann G (2005). Sequence-specific potent induction of IFN-alpha by short interfering RNA in plasmacytoid dendritic cells through TLR7. *Nature Medicine* **11**: 263-270.

Hosoya K, Tachikawa M (2012). The inner blood-retinal barrier: molecular structure and transport biology. *Advances in Experimental Biology and Medicine* **763**: 85-104.

Huber G, Heynen S, Imsand C, vom Hagen F, Muehlfriedel R, Tanimoto N, Feng Y, Hammes HP, Grimm C, Peichl L, Seeliger MW, Beck SC (2010). Novel rodent models for macular research. PLoS One 5: e13403.

Humphries MM, Rancourt D, Farrar GJ, Kenna P, Hazel M, Bush RA, Sieving PA, Sheils DM, McNally N, Creighton P, Erven A, Boros A, Gulya K, Capecchi MR, Humphries P (1997). Retinopathy induced in mice by targeted disruption of the rhodopsin gene. *Nature Genetics* **15**: 216-219.

Imai S, Shimazawa M, Nakanishi T, Tsuruma K, Hara H (2010). Calpain inhibitor protects cells against light-induced retinal degeneration. *Journal of Pharamacology and Experimental Therapeutics* **335**: 645-652.

Inomata Y, Nakamura H, Tanito M, Teratani A, Kawaji T, Kondo N, Yodoi J, Tanihara H (2006). Thioredoxin inhibits NMDA-induced neurotoxicity in the rat retina. *Journal of Neurochemistry* **98**: 372-385.

Jackson AL, Bartz SR, Schelter J, Kobayashi SV, Burchard J, Mao M, Li B, Cavet G, Linsley PS (2003). Expression profiling reveals off-target gene regulation by RNAi. *Nature Biotechnology* **21**: 635-637.

Jacobson SG, Sumaroka A, Luo X, Cideciyan AV (2013). Retinal optogenetic therapies: clinical criteria for candidacy. *Clinical Genetics* **84**: 175-182.

Jacobson SG, Acland GM, Aguirre GD, Aleman TS, Schwartz SB, Cideciyan AV, Zeiss CJ, Komaromy AM, Kaushal S, Roman AJ, Windsor EA, Sumaroka A, Pearce-Kelling SE, Conlon TJ, Chiodo VA, Boye SL, Flotte TR, Maguire AM, Bennett J, Hauswirth WW (2006). Safety of recombinant adeno-associated virus type 2-RPE65 vector delivered by ocular subretinal injection. *Molecular Therapy* **13**: 1074-1084.

Jaeschke H, Woolbright BL (2012). Current strategies to minimize hepatic ischemia-reperfusion injury by targeting reactive oxygen species. *Transplant Reviews* **26**: 103-114.

Jiang L, Li TZ, Boye SE, Hauswirth WW, Frederick JM, Baehr W (2013). RNAi-mediated gene suppression in a GCAP1(L151F) cone-rod dystrophy mouse model. *PLoS One* **8**: e57676.

Johnson CJ, Berglin L, Chrenek MA, Redmond TM, Boatright JH, Nickerson JM (2008). Technical brief: subretinal injection and electroporation into adult mouse eyes. *Molecular Vision* **14**: 2211-2226.

Jones BJ, Roberts DJ (1968). The quantiative measurement of motor inco-ordination in naive mice using an acelerating rotarod. *Journal of Pharmacy and Pharmacology* **20**: 302-304.

Judge A, MacLachlan I (2008). Overcoming the innate immune response to small interfering RNA. *Human Gene Therapy* **19**: 111-124.

Judge AD, Sood V, Shaw JR, Fang D, McClintock K, MacLachlan I (2005). Sequence-dependent stimulation of the mammalian innate immune response by synthetic siRNA. *Nature Biotechnology* **23**: 457-462.

Jurk M, Chikh G, Schulte B, Kritzler A, Richardt-Pargmann D, Lampron C, Luu R, Krieg AM, Vicari AP, Vollmer J (2011). Immunostimulatory potential of silencing RNAs can be mediated by a non-uridine-rich toll-like receptor 7 motif. *Nucleic Acids Research* **21**: 201-214.

Kachi S, Oshima Y, Esumi N, Kachi M, Rogers B, Zack DJ, Campochiaro PA (2005). Nonviral ocular gene transfer. *Gene Therapy* **12**: 843-851.

Kajiwara K, Berson EL, Dryja TP (1994). Digenic retinitis pigmentosa due to mutations at the unlinked peripherin/RDS and ROM1 loci. *Science* **264**: 1604-1608.

Karikó K, Bhuyan P, Capodici J, Weissman D (2004). Small interfering RNAs mediate sequence-independent gene suppression and induce immune activation by signaling through toll-like receptor 3. *Journal of Immunology* **172**: 6545-6549.

Kauper K, McGovern C, Sherman S, Heatherton P, Rapoza R, Stabila P, Dean B, Lee A, Borges S, Bouchard B, Tao W (2012). Two-year intraocular delivery of ciliary neurotrophic factor by encapsulated cell technology implants in patients with chronic retinal degenerative diseases. *Investigative Ophthalmology and Visual Science* **53**: 7484-7491.

Kaur J, Mencl S, Sahaboglu A, Farinelli P, van Veen T, Zrenner E, Ekström P, Paquet-Durand F, Arango-Gonzalez B (2011). Calpain and PARP activation during photoreceptor cell death in P23H and S334ter rhodopsin mutant rats. *PLoS One* **6**: e22181.

Kaiser PK, Symons RC, Shah SM, Quinlan EJ, Tabandeh H, Do DV, Reisen G, Lockridge JA, Short B, Guerciolini R, Nguyen QD (2010). RNAi-based treatment for neovascular age-related macular degeneration by Sirna-027. *American Journal of Ophthalmology* **150**: 33-39.

Kawakami S, Harada A, Sakanaka K, Nishida K, Nakamura J, Sakaeda T, Ichikawa N, Nakashima M, Sasaki H (2004). In vivo gene transfection via intravitreal injection of cationic liposome/plasmid DNA complexes in rabbits. *International Journal of Pharmaceutics* **278**: 255-262.

Kay MA, Manno CS, Ragni MV, Larson PJ, Couto LB, McClelland A, Glader B, Chew AJ, Tai SJ, Herzog RW, Arruda V, Johnson F, Scallan C, Skarsgard E, Flake AW, High KA (2000). Evidence for gene transfer and expression of factor IX in haemophilia B patients treated with an AAV vector. *Nature Genetics* **24**: 257-261.

Keeler CE (1947). Gene Therapy. *Journal of Heredity* **38**: 294-298.

Kefalov VJ (2012). Rod and cone visual pigments and phototransduction through pharmacological, genetic, and physiological approaches. *Journal of Biological Chemistry* **287**: 1635-1641.

Kiang AS, Palfi A, Ader M, Kenna PF, Millington-Ward S, Clark G, Kennan A, O'reilly M, Tam LC, Aherne A, McNally N, Humphries P, Farrar GJ (2005). Toward a gene therapy for dominant disease: validation of an RNA interference-based mutation-independent approach. *Molecular Therapy* **12**: 555-561.

Kleinman ME, Kaneko H, Cho WG, Dridi S, Fowler BJ, Blandford AD, Albuquerque RJ, Hirano Y, Terasaki H, Kondo M, Fujita T, Ambati BK, Tarallo V,

Gelfand BD, Bogdanovich S, Baffi JZ, Ambati J (2012). Short-interfering RNAs induce retinal degeneration via TLR3 and IRF3. *Molecular Therapy* **20**: 101-108.

Kleyn PW, Fan W, Kovats SG, Lee JJ, Pulido JC, Wu Y, Berkemeier LR, Misumi DJ, Holmgren L, Charlat O, Woolf EA, Tayber O, Brody T, Shu P, Hawkins F, Kennedy B, Baldini L, Ebeling C, Alperin GD, Deeds J, Lakey ND, Culpepper J, Chen H, Glücksmann-Kuis MA, Carlson GA, Duyk GM, Moore KJ (1996). Identification and characterization of the mouse obesity gene tubby: a member of a novel gene family. *Cell* **85**: 281-290.

Komeina K, Rogers BS, Lu L, Campochiaro PA (2006). Antioxidants reduce cone cell death in a model of Retinitis Pigmetosa. *Proceedings of the National Academy of Sciences USA* **103**: 11,300-11,305.

Komeima K, Usui S, Shen J, Rogers BS, Campochiaro PA (2008). Blockade of neuronal nitric oxide synthase reduces cone cell death in a model of retinitis pigmentosa. *Free Radical Biology and Medicine* **45**: 905-912.

Kong J, Kim SR, Binley K, Pata I, Doi K, Mannik J, Zernant-Rajang J, Kan O, Iqball S, Naylor S, Sparrow JR, Gouras P, Allikmets R (2008). Correction of the disease phenotype in the mouse model of Stargardt disease by lentiviral gene therapy. *Gene Therapy* **15**: 1311-1320.

Kong L, Zhou X, Li F, Yodoi J, McGinnis J, Cao W (2010). Neuroprotective effect of overexpression of thioredoxin on photoreceptor degeneration in Tubby mice. *Neurobiology of Disease* **38**: 446-455.

Kostic C, Crippa SV, Pignat V, Bemelmans AP, Samardzija M, Grimm C, Wenzel A, Arsenijevic Y (2011). Gene therapy regenerates protein expression in cone photoreceptors in Rpe65 (R91W/R91W) mice. *PLoS One* **3**: e16588.

Kostic C, Chiodini F, Salmon P, Wiznerowicz M, Deglon N, Hornfeld D, Trono D, Aebischer P, Schorderet DF, Munier FL, Arsenijevic Y (2003). Activity analysis of

housekeeping promoters using self-inactivating lentiviral vector delivery into the mouse retina. *Gene Therapy* **10**: 818-821.

Kowluru RA, Koppolu P, Chakrabarti S, Chen S (2003). Diabetes-induced activation of nuclear transcriptional factor in the retina, and its inhibition by antioxidants. *Free Radical Research* **37**: 1169-1180.

Kumar-Singh R, Bradley DG, Farrar GJ, Lawler M, Jordan SA, Humphries P (1991). Autosomal dominant retinitis pigmentosa: a new multi-allelic marker (D3S621) genetically linked to the disease locus (RP4). *Human Genetics* **86**: 502-504.

Kunte MM, Choudhury S, Manheim JF, Shinde VM, Miura M, Chiodo VA, Hauswirth WW, Gorbatyuk OS, Gorbatyuk MS (2012). ER stress is involved in T17M rhodopsin-induced retinal degeneration. *Investigative Ophthalmology and Visual Science* **20**: 3792-3800.

Lamoke F, Ripandelli G, Webster S, Montemari A, Maraschi A, Martin P, Marcus DM, Liou GI, Bartoli M (2012). Loss of thioredoxin function in retinas of mice overexpressing amyloid β. *Free Radical Biology and Medicine* **53**: 577-588.

Laurent TC, Moore EC, Reichard P (1964). Enzymatic Synthesis of Deoxyribonucleotides: IV. Isolation and Characterisation of Thioredoxin, the Hydrogen donor from Escherichia coli B. *Journal of Biological Chemistry* **239**: 3436-3444.

Lebiedzinska M, Karkucinska-Wieckowska A, Wojtala A, Suski JM, Szabadkai G, Wilczynski G, Wlodarczyk J, Diogo CV, Oliveira PJ, Tauber J, Ježek P, Pronicki M, Duszynski J, Pinton P, Wieckowski MR (2012). Disrupted ATP synthase activity and mitochondrial hyperpolarisation-dependent oxidative stress is associated with p66Shc phosphorylation in fibroblasts of NARP patients. *International Journal of Biochemistry and Cell Biology*, http://dx.doi.org/10.1016/j.biocel.2012.07.020

Lee SY, Usui S, Zafar AB, Oveson BC, Jo YJ, Lu L, Masoudi S, Campochiaro PA (2011). N-Acetylcysteine promotes long-term survival of cones in a model of retinitis pigmentosa. *Journal of Cellular Physiology* **226**: 1843-1849.

Li J, Wang JJ, Yu Q, Chen K, Mahadev K, Zhang SX (2010b). Inhibition of reactive oxygen species by Lovastatin downregulates vascular endothelial growth factor expression and ameliorates blood-retinal barrier breakdown in db/db mice: role of NADPH oxidase 4. *Diabetes* **59**: 1528-1538.

Li Q, Dinculescu A, Shan Z, Miller R, Pang J, Lewin AS, Raizada MK, Hauswirth WW (2008). Downregulation of p22phox in retinal pigment epithelial cells inhibits choroidal neovascularization in mice. *Molecular Therapy* **16**: 1688-1694.

Li T, Snyder WK, Olsson JE, Dryja TP (1996). Transgenic mice carrying the dominant rhodopsin mutation P347S: evidence for defective vectorial transport of rhodopsin to the outer segments. *Proceedings of the National Academy of Sciences USA* **93**: 14176-14181.

Li Y, Tao W, Luo L, Huang D, Kauper K, Stabila P, Lavail MM, Laties AM, Wen R (2010). CNTF induces regeneration of cone outer segments in a rat model of retinal degeneration. *PLoS One* **5**: e9495.

Li J, Li Y, Zhang M, Hu Z (2012). Silencing of Rac1 expression via RNA interference inhibits retinal neovascularization in rats. *Molecular Vision* **18**: 1354-1360.

Liang FQ, Aleman TS, Dejneka NS, Dudus L, Fisher KJ, Maguire AM, Jacobson SG, Bennett J (2001). Long-term protection of retinal structure but not function using RAAV.CNTF in animal models of retinitis pigmentosa. *Molecular Therapy* **4**: 461-472.

Liao HW, Yau KW (2007). In vivo gene delivery in the retina using polyethylenimine. *BioTechniques* **42**: 285-288.

Lin CS, Sharpley MS, Fan W, Waymire KG, Sadun AA, Carelli V, Ross-Cisneros FN, Baciu P, Sung E, McManus MJ, Pan BX, Gil DW, Macgregor GR, Wallace DC (2012). Mouse mtDNA mutant model of Leber hereditary optic neuropathy. *Proceedings of the National Academy of Sciences USA* **109**: 20065-20070.

Liu Y, Tang L, Chen B (2012). Effects of antioxidant gene therapy on retinal neurons and oxidative stress in a model of retinal ischemia/reperfusion. *Free Radical Biology and Medicine* **52**: 909-915.

Liu Y, Li Y, Yu S, Zhao G (2012). Recent advances in the development of thioredoxin reductase inhibitors as anticancer agents. *Current Drug Targets* **13**: 1432-1444.

Lorenzetto E, Ettorre M, Pontelli V, Bolomini-Vittori M, Bolognin S, Zorzan S, Laudanna C, Buffelli M (2013). Rac1 selective activation improves retina ganglion cell survival and regeneration. *PLoS One* **8**: e64350.

Loscher CJ, Hokamp K, Kenna PF, Ivens AC, Humphries P, Palfi A, Farrar GJ (2007). Altered retinal microRNA expression profile in a mouse model of retinitis pigmentosa. *Genome Biology* **8**: R248.

Lu L, Oveson BC, Jo YJ, Lauer TW, Usui S, Komeima K, Xie B, Campochiaro PA (2009). Increased expression of glutathione peroxidase 4 strongly protects retina from oxidative damage. *Antioxidants and Redox Signalling* **11**: 715-724.

Lynch RE, Fridovich I (1978). Permeation of the erythrocyte stroma by superoxide radical. *Journal of Biological Chemistry* **253**: 4697-4699.

Maclachlan TK, Lukason M, Collins M, Munger R, Isenberger E, Rogers C, Malatos S, Dufresne E, Morris J, Calcedo R, Veres G, Scaria A, Andrews L, Wadsworth S (2011). Preclinical safety evaluation of AAV2-sFLT01- a gene therapy for age-related macular degeneration. *Molecular Therapy* **19**: 326-334.

Maguire AM, Simonelli F, Pierce EA, Pugh EN Jr, Mingozzi F, Bennicelli J, Banfi S, Marshall KA, Testa F, Surace EM, Rossi S, Lyubarsky A, Arruda VR, Konkle B, Stone E, Sun J, Jacobs J, Dell'Osso L, Hertle R, Ma JX, Redmond TM, Zhu X, Hauck B, Zelenaia O, Shindler KS, Maguire MG, Wright JF, Volpe NJ, McDonnell JW, Auricchio A, High KA, Bennett J (2008). Safety and efficacy of gene transfer for Leber's congenital amaurosis. *New England Journal of Medicine* **358**: 2240-2248.

Maguire AM, High KA, Auricchio A, Wright JF, Pierce EA, Testa F, Mingozzi F, Bennicelli JL, Ying GS, Rossi S, Fulton A, Marshall KA, Banfi S, Chung DC, Morgan JI, Hauck B, Zelenaia O, Zhu X, Raffini L, Coppieters F, De Baere E, Shindler KS, Volpe NJ, Surace EM, Acerra C, Lyubarsky A, Redmond TM, Stone E, Sun J, McDonnell JW, Leroy BP, Simonelli F, Bennett J (2009). Age-dependent effects of RPE65 gene therapy for Leber's congenital amaurosis: a phase 1 dose-escalation trial. *Lancet* **374**: 1597-1605.

Malhotra JD, Miao H, Zhang K, Wolfson A, Pennathur S, Pipe SW, Kaufman RJ (2008). Antioxidants reduce endoplasmic reticulum stress and improve protein secretion. *Proceedings of the National Academy of Sciences of the USA* **105**: 18525-18530.

Mandal MN, Patlolla JM, Zheng L, Agbaga MP, Tran JT, Wicker L, Kasus-Jacobi A, Elliott MH, Rao CV, Anderson RE (2009). Curcumin protects retinal cells from light-and oxidant stress-induced cell death. *Free Radical Biology and Medicine* **46**: 672-679.

Mao Y, Finneman SC (2012). Essential diurnal Rac1 activation during retinal phagocytosis requires αvβ5 integrin but not tyrosine kinases focal adhesion kinase or Mer tyrosine kinase. *Molecuclar Biology of the Cell* **23**: 1104-1114.

Marano RJ, Toth I, Wimmer N, Brankov M, Rakoczy PE (2005). Dendrimer delivery of an anti-VEGF oligonucleotide into the eye: a long-term study into inhibition of laser-induced CNV, distribution, uptake and toxicity. *Gene Therapy* **12**: 1544-1550.

Martin KR, Klein RL, Quigley HA (2002). Gene delivery to the eye using adeno-associated viral vectors. *Methods* **28**: 267-275.

Martínez T, Wright N, López-Fraga M, Jiménez AI, Pañeda C (2013). Silencing human genetic diseases with oligonucleotide-based therapies. *Human Genetics* **132**: 481-493.

Masuda I, Matsuo T, Yasuda T, Matsuo N (1996). Gene transfer with liposomes to the intraocular tissues by different routes of administration. *Investigative Ophthalmology and Visual Science* **37**: 1914-1920.

Matsuda T, Cepko CL (2004). Electroporation and RNA interference in the rodent retina in vivo and in vitro. *Proceedings of the National Academy of Sciences USA* **101**: 16-22.

Matsui M, Oshima M, Oshima H, Takaku K, Maruyama T, Yodoi J, Taketo MM (1996). Early embryonic lethality caused by targeted disruption of the mouse thioredoxin gene. *Developmental Biology* **178**: 179-185.

Mattson MP (2009). Roles of the Lipid Peroxidation Product 4-Hydroxynonenal in Obesity, the Metabolic Syndrome, and Associated Vascular and Neurodegenerative Disorders. *Experimental Gerontology* **44**: 625-633.

McClements ME, MacLaren RE (2013). Gene therapy for retinal disease. *Translational Research* **161**: 241-254.

Meuillet EJ, Mahadevan D, Berggren M, Coon A, Powis G (2004). Thioredoxin-1 binds to the C2 domain of PTEN inhibiting PTEN's lipid phosphatase activity and membrane binding: a mechanism for the functional loss of PTEN's tumor suppressor activity. *Archives of Biochemistry and Biophysics* **429**: 123-133.

Milam AH, Li ZY, Fariss RN (1998). Histopathology of the human retina in retinitis pigmentosa. *Progress in Retinal and Eye Research* **17**: 175-205.

Millington-Ward S, Chadderton N, O'Reilly M, Palfi A, Goldmann T, Kilty C, Humphries M, Wolfrum U, Bennett J, Humphries P, Kenna PF, Farrar GJ (2011). Suppression and replacement gene therapy for autosomal dominant disease in a murine model of dominant retinitis pigmentosa. *Molecular Therapy* **19**: 642-649.

Mitchell DC, Bryan BA, Liu JP, Liu WB, Zhang L, Qu J, Zhou X, Liu M, Li DW (2007). Developmental expression of three small GTPases in the mouse eye. *Molecular Vision* **13**: 1144-1153.

Mitsushima M, Toyoshima F, Nishida E (2009). Dual role of Cdc42 in spindle orientation control of adherent cells. *Molecular and Cellular Biology* **29**: 2816-2827.

Miyano K, Sumimoto H (2007). Role of the small GTPase Rac in $p22^{phox}$ dependent NADPH oxidases. *Biochimie* **89**: 1133-1144.

Mohr SE, Perrimon N (2012). RNAi screening: new approaches, understandings, and organisms. *Wiley Interdisciplinary Reviews RNA* **3**: 145-158.

Mukhopadhyay S, Jackson PK (2013). Cilia, tubby mice, and obesity. *Cilia* 2:1.

Mukhopadhyay P, Rajesh M, Yoshihiro K, Haskó G, Pacher P (2007). Simple quantitative detection of mitochondrial superoxide production in live cells. *Biochemical and Biophysical Research Communications* **358**: 203-208.

Muller FL, Lustgarten MS, Jang Y, Richardson A, Van Remmen H (2007). Trends in oxidative aging theories. *Free Radical Biology and Medicine* **43**: 477-503.

Mumbengegwi DR, Li Q, Li C, Bear CE, Engelhardt JF (2008). Evidence for a superoxide permeability pathway in endosomal membranes. *Molecular and Cellular Biology* **28**: 3700-3712.

Munemasa Y, Kwong JM, Kim SH, Ahn JH, Caprioli J, Piri N (2010). Thioredoxins 1 and 2 protect retinal ganglion cells from pharmacologically induced oxidative stress, optic nerve transection and ocular hypertension. *Advances in Experimental Medicine and Biology* **664**: 355-363.

Murakami Y, Ikeda Y, Yoshida N, Notomi S, Hisatomi T, Oka S, De Luca G, Yonemitsu Y, Bignami M, Nakabeppu Y, Ishibashi T (2012). MutT Homolog-1 Attenuates Oxidative DNA Damage and Delays Photoreceptor Cell Death in Inherited Retinal Degeneration. *The American Journal of Pathology* **181**: 1378-1386.

Murata M, Fukushima K, Takao T, Seki H, Takeda S, Wake N (2012). Oxidative Stress Produced by Xanthine Oxidase Induces Apoptosis in Human Extravillous Trophoblast Cells. *The Journal of Reproduction and Development* epub: September 14.

Mussolino C, della Corte M, Rossi S, Viola F, Di Vicino U, Marrocco E, Neglia S, Doria M, Testa F, Giovannoni R, Crasta M, Giunti M, Villani E, Lavitrano M, Bacci ML, Ratiglia R, Simonelli F, Auricchio A, Surace EM (2011). AAV-mediated photoreceptor transduction of the pig cone-enriched retina. *Gene Therapy* **18**: 637-645.

Mustafi D, Engel AH, Palczewski (2009). Structure of cone photoreceptors. *Progress in Retinal and Eye Research* **28**: 289-302.

Nag TC, Wadhwa S, Alladi PA, Sanyal T (2011). Localization of 4-hydroxy 2-nonenal immunoreactivity in aging human retinal Müller cells. *Annals of Anatomy* **193**: 205-210.

Nakamura H, Hoshino Y, Okuyama H, Matsuo Y, Yodoi J (2009). Thioredoxin 1 delivery as new therapeutics. *Advanced Drug Delivery Reviews* **61**: 303-309.

Napoli C, Lemieux C, Jorgensen R (1990). Introduction of a chimeric chalcone synthase gene into petunia results in reversible co-suppression of homologouse genes in trans. *Plant Cell* **2**: 279-289.

Nathwani AC, Tuddenham EG, Rangarajan S, Rosales C, McIntosh J, Linch DC, Chowdary P, Riddell A, Pie AJ, Harrington C, O'Beirne J, Smith K, Pasi J, Glader B, Rustagi P, Ng CY, Kay MA, Zhou J, Spence Y, Morton CL, Allay J, Coleman J, Sleep S, Cunningham JM, Srivastava D, Basner-Tschakarjan E, Mingozzi F, High KA, Gray JT, Reiss UM, Nienhuis AW, Davidoff AM (2011). Adenovirus-associated virus vector-mediated gene transfer in hemophilia B. *The New England Journal of Medicine* **365**: 2357-2365.

Natkunarajah M, Trittibach P, McIntosh J, Duran Y, Barker SE, Smith AJ, Nathwani AC, Ali RR (2008). Assessment of ocular transduction using single-stranded and self-complementary recombinant adeno-associated virus serotype 2/8. *Gene Therapy* **15**: 463-467.

Nielsen CB, Shomron N, Sandberg R, Hornstein E, Kitzman J, Burge CB (2007). Determinants of targeting by endogenous and exogenous microRNAs and siRNAs. *RNA* **13**: 1894-1910.

Noben-Trauth K, Naggert JK, North MA, Nishina PM (1996). A candidate gene for the mouse mutation tubby. *Nature* **380**: 534-538.

Nonnemacher M, Weber T (2012). Intracellular transport of recombinant adeno-associated virus vectors. *Gene Therapy* **19**: 649-658.

Obolensky A, Berenshtein E, Lederman M, Bulvik B, Alper-Pinus R, Yaul R, Deleon E, Chowers I, Chevion M, Banin E (2011). Zinc-desferrioxamine attenuates retinal degeneration in the rd10 mouse model of retinitis pigmentosa. *Free Radical Biology and Medicine* **51**: 1482-1491.

Oblander SA, Brady-Kalnay SM (2010). Distinct PTPmu-associated signaling molecules differentially regulate neurite outgrowth on E-, N-, and R-cadherin. *Molecular and Cellular Neurosciences* **44**: 78-93.

O'Driscoll C, Doonan F, Sanvicens N, Messeguer A, Cotter TG (2011). A novel free radical scavenger rescues retinal cells *in vivo*. *Experimental Eye Research* **93**: 65-74.

Ohnaka M, Miki K, Gong YY, Stevens R, Iwase T, Hackett SF, Campochiaro PA (2012). Long-term expression of glial cell line-derived neurotrophic factor slows, but does not stop retinal degeneration in a model of retinitis pigmentosa. *Journal of Neurochemistry* **122**: 1047-1053.

Olsson JE, Gordon JW, Pawlyk BS, Roof D, Hayes A, Molday RS, Mukai S, Cowley GS, Berson EL, Dryja TP (1992). Transgenic mice with a rhodopsin mutation (Pro23His): a mouse model of autosomal dominant retinitis pigmentosa. *Neuron* **9**: 815-830.

O'Mahony AM, Godinho BM, Ogier J, Devocelle M, Darcy R, Cryan JF, O'Driscoll CM (2012). Click-modified cyclodextrins as nonviral vectors for neuronal siRNA delivery. *ACS Chemical Neuroscience* **3**: 744-752.

O'Mahony AM, Ogier J, Darcy R, Cryan JF, O'Driscoll CM (2013). Cationic and PEGylated Amphiphilic Cyclodextrins: Co-Formulation Opportunities for Neuronal Sirna Delivery. *PLoS One* **8**: e66413

Onyango AN (2012). Small reactive carbonyl compounds as tissue lipid peroxidation products; and the mechanisms of their formation thereby. *Chemistry and Physics of Lipids* **165**: 777-786.

O'Reilly M, Palfi A, Chadderton N, Millington-Ward S, Ader M, Cronin T, Tuohy T, Auricchio A, Hildinger M, Tivnan A, McNally N, Humphries MM, Kiang AS, Humphries P, Kenna PF, Farrar GJ (2007). RNA interference-mediated suppression

and replacement of human rhodopsin in vivo. *American Journal of Human Genetics* **81**: 127-135.

Padnick-Silver L, Kang Derwent JJ, Giuliano E, Narfström K, Linsenmeier RA. Retinal oxygenation and oxygen metabolism in Abyssinian cats with a hereditary retinal degeneration. *Investigative Ophthalmology and Visual Science* **47**: 3683-3689.

Palfi A, Chadderton N, McKee AG, Blanco Fernandez A, Humphries P, Kenna PF, Farrar GJ (2012). Efficacy of codelivery of dual AAV2/5 vectors in the murine retina and hippocampus. *Human Gene Therapy* **23**: 847-858.

Pang JJ, Chang B, Kumar A, Nusinowitz S, Noorwez SM, Li J, Rani A, Foster TC, Chiodo VA, Doyle T, Li H, Malhotra R, Teusner JT, McDowell JH, Min SH, Li Q, Kaushal S, Hauswirth WW (2006). Gene therapy restores vision-dependent behavior as well as retinal structure and function in a mouse model of RPE65 Leber congenital amaurosis. *Molecular Therapy* **13**: 565-572.

Park JS, Li YF, Bai Y (2007). Yeast NDI1 improves oxidative phosphorylation capacity and increases protection against oxidative stress and cell death in cells carrying a Leber's hereditary optic neuropathy mutation. *Biochimica et Biophysica Acta* **1772**: 533-542.

Peng YW, Zallocchi M, Wang WM, Delimont D, Cosgrove D (2011). Moderate light-induced degeneration of rod photoreceptors with delayed transducin translocation in shaker1 mice. *Investigative Ophthalmology and Visual Science* **52**: 6421-6427.

Petrs-Silva H, Dinculescu A, Li Q, Deng WT, Pang JJ, Min SH, Chiodo V, Neeley AW, Govindasamy L, Bennett A, Agbandje-McKenna M, Zhong L, Li B, Jayandharan GR, Srivastava A, Lewin AS, Hauswirth WW (2011). Novel properties of tyrosine-mutant AAV2 vectors in the mouse retina. *Molecular Therapy* **19**: 293-301.

Phillips MI (2012). Gene, Stem Cell, and Future Therapies for Orphan Diseases. *Clinical Pharmacology and Therapeutics* **92**: 182-192.

Punzo C, Xiong W, Cepko CL (2012). Loss of daylight vision in retinal degeneration: are oxidative stress and metabolic dysregulation to blame? *Journal of Biological Chemistry* **287**: 1642-1648.

Purves D, Augustine GS, Fitzpatrick D, Hall WC, La Mantia AS, McNamara JO, White LE (2008) Neuroscience, 4th edition. Sunderland Massachusetts. Sinauer Asssociates Inc.

Qi X, Cai J, Ruan Q, Liu L, Boye SL, Chen Z, Hauswirth WW, Ryals RC, Shaw L, Caballero S, Grant MB, Boulton ME (2012). γ-Secretase inhibition of murine choroidal neovascularization is associated with reduction of superoxide and proinflammatory cytokines. *Investigative Ophthalmology and Visual Science* **53**: 574-585.

Raden D, Hildebrandt S, Xu P, Bell E, Doyle FJ 3rd, Robinson AS (2005). Analysis of cellular response to protein overexpression. *IEE Proceedings-Systems Biology* **152**: 285-289.

Raffaello A, Rizzuto R (2011). Mitochondrial Longevity Pathways. *Biochima et Biophysica Acta* **1813**: 260-268.

Ralph GS, Radcliffe PA, Day DM, Carthy JM, Leroux MA, Lee DCP, Wong L, Bilsland LG, Greensmith L, Kingsman SM, Mitrophanous KA, Mazarakis ND, Azzouz M (2005). Silencing mutant SOD1 using RNAi protects against neurodegeneration and extends survival in an ALS model. *Nature Medicine* **11**: 429-433.

Ramsden CM, Powner MB, Carr AJ, Smart MJ, da Cruz L, Coffey PJ (2013). Stem cells in retinal regeneration: past, present and future. *Development* **140**: 2576-2585.

Rand TA, Petersen S, Du F, Wang X (2005). Argonaute2 cleaves the anti-guide strand of siRNA during RISC activation. *Cell* **123**: 621-629.

Rex TS, Tsui I, Hahn P, Maguire AM, Duan D, Bennett J, Dunaief JL (2004). Adenovirus-mediated delivery of catalase to retinal pigment epithelial cells protects neighboring photoreceptors from photo-oxidative stress. *Human Gene Therapy* **15**: 960-967.

Rezaie T, McKercher SR, Kosaka K, Seki M, Wheeler L, Viswanath V, Chun T, Joshi R, Valencia M, Sasaki S, Tozawa T, Satoh T, Lipton SA (2012). Protective effect of carnosic acid, a pro-electrophilic compound, in models of oxidative stress and light-induced retinal degeneration. *Investigative Ophthalmology and Visual Science* **53**: 7847-7854.

Roddy GW, Rosa RH Jr, Oh JY, Ylostalo JH, Bartosh TJ Jr, Choi H, Lee RH, Yasumura D, Ahern K, Nielsen G, Matthes MT, LaVail MM, Prockop DJ (2012). Stanniocalcin-1 rescued photoreceptor degeneration in two rat models of inherited retinal degeneration. *Molecular Therapy* **20**: 788-797.

Rogers BS, Symons RC, Komeima K, Shen J, Xiao W, Swaim ME, Gong YY, Kachi S, Campochiaro PA (2007). Differential sensitivity of cones to iron-mediated oxidative damage. *Investigative Ophthalmology and Visual Science* **48**: 438-445.

Romano N, Macino G (1992). Quelling: transient inactivation of gene expression in Neurospora crassa by transformation with homologous sequences. *Molecular Microbiology* **6**: 3343-3353.

Rossmiller B, Mao H, Lewin AS (2012). Gene therapy in animal models of autosomal dominant retinitis pigmentosa. *Molecular Vision* **18**: 2479-2496.

Rothe G, Valet G (1990). Flow cytometric analysis of respiratory burst activity in phagocytes with hydroethidine and 2',7'-dichlorofluorescin. *Journal of Leukocyte Biology* **47**: 440-448.

Saari JC (2012). Vitamin A metabolism in rod and cone visual cycles. *Annual Review of Nutrition* **32**: 125-145.

Saitoh M, Nishitoh H, Fujii M, Takeda K, Tobiume K, Sawada Y, Kawabata M, Miyazono K, Ichijo H (1998). Mammalian thioredoxin is a direct inhibitor of apoptosis signal-regulating kinase (ASK) 1. *EMBO Journal* **17**: 2596-2606.

Saliba RS, Munro PMG, Luthert PJ, Cheetham ME (2002). The cellular fate of mutant rhodopsin: quality control, degradation and aggresome formation. *Journal of Cell Science* **115**: 2907-2918.

Salvador A, Sousa J, Pinto RE (2001). Hydroperoxyl, superoxide and pH gradients in the mitochondrial matrix: a theoretical assessment. *Free Radical Biology and Medicine* **31**: 1208-1215.

Sarra GM, Stephens C, Schlichtenbrede FC, Bainbridge JW, Thrasher AJ, Luthert PJ, Ali RR (2002). Kinetics of transgene expression in mouse retina following sub-retinal injection of recombinant adeno-associated virus. *Vision Research* **42**: 541-549.

Sasaki M, Ozawa Y, Kurihara T, Kubota S, Yuki K, Noda K, Kobayashi S, Ishida S, Tsubota K (2010). Neurodegenerative influence of oxidative stress in the retina of a murine model of diabetes. *Diabetologia* **52**: 971-979.

Scherr M, Venturini L, Battmer K, Schaller-Schoenitz M, Schaefer D, Dallmann I, Ganser A, Eder M (2007). Lentivirus-mediated antagomir expression for specific inhibition of miRNA function. *Nucleic Acids Research* **35**: e149.

Schmidt A, Hall A (2002). Guanine nucleotide exchange factors for Rho GTPases: turning on the switch. *Genes and Development* **16**: 1587-1609.

Segal AW, Jones AT, Webster D, Allison AC (1978). Absence of a newly described cytochrome b from neutrophils of patients with chronic granulomatous disease. *Lancet* **2**: 446-449.

Sen GL, Blau HM (2006). A brief history of RNAi: the silence of the genes. *FASEB Journal* **20**: 1293-1299.

Shan H, Ji D, Barnard AR, Lipinski DM, You Q, Lee EJ, Kamalden TA, Sun X, MacLaren RE (2011). AAV-mediated gene transfer of human X-linked inhibitor of apoptosis protects against oxidative cell death in human RPE cells. *Investigative Ophthalmology and Visual Science* **52**: 9591-9597.

Shen J, Yang X, Dong A, Petters RM, Peng YW, Wong F, Campochiaro PA (2005). Oxidative damage is a potential cause of cone cell death in retinitis pigmentosa. *Journal of Cellular Physiology* **203**: 457-464.

Sherry DM, Blackburn BA (2013). P-Rex2, a Rac-guanine nucleotide exchange factor, is expressed selectively in ribbon synaptic terminals of the mouse retina. *BMC Neuroscience* **14**: 70-84.

Shibuki H, Katai N, Yodoi J, Uchida K, Yoshimura N (2000). Lipid peroxidation and peroxynitrite in retinal ischemia-reperfusion injury. *Investigative Ophthalmology and Visual Science* **41**: 3607-3614.

Shinde VM, Sizova OS, Lin JH, LaVail MM, Gorbatyuk MS (2012). ER stress in retinal degeneration in S334ter Rho rats. *PLoS One* **7**: e33266.

Sieving PA, Caruso RC, Tao W, Coleman HR, Thompson DJ, Fullmer KR, Bush RA (2006). Ciliary neurotrophic factor (CNTF) for human retinal degeneration: phase I trial of CNTF delivered by encapsulated cell intraocular implants. *Proceedings of the National Academy of Sciences of the USA* **103**: 3896-3901.

Simonelli F, Maguire AM, Testa F, Pierce EA, Mingozzi F, Bennicelli JL, Rossi S, Marshall K, Banfi S, Surace EM, Sun J, Redmond TM, Zhu X, Shindler KS, Ying GS, Ziviello C, Acerra C, Wright JF, McDonnell JW, High KA, Bennett J, Auricchio A (2010). Gene therapy for Leber's congenital amaurosis is safe and

effective through 1.5 years after vector administration. *Molecular Therapy* **18**: 643-650.

Singer TP, Ramsay RR (1994). The reaction sites of rotenone and ubiquinone with mitochondrial NADH dehydrogenase. *Biochimica et Biophysica Acta* **1187**: 198-202.

Smith LEH, Wesolowski E, McLellan A, Kostyk SK, D'Amato R, Sullivan R, D'Amore PA (1993). Oxygen-Induced Retinopathy in the Mouse. *Investigative Ophthalmology and Visual Science* **35**: 101-111.

Smith RA. Murphy MP (2010). Animal and human studies with the mitochondria-targeted antioxidant MitoQ. Annals *of the New York Academy of Sciences* **1201**: 96-103.

Snow BJ, Rolfe FL, Lockhart MM, Frampton CM, O'Sullivan JD, Fung V, Smith RA, Murphy MP, Taylor KM; Protect Study Group (2010). A double-blind, placebo-controlled study to assess the mitochondria-targeted antioxidant MitoQ as a disease-modifying therapy in Parkinson's disease. *Movement Disorders* **25**: 1670-1674.

Sohocki MM, Daiger SP, Bowne SJ, Rodriquez JA, Northrup H, Heckenlively JR, Birch DG, Mintz-Hittner H, Ruiz RS, Lewis RA, Saperstein DA, Sullivan LS (2001). Prevalence of mutations causing retinitis pigmentosa and other inherited retinopathies. *Human Mutation* **17**: 42-51.

Sopko R, Huang D, Preston N, Chua G, Papp B, Kafadar K, Snyder M, Oliver SG, Cyert M, Hughes TR, Boone C, Andrews B (2006). Mapping pathways and phenotypes by systematic gene overexpression. *Molecular Cell* **21**: 319-330.

Souied EH, Reid SN, Piri NI, Lerner LE, Nusinowitz S, Farber DB (2008). Non-invasive gene transfer by iontophoresis for therapy of an inherited retinal degeneration. *Experimental Eye Research* **87**: 168-175.

Stevenson L, Matesanz N, Colhoun L, Edgar K, Devine A, Gardiner TA, McDonald DM (2010). Reduced nitro-oxidative stress and neural cell death suggests a protective role for microglial cells in TNFalpha-/- mice in ischemic retinopathy. *Investigative Ophthalmology and Visual Science* **51**: 3291-3299.

Stieger K, Colle MA, Dubreil L, Mendes-Madeira A, Weber M, Le Meur G, Deschamps JY, Provost N, Nivard D, Cherel Y, Moullier P, Rolling F (2008). Subretinal delivery of recombinant AAV serotype 8 vector in dogs results in gene transfer to neurons in the brain. *Molecular Therapy* **16**: 916-923.

Stieger K, Schroeder J, Provost N, Mendes-Madeira A, Belbellaa B, Le Meur G, Weber M, Deschamps JY, Lorenz B, Moullier P, Rolling F (2009). Detection of intact rAAV particles up to 6 years after successful gene transfer in the retina of dogs and primates. *Molecular Therapy* **17**: 516-523.

Styskal J, Van Remmen H, Richardson A, Salmon AB (2012). Oxidative stress and diabetes: what can we learn about insulin resistance from antioxidant mutant mouse models? *Free Radical Biology and Medicine* **52**: 46-58.

Sugano E, Isago H, Murayama N, Tamai M, Tomita H (2013). Different anti-oxidant effects of thioredoxin 1 and thioredoxin 2 in retinal epithelial cells. Cell Structure and Function 38: 81-88.

Takahashi Y, Moiseyev G, Chen Y, Nikolaeva O, Ma JX (2011). An alternative isomerohydrolase in the retinal Müller cells of a cone-dominant species. *The FEBS Journal* **278**: 2913-2926.

Tam BM, Moritz OL (2006). Characterization of Rhodopsin P23H-Induced Retinal Degeneration in a Xenopus laevis Model of Retinitis Pigmentosa. *Investigative Ophtalmology and Visual Science* **47**: 3234-3241.

Tan SM, Stefanovic N, Tan G, Wilkinson-Berka JL, de Haan JB (2013). Lack of the antioxidant glutathione peroxidase-1 (GPx1) exacerbates retinopathy of prematurity in mice. *Investigative Ophthalmology and Visual Science* **54**: 555-562.

Tanito M, Agbaga MP, Anderson RE (2007). Upregulation of thioredoxin system via Nrf2-antioxidant responsive element pathway in adaptive-retinal neuroprotection in vivo and in vitro. *Free Radical Biology and Medicine* **42**: 1838-1850.

Tanito M, Masutani H, Nakamura H, Oka S, Ohira A, Yodoi J (2002). Attenuation of retinal photooxidative damage in thioredoxin transgenic mice. *Neuroscience Letters* **326**: 142-146.

Tanito M, Elliott MH, Kotake Y, Anderson RE (2005). Protein modifications by 4-hydroxynonenal and 4-hydroxyhexenal in light-exposed rat retina. *Investigative Ophthalmology and Visual Science* **46**: 3859-3868.

Trifunović D, Sahaboglu A, Kaur J, Mencl S, Zrenner E, Ueffing M, Arango-Gonzalez B, Paquet-Durand F (2012). Neuroprotective strategies for the treatment of inherited photoreceptor degeneration. *Current Molecular Medicine* **12**: 598-612.

Tsuruma K, Tanaka Y, Shimazawa M, Mashima Y, Hara H (2011). Unoprostone reduces oxidative stress- and light-induced retinal cell death, and phagocytotic dysfunction, by activating BK channels. *Molecular Vision* **17**: 3556-3565.

Uğurlu N, Aşık MD, Yülek F, Neselioglu S, Cagil N (2013). Oxidative stress and anti-oxidative defence in patients with age-related macular degeneration. *Current Eye Research* **38**: 497-502.

Urtti A, Polansky J, Lui GM, Szoka FC (2000). Gene delivery and expression in human retinal pigment epithelial cells: effects of synthetic carriers, serum, extracellular matrix and viral promoters. *Journal of Drug Targeting* **7**: 413-421.

Usui S, Oveson BC, Lee SY, Jo YJ, Yoshida T, Miki A, Miki K, Iwase T, Lu L, Campochiaro PA (2009). NADPH oxidase plays a central role in cone cell death in retinitis pigmentosa. *Journal of Neurochemistry* **110**: 1028-1037.

Usui S, Komeima K, Lee SY, Jo YJ, Ueno S, Rogers BS, Wu Z, Shen J, Lu L, Oveson BC, Rabinovitch PS, Campochiaro PA (2009b). Increased expression of catalase and superoxide dismutase 2 reduces cone cell death in retinitis pigmentosa. *Molecular Therapy* **17**: 778-786.

Usui S, Oveson BC, Iwase T, Lu L, Lee SY, Jo YJ, Wu Z, Choi EY, Samulski RJ, Campochiaro PA (2011). Overexpression of SOD in retina: need for increase in H2O2-detoxifying enzyme in same cellular compartment. *Free Radical Biology and Medicine* **51**: 1347-1354.

Valko M, Rhodes CJ, Moncol J, Izakovic M, Mazur M (2006). Free radicals, metals and antioxidants in oxidative stress-induced cancer. *Chemico-Biological Reactions* **10**: 1-40.

Valko M, Leibfritz D, Moncol J, Cronin MT, Mazur M, Telser J (2007). Free radicals and antioxidants in normal physiological functions and human disease. *International Journal of Biochemistry and Cell Biology* **39**: 44-84.

Verma A, Shan Z, Lei B, Yuan L, Liu X, Nakagawa T, Grant MB, Lewin AS, Hauswirth WW, Raizada MK, Li Q (2012). ACE2 and Ang-(1-7) confer protection against development of diabetic retinopathy. *Molecular Therapy* **20**: 28-36.

Verrier JD, Madorsky I, Coggin WE, Geesey M, Hochman M, Walling E, Daroszewski D, Eccles KS, Ludlow R, Semple-Rowland SL (2011). Bicistronic lentiviruses containing a viral 2A cleavage sequence reliably co-express two proteins and restore vision to an animal model of LCA1. *PLoS One* **6**: e20553.

Wang H, Zhang SX, Hartnett ME (2013). Signaling pathways triggered by oxidative stress that mediate features of severe retinopathy of prematurity. *JAMA Ophthalmology* **131**: 80-85.

Wang H, Geisen P, Wittchen ES, King B, Burridge K, D'Amore PA, Hartnett ME (2011). The role of RPE cell-associated $VEGF_{189}$ in choroidal endothelial cell

transmigration across the RPE. *Investigative Ophthalmology and Visual Science* **52**: 570-578.

Wang JS, Kefalov VJ (2009). An alternative pathway mediates the mouse and human cone visual cycle. *Current Biology* **19**: 1665-1669.

Wang JS, Kefalov (2011). The Cone-specific visual cycle. *Progress in Retinal and Eye Research* **30**: 115-128.

Wang XW, Tan BZ, Sun M, Ho B, Ding JL (2008). Thioredoxin-like 6 protects retinal cell line from photooxidative damage by upregulating NF-kappaB activity. *Free Radical Biology and Medicine* **45**: 336-344.

Watanabe S, Sanuki R, Ueno S, Koyasu T, Hasegawa T, Furukawa T (2013). Tropisms of AAV for subretinal delivery to the neonatal mouse retina and its application for in vivo rescue of developmental photoreceptor disorders. *PLoS One* **8**: e54146.

Weber M, Rabinowitz J, Provost N, Conrath H, Folliot S, Briot D, Chérel Y, Chenuaud P, Samulski J, Moullier P, Rolling F (2003). Recombinant adeno-associated virus serotype 4 mediates unique and exclusive long-term transduction of retinal pigmented epithelium in rat, dog, and nonhuman primate after subretinal delivery. *Molecular Therapy* **7**: 774-781.

Welsh SJ, Bellamy WT, Briehl MM, Powis G (2002). The redox protein thioredoxin-1 (Trx-1) increases hypoxia-inducible factor 1alpha protein expression: Trx-1 overexpression results in increased vascular endothelial growth factor production and enhanced tumor angiogenesis. *Cancer Research* **62**: 5089-5095.

Wilkinson-Berka JL, Rana I, Armani R, Agrotis A (2013). Reactive oxygen species, Nox and angiotensin II in angiogenesis: implications for retinopathy. *Clinical Science* **124**: 597-615

Williams M, Hogg RE, Chakravarthy U (2013). Antioxidants and diabetic retinopathy. *Current Diabetes Reports* **13**: 481-487.

Witt J, Marks Jr WJ (2011). An update on Gene Therapy in Parkinson's Disease. *Current Neurology and Neuroscience Reports* **11**: 362-370.

Wojewoda M, Duszyński J, Szczepanowska J (2010). Antioxidant defence systems and generation of reactive oxygen species in osteosarcoma cells with defective mitochondria: effect of selenium. *Biochimica et Biophysica Acta* **1797**: 890-896.

Wright AF, Chakarova CF, Abd El-Aziz MM, Bhattacharya SS (2010). Photoreceptor degeneration: genetic and mechanistic dissection of a complex trait. *Nature Reviews Genetics* **11**: 273-284.

Wu M, Yang S, Elliott MH, Fu D, Wilson K, Zhang J, Du M, Chen J, Lyons T (2012). Oxidative and endoplasmic reticulum stresses mediate apoptosis induced by modified LDL in human retinal Müller cells. *Invest Ophthalmol Vis Sci* **53**: 4595-4604.

Wu Z, Yang H, Colosi P (2010). Effect of genome size on AAV vector packaging. *Molecular Therapy* **18**: 80-86.

Xiao X, Li J, Samulski RJ (1998). Production of high-titer recombinant adeno-associated virus vectors in the absence of helper adenovirus. *Journal of Virology* **72**: 2224-2232.

Yamamoto S, Sugawara T, Murakami A, Nakazawa M, Nao-I N, Machida S, Wada Y, Mashima Y, Myake Y (2012). Topical Isopropyl Unoprostone for Retinitis Pigmentosa: Microperimetric Results for the Phase 2 Clinical Study. *Ophthalmology and Therapy* 10.1007/s40123-012-0005-9.

Yan Z, Zak R, Zhang Y, Engelhardt JF (2005). Inverted terminal repeat sequences are important for intermolecular recombination and circularization of adeno-associated virus genomes. *Journal of Virology* **79**: 364-379.

Yang Y, Mohand-Said S, Danan A, Simonutti M, Fontaine V, Clerin E, Picaud S, Léveillard T, Sahel JA (2009). Functional cone rescue by RdCVF protein in a dominant model of retinitis pigmentosa. *Molecular Therapy* **17**: 787-795.

Yeom KH, Lee Y, Han J, Suh MR, Kim VN (2006). Characterization of DGCR8/Pasha, the essential cofactor for Drosha in primary miRNA processing. *Nucleic Acids Research* **34**: 4622-4629.

Yu DY, Cringle SJ, Su EN, Yu PK (2000). Intraretinal oxygen levels before and after
photoreceptor loss in the RCS rat. *Investigative Ophthalmology and Visual Science* **41**: 3999–4006.

Yu DY, Cringle S, Valter K, Walsh N, Lee D, Stone J (2004). Photoreceptor death, trophic factor expression, retinal oxygen status, and photoreceptor function in the P23H rat. *Investigative Ophthalmology and Visual Science* **45**: 2013-2019.

Zahedi Avval F, Holmgren A (2009). Molecular mechanisms of thioredoxin and glutaredoxin as hydrogen donors for Mammalian s phase ribonucleotide reductase. *Journal of Biological Chemistry* **284**: 8233-8240.

Zafrilla P, Losada M, Perez A, Caravaca G, Mulero J (2013). Biomarkers of oxidative stress in patients with wet age related macular degeneration. *Journal of Nutrition, Health and Ageing* **17**: 219-222.

Zhang X, Jones D, Gonzalez-Lima F (2002). Mouse model of optic neuropathy caused by mitochondrial complex I dysfunction. *Neuroscience Letters* **326**: 97-100.

Zhao H, Kalivendi S, Zhang H, Joseph J, Nithipatikom K, Vásquez-Vivar J, Kalyanaraman B (2003). Superoxide reacts with hydroethidine but forms a fluorescent product that is distinctly different from ethidium: potential implications in intracellular fluorescence detection of superoxide. *Free Radical Biology and Medicine* **34**: 1359-1368.

Xia H, Mao Q, Paulson HL, Davidson BL (2002). siRNA-mediated gene silencing in vitro and in vivo. *Nature Biotechnology* **20**: 1006-1010.

Xia H, Mao Q, Eliason SL, Harper SQ, Martins IH, Orr HT, Paulson HL, Yang L, Kotin RM, Davidson BL (2004). RNAi suppresses polyglutamine-induced neurodegeneration in a model of spinocerebellar ataxia. *Nature Medicine* **10**: 816-820.

Summary

The focus of this thesis was the exploration of genetic modulators of oxidative stress in transgenic mouse models of Retinitis Pigmentosa (RP). This disease can be inherited both dominantly and recessively and can be either X-linked or autosomal depending of the disease causing mutation. Patients of RP gradually lose their peripheral eyesight over years as rod cells die in the retina. Cone cells then begin to die leading to complete blindness. Evidence amassed over the past ten years has suggested that increasing levels of oxidative stress in the retina of these patients is causing cell death of rod and cone photoreceptor cells. In particular, cone cells seem to die secondary to rods as the levels of oxidative stress dramatically increase when rods die. In addition, this increase in oxidative stress appears to be common in many inherited and non-inherited retinal degenerations.

Based on these observations, two genetic therapies were created. The first of these was an RNA interference (RNAi) based therapy targeted at the *Rac1* gene. The protein encoded by this gene is known to activate the NADPH oxidase complex which produces ROS. Previous studies have shown that depleting this gene in the retina preserves eyesight in mouse models of RP. Therefore short interfering RNAs (siRNAs) were generated to target *Rac1* mRNA and were demonstrated to suppress expression of this gene *in vitro*. Subsequently, short hairpin RNAs (shRNAs) were developed based on the sequence of successful siRNAs for Adeno Aassociated Virus (AAV) mediated delivery to the mouse retina *in vivo*. This also resulted in suppression of endogenous mouse *Rac1* expression. Furthermore, of the two shRNA AAV vectors created, one was demonstrated to preserve visual function and rod and cone photoreceptor viability in a mouse model of RP.

In addition to the suppression of *Rac1*, a parallel project explored the use of *Thioredoxin1* (Trx) over-expression in the retina and the effect of this over-expression in two mouse models of RP. The *Trx* gene encodes an anti-oxidant protein which acts as a reducing agent within the cell cytoplasm. Previous studies have demonstrated that over-expression of this gene preserves retinal ganglion cell function and viability in several models of retinal degeneration. Furthermore, over-expression of *Trx* was shown to be protective of retinal photoreceptor cells in a

mouse model of RP. Therefore an AAV plasmid was generated which expresses the *Trx* gene. This plasmid was demonstrated to drive strong expression of *Trx in vitro*. Subsequently this plasmid was used to generate recombinant AAV vector to deliver this plasmid to retinal cells *in vivo*. The vector was demonstrated to drive strong expression of *Trx* in the photoreceptor cells *in vivo*. Delivery of the *Trx* AAV vector to two mouse models of RP failed to protect photoreceptor cell function or viability in these models. Possible reasons for this failure are also explored in this thesis.

Finally, a stain for ROS named dihydroethidium (DHE) was used to evaluate the levels of ROS in three mouse models of retinal degeneration frequently used by the TCD Ocular Genetics laboratory. Of these three, two were demonstrated to exhibit increased staining for ROS in the retina. In addition, ROS production in the retina was monitored using this stain after treatment of RP model mice with a *Rac1* targeted shRNA or a plasmid over-expressing *Trx*. No decrease in staining was observed for any constructs evaluated except for one shRNA which targets *Rac1*. This shRNA was the same construct which elicited an improvement in photoreceptor function and cell viability, suggesting that shRNA suppression of *Rac1* decreased the production of ROS and in turn increased the functionality of the retina by reducing ROS mediated pathology.

The experiments detailed in this thesis provide an indication that modulation of the retinal levels of reactive Oxygen species can provide functional benefit in mouse models of RP. Furthermore, it provides the motivation to carry out further characterisation of RNAi mediated suppression of *Rac1* expression within other animal models of RP as well as mouse models of other retinal degenerations for which oxidative stress is a contributing pathological factor.

TCD THESIS 10400